UNIVERSITY OF Southampton

University of Southampton Research Repository
ePrints Soton

Copyright © and Moral Rights for this thesis are retained by the author and/or other copyright owners. A copy can be downloaded for personal non-commercial research or study, without prior permission or charge. This thesis cannot be reproduced or quoted extensively from without first obtaining permission in writing from the copyright holder/s. The content must not be changed in any way or sold commercially in any format or medium without the formal permission of the copyright holders.

When referring to this work, full bibliographic details including the author, title, awarding institution and date of the thesis must be given e.g.

AUTHOR (year of submission) "Full thesis title", University of Southampton, name of the University School or Department, PhD Thesis, pagination

http://eprints.soton.ac.uk

**University of Southampton**

**Faculty of Engineering and the Environment**


# Investigation of Hybrid Systems for Diesel Powered Ships

By

Eleftherios K. Dedes

Thesis submitted for the Degree of Doctorate of Philosophy

July 2013

# Abstract

The combination of a prime mover and an energy storage device for reduction of fuel consumption has been successfully used in the automotive industry. The potential of a load levelling strategy and the energy management optimisation through the use of a Hybrid Diesel propulsion system for ocean going ships is investigated. The goal of Diesel Hybrid systems is to reduce exhaust gas emissions by reducing fuel oil consumption though an introduction of an energy storage medium. Part of the research is based on operational data for a shipping fleet containing all types of bulk carriers. The engine loading and energy requirements are estimated and the sizing of suitable propulsion and the battery storage system is proposed. The changes in overall emissions are estimated and the potential for fuel savings is identified. The emission estimation is made by applying a bottom up approach, and the use of fuel based factors. The thesis includes an assessment of the calculation error imposed by the usage of fuel-based factors, and a determination of the uncertainty in the approximation of global shipping emissions is made. Constructional and volume constraints are identified and a concept feasibility is performed.

The thesis demonstrates the use of developed ship voyage simulator, which is a time domain quasi-steady simulation tool. The system components of the Hybrid and the conventional machinery system are modelled, the weather characteristics and the hull-fluid interaction are implemented in a modular, scalable and expandable manner. Using the simulation tool, an assessment of simulated bottom up approach with the results of the IMO formula is presented for a number of examined voyages. Moreover, simulator outputs of the propulsive demand are fed to the optimisation algorithm, which is based on the equivalent cost minimisation strategy. In addition, a pseudo multi-objective optimisation algorithm for $CO_2$ and PM reduction is also presented. The results indicate that the ship simulator estimates shipping emissions with a significantly smaller error than the adopted formulae of the IMO.

The hybrid solution for diesel powered ships is under specific scenarios financially viable, and the fuel savings based on the statistical analysis are notable when ageing of the engines and performance deterioration models are included. Nevertheless, when the optimised performance of the Hybrid power layouts is compared to optimally tuned engines at ISO conditions, instead of the actual prime mover performance, the the fuel saving potential for auxiliary loads is reduced and also leads to non-feasible results for propulsive loads. Nonetheless, the Hybrid power systems permit the use of sophisticated prime mover energy management for both propulsive and auxiliary loads. This proved to lead to notable fuel savings for the combined shipboard power trains.

(Page left intentionally blank)

# Table of Contents

# List of Figures

## Chapter 1



## Chapter 2



## Chapter 3

## Chapter 4



## Chapter 5

## Chapter 6



## Appendices

(Page left intentionally blank)

# List of Tables

## Chapter 1



## Chapter 2



## Chapter 3



## Chapter 4

**Chapter 5**



**Chapter 6**

## Appendices

(Page left intentionally blank)

# Nomenclature

| | | | |
|---|---|---|---|
| $\nabla$ | : | Displacement volume of the ship | [$m^3$] |
| a | : | Correction factor for $C_B$ and Froude number (Kwon, 2008) | [-] |
| A | : | Number of fissions | [-] |
| $A_{BT}$ | : | Transverse area of the bulbous bow | [$m^2$] |
| $A_E/A_o$ | : | Expanded blade area ratio | [-] |
| $A_F$ | : | Frontal projected area | [$m^2$] |
| $A_i$ | : | Coefficients determined in Isherwood (1974) | [-] |
| $A_L$ | : | Lateral projected area of the ship | [$m^2$] |
| $A_n$ | : | Wave amplitude | [-] |
| $A_R$ | : | Rudder area | [$m^2$] |
| $A_T$ | : | Transverse projected area of the ship | [$m^2$] |
| $A_{TR}$ | : | Immersed transom area | [$m^2$] |
| $a_w$ | : | shape factor of Weibul/ Rayleigh probability density functions | [-] |
| B | : | Breadth of the ship | [m] |
| $Bat_{cap}$ | : | Battery Energy Capacity | [kWh] |
| $b_e$ | : | Specific Fuel Oil Consumption at examined load | [g/kWh] |
| $B_i$ | : | Coefficients determined in Isherwood (1974) | [-] |
| bkW | : | Engine's break Power | [kW] |
| BN | : | Beaufort number | [-] |
| C | : | Distance from bow of centroid to the $A_L$ | [m] |
| $C_A$ | : | Correlation allowance coefficient in Hotrop (1981) | [-] |
| $C_B$ | : | Block coefficient | [-] |
| $C_F$ | : | Frictional resistance coefficient ITTC 1957 | [-] |
| $C_{F\,A/E}$ | : | A/E fuel carbon content | [-] |
| $C_{F\,M/E}$ | : | M/E fuel carbon content | [-] |
| $C_F$ | : | Friction coefficient | [-] |
| $C_{Fi}$ | : | Fuel type coefficient | [-] |
| $C_i$ | : | Coefficients determined in Isherwood (1974) | [-] |
| $c_{KB}$ | : | Constant dependent on the battery technology | [-] |
| $C_n$ | : | Coefficient (Oosterveld and Oossanen, 1975) | [-] |
| $C_{nom}$ | : | Nominal battery capacity | [MWh] |
| $C_P$ | : | Prismatic coefficient | [-] |
| $CR_i$ | : | Correction factors imposed by engine manufacturers | [-] |
| $CR_{LCVF}$ | : | Correction for fuel oil low calorific value | [-] |

| | | | |
|---|---|---|---|
| $C_{stern}$ | : | Stern type as described in Holtrop and Mennen (1981) | [-] |
| $C_V$ | : | Viscous resistance coefficient | [-] |
| $C_{WP}$ | : | Water plane coefficient | [-] |
| D | : | Drought of the ship | [m] |
| $D_i$ | : | Sailed distance | [n. m.] |
| $DoD_{in}$ | : | Battery Depth of Discharge at simulation time step | [%] |
| $DoD_{t-1}$ | : | Battery Depth of Discharge at previous simulation time step | [%] |
| $D_p$ | : | Propeller diameter | [m] |
| dV | : | Voltage drop/ excess during discharging/ charging | [V] |
| DWT | : | Vessels deadweight | [tonnes] |
| $E_o$ | : | Electromotive force or open-circuit voltage of cell | [V] |
| $E_{bat}$ | : | Installed Battery Energy Density | [kWh] |
| F | : | Fetch distance | [km] |
| $f_{ci}$ | : | Correction factor to account ship specific design elements | [-] |
| $f_{eff}$ | : | Availability factor of innovative energy saving technology | [-] |
| $f_i$ | : | Coefficients for E/R volume approximation (SNAME, 1990) | [-] |
| $f_j$ | : | Capacity factor for technical/regulatory limitation on capacity | [-] |
| Fn | : | Froude number | [-] |
| $Fn_i$ | : | Froude number based on the immersion | [-] |
| Fo | : | Oversizing factor and is determined by the designer | [-] |
| $F_T$ | : | Turbulence scale | [-] |
| $f_w$ | : | Non-dimentional deduction coefficient of sea condtions | [-] |
| g | : | Acceleration of gravity | [m/s²] |
| g(x) | : | Specific Fuel Oil Consumption curve | [g/kWh] |
| h(x) | : | SFOC curve for type II Diesel Generator Set | [g/kWh] |
| $h_B$ | : | Vertical position of $A_{BT}$ from the keel plane | [m] |
| $h_i$ | : | Enthalpies at certain temperature and dryness | [kJ] |
| $h_p$ | : | Enthalpy at condenser | [kJ] |
| i | : | Operating current of battery on load | [A] |
| J | : | Advance speed | [-] |
| k | : | Coefficient determined by Hollenbach method | [-] |
| k’ | : | Coefficient determined by Manwell et al. (2005) | [-] |
| $k_{Boss}$ | : | Boss coefficient | [-] |
| $k_{Brac}$ | : | Bracket coefficient | [-] |
| $K_N$ | : | The surface drag coefficient equal | [-] |
| $K_Q$ | : | Non-dimensional propeller torque coefficient | [-] |
| $K_R$ | : | Rudder velocity distance corrective factor | [-] |

| | | | |
|---|---|---|---|
| $k_{Rudd}$ | : | Rudder coefficient | [-] |
| $K_T$ | : | Non-dimensional propeller thrust coefficient | [-] |
| L | : | Equivalent ship length (Schneekluth and Bertram, 1998) | [-] |
| LCB | : | Longitudinal Centre of Buoyancy | [m] |
| lcb | : | LCB expressed in percentage from amidships | [%] |
| LCG | : | Longitudinal Centre of Gravity | [m] |
| LF | : | Engine load factor | [-] |
| $L_{OA}$ | : | Length overall | [m] |
| $L_{OS}$ | : | Length over surface determined in Hollenbach method | [m] |
| $L_{PP}$ | : | Length between perpendiculars | [m] |
| $L_{WL}$ | : | Length of waterline | [m] |
| $\dot{m}$ | : | Steam mass flow | [kg/m³] |
| $Max_{d.c}$ | : | Battery Maximum Discharge current | [A] |
| $MCR_{A/E}$ | : | Maximum Continuous Rating of Auxiliary Diesel Engine | [kW] |
| $MCR_m$ | : | Maximum Continuous Rating of electric machine | [kW] |
| $MCR_{M/E}$ | : | Maximum Continuous Rating of Main Diesel Engine | [kW] |
| $m_f$ | : | Mass of injected fuel | [kg] |
| MTC | : | Moment to change trim | [tm] |
| $M_{XG}$ | : | Gust peak | [m/s] |
| $MX_R$ | : | Ramp maximum value | [m/s] |
| n | : | Revolutions of the propeller | [rps] |
| N | : | Number of measurements | [-] |
| $N'_{uu\delta}$ | : | Static non-dimensional yawing moment coefficient | [-] |
| $N'_{uv}$ | : | Static non-dimensional rudder yawing moment coefficient | [-] |
| $N_{BB}$ | : | Number of Battery Banks | [-] |
| $N_{Boss}$ | : | Number of bosses | [-] |
| $N_{Brac}$ | : | Number of brackets | [-] |
| $n_{bs}$ | : | Number of batteries in DC bus | [-] |
| $NF_{cons.}$ | : | Nuclear fuel consumption | [tonnes] |
| $No_{atoms}$ | : | Required number of atoms to achieve the number of fissions | [-] |
| $NR_{cons.}$ | : | Nuclear Reactor specific fuel depletion | [g/kWh] |
| $NR_{max}$ | : | Nuclear Reactor maximum power output | [kW] |
| $N_{Rudd}$ | : | Number of rudders | [-] |
| P | : | Engine Output Power | [kW] |
| p(x) | : | Power limit curve dictated by the Main Engine | [kW] |
| P/D | : | Pitch to diameter ratio | [-] |
| $P_{A/E}$ | : | A/E power output | [kW] |

| | | | |
|---|---|---|---|
| $P_{AES}$ | : | All electric ship power demand | [kW] |
| $P_B$ | : | Emergence of the bow | [-] |
| $P_{demand}$ | : | Demanded power by the propulsion and/ or auxiliary loads | [kW] |
| $P_{eff}$ | : | 75% Power of the M/E due to innovative technology | [kW] |
| $P_{M/E}$ | : | M/E power output | [kW] |
| $P_{prd}$ | : | Produced Power | [kW] |
| $P_{PTI}$ | : | Power Take In output power | [kW] |
| $P_{PTI}$ | : | Power take off (PTI) power output | [kW] |
| $P_{req.}$ | : | Required Power | [kW] |
| $P_{total}$ | : | Required voyage propulsive power | [kW] |
| $P_{WHR}$ | : | Waste heat recovery (WHR) equivalent power output | [kW] |
| $P_{WHR}$ | : | Waste Heat Recovery system power output | [kW] |
| q | : | Dynamic pressure of the apparent wind | [Pa] |
| $Q_o$ | : | Open water developed torque | [Nm] |
| $Q_1$ | : | Energy supplied by the nuclear reactor | [kW] |
| $Q_F$ | : | Fuel Chemical Power | [kW] |
| R | : | Uniformly distributed number [0, 1] | [-] |
| $R_A$ | : | Model-ship correlation | [N] |
| $R_{APP}$ | : | Appendage resistance | [N] |
| $R_B$ | : | Pressure resistance of bulbous bow | [N] |
| $R_F$ | : | Frictional resistance according to ITTC 1957 | [N] |
| $R_i$ | : | Internal resistance of the battery | [Ω] |
| RPM | : | Engine Rotational speed | [RPM] |
| $R_R$ | : | Residual Resistance | [N] |
| $R_T$ | : | Total Resistance | [N] |
| $R_{TR}$ | : | Pressure resistance of immersed transom stern | [N] |
| $R_W$ | : | Wave-making and wave-breaking resistance | [N] |
| $S_P$ | : | Perimeter of the lateral projection | [m] |
| S | : | Wetted surface area | [m²] |
| $S_{APP}$ | : | Appendage wetted surface area | [m²] |
| $SFOC_{A/E}$ | : | A/E specific fuel oil consumption | [g/kWh] |
| $SFOC_{M/E}$ | : | M/E specific fuel oil consumption | [g/kWh] |
| $SFOC_{min}$ | : | Minimum SFOC of Auxiliary Engine | [g/kWh] |
| $SFOC_{min}$ | : | Minimum SFOC of Diesel Generator Sets | [g/kWh] |
| $S_n$ | : | Coefficient (Oosterveld and Oossanen, 1975) | [-] |
| $SoC_{ref}$ | : | Reference Battery State of Charge, user defined | [%] |
| $SoC_t$ | : | Battery State of Charge at simulation time t | [%] |

| | | | |
|---|---|---|---|
| $S_{total}$ | : | Wetted surface area approximated by Hollenbach method | [m²] |
| T | : | Developed thrust | [N] |
| t | : | Thrust deduction factor | [-] |
| $T_o$ | : | Open water developed thrust | [N] |
| $T_{1G}$ | : | Gust starting time | [s] |
| $T_{1R}$ | : | Ramp start time | [s] |
| $T_{2R}$ | : | Ramp maximum time | [s] |
| $T_{air}$ | : | Air temperature | [°C] |
| $T_G$ | : | Gust period | [s] |
| $t_{ref}$ | : | Reference time where the $SoC_t$ must be equal to $SoC_{ref}$ | [h] |
| $t_{sim}$ | : | Simulation elapsed time | [h] |
| $T_W$ | : | Water temperature | [°C] |
| $u_n$ | : | Coefficients (Oosterveld and Oossanen, 1975) | [-] |
| $u_w$ | : | Wind speed | [m/s] |
| V | : | Vessel speed | [m/s] |
| v | : | Ship's lateral velocity | [m/s] |
| $V_o$ | : | Undisturbed fluid speed at propeller | [m/s] |
| $V_1$ | : | accelerated speed at the propeller disk | [m/s] |
| $V_2$ | : | accelerated speed downstream of propeller disk | [m/s] |
| $V_A$ | : | Velocity of advance | [m/s] |
| $V_{Bat}$ | : | Battery Voltage | [V] |
| $V_{EP}$ | : | Engine Room Volume | [m³] |
| $v_n$ | : | Coefficients (Oosterveld and Oossanen, 1975) | [-] |
| $V_{nominal}$ | : | Battery Nominal Voltage | [V] |
| $V_{OP}$ | : | DC bus voltage | [V] |
| $V_R$ | : | Relative wind speed | [m/s] |
| $V_R$ | : | Relative wind velocity | [m/s] |
| $V_{ref}$ | : | Vessel desing/ reference speed | [knots] |
| $V_{ref}$ | : | Vessel reference speed defined by IMO | [knots] |
| $V_{RR}$ | : | Relative rudder velocity | [m/s] |
| $V_{WB}$ | : | Base wind velocity | [m/s] |
| $V_{WG}$ | : | Gust wind component | [m/s] |
| $V_{WN}$ | : | Noise wind component | [m/s] |
| $V_{WR}$ | : | Ramp wind component | [m/s] |
| w | : | Wake friction | [-] |
| w(x) | : | Battery Discharge/ Charge efficiency curves | [-] |
| $W_{cargo}$ | : | Weight of transported cargo | [tonnes] |

| | | | |
|---|---|---|---|
| $W_{Fuel}$ | : | Consumed fuel weight | [tonnes] |
| $W_P$ | : | Work required at pressuriser | [kW] |
| $W_T$ | : | Work in the Turbine | [kW] |
| X | : | Distance between rudder and propeller | [m] |
| $Y'_{cc\delta}$ | : | Non-dimensional rudder force coefficient | [-] |
| $Y'_{uv\,\delta}$ | : | Vessel Hydrodynamic coefficient | [-] |
| $Y'_{uv}$ | : | Non-dimensional static force coefficient | [-] |
| $Y_{i,o}$ | : | Amount of available and bound charge | [Ah] |
| z | : | Number of blades | [-] |
| $\beta$ | : | scale factor of Weibul probability density function | [-] |
| $\Gamma$ | : | Gamma function | [-] |
| $\Delta$ | : | Vessel displacement | [tonnes] |
| $\delta_B$ | : | Coefficient determined in Blendermann (1994) | [-] |
| $\Delta t_{sim}$ | : | Simulation time step | [h] |
| $\varepsilon$ | : | Wind angle of attack | [rad] |
| $(\eta_c)_a$ | : | Concentration polarisation at anode and cathode | [-] |
| $(\eta_c)_c$ | : | Concentration polarisation at anode and cathode | [-] |
| $(\eta_{ct})_a$ | : | Activation polarisation or charge-transfer overvoltage at anode | [-] |
| $(\eta_{ct})_c$ | : | Activation polarisation or charge-transfer overvoltage at cathode | [-] |
| $\eta_c$ | : | Propulsion converter efficiency | [-] |
| $\eta_{conv.}$ | : | Propulsion converter efficiency | [-] |
| $\eta_g$ | : | Gearbox/ clutch efficiency | [-] |
| $\eta_{gen}$ | : | Electric generator efficiency | [-] |
| $\eta_{isHP}$ | : | High Pressure turbine isentropic efficiency | [-] |
| $\eta_{isLP}$ | : | High Pressure turbine isentropic efficiency | [-] |
| $\eta_{loss}$ | : | Electric conversion losses | [-] |
| $\eta_m$ | : | Electric motor efficiency curve | [-] |
| $\eta_{mHP}$ | : | High pressure turbo generator efficiency curve | [-] |
| $\eta_{mLP}$ | : | Low pressure turbo generator efficiency curve | [-] |
| $\eta_{overall}$ | : | Turbine system overall efficiency | [-] |
| $\eta_R$ | : | Relative rotative efficiency | [-] |
| $\eta_{Rankine}$ | : | Rankine cycle efficiency | [-] |
| $\eta_{reactor}$ | : | Nuclear reactor efficiency | [-] |
| $\eta_{T/F}$ | : | Propulsion transformer efficiency | [-] |
| $\eta_{T/F,inv}$ | : | Battery Transformer and inverter efficiency | [-] |
| $\eta_{trans}$ | : | Conversion losses due to power transmission | [-] |
| $\Theta_u$ | : | Fuel Oil Lower Calorific Value | [kJ/kg] |

| | | | |
|---|---|---|---|
| $\mu$ | : | Correlation factor defined by Kwon method | [-] |
| $\mu_{sw}$ | : | Salt water kinematic viscosity | [$m^2/s$] |
| $\xi_n$ | : | Uniformly distributed random variables between [0, $2\pi$] | [-] |
| $\rho_{air}$ | : | Air density | [$kg/m^3$] |
| $\rho_w$ | : | Water density | [$kg/m^3$] |
| $\varphi_i$ | : | Random variable with uniform probability density [0, $2\pi$] | [-] |
| $\omega_o$ | : | Encounter frequency | [rad/s] |
| 1+k1 | : | Form factor of hull viscous resistance | [-] |

(Page left intentionally blank)

# Abbreviations

| | | |
|---|---|---|
| AC | : | Alternative current |
| A/E | : | Auxiliary Diesel engine |
| AES | : | All electric ship |
| BSRA | : | British ship research association |
| BWR | : | Boiling water reactor |
| CO | : | Carbon monoxide |
| $CO_2$ | : | Carbon dioxide |
| CODOG | : | Combined Diesel or gas |
| CODAG | : | Combined Diesel and gas |
| CPD | : | Continuous professional development |
| DC | : | Direct current |
| DWT | : | Deadweight |
| EC | : | Elementary carbon |
| ECA | : | Emission control area |
| ECMS | : | Equivalent cost minimisation strategy |
| EEDI | : | Energy efficiency design index |
| EEOI | : | Energy efficiency operational indicator |
| EGR | : | Exhaust gas recirculation |
| EPR | : | European pressurised reactor |
| E/R | : | Engine room |
| FEP | : | Full electric propulsion |
| FEU | : | Fifty-foot equivalent unit container |
| GCFR | : | Gas-cooled breeder reactor |
| GHG | : | Green house gasses |
| GTO | : | Gate turnoff thyristors |
| GUI | : | Graphical user interface |
| HC | : | Unburnt hydrocarbons |
| HEU | : | High enriched Uranium |
| HFO | : | Heavy fuel oil |
| HVAC | : | Heating, ventilation and air conditioning system |
| ICE | : | Internal combustion engine |
| IFEP | : | Integrated full electric propulsion |
| IGCT | : | Integrated gate-commutated thyristors |
| IMO | : | International maritime organisation |

| | | |
|---|---|---|
| IRR | : | Internal rate of return |
| ISO | : | International standardisation organisation |
| ITTC | : | International towing tank conference |
| JIT | : | Just in time arrival |
| LCB | : | Longitudinal centre of buoyancy |
| LEU | : | Low enriched Uranium |
| LMFBR | : | Liquid metal cooled breeder reactor |
| LNG | : | Liquefied natural gas |
| LWBR | : | Light-water breeder reactor |
| M/E | : | Main Diesel engine |
| MARPOL | : | Marine pollution |
| MCR | : | Maximum continuous rating |
| MDO | : | Marine Diesel oil |
| MEPC | : | Marine environmental pollution committee |
| MSBR | : | Molten salt breeder reactor |
| NCR | : | Nominal continuous rating |
| $NO_x$ | : | Nitrogen oxides |
| OC | : | Organic compounds |
| OGV | : | Ocean going vessel |
| PHEV | : | Plug-in hybrid electric vehicle |
| PM | : | Particulate matter |
| PTI | : | Power take-in |
| PTO | : | Power take-off |
| PWR | : | Pressurised water reactor |
| RBMK | : | Reaktor Bolshoy Moshchnosti Kanalniy (Russian) |
| RPM | : | Rotations per minute |
| SCR | : | Selective catalytic reaction |
| SCRe | : | Silicon controlled rectifier |
| SFOC | : | Specific fuel oil consumption |
| SMES | : | Superconducting Magnetic Energy Storage |
| SMR | : | Small modular reactor |
| $SO_x$ | : | Sulphur oxides |
| TEU | : | Twenty-foot equivalent unit container |
| VSC | : | Voltage source converter |
| WED | : | Wake equalising duct |
| WIT | : | Water in Fuel technology |
| ZEBRA | : | Zero emission battery research activity |

# Declaration of Authorship

I, Eleftherios K. Dedes declare that the thesis entitled 'Investigation of Hybrid Systems for Diesel Powered Ships' and the work presented in the thesis are both my own, and have been generated by me as the result of my own original research. I confirm that:

- this work was done wholly or mainly while in candidature for a research degree at this University;
- where any part of this thesis has previously been submitted for a degree or any other qualification at this University or any other institution, this has been clearly stated;
- where I have consulted the published work of others, this is always clearly attributed;
- where I have quoted from the work of others, the source is always given. With the exception of such quotations, this thesis is entirely my own work;
- I have acknowledged all main sources of help;
- where the thesis is based on work done by myself jointly with others, I have made clear exactly what was done by others and what I have contributed myself;
- parts of this work have been published as: E. K. Dedes, D. A. Hudson and S. R. Turnock
  - *Modifications on the Activity based approach for accurate estimation of fuel consumption from global shipping,* Transportation Research Part D: Transport and Environment, to be submitted, 2013c.
  - *Diesel Hybrid systems for increase of fuel efficiency and reduction of exhaust emissions from ocean going ships,* Journal of Energy, to be submitted, 2013b.
  - *Technical feasibility of Hybrid Powering systems to reduce emissions from bulk carriers*, IJME Transactions of RINA, 2013a.
  - *Design and Simulation of Hybrid Powering Systems for Reduction of Fuel Oil Consumption and Shipping Emissions*, 1rst International MARINELIVE Conference on 'All Electric Ship', NTUA, Athens, Greece, 2012b
  - *Assessing the potential of hybrid energy technology to reduce exhaust emissions from global shipping*, Energy Policy 40, p.p. 204-218, 2012a

- …and S. Hirdaris. *Possible Power Train Concepts for Nuclear Powered Merchant Ships*. LCS conference, Glasgow, Vol. 1 p.p. 263-273, University of Strathclyde, 2011.
- *Design of Hybrid Diesel-Electric Energy Storage Systems to Maximize Overall Ship Propulsive Efficiency*, 11th PRADS conference R.J. Brazil, Vol. 1 p.p. 703-713, COPPE UFRJ, 2010

**Signed:**

**Date:** 22/07/2013

# Acknowledgements

Firstly, I want to express my deep appreciation to my academic supervisors Professor Stephen Turnock and Dr Dominic Hudson who guided me with their expertise and most importantly who supported me in some difficult decisions. I would like to express my gratitude as well to Professor Ajit Shenoi for offering me a place at the Fluid Structure Interactions Group and for his support.

Secondly, I would like to thank my parents Konstantinos and Chrysanthi for encouraging me to continue my studies, apply for research post-graduate degree and for supporting my decisions.

I wish to thank Foundation Propondis, Eugenides Foundation, Union of Greek Ship Owners, Lloyd's Register UK and Lloyd's Register Educational Trust for the financial support of the research project throughout the three years of study. Especially I would like to thank the chairman of Propondis Foundation Mr D. Diamantides and the director Mr G. Baveas, Dr S. Hirdaris from Lloyds' Register UK strategic R&D and the regional manager of Hellenic Lloyds Mr. A. Poulovassilis.

Furthermore I would like to express my gratitude to the Technical and Operational departments of the Greek shipping company which provided the data, especially to the Technical Manager Mr P. Provias, to the superintendent engineers Mr A. Giantsis, Mr P. Triantafylos and Mr G. Gavrilis and to the technical department of Carnival Corporation and plc.

Additionally, I wish to thank to Dr R. Wills from Faculty of Engineering and the Environment of University of Southampton, Dr M. Ioannou from Wartsila R&D Swiss and Professor C. Frangopoulos, Associate Professor J. Prousalidis and Mr G. Georgiou from National Technical University of Athens.

Personally I would like to thank my friend and superintendent engineer Mr P. Georgakis for his support and his professional opinion in the aspects of actual shipping operations. Finally but not of least importance, a special thanks to Ms V. Maseli for her sincere support and her belief for the successful continuation of my studies.

With the oversight of my main supervisor Professor S. R. Turnock, editorial advice by Ms D. Kapsali has been sought. No changes of intellectual content were made as a result of this advice.

(Page left intentionally blank)

*To my parents*
*Chrysanthi and Konstantinos*

(Page left intentionally blank)

# 1 Introduction

## 1.1 Background

Approximately 80% of world trade by volume is carried by sea (UNCTAD 2008). In 2007 it is estimated that international shipping was responsible for approximately 870 million tonnes of $CO_2$ emissions, or 2.7% of global anthropogenic $CO_2$ emissions. By way of comparison, this level of emissions is between those of Germany and Japan for the same year. Domestic shipping and fishing activity bring these totals to 1050 million tonnes of $CO_2$, or 3.3% of global anthropogenic $CO_2$ emissions. Despite the undoubted $CO_2$ efficiency of shipping in terms of grammes of $CO_2$ emitted per tonne-km, it is recognised within the maritime sector that reductions in these totals must be made (IMO, 2009). Nonetheless, exhaust emissions from global shipping contribute significantly to the total emissions of the transportation sector (Corbett et al, 1999; Eyring et al., 2005). Eyring et al., (2010) mention that $NO_x$ emissions are currently estimated to be around 15% of global anthropogenic $NO_x$ emissions and 4-9% of $SO_x$, respectively, and recent legislation is aimed at reducing these emissions through the introduction of emission control areas and requirements on newly built marine diesel engines (MARPOL, 2005). The expected changes in $CO_2$ emissions from shipping from 2007 to 2050 were modelled for the International Maritime Organisation with reference to the emissions scenarios developed for the UN IPCC. These scenarios are based on global differences in population, economy, land-use and agriculture (IMO, 2009). The base scenarios indicate annual increases of $CO_2$ emissions in the range 1.9-2.7%, with the extreme scenarios predicting changes of 5.2% and -0.8%, respectively. The increase in emissions is related to predicted growth in seaborne transport. If global emissions of $CO_2$ are to be stabilised at a level consistent with a 2°C rise in global average temperature by 2050, it is clear that the shipping sector must find ways to stabilise, or reduce, its emissions – or these projected values will account for 12% to 18% of all total permissible $CO_2$ emissions.

Carbon dioxide and Suplhur oxides emissions from world shipping are directly related to the fuel consumption of the fleet. In 2007, approximately 277 million tonnes of fuel were consumed by international shipping. Three categories of ship account for almost two thirds of this consumption. The liquid bulk sector accounts for ~65 million tonnes fuel/year, container vessels for ~55 million tonnes fuel/year and the dry bulk sector for ~53 million tonnes fuel/year (IMO, 2009). Figure 1.1 depicts the actual share of Carbon dioxide per vessel category, which is the most important GHG emitted by ships. In addition, nitrogen oxides and particulate matter is directly related to the engine fuel efficiency and working point.

From a ship-owner/ managing Company perspective, the shipping sector is facing the severe consequences of global recession. Increased vessel capacity, which affects the balance between supply and demand, had led the older or the most inefficient vessels to be unchartered. The ones that remain into the trading play are subject to low income, affecting the prosperity of the sector. For that reason, the IMO, on the one hand, and shipping companies on the other (the former for the purpose of lowering emissions), are seeking ways to further reduce fuel consumption, which is directly related to net income and to total emissions. Working towards improved ship energy efficiency, shipyards have adapted their approach to ship design for newly-built ships, mainly under pressure from the adopted legislation of the IMO, the Energy Efficiency Design Index and from the shipping companies, which now demand an energy efficient ship in order to maximise their profit in the longer term.

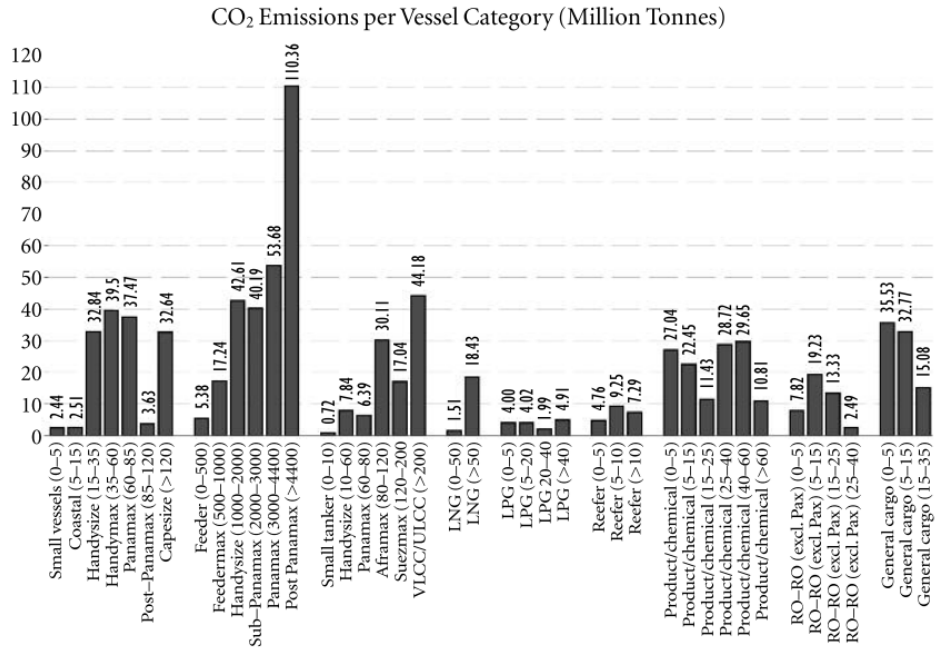


**Figure 1.1: World fleet CO2 emission share in million tonnes per vessel category, year (Psaraftis and Kontovas, 2009)**

This thesis, deals with the complex problem of ship fuel consumption which is related to the total emitted exhaust gasses, the accurate measurement of the emission percentages and the thermodynamic efficiency of marine Diesel engines. The latter efficiency is directly related to the operational envelope of each ocean going vessel. Therefore, a suitable proposal to minimise fuel consumption, reduce fuel emissions and be able to be installed on current and future designs should be found.

The combination of a prime mover and an energy storage device for the reduction of fuel consumption has been successfully used in the automotive industry (Mohamed et al., 2009) and has been shown to contribute to reduced $CO_2$ emissions (Alvarez et al., 2010;

Fontaras et al., 2008). The shipping industry has utilised this for conventional submarines where no oxygen is present during dive conditions. The question to be raised is whether the hybrid solution consisting of a Diesel prime movers and batteries is suitable as a method of increasing fuel efficiency and consequently for emission reduction in marine applications.

The main reason for investigating a potential solution that uncouples the production and the demand is primarily because the optimisation of marine diesel engines is aimed at reducing fuel consumption for a broad range of operations. This implies that the tuning of engine parameters such as injection and valve timing, the selection of the turbochargers are made for a wide range of operational conditions, especially for camshaft controlled engines. However, this range affects the local efficiency and more suitable components for smaller operational profiles are not installed (Kyrtatos, 1993). Marine engines operate in changing conditions at sea due to vessel interaction with hydrodynamic and wind induced loads. In addition, the operations department/ charterer voyage orders, may include voyage deviations and speed alterations which is another factor that affects the propulsion system operational point. In order to serve this operational envelope, the designers optimise engines for a broad operational range; there is, however, a specific optimised point of minimum fuel consumption for a given speed. Unfortunately, the operation of the engine at that point or near that point is not always possible. Thus the specific fuel oil consumption (SFOC) is increased and both the thermodynamic and the mechanical efficiencies of the engine drop (Klein Woud and Stapersma, 2003).

The efficiencies of marine diesel engines have increased in recent decades (Kyrtatos, 2009) and efforts are continuing to reduce specific fuel consumption and exhaust pollutant gases, such as $NO_x$ and $SO_x$ and shoot (PM and smoke) but still, the broad range of operational conditions limits their overall efficiency.

The use of work investigates hybrid power system topologies allows the propulsor (propellers in ocean going fleet) to be uncoupled from the process of the production of rotational speed and torque by the Diesel prime movers. This concept requires the existence of an intermediate energy storage medium or a sophisticated energy management system to deal with the power demand. A preliminary concept for battery electric propulsion was made in Barabino et al. (2009). The Hybrid propulsion system was initially discussed by Nilsen and Sørfonn (2009) by coupling a Diesel engine and Diesel generator set in a system with the Power take off (PTO-PTI) feature, in order to switch propulsion unit while sailing into emission control areas (ECAs). It was believed that it is easier to switch fuel type without stopping by having a generator set supplying energy to the propulsion, burning lighter fuel only. Moreover, de Vos and Versuijs (2010) investigated the potential for a Hybrid tug vessel to operate at low loads using a fuel cell,

and to use the installed Diesel engine when in tug operation, for emission reduction and optimised use of the power trail inside the port.

Grimmelious et al. (2011) state that ships having short-term peaks or long periods of very low load, benefit the most from Hybrid Power systems. However, it is argued among the shipping industry that other types of vessels can benefit from hybrid (consisting of energy storage and Diesel engines) concepts. The primary feasibility analysis of hybrid power systems for slow speed vessels published by Dedes et al. (2010) demonstrated that the potential application of Hybrid systems in bulk carrier vessels can be feasible. It has been determined that Hybrid Power system that can apply load levelling in propulsion loads, control the energy production by optimally loading the prime mover for the total duration of the voyage, is promising and has yet to be performed. However, the concept of retrofit slow speed vessels with All Electric Hybrid propulsion to minimise electromechanical losses from and to the battery system proved to be inefficient (Dedes et al., 2012a).

## 1.2 Aim and Objectives

The aim of this thesis is to investigate the use of a conventional Diesel Mechanical system for main propulsion, incorporating a PTO/PTI module and an appropriate energy storage medium. For a conventional ship, the objective is to produce the required energy at near optimum conditions by finding the optimum power split between the Diesel Engine and the hybrid module. For the system to have a high energy efficiency, the engine specific fuel oil consumption (SFOC) has to be near the minimum value. The energy storage system or the sophisticated energy management is responsible for covering the energy demand and maintaining the optimum energy production. Energy management and load levelling result in reductions of the total fuel bill. In addition, a decrease of sea margin, hence a decrease of the size of the total installed power as the peak demands, can be covered by the storage medium without affecting the overall fuel efficiency. Nevertheless, to apply load levelling and/or reduce the power output of the Diesel prime movers, the Hybrid Power concept uses devices capable of storing large amounts of energy for a non-uniform charging/discharging time profile. Specific objectives are to:

i. Investigate different storage systems and identifies high temperature batteries as the most promising solution with their low installation cost, high power density and high recyclability. For the conventional Diesel or Diesel-electric propulsion layouts, it is expected that this system will allow a more flexible approach to the overall propulsion system, permitting further application of external emission reduction techniques. The application of sustainable

technologies (such as solar panels, wind turbines, etc.) as auxiliary installations to the charging circuit of the storage system is also feasible.

ii. Process a set of actual operational data which consists of fuel consumption and the actual vessel operation for a fleet of dry bulk carrier vessels. Calculation of $CO_2$, $NO_x$ and $SO_x$ emissions and estimation of the engine loading for laden and ballast voyages is then possible. The statistical data provided the information necessary to estimate the size of the storage medium and identify the optimisation point of the propulsion engines using an overall daily energy consumption approach.

iii. Consider the connection of batteries and operational parameters using a suitable modelling and simulation approach using a systematic energy approach. The selection of the prime mover is crucial for any potential changes in cargo capacity or vessel displacement. The energy storage media and diesel generators will not make major changes in the ship weight and longitudinal distribution that would reduce the carrying capacity of the vessel. Preliminary economic feasibility of the project is to demonstrated for a Diesel-Hybrid Power layout.

iv. Develop a ship voyage analysis simulation in Matlab/Simulink® environment in order to extrapolate the results and investigate the emission profile of the global fleet for a number of actual and fictional scenarios. The simulator is built in a modular, scalable and extendable manner so that the simulation library could be updated with higher complexity models or with updates of the mathematical implementation of the existing ones.

v. Assess the benefit of Hybrid Power using non-linear optimisation algorithms based on the Equivalent Cost Minimisation Strategy (ECMS) of Guzzella and Sciarretta (2005), and a pseudo multi-objective optimisation algorithm, with the primary target of reducing fuel consumption when the storage medium is not depleted and minimising the PM emissions while the system is in charging mode. The algorithm is to incorporate laboratory efficiency data for the main propulsion marine Diesel engine and for the auxiliary Diesel generator sets. Moreover, the sea trial and model test data for the thrust deduction factor, relative rotational efficiency and wake friction coefficient for the examined ships were inserted in the calculations and the simulation. In addition, detailed experimental efficiency curves for the selected battery type were used. Furthermore, for the electrical components, with the exception of the electric machine efficiency curve, static efficiency factors were used. Due to the fact that the latter proved to be of the most importance in terms of the feasibility of the

Hybrid Power system, a sensitivity analysis was performed and the results are discussed in detail.

## 1.3 Dry bulk sector

This study concentrates on the dry bulk sector as one of the major contributors to $CO_2$ emissions of international shipping and a key sector underpinning global seaborne trade. Between 1986 and 2006 average annual growth in the transport of coal and iron ore was greater than that in the transport of oil and oil products and outstripped global GDP growth (IMO, 2009). Within the dry bulk sector, the vessel types commonly used may be classified according to Table 1.1.

It may be noted that the design of Post-Panamax bulk carriers has significant similarities with liquid carrying tankers of a similar size (commonly referred to as Aframax tankers) and the conclusions are of relevance to this sector and directly applicable to this design. Aframax tankers account for approximately one third of all tankers (Lloyds Maritime Information Services, 2007). Moreover, the Post-Panamax vessel category is making itself apparent due to the new widened Panama Canal. However, due to this novel ship sub-category the question of their propulsive efficiency in off design conditions is a topic of discussion among the designers. For that particular reason, the hybrid layout presented in this thesis might be for up discussion with the ultimate aim of increasing propulsive efficiency by focusing on their propeller engine matching.

Table 1.1: Ship type description (Molland et al., 2012)

| **Bulk carrier type** | **Dimensions** | **Ship size (scantling)** |
|---|---|---|
| Small Overall ship length up to | approx 115 m | Up to 10,000 dwt |
| Handysize Scantling draught up to | approx 10 m | 10,000 – 35,000 dwt |
| Handymax Overall ship length | max 190 m | 35,000 – 55,000 dwt |
| Panamax<br>Ship breadth equal to<br>Overall ship length up to<br>Passing ship draught up to | 32.2 / 32.3 m<br>289.6 m<br>12.04 m | 60,000 – 80,000 dwt |
| Post Panamax (Small capes) | Breadth approx 43 - 45 m for 120,000 - 180,000 dwt | 80,000 – 120.000 dwt |
| Capesize | | 120– 200,000 dwt |
| VLBC – Very Large Bulk Carrier | $L_{OA}$ above 300 m | > 200,000 dwt |
| **Oil Tanker type** | **Dimensions** | **Ship size (scantling)** |
| Small Overall ship length up to | approx. 115 m | Up to 10,000 dwt |
| Handysize Scantling draught up to | approx. 10 m | 10,000 – 30,000 dwt |
| Handymax Overall ship length | max 180 m | 30000 – 50,000 dwt |
| Panamax<br>Ship breadth equal to<br>Overall ship length up to<br>Passing ship draught up to | max:<br>32.2 / 32.3 m<br>225 m (port facilities)<br>12.04 m | 60,000 – 75,000 dwt |
| Aframax | Breadth approx. 41 - 44 m | 80,000 – 120.000 dwt |
| Suezmax<br>Ship breadth equal to<br>Drought x Breadth<br>Overall Length up to<br>Ship draught up to | 70 m<br>Approx. 820 - 945 $m^2$<br>500m<br>21.3 m | 120,000 – 200,000 dwt |
| VLCC – Very Large Crude Carrier | $L_{OA}$ above 300 m | >250– 320,000 dwt |
| ULCC – Ultra Large Crude Carrier | $L_{OA}$ above 300 m | >320,000 dwt |
| **Containership type** | **Dimensions** | **Ship size (scantling)** |
| Small, overall ship length up to | approx. 115 m | Up to 1,000 Teu |
| Feeder, ship breath up to | approx. 23 m | 1,000 – 2,800 Teu |
| Panamax<br>Ship breadth equal to<br>Overall ship length up to<br>Overall ship length up to<br>(re canal lock chamber)<br>Passing ship draught up to | max:<br>32.2 / 32.3 m 225 m<br><br>294.1 m<br>12.04 m | 2,800– 5,100 Teu |
| Post-Panamax (existing), Breadth | Approx. 39.8–45.6m | 5,500 – 10,000 Teu |
| New Panamax<br>Breadth up to<br>Draught (TFW) up<br>Length OA up to | 48.8m<br>15.2m<br>365.8m | 12,000 – 14,500 Teu |

## 1.4 Layout of thesis

This thesis is divided into a total of seven chapters and four appendices. The second chapter outlines the state of the art work in ship Energy efficiency and attempts to classify the equivalent measures to hybrid system on the basis of installation cost, implementation effectiveness and operational simplicity. Furthermore, in accordance with the latest guidelines of the International Maritime Organisation (IMO), these measures are connected to the energy efficiency operational indicator (EEOI). The trade-off between the implied Nitrogen Oxides limits with the adoption of EEDI which targets fuel consumption is also discussed. This chapter also explains the formation of exhaust pollution of ships and correlations emissions with the Diesel Engine cycle. For that purpose, it also defines the scope of work for emission calculation, which outlines the globally adopted formulae and how these are implemented in this project. A comparison of the assumption of global emission inventories is made.

Chapter 3 explains in detail the investigated Hybrid power system layouts. The prime mover types, energy storage and miscellaneous electronic and electrical components suitable for the Hybrid system are outlined, compared and selected. Detailed explanation of component efficiency, their potential improvements in the near future and the basic assumptions are presented. Moreover, vessel energy demand and analysis of the operational profile is performed for a conceptual test case. For this case analytical calculations are undertaken in order to assess, constructional and financial feasibility of the Hybrid system.

Chapter 4 contains the mathematical modelling of every simulation block that was constructed, as well as a detailed presentation of the adopted mathematical implementation of the ECMS optimisation algorithm and of the pseudo multi-objective optimisation for PM, $NO_x$ and $CO_2$. This Chapter includes also a methodology example which starts from this Chapter covering the problem formulation and its mathematical representation and continues to Chapter 5 and 6.

Chapter 5 includes the library of simulation blocks that was constructed, as they are implemented in Matlab/ Simulink environment, based on the mathematical modelling of Chapter 4. Signal inputs and outputs are denoted, and the units that were used are presented for each block, along with explanation of how each block is connected to the rest. In this Chapter, the methodology example is continued and presents the procedure on how to select the suitable mathematical models and how to perform the required simulation.

Chapter 6 comprises test cases that were performed in order to assess the accuracy of the simulation block, and of results concerning the ship voyage simulator and the optimisation algorithm for the Hybrid Powerlayout. For demonstration purposes, the complete procedure of selecting the models, inserting the data and simulating the actual

voyage which then feeds the optimisation algorithm input is undertaken. Thus, the energy requirement calculations can be performed and a record of power load fluctuations on the examined voyages can be obtained. As a result, more propulsive and auxiliary power scenarios are investigated and based on these cases, an attempt to define the actual required sea margin is endeavoured.

In chapter 7, states the ocnclusions of the work including a discussion of their implications and likely areas for future investigation.

The thesis comprises of four Appendices. Appendix I presents a set of background mathematical formulations which support the mathematical models of Chapter 4. In addition mathematical models that were implemented but were not further used in the project are also given in this Appendix.

Appendix II contains tables of machinery equipment, vessel constructional data and tables of machinery layouts, which were used in order to assess the constructional feasibility of the Hybrid Power concepts.

Appendix III includes the regression analysis of the statistical data obtained from the examination of the daily performance reports. This analysis was performed for the sampled fleet in order to size the energy storage system for bulkers for each vessel size category.

Appendix IV includes the work undertaken for potential Nuclear Hybrid power concepts. This appendix includes assessment of reactor types suitable for marine applications, discussion on the constructional and social implications of Nuclear powered shipping. The goal of this work was to identify if a modular ship type is capable of operating in a liner ocean going voyage having increased energy storage capacity so the Nuclear reactor (pusher) can always remain in international waters. For this reason the ECMS strategy is applied so to minimize the nuclear fuel consumption. The analysis of the power requirements and the selection of suitable energy storage system are obtained from the Hybrid Diesel power layouts research. The auxiliary power data have been sampled during ship board energy audit of a conventional bulk carrier. Furthermore, data regarding the different types of bulkers have been used after analysing voyage reports. Finally, regarding the propulsion loads, the developed ship voyage simulator was used.

(Page left intentionally blank)

# 2 Shipping Emissions, Policy and Energy Efficiency

Fuel efficiency on board commercial vessels became the top priority after the first oil crisis in the 70s. However, rapid economic growth right up to the beginning of the global recession of 2007 led the ship industry to build deadweight (DWT) optimised vessels, disregarding the energy efficiency of the ships. In 2000, the IMO published the first greenhouse emission study, which correlates the effect of vessel operation with its environmental impact in terms of exhaust gas emissions. This issue is one of the most important documents in the international environmental agenda. In November 2003, the IMO adopted Resolution A.963(23) 'IMO Policies and practices related to the reduction of Ggreenhouse House Gas emissions from ships'. Furthermore, the IMO marine environmental protection comitee (MEPC) has developed a package of measures aimed at reducing the shipping sector's $CO_2$ emissions. Governments at IMO have also agreed on key principles for the development of regulations on $CO_2$ emissions from ships so that they will:

- effectively reduce $CO_2$ emissions;
- be binding and include all flag states;
- be cost effective;
- not distort competition;
- be based on sustainable development without restricting trade and growth;
- be goal-based and not prescribe particular methods;
- stimulate technical research and development in the entire maritime sector;
- take into account new technology; and
- be practical, transparent, free of fraud and easy to administer.

In 2007, the second greenhouse study updated the findings of the first study and introduced the discussion about Ship Energy Efficiency. The Ship Energy Efficiency management plan is mandatory for all vessels that are subject to MARPOL from January 2013. This means that the IMO takes the environmental impact of global shipping and fuel sustainability very seriously.

The energy used for the propulsion and auxiliary loads of each ship comes mainly from the combustion of fossil fuels. The exhaust gas emissions are carbon monoxide (CO), carbon dioxide ($CO_2$), sulphur oxides ($SO_x$), nitrogen oxides ($NO_x$), unburnt hydrocarbons ($H_xC_x$) and particulate matter (PM). These emissions have an environmental impact, since they are known to contribute to global warming, acid rain, eutrophication, and rising levels of ground level ozone, affecting both ecosystems and human health (Eyring et al., 2010).

This chapter is focusing on the problem of shipping emissions and how the industry up to this date tries to identify the formulation of exhaust gases, measure the quantity and effectively reduce it. The types of emissions are presented, the trade-offs between emission reduction and engine efficiency are discussed, the emission estimation methods are presented and their accurary is questioned. Regarding the trade off between Nitrogen oxides and Carbon dioxide, the trade off is analytacaly discussed as the energy efficiency desing index (EEDI) imposed by IMO and MARPOL Tier I – III limits make complex the emission reduction approach. Finally, in order to compare the Hybrid power layouts potential fuel savings, all the industry operational and technical measures are classified based on their type, cost, retrofit capability and their claimed savings.

## 2.1 Diesel engine operation

In the diesel engine combustion process, high pressured fine droplets of diesel fuel are mixed with air. The mixture is pressurised by the piston movement and the mixture spontaneously combusts. A typical turbocharged two-stroke marine Diesel engine with a normal stroke, controlled by a camshaft, requires 170 grams of fuel per produced kWh at optimum conditions; 7.8 kg of air is used as the combustion process requires large amounts of oxygen (21% in volume of air). In the combustion process, volatile carbon compounds react with oxygen, forming carbon dioxide, carbon monoxide and water, and simultaneously releasing a significant amount of thermal energy. Diesel engines are not a major source of Carbon monoxide. The exhaust gas contains approximately 0.5 kg of $CO_2$, 0.2kg of vaporized water and also 1.1kg of excess oxygen (Wright, 2000). Air is mostly (78%) nitrogen and thus a large amount of nitrogen is involved in the combustion process.

Although Nitrogen is an inert gas, under combustion temperatures, which can exceed to 2700 degrees Kelvin, it can connect with the Oxygen molecules. The term $NO_x$ usually consists of nitric oxide (NO) and nitrogen dioxide ($NO_2$), but could also consist of several other oxides of nitrogen, such as dinitrogen oxide ($N_2O$), dinitrogen tetrooxide ($N_2O_4$) and dinitrogen pentoxide ($N_2O_5$). In combustion, the amount of NO is normally dominates followed by a much smaller amount of $NO_2$. The other oxides of nitrogen normally occur in very small quantities. $NO_x$ is produced during combustion and can be divided into three formation types. These are the thermal $NO_x$ formation, which occurs during the combustion, the fuel $NO_x$ formation and, finally, the prompt $NO_x$ formation. Important factors that contribute to the thermal $NO_x$ formation are residence time, which describes how long time the combustion gas remains at the highest temperature, turbulence and the amount of excess oxygen. A uniform flame contributes to reduced formulation of thermal $NO_x$. The process is mainly governed by the following three

equations described as the extended Zeldovich mechanism. These are presented here below in the form of equilibrium reaction equations:

$$\begin{aligned} N_2 + O &\leftrightarrow NO + N \\ N + O_2 &\leftrightarrow NO + O \\ N + OH &\leftrightarrow NO + H \end{aligned} \tag{2.1.1}$$

The mechanism for the fuel $NO_x$ formation process is not fully understood yet. Prompt $NO_x$ formation is the last process describing the $NO_x$ formation. In this process, radical hydrocarbons are produced during the combustion of the fuel. These radicals quickly react with the nitrogen in the combustion air to form transition substances, which then oxidize to $NO_x$ when they react with the oxygen in the combustion air. The formation of NO depends on excess oxygen and high temperatures. Gas that burns before the time of peak cylinder pressure is particularly important. After the gas has burned, it is compressed to a higher pressure and temperature, and so reaches the highest temperature of any portion of the cylinder charge. Thus, the early part of combustion is important for $NO_x$; almost all $NO_x$ is formed in the first 20° of crank angle after the start of combustion. Dominating influences in the formation of $NO_x$ are temperature and oxygen concentration. According to measurements, the higher the temperature and the higher the residence time at high temperature in the cylinder, the greater the amount of thermal $NO_x$ that will be created. The dependence of $NO_x$ and temperature can be explained by the following equation (Heywood, 1988):

$$\frac{d[NO]}{dt} = \frac{6 \cdot 10^6}{\sqrt{T}} \cdot e^{\left(\frac{-69090}{T}\right)} \cdot \sqrt{[O_2]_e} \cdot [N_2]_e \tag{2.1.2}$$

Concerning $NO_x$ emissions, marine engine manufacturers strive to comply with the standards of MARPOL ANNEX VI at all loads using pre-combustion and combustion techniques and exhaust after-treatment (Kyrtatos, 2009). For that reason, a $NO_x$ cycle coefficient has been introduced and certain limits are already applied (MARPOL, 2005). Marine Diesel Engines however, have a significant efficiency problem at low loads, especially when in transient operation due to air supply mismatch (inefficiency of the Turbocharger which is not running near the surge line), and low mechanical efficiency, which decreases significantly by more than 4%. Furthermore, heat recapture is not performed as before, and significantly less heat is recovered.

Finally, after-treatment technologies, such as scrubbers and Exhaust Gas Recirculation, have minimum operational exhaust mass flow, which occurs at over 60% of the MCR. Exhaust gas re-circulation decreases the amount of oxygen that is supplied to

the cylinder. The operation of engines at a specific load permits the best match between turbocharger and EGR system. Furthermore, a two-stage turbocharger can be installed as the engine can have a higher compressed ratio, which can limit the range of pressure increase required from combustion, thus reducing latter's temperature and consequently $NO_x$ formation.

Based on a study by Corbett and Koehler (2003), it can be extracted that the total amount of $NO_x$ (tonnes) drops while the load is higher because the fuel efficiency increases. However, the combustion temperatures and pressures are higher, leading to higher specific $NO_x$ (g/kWh). However, this can be justified by the fact that external after-treatment is possible in higher loads and, in addition, higher thermal efficiency exists, causing a drop in the total emission of $NO_x$ in terms of kg per tonne of burnt fuel. In four-stroke engines, the behaviour of $NO_x$ is lower than the two-stroke due to the fact that combustion time (which is dependent on the engine RPM) is lower, and scavenging and injection timing are completely different as compared to slow speed engines, hence higher loads lead to higher $NO_x$, but lower than two-stroke Diesel Engines of the equivalent output (Woodyard, 2009).

$NO_x$ emission abatement targets three areas: fuel, charge air and combustion. Gas fuels have significantly lower $NO_x$ emissions and zero $SO_x$. High Cetane rating also reduces the ppm values along with emulsified fuels, which is homogenisation of clean water into the fuel oil, in the form of micronic particles of water dispersed throughout the fuel volume (Thomson, 1985). Charge air plays a significant role in the formation of $NO_x$ as cooler air keeps the maximum temperature lower after combustion occurs. However, cooling the air inlet entails the risk of vapour droplets. Charge air Temperature may lower $NO_x$ from 5-15% (Wright, 2000). Two techniques of introducing water are also examined. Air fumigation concerns the inlet manifold, and direct water injection is performed by injectors inside the cylinder. Both technologies aim to maintain the temperature at lower levels than the current developed ones (Chryssakis et al., 2010). The solution proved to have potential for future applications. However, an increase in specific fuel oil consumption (SFOC) arose. As seen in this paper, air fumigation is associated with a linear relation between NO decrease and SFOC increase. The Exhaust Gas recirculation system is a popular method to reduce $NO_x$. It is reported that a 50% reduction is achieved by using 5 -10% re-circulated and cooled exhaust gas, which lowers the overall availability of $O_2$ for combustion. Further details can be found in Wright (2000), Abd-Alla (2002), Hountalas et al. (2008) and Zheng et al. (2004). A typical representation of the $NO_x$ and SFOC trade-off is depicted in Figure 2.1.

The injection system, responsible for how the fuel is sprayed, has a contributing role in the formation of Nitrogen Oxides. Non-atomised fuel and non-uniform injection

leads to local high flame temperatures, which increase their formation. Research is performed in novel strategies for combustion (Andreadis et al., 2009). Another method is the 'Miller cycle' system, which reduced the temperature and the maximum pressure developed in the cylinder by supplying higher-pressure air at the inlet, something that requires the Turbocharger to have a high pressure ratio. The latter can only occur with two-stage turbocharger system.

Secondary control methods are applied after the heat recovery systems before the ambient exhaust, and convert the noxious components into a less polluting and hazardous waste stream. Selective catalytic reaction (SCR) and scrubbers are used. The SCR system injects urea instead of ammonia (which is toxic and flammable) under the right conditions (exhaust temperature) and in the presence of a suitable catalyst, in order to separate $NO_x$ and to convert to $N_2$ and water vapour (Amiridis et al., 1996; Andersson and Winnes, 2011).

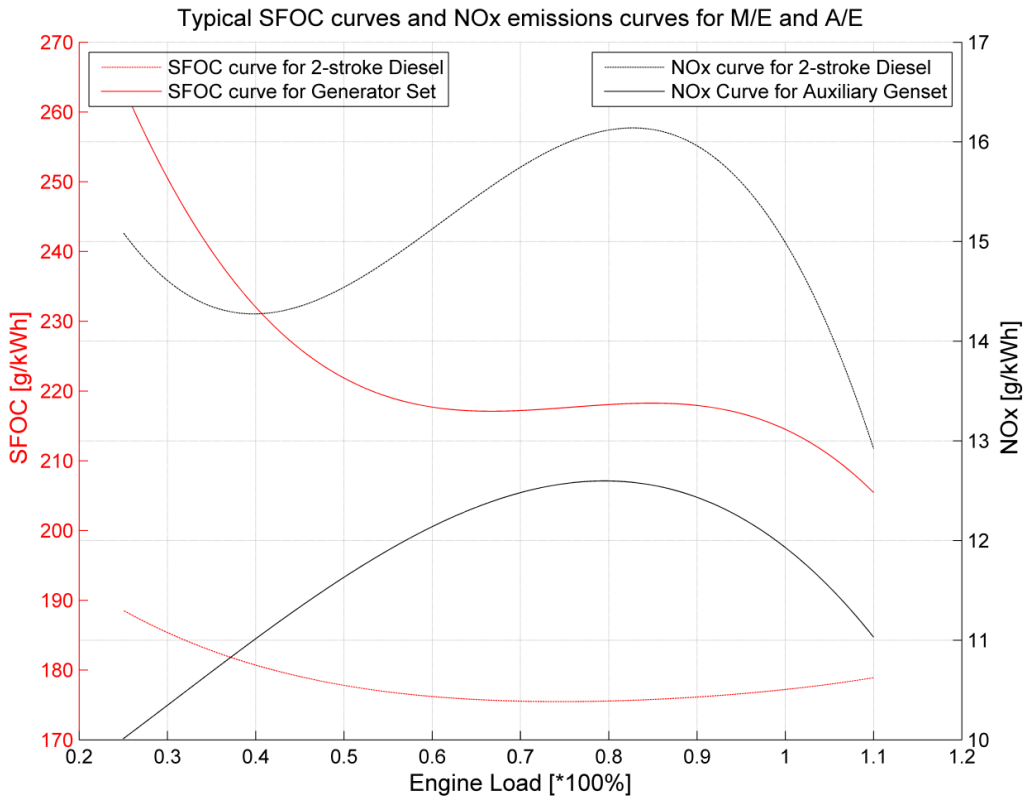


**Figure 2.1: Specific Fuel Oil Consumption curves and specific NOx curves for 2-stroke and 4-stroke Diesel engines, obtained from shop Trials**

In addition to the above, the Sulphur content of the fuel reacts with the excess of oxygen of the charge air, forming Sulphur Oxides. 95% of $SO_x$ are $SO_2$ and the remaining $SO_3$. $SO_x$ are directly related to the percentage of Sulphur in the fuel. Nonetheless, in order to achieve a drop in $SO_x$, high temperatures (high loads) are required, and the engine designer has to balance the $NO_x$ $SO_x$ trade-off.

Primary measures to reduce SOx are aimed at improving the quality of marine fuel. Currently low sulphur oil is to be introduced from 1st of January 2015 inside ECA zones which brings down $SO_x$ emissions to almost zero. From an operational point of view, higher temperatures, hence engine loading, reduces the production of $SO_x$ soot and smoke.

Due to engine lubrication, a percentage of the amount of cylinder oil is burned during combustion. The lubrication oil may contain heavy and alkaline metals, which are released in the exhaust gas. Unlike other emissions, which are chemically defined, particulate matter (PM) is defined by the international standard ISO 8178. PM with diameter less than 2.5μm from marine emissions is defined to include ash particles, organic compounds and elementary carbon (EC) and Sulphate and its associated water molecules. Fuel Sulphur content has been found to significantly affect the amount of PM emissions, because all of the Sulphate and its associated water molecules originate from the Sulphur content of the fuel.

A final source of hazardous emissions from Diesel engines is the unburnt Hydrocarbons, shoot and smoke. IMO has imposed no limits to these pollutant gass.

The formulation is caused by incomplete combustion due to bulk quenching of the flame, when combustion is especially slow. Such conditions are more likely to occur during engine transient loads when the air/fuel ratio ignition timing and fraction of exhaust gas recirculation (EGR, if applicable) for emission control may not be properly matched (Heywood, 1988). To remove the parameter of EGR system, in marine Diesel engines, bypass valves are installed and the system is not operational at low loads. Additionally, the unburnt Hydrocarbon emissions are likely to form due to the increasing cylinder pressure that forces some of the gas into crevices and narrow volumes that are connected to the combustion chambers (e.g. volumes between the piston rings and cylinder walls). As a result, the combustion flame cannot enter. Furthermore, before reaching the combustion chamber walls, the flame is extinguished and leaves sprayed fuel unburnt. The existence of a thin layer of cylinder oil remaining on the cylinder wall and/or the cylinder head can absorb and desorb hydrocarbon components of the fuel. This permits a fraction of the fuel to escape the combustion process unburnt. The work of Papalambrou et al. (2007) is aimed at the development of pulse turbocharging, the use of electric blowers in broad operational range and compressed air systems, which reduced the opacity of smoke significantly (80-85%). During transient loading, the development of control strategies has been investigated in Papalambrou and Kyrtatos (2009), in order to reduce smoke emissions. Concerning the unburnt hydrocarbons, it can be extracted that the operation of marine Diesel engines at low loads increases the PM and unburnt Hydrocarbon emissions, while the associated $NO_x$ in terms of g/kwh are low; the engine

fuel efficiency, however, is significantly lower, increasing the total engine emissions in terms of produced energy.

## 2.2 Methods for estimating ship emissions

Policy makers cannot be effective in reducing health problems caused by marine operation and traffic near coastal areas without sufficient information about the total fuel consumption amounts and geographical distribution of the emissions. Therefore emissions are estimated by means of several different models that produce information about the location, total emission amounts and pollutant sources. In recent studies of emissions from global shipping, there are two methods applied to determine greenhouse gas emissions. The first method relies on knowledge of marine fuel bunker sales in combination with a fuel-related emissions factor. In principle, this method should be accurate, but the absence of worldwide fuel sales data, along with unreliable estimates of the number of marine bunker fuel sales, makes its application problematic (Psaraftis and Kontovas, 2009). The second method is referred to as a 'bottom-up' or 'activity based' method and is often considered the more accurate in practice (Corbett and Koehler, 2003; Eyring, et al., 2010). A comparison of both methods is performed in the recent IMO (2009) greenhouse gas study, which indicates a difference of 30% between the two approaches, with the 'activity based' method being considered the more accurate. Endresen, et al. (2003) used an indirect bottom-up approach for emissions calculation. This activity-based approach calculates the engine power from data entered in the ship registry and the main ship characteristics, such as deadweight tonnage (DWT) and gross tonnage, and applies a statistical model for ship operation and fuel consumption. However, the absence of operational data and engine performance data introduce an uncertainty into the calculation (Corbett and Koehler, 2003). In determining emissions, it is possible to use either a 'power based emission factor' that relates emitted pollutant (g) to main engine power (kWh), or to use a 'fuel based emission factor' relating emitted pollutant (tonnes) to daily total fuel consumption (tonnes/day) (Corbett et al., 1999; Corbett and Koehler, 2003; Endresen et al., 2003, 2007; Eyring et al., 2005; Psaraftis and Kontovas, 2008).

Ship emission inventories have been introduced mainly for arctic regions where the shipping emissions pose direct threats to the marine environment, especially in terms of the PM and unburnt Hydrocarbons and their effect on the ice (Corbett et al., 1999, 2010; Paxian et al., 2010; Eyring et al., 2009). Various regional ship emission inventories have been introduced (Matthias et al., 2010; De Meyer et al., 2008) and evaluations have shown that the previously significant uncertainties in the estimated emissions of global ship traffic have decreased during the last decade (Paxian et al., 2010; Lack et al., 2008). Although there is no shortage of information concerning the global distribution of

emissions, there are currently very few statistics regarding the geographical distribution and chemical composition of emissions arising from ship traffic available. Moreover, chemical composition details have not generally been introduced to global bottom-up inventories of ship emissions.

Engine loading is crucial for estimating fuel consumption and thus emissions. . The curves depicted in Figure 2.1 suggest that total emissions, which are directly connected to the SFOC of the engine, are dependent on the loading. Any transient operation away from the minimum leads to an increased SFOC and, by extension, higher emissions in terms of g/kWh. Previous studies attempt to assume the engine loading and calculate the consumed fuel per voyage day indirectly, by multiplying SFOC, engine loading factor, the kW of the engine's MCR and the activity time (Corbett & Koehler, 2003; Endresen, et al., 2003). This loading factor is found using (IMO, 2009):

$$LF = \frac{\text{Actual Speed}}{\text{Max. Speed}} \tag{2.1.3}$$

In this study, the consumed fuel is reported and measured by the flow meters inside the engine rooms of each examined vessel. The measurement of the actual fuel consumption is performed by the crew. Three ways to measure fuel consumption exist. The first relies on the sounding of the fuel service tank and settling tank. Although the purifier system constantly feeds fuel the settling tank, if the quantities of the two tanks are measured with a time difference, the consumed fuel can be approximated. However, the actual breakdown of fuel consumption is unknown and only estimations e.g. Diesel generator consumption and auxiliary boiler consumption can be made. Nevertheless, in bulk carriers during at sea condition, economiser steam generation can serve the demand so boiler consumption equals zero, therefore only A/E consumption should be assumed. Consequently the first uncertainty factor is introduced. The second uncertainty factor is how the engineer on board takes the measurement. The instrument has a conical weight at the end that hits the bottom of the tank. If more tape is used and the weight trends to flatten on the bottom, this means less consumption, which results in negligible or serious errors (depending on the tank capacity). Finally, the vessel trim due to ship motions is difficult to read, thus differences in the interpolation tables will exist.

A second method relies on the gauge system which utilises compressed air to determine the quantity that exists inside the measured tank. This method is only for indication as the error percentage is high. The last method for fuel consumption is by flow meters. The measurement is accurate for each consumer (M/E, A/E and Boiler) but corrections should be applied. The temperature of the fuel has great influence on the actual fuel mass, so temperature reading before the flow meter should be obtained. Typically,

engineers obtain temperature measurement at the centrifugal separator or at the service tank. Therefore uncertainty factor is again introduced. Flow meters are also sensitive to the quality of the fuel and to the vessel trim. Based on measurements obtained during ship-board attendances, differences between flow meter reading and soundings that exceed 4% were observed. Nevertheless, during the sampling of the data, the fuel consumption between fuel meters and sounding converged with very small difference which was less than 1.4%. Thus, it is considered in this thesis that the fuel measurement is accurate enough. Any remaining differences can be explained by sea and air inlet temperatures that affect the performance of the engine (MAN Diesel, 2007) and the actual operation in non-laboratory environment, which leads to an increase in the actual fuel consumption of up to 8% of the initial, assuming the same fuel type is used.

An activity based approach is to be used later in this thesis using actual operational data for a fleet of dry bulk vessels, together with the 'noon reports' of engine performance and 'as measured' main engine fuel consumption, to calculate quantities of emissions. In determining emissions, it is possible to use either a 'power based emission factor' that relates emitted pollutant (g) to main engine power (kWh), or a 'fuel based emission factor' relating emitted pollutant (tonnes) to daily total fuel consumption (tonnes/day) (Psaraftis and Kontovas, 2008). These emissions factors are given in Table 2.1.

**Table 2.1: Emission factors for low speed engines (TIER I) (IMO, 2009; EMEP/CORINAIR, 2002) for 'at sea operation'. Static average power based factors and fuel based factors.**

| Pollutant type | Static average Power based factor [g/kWh] | Fuel based factor [tonnes/day] |
|---|---|---|
| $PM_{10}$ | 1.5 | - |
| $PM_{2.5}$ | 1.2 | - |
| DPM | 1.5 | - |
| $NO_x$ | 17 | 0.087 |
| $SO_x$ | 10.5 | 0.02*%Sulphur |
| CO | 1.4 | 0.0074 |
| HC | 0.6 | - |
| $CO_2$ | 620 | 3.114 |
| $N_2O$ | 0.031 | - |
| $CH_4$ | 0.006 | 0.0003 |

The second IMO Greenhouse Gas study (IMO, 2009) used fuel based emission factors, as each engine map is vessel specific. Where the operational data for the ship are known, it is possible to account for the fluctuations in loading of the main engine from day to day by using power based emissions factors for a broad range of loads. Although the key to the efficiency of the proposed Hybrid Power system is in accurately assessing the effects

of fluctuating engine loading in SFOC, limited access to engine pollution maps make it necessary to adopt a fuel based factor for $CO_2$ emissions as well as $NO_x$ emissions and $SO_x$, since the composition of fuel is known by the bunker analysis. A reasonable modern engine efficiency of 42% is used, without heat recovery, and judging from the correlation of SFOC and g/kWh of pollutant gas, it can be surmised that fuel based factors take into account engine efficiency and remain constant for 'at sea operation' and change at 'at berth' or 'in manoeuvring' conditions.

An attempt to measure the implied error and the uncertainty to the calculations by the use of a fuel based factor is presented in Table 2.2 for a modern two-stroke Diesel Engine. It can be extracted from this table that the fluctuation of error from the engine tuning point versus load is lower than 0.05%.

However, the fuel based factor for $CO_2$ for this engine is significantly different to the fuel based factor suggested by the literature and the IMO.

The means by which emissions were calculated for this study may be summarised as follows:

- $CO_2$ emissions depend on engine efficiency, which is directly related to SFOC. The higher the SFOC, the higher the $CO_2$ emissions. $CO_2$ is dependent on fuel composition. Marine Fuels are considered to have 86.2 – 86.7 % Carbon. Hence 3.114 tonne/tonne fuel is used as an emission factor, which is within the range of the study of Corbett & Koehler, (2003) and is adopted by the IMO (2009) for EEOI and EEDI approximation.
- $SO_x$ emissions depend on the fuel composition, which is known for each voyage, thus the total bunker consumption (in tonnes per day) is multiplied by the percentage of Sulphur times the emission factor.
- For $NO_x$ emissions, the IMO established propulsion engine standards for Ocean Going vessels (OGV), in Annex VI of MARPOL (2005). Engine manufacturers have built engines to comply with that standard. Hence the limit value of 17g/kWh is used for slow speed engines (MARPOL, 2005) which lead to a fuel based factor of 0.087 tonnes per day, which is empirical and adopted by EMEP/CORINAIR (2002).

Ageing of engines, poor maintenance and actual operation in non-ISO conditions result in a decrease of engine efficiency and an increase of the SFOC. Consequently the 'as measured' fuel consumption will still imply a degree of uncertainty for the $NO_x$ emissions, although the real engine is likely to emit more than what is assumed in this study.

**Table 2.2: Comparison and calculation of implied error of fuel based factors and power based factors for a Marine Diesel Engine of K98MC-C Tier II**

| Load | SFOC | Difference% | $CO_2$ | Fuel Factor | Difference % | $SO_x$ | | | $NO_x$ | | |
|---|---|---|---|---|---|---|---|---|---|---|---|
| 1.00 | 170.5 | 2.3 | 559 | 3.279 | 0.039 | 11.94 | 0.07003 | 0.059 | 13.5 | 0.079 | -10.264 |
| 0.90 | 168.4 | 1.1 | 552 | 3.278 | 0.018 | 11.79 | 0.07001 | 0.034 | 14.2 | 0.0843 | -4.434 |
| 0.80 | 167 | 0.2 | 547 | 3.275 | -0.057 | 11.69 | 0.07000 | 0.017 | 14.6 | 0.0874 | -0.918 |
| 0.75 | 166.7 | 0.1 | 546 | 3.275 | -0.060 | 11.67 | 0.07001 | 0.026 | 14.7 | 0.0882 | -0.060 |
| 0.70 | 166.6 | | 546 | 3.277 | | 11.66 | 0.06999 | | 14.7 | 0.0882 | |
| 0.65 | 167 | 0.2 | 547 | 3.275 | -0.057 | 11.69 | 0.07000 | 0.017 | 14.7 | 0.0880 | -0.240 |
| 0.60 | 167.8 | 0.7 | 550 | 3.278 | 0.012 | 11.75 | 0.07002 | 0.051 | 14.6 | 0.0870 | -1.391 |
| 0.55 | 168.8 | 1.3 | 553 | 3.276 | -0.038 | 11.82 | 0.07002 | 0.051 | 14.5 | 0.0859 | -2.646 |
| 0.50 | 170 | 2.0 | 557 | 3.276 | -0.026 | 11.9 | 0.07000 | 0.017 | 14.5 | 0.0853 | -3.333 |
| 0.45 | 171.4 | 2.9 | 562 | 3.279 | 0.0479 | 12 | 0.07001 | 0.034 | 14.4 | 0.0840 | -4.784 |
| 0.35 | 174.6 | 4.8 | 572 | 3.276 | -0.038 | 12.22 | 0.06999 | 0.001 | 14.4 | 0.0825 | -6.529 |

In order to evaluate the effectiveness with the static power based factor and the fuel based factor, a set of voyages in laden and ballast was evaluated using both types of factors. Table 2.3 describes the operational routes examined for this study.

Table 2.3: Examined set of voyages for emission factor evaluation

| Vessel | Departure port | Arrival port | Travelled distance | Quantity (MT) | Vessel condition |
|---|---|---|---|---|---|
| PPVSL 1 | Rio Grande | Marin | 5168 | 60600 | Laden |
| | Hong Kong | Tubarao | 9435 | 39063 | Ballast |
| PPVSL 2 | Tubarao | Amsterdam | 5045 | 80000 | Laden |
| | Port Talbot | Port Cartier | 2610 | 39060 | Ballast |
| PPVSL 3 | Dalrymple Bay | Taranto | 9535 | 89524 | Laden |
| | Luoyan | Dalrymple bay | 3906 | 39121 | Ballast |

Emission calculations are performed for each voyage and for every vessel. As an outcome, emissions per tonne mile can be calculated by dividing the emitted tonnes by the cargo capacity and travelled miles (Psaraftis and Kontovas, 2008). Figures 2.2, 2.3 and 2.4 show the gasses emitted during the voyages, and a comparison of emission studies and factors is performed.

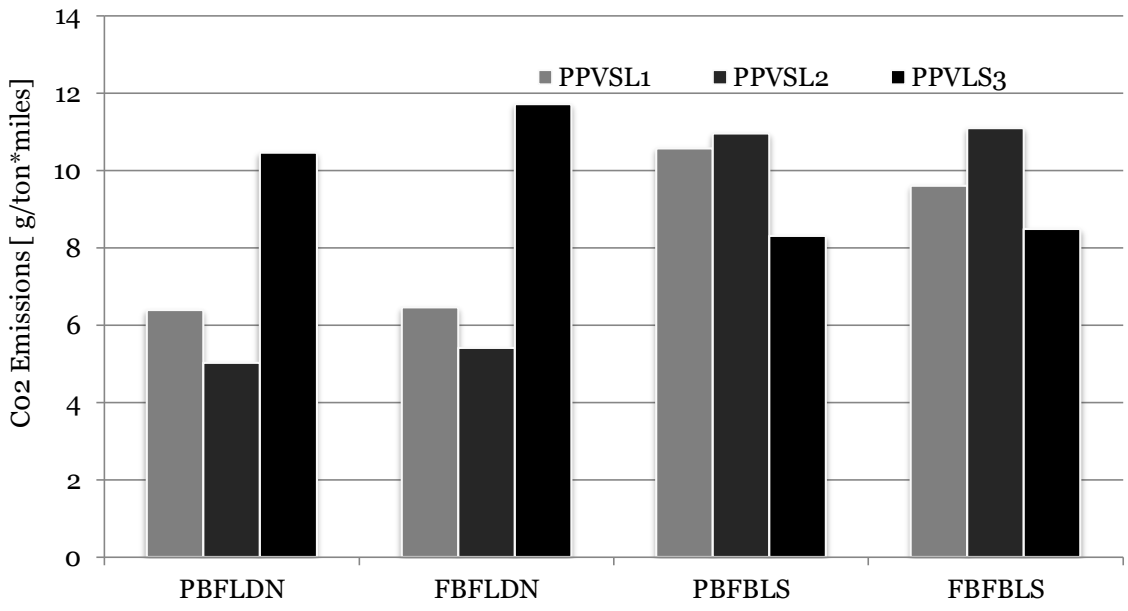


Figure 2.2: Comparison of 'Activity' method of power based factors (PBF) and fuel based factors (FBF) with LMT assumptions, for $CO_2$ emissions

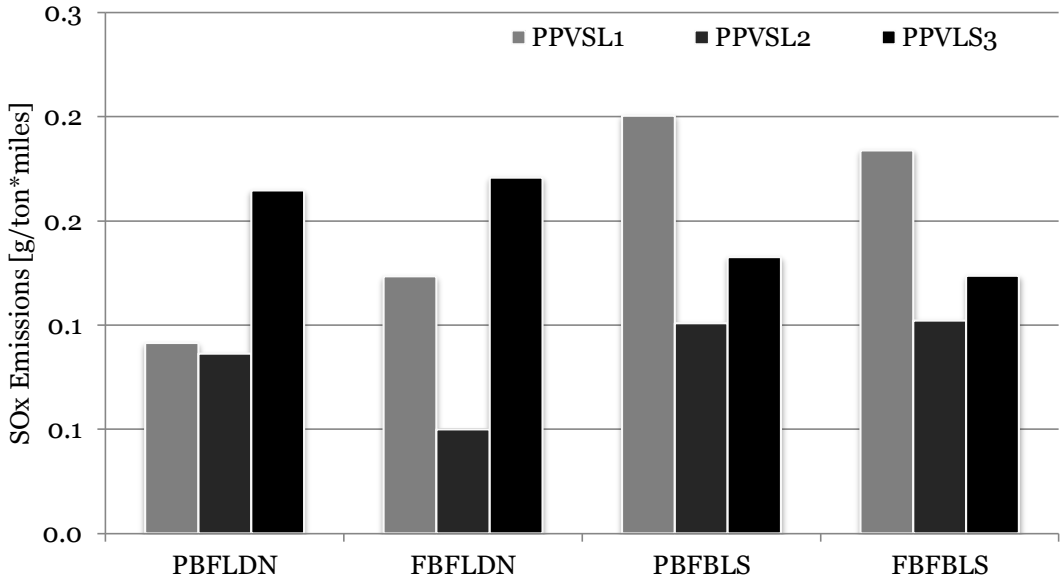


**Figure 2.3: Comparison of 'Activity' method of power based factors (PBF) and fuel based factors (FBF) with LMT assumptions, for $SO_x$ emissions**

The calculation of emissions showed differences between fuel based and power based emission factors. This deviation, along with the general assumption of ship operation, introduces uncertainty and, as can be seen in the comparison graphs, it overestimates emissions such as $CO_2$ and underestimates $NO_x$. However, in cases where daily reports do not exist, the rough assumptions of engine loading and vessel speed can represent voyage emissions with acceptable accuracy.

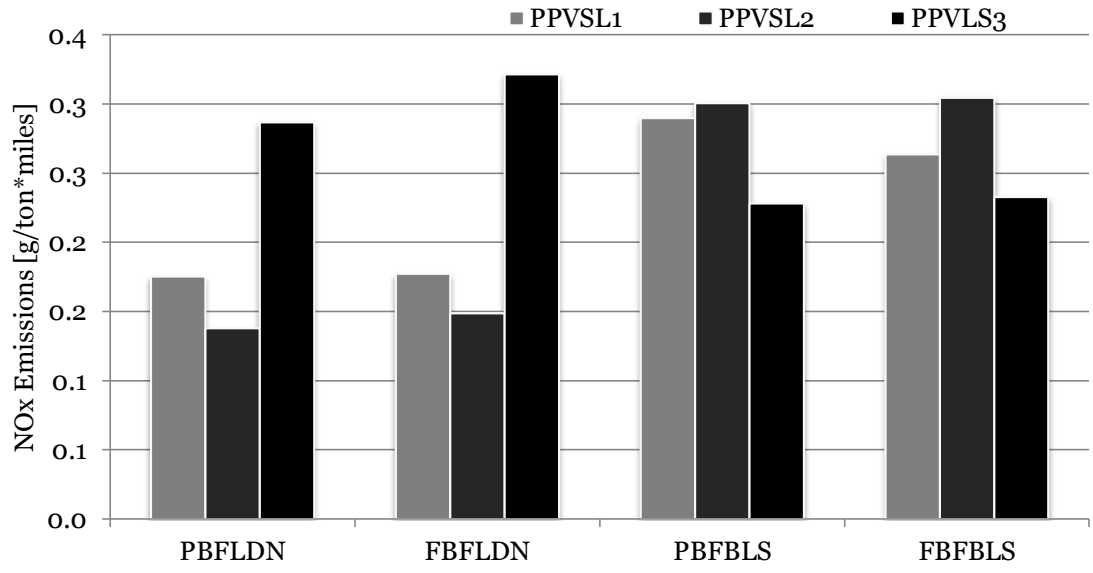


**Figure 2.4: Comparison of 'Activity' method of power based factors (PBF) and fuel based factors (FBF) with LMT assumptions, for $NO_x$ emissions**

IMO through the adoption of the MEPC62 and resolution 203 had officially linked shipping emissions with vessel energy efficiency. For this reason, the IMO adopted a set of formulae that attempt to estimate the vessels' environmental impact and in more detail, their carbon footprint. The latter formulae relate the installed power to the energy efficiency index, taking into account the auxiliary engines, the specific fuel consumption curves, the existence of heat recovery systems and push and pull systems that reduce the propulsive energy (e.g. kites, sails etc.) and innovative sustainable energy devices, such as wind turbines and photovoltaic systems. In addition, they consider the vessel's design speed and the Deadweight and correction factors for sea-vessel interaction and for Ice Class ships. However, many scientific objections have been raised during last 5 years IMO MEPC meetings with regards to the EEDI reduction, benchmarking, specific vessel types applicability, contribution factors of hydrodynamic energy saving devices and the reduction factors for large vessels and the and applicability dates. Nonetheless, problems arise when the emission policy and the measures to improve the EEDI are taken into account. The main problem identified in this formula is measrues in order to decrease the EEDI, and thus reduce the environmental impact, serious concerns raised for underpowered ships, with implications on safety and manoeuvrability, weather margin performance and easy solution to reduce speed instead of optimise the hull forms. In addition, the shipyards shift towards increasing the DWT, maintaining the same displacement and reducing the lightweight, which results in a potential decrease of the vessel's lifecycle, rasing concerns about the structural ability. During MEPC 62 meeting Greece opposed to Japan regarding the structural enchacements that proposed in order to tackle the structural concerns, convincing the committee that structural safety cannot be compromised.

The formula of EEDI is given by the equation (2.1.4). It can be identified from the formula (2.1.4) that the fuel type expressed with the coefficient $C_F$ inserts the emission factor into the EEDI formula. The rest combine the vessel's energy efficiency with the emissions at the design stage. This formula is due to be updated in order to take into account the Diesel Electric installations and the Hybrid Power systems.

$$EEDI = \frac{\left(\prod_{j=1}^{m} f_{ci}\right)\cdot\left(\sum_{i=1}^{nM/E} C_{F_{M/E}}\cdot SFOC_{M/E}\cdot P_{M/E}\right) + P_{A/E}\cdot C_{F_{A/E}}\cdot SFOC_{A/E} + \left(\sum_{i=1}^{nM/E} P_{PTI} - \sum_{i=1}^{nWHR} P_{WHR}\right)\cdot C_{F_{A/E}}\cdot SFOC_{A/E} - \left(\sum_{i=1}^{reff} f_{eff}\cdot P_{eff}\cdot C_{F_{M/E}}\cdot SFOC_{M/E}\right)}{f_j\cdot DWT\cdot V_{ref}\cdot f_w} \quad (2.1.4)$$

where,

$f_{ci}$ : Correction factor to account ship specific design elements [-]

$C_{F\,M/E}$ : M/E fuel carbon content [-]

$SFOC_{M/E}$: M/E specific fuel oil consumption [g/kWh]

$P_{M/E}$ : M/E power output [kW]

$C_{F\,A/E}$ : A/E fuel carbon content [-]

$SFOC_{A/E}$ : A/E specific fuel oil consumption [g/kWh]

$P_{A/E}$ : A/E power output [kW]

$P_{PTI}$ : Power take off (PTI) power output [kW]

$P_{WHR}$ : Waste heat recovery (WHR) equivalent power output [kW]

DWT : Vessels deadweight [tonnes]

$f_{eff}$ : Availability factor of innovative energy saving technology [-]

$P_{eff}$ : 75% of the M/E power reduction due to application of innovative technology [kW]

$V_{ref}$ : Vessel desing/ reference speed [knots]

$f_w$ : Non-dimentional coefficient indicating decrease due to environmental condtions [-]

$f_j$ : Capacity factor for any technical/regulatory limitation on capacity [-]

Unfortunately, the modern regulations regarding the Nitrogen Oxides, insert a penalty parameter to the EEDI calculation. In terms of grammes of specific pollutant per kWh, a trade-off between $NO_x$ and SFOC exists. The first marine slow speed Diesel engines meeting Tier II requirements ($NO_x$ less than 14.4g/kwh) in order to reduce the amount of these oxides, decreased the combustion pressure. This method directly affected the engine fuel efficiency and thus, the SFOC increased by up to 6g/kWh for camshaft controlled engines and by 4g/kWh for the electronically controlled engines (MAN Diesel, 2009b). The observed difference between the electronic and camshaft engines is explained by the existence of better control of valve timing, injection parameters (rate shaping) and finally due to design improvements as the electronic engines are newer compared to the camshaft ones. Nonetheless, in order to meet the nitrogen oxides limits, modifications on the combustion process are implemented. The introduction of lower combustion temperatures despite the $NO_x$ reduction, the SFOC is increased. In addition, a very promising technology of exhaust gas recirculation (EGR) which reduces the oxygen content inside the cylinder during scavenging process also reduces fuel efficiency. Furthermore, the application of two-stage turbocharging inserts a fuel penalty which is less than the previous depicted values and is considered as a very promising technology as well. In addition, the water in fuel technology (WIF) may increase SFOC (in TIER II engines) by up to 5% at the 75%

engine load (MAN Diesel, 2009b). The latter operational point is directly related to the EEDI calculation and has the largest contribution to the estimation of $NO_x$ of E3 cycle type (Propeller law operated Main or Auxiliary engines). This relationship is found in MARPOL Annex VI can be seen in equation (2.1.5).

$$E_3 = 0.2 \cdot SNO_{X\,100\%} + 0.5 \cdot SNO_{X\,75\%} + 0.15 \cdot SNO_{X\,50\%} + 0.15 \cdot SNO_{X\,25\%} \qquad (2.1.5)$$

It is evident from equation (2.1.5) that the weighting factor of $NO_x$ cycle is large at the 75% of the MCR. Thus, the technologies to reduce $NO_X$ primarily target this point. However, to increase the SFOC there in order to reduce $NO_x$ increase the EEDI and vice versa (MAN Diesel, 2009a: 2009b). During the research performed to meet Tier II requirements, multiple engine component variations have been implemented which resulted in lower SFOC in part or low load operation than the initial reported values (IMarEST, 2011; MAN Diesel, 2009a). Although, the reduced SFOC in these loads has increased the specific $NO_x$ emissions, the engine $NO_x$ cycle remains below the limit due to the weighted relationship of equation (2.1.5). The designers now decide which load to penalties and is always the ones which are considered outside the main operational envelope of the engine (IMarEST, 2011).

There are further implications when Diesel engines need to meet Tier III requirements in ECA zones. Currently, the dominant technologies to meet Tier III is by applying external means such as excessive heat recovery (gaining electrical energy from turbo-generators using the exhaust heat) and using EGR. The last method further reduces the fuel efficiency by approximately 3g/kWh, something that affects the EEDI for vessels constructed to sail only in ECA zones. On the other hand, MAN Diesel which was the first engine manufacturer that announced Tier III compliance claims that this particular engine having part load optimisation and under Tier II compliance, is more energy efficient during transoceanic crossings. This occurs because the engine is capable of switching from low emission running to fuel efficient operation when sailing outside the areas governed by Tier III regulations. Thus, the fuel efficiency is achieved only by a technicality and not by actual fuel efficiency meeting Tier III limits.

The EEDI is only dependent on the value of SFOC at 75% (which is depicted on the International Air Pollution Prevention (IAPP) certificate). For the remaining operational time of the vessel, the Energy Efficiency Operation Index (EEOI) formula is proposed. This simple formula accounts only for the vessel's total fuel consumption (M/E, A/E and auxiliary boilers), the steamed miles and the on-board cargo. It is calculated for round trips only, since in ballast condition no cargo is present, leading to infinite results.

$$EEOI = \frac{\sum_{i=1}^{n} C_{F_i} \cdot W_{Fuel_i}}{\sum_{i=1}^{m} W_{\text{cargo}_i} \cdot D_i} \tag{2.1.6}$$

This formula does not take into account the lower calorific value of the fuel, which has a significant impact on fuel consumption. For that reason it is proposed to re-calculate the formula as follows:

$$EEOI' = \frac{\sum_{i}^{n}\sum_{j}^{m}\left(\text{CR}_{\text{LCVF}_j} \cdot C_{F_{i,j}} \cdot W_{Fuel_{i,j}}\right)}{\sum_{i=1}^{m} W_{\text{cargo}_i} \cdot D_i} \tag{2.1.7}$$

Although Hybrid ships are currently excluded from the calculation of EEDI, the EEOI formula is applicable to every ship that is subject to the MARPOL convention. Thus, a SFOC curve that best fits the operational envelope and is optimised for the majority of the operational time, reduces significantly the EEOI. In addition, the Hybrid Power system, which reduces the total fuel consumption either in propulsion or auxiliary systems, improves the operational environmental impact of the vessel. This is crucial in terms of future vessel sustainability, as policy makers are very close to reaching an agreement on taxation and establishing an emission trading scheme. Consequently, in order to improve the total energy efficiency and assess the Hybrid potential in terms of application restrictions, installation cost and ease of implementation, a global identification and classification of up to date energy efficiency measures should be made.

## 2.3 Improving the energy efficiency of the vessels

The term 'system efficiency' refers to the ability of the energy system to have its output as close as possible to its input, minimising the losses. For the vessel, the energy efficiency targets the propulsion system, whose input is the fuel (whether it is petroleum or LNG) and its output the propulsive power (thrust) and electricity for auxiliary loads. Energy efficiency is making the best possible use of the energy expended to obtain the maximum work done in order to achieve fuel savings. Energy efficiency increases either when the energy input is reduced for a given level of service, or when services are increased and enhanced for a given amount of energy input. Proposed ways of increasing fuel efficiency can be broken down into four categories, depending on their targeting area, as follows: Thus,

- Improving vessel operations
- Improving the ship's total resistance
- Improving propulsion (hydrodynamic side)
- Improving power generation and on-board consumption

With the aim of enhancing ship energy efficiency, the baseline vessel has to be defined. The baseline vessel is an ideal vessel, which is hydro-dynamically highly optimised, the coupling of propeller and engine is ideal, and the superstructure design secures minimum air-drag. This explains the fact that many energy saving devices have valid savings for initially bad designs, where the aforementioned hydrodynamic vessels never can reach the claims made about them (VLCC workgroup, 2009). In terms of machinery efficiency, the vessel is equipped with state of the art technologies, and external abatement techniques for $NO_x$ and $SO_x$ reduction are installed. The energy saving devices that will be presented below do not increase the baseline vessel dramatically. Nevertheless, as it was stated earlier, modern vessels are DWT optimised and their reference line is well below the baseline vessel. As a result, the saving potentials should not be summed up and, of course, the outcome will not lead to an energy independent ship. In order to improve energy efficiency resulting in the reduction of the power requirement, two categories of measures/practices have been identified.

Operational practices target ship operations and management. These practices aim to improve the energy efficiency with zero investment cost. Their implementation ranges from easy adoption to very hard/impossible implementation by the crew or impossible for the examined ship type due to constraint parameters, such as the ship safety, operational restrictions by ports and/or charterers, etc.

Technical measures target vessel retrofitting and installation of energy saving devices. This category includes the hydrodynamic improvement devices and machinery optimisation and retrofitting. Usually, these practices have a notable cost and their selection should be made in accordance with a detailed financial calculation. The implementation period is during dry-docking, and the crew's working environment and procedures after the implementation of these measures is not significantly affected.

In order to evaluate the effectiveness of the adopted measures and practices, performance monitoring tools should be installed on-board. Performance monitoring is usually executed by specific electronic software and hardware sensors. The results are transmitted to the managing company for evaluation. In the event that there are indications of vessel performance deterioration, the company can take immediate action within a very short response time, thus ensuring that energy efficiency would remain high.

## 2.4 Operational and port methods to reduce emissions

'Slow steaming' is a term used to describe the method of decreasing the average vessel sailing speed. The range of operational speeds is determined by the charterers and is related to the shipping business. When speed is reduced, engine loading decreases by a cubic relationship, thus the total amount of fuel burnt is significantly lower. However, in terms of specific fuel oil consumption, slow steaming reduces fuel efficiency. Moreover, carbon emissions are connected to fuel consumption only. Hence, carbon emissions are a new parameter in the shipping transportation system. Corbett et al. (2009) and Cariou (2011) have demonstrated that slow steaming is applicable to container vessels that are high-speed ships and hence the installed power is high. They have shown that, although it may require more ships (Psaraftis and Kontovas, 2009; 2010), slow steaming in containerships has so far led to an 11% decrease of $CO_2$ emissions.

Pollution in ocean going ships is important, however, significant pollution occurs in high traffic ports. In-port emissions make up a small percentage of the overall emissions from shipping (Whall et al., 2002; Dalsøren et al., 2009); ports attract shipping traffic and inevitably constitute points of concentrated ship exhaust emissions. The unified port of San Diego in the United States has employed Starcrest Consulting (2006) to apply a bottom-up approach to estimate emissions from all port operations. Furthermore, Tzannatos (2010) underlines the importance of Piraeus' harbour shipping operations in emission percentages, which significantly downgrade the air quality around the harbour and affect human health. Furthermore, the impact of Los Angeles port on air quality is discussed in Ault et al. (2009). The examined studies conclude that emission factors are not accurate for in-port emission estimation, and detailed pollution engine maps are

required. Nevertheless, the total amount of local $CO_2$, $NO_x$, $SO_x$ and particulate matter emissions is noteworthy and cannot be excluded from emission inventories.

Following the importance of local ship emissions, technology considerations and available ways to plug ships with shore power, a method commonly known as 'cold ironing', are presented in Khersonsky et al. (2007). This feature makes it possible to cease utilising generator engines that burn fuel inside the harbours, making the ship operation carbon free. However, Hall (2010) demonstrated that shore power leads to a decrease in emissions only when electricity from the grid is produced and transferred more efficiently than the power that ships can generate themselves. However, in terms of local emissions in every port, significant reductions are possible.

Weather Routing is the optimisation of a ship's course and speed that may reduce the average added resistance in seaways. IMO (2009) state that fuel savings can be as high as 5%. However, some experts estimate the saving potential to lower than 1% for more realistic scenarios. Weather routing should be combined with the tactic of slow steaming or optimised voyage control, and just in time arrival (JIT). Optimum voyage control refers to the optimum route, and improved efficiency can be achieved through the careful planning and execution of the voyages, reducing the total voyage miles, hence fuel consumption. JIT is a voluntary speed reduction upon agreement with the charterers to reduce speed and thus the total fuel consumption, because of known delays at the next port. This approach increases the time spent in laden or ballast and reduces the time spent in anchorage or alongside.

Based on hydrodynamic performance, the trim is a significant parameter in a vessel's fuel consumption. IMO (2009) INTERTANKO and INTERCARGO underline the importance of the trim and encourage crew performing trials in order to identify the trim that leads to the lowest fuel consumption under specific weather conditions.

Pumps and fans should be operated according the electric load analysis provided by the Yard. The crew should use port cooling pumps at port or anchorage, when available. This minimises the fuel consumption of auxiliaries. Cooling/ventilation systems are not always under full load/RPM. Installation of a speed/power control unit for engine room pumps and fans will conserve electrical energy demand, where pumps are not required to operate at their full-speed rating.

The cargo/voyage-specific heating requirements and the Charterer/Cargo Receiver requirements should be taken into account when carrying crude oil. Excessive use of auxiliary boilers leads to significant fuel costs, and managing companies have established that optimised cargo heating may reduce Auxiliary Boiler consumption by up to 20%. In addition to the above, it is proposed to perform optimum lighting management and to promote smart lighting controllers, by turning off all unnecessary lights. Moreover,

it is also advisable to adopt a sequential method in ballast water exchange, which is more energy efficient, since it requires ballast pumps to operate for a shorter time, if no restrictions apply.

## 2.5 Technical measures to reduce emissions

### 2.5.1 Rudder modifications

The goal of the application of energy saving devices in rudders is to increase the energy recovery ratio from the propeller losses, since the rudder is located downstream of the propeller. There are three main sources of propeller losses: frictional, axial and rotational. Hollenbach and Friesch (2007) claim that twisted rudder with a costa bulb may lead to 4% lower consumption. High efficiency rudders combine various approaches to save fuel. Rudder surf bulb is a combination of thrust fins and costa bulb, which improves the flow to the rudder (Beek, 2004; Lehman, 2007), and the fins are designed to generate thrust in the rotating propeller slipstream. Moreover, rotational losses are recovered. Rudder Surf Fins is a simpler system developed on the same principle as the rudder surf bulb. It consists only of transversal fins installed on the rudder, which recovers energy lost due to the propeller rotation. Both x-shaped thrust configurations and configurations with only two blades have been proposed. Full hull forms are expected to benefit more from such fins than slender vessels. IMO (2009) reports savings up to 9%.

### 2.5.2 Improvement of propeller up flow and down flow

A propeller generates vortices from its hub, which reduce its efficiency, and is prone to cavitation. The magnitude of these vortices will depend on the blade radial loading distribution, and on the size and design of the hub. Vortices from the hub tend to be steadier than those generated from the propeller tips, and consequently have an influence at the higher frequency range, rather than direct harmonics of the blade rate frequency. PBCF (Propeller Boss Cap Fins) developed in Japan and composed of small fins attached to a propeller boss cap, were proposed as a novel energy saving device (Gearhard and McBride, 1989; ITTC, 1999). Currently more than 130 PBCF's are attached to full-scale propellers and have, to date, demonstrated energy savings reaching up to 4% (Ouchi et al, 1989, 1992). A similar system to the PBCF is the Hub Vortex Vane (HVV. The HVV is a small vane propeller fixed to the tip of a cone-shaped boss cap. It may have more blades than the propeller (Schulze, 1995). Vendors claim increases of up to 3% in propeller efficiency but, according to Junglewitz (1996), reported gains are highly doubtful. The purpose of these devices is generally to improve the hydrodynamic flow before the propeller. The main application is to reduce the swirl resistance of the hull form, hence

reducing the viscous pressure resistance. Devices aiming to fix the flow to the propeller are the Sanoyas Tandem Fins, the IHI low Viscous Resistance Fins, the Grotheus Spoilers, the Oshima Wake Acceleration Fin and the Namura flow Control Fin. Although these vortex generators have been employed to fix design flaws leading to vibration, it is expected that they increase fuel consumption rather than lead to any fuel savings.

The purpose of the Pre-swirl Stator system is to produce a swirling flow opposed to the direction of rotation of the propeller, thereby annulling the swirl induced by the propeller and, at the same time, increasing the relative tangential velocity of the propeller blades. Thus, propulsive efficiency is increased and the cavitation of the propeller is reduced (Linjenberg, 2006).

The Mewis Duct is a novel power saving device which has been developed for slower ships with full form hull shape, that allows either a significant fuel saving at a given speed or alternatively for the vessel to travel faster for a given power level. The duct diameter is smaller than the propeller diameter and the fins chord length only covers part of the duct's length. The MD combines the effects of a wake equalizing duct and pre-swirl fins within a single unit. By pre-correcting the flow into the propeller, the device essentially reduces the rotational losses and increases the flow velocity towards the inner radii of the propeller (Hollenbach and Reinholz, 2011). The pre swirl is claimed to reduce rotational losses and also to contribute to a reduction of energy loss due to generation of hub vorticity. The achievable power savings from the Mewis Duct are strongly dependent on the propeller thrust loading, ranging from 3% for small multi-purpose ships to up to 9% for large tankers and bulk carriers. HSVA denotes that the power saving is about 6.0% at 16 knots sailing speed, which corresponds to a speed increase of 0.27 knots (Hollenbach and Reinholz, 2011). Ouchi (1989) states that the power saving is virtually independent of ship draught and speed. The Mewis Duct is ideally suited to both new-builds and retrofit applications. There are two types of duct that are applicable to marine propellers. The first type is called accelerating Duct and the second decelerating. The proprietary brand of accelerating propeller is the Kort nozzle. Attention should be paid to the fact that the efficiency of ducted propellers when free-running and lightly loaded tends to be less than that of a non-ducted propeller, because of the additional shrouding which adds drag, resulting in the Kort nozzles losing their advantage at around 10 knots. Ducted propellers have been around for many decades and very few ships, mainly tankers, were fitted in the 1970s. The practice was abandoned reportedly due to problems with vibration and cavitation. According to IMO (2009), potential savings can be as high as 20%.

The wake behind single-screw ships is non-homogenous (i.e. there are very low velocities at the top of the propeller disc). This induces pressure fluctuations on the propeller and the ship hull above the propeller, which in turn excite vibrations. The magnitude of these

vibrations poses more or less restrictive constraints on the propeller design. It is assumed that improving the homogeneity of the wake will improve propulsion efficiency (the results mainly affect open water propeller efficiency). Optimising the angle of the partial duct to the stern under load conditions is said to improve the homogeneity of the wake. Wake equalising devices, such as Schneeklith nozzles (or Wake Equalising Ducts (WED)) (Schneekluth, 1986; Schneekluth and Bertram, 1998), the Sumitomo integrated Lammeren Duct (SILD) or the Hitachi Zosen Nozzle, may improve propulsion. Nonetheless, independent analyses result in contradicting evaluations of the effectiveness of WEDs (Celik (2007; ITTC, 1999).

The above technologies may increase propeller performance, leading to higher fuel efficiency because of the reduction in required torque. Reduction in friction resistance, by means of advanced painting or regular cleaning, or by using novel systems, such as air lubrication, should also be considered. In addition, wave added resistance plays a significant part in bad weather, or when sailing at high speeds.

### 2.5.3 Minimisation of ship total resistance

Coatings may effectively reduce frictional resistance. Silicon based antifouling is a new generation of paints that employ a Foul Release mechanism. 'Foul release' is the name given to the technology that does not use biocides to control fouling, but provides an ultra-smooth, slippery, low friction, hydrophobic or hydrophobic/hydrophilic combination surface, onto which fouling organisms have difficulty in settling. The available Foul Release products contain no added biocides and are based on silicone/fluoro-polymer technology. Some publications claim improvements in excess of 10%. However, this is partially true after dry-docking. Over longer periods, this notable effect fades out.

Routine in-service polishing of the propeller reduces its surface roughness caused by organic growth and fouling. There is evidence that the effects of a poorly maintained propeller can decrease speed and fuel efficiency by up to 3% compared to that of a propeller maintaining an 'A' finish on the Rupert Scale.

Hull cleaning should be carried out on a condition assessment basis, as the increased roughness significantly increases the friction resistance. Therefore, in conjunction with every propeller polishing, the hull should be inspected for damage and marine growth. If there is significant growth on the hull, an immediate decision to clean the hull could be made by the Company, taking into account the report/notification by the Master.

The main components of ship resistance consist of resistance due to wave drag, pressure drag, and frictional drag. A promising alternative technique to obtain lower frictional resistance is to use air as a lubricant in order to reduce the wetted surface of the ship. Three

distinct approaches are identified: the injection of bubbles, air films, and air cavity ships (Foeth et al., 2008; Ceccio, 2010).

Hirota et al. (2004), based on model test results, state that the sharpness of the bow shape above the calm waterline could reduce added resistance. With a blunter bow shape, such as that of tankers or bulk carriers, waves are mostly reflected forward and so the resistance increases. The increase in wave resistance acting on such full-form ships with a blunt bow is therefore larger than that on slender ships. For blunt-bow shaped full-form ships with a smaller power engine, the speed loss is estimated to be larger than that for ships with a conventional high power engine. To improve the performance in waves for ships with a low power engine, the resistance increase in waves needs to be reduced. To achieve this, the bow should be made less blunt. Results of a study on the effect of bow bluntness on the resistance increase indicated that the most effective way was to sharpen the bow shape above the still water level, where the wave surface is elevated and reflected. By sharpening this part, the incident wave is reflected mostly to the side, not forwards, thus reducing the wave resistance acting backward. Ax-Bow design may reduce the resistance increase in waves by 20% to 30% in almost the entire range of wavelength. This enables a 4 to 6% reduction of horsepower, or fuel consumption, in the case of sea conditions corresponding to a 20% sea margin. This new bow shape has been applied to ships already and, according to NKK (2002), trials showed that the Ax-bow indeed leads to reduced speed loss in waves.

Wind assisted concepts predominantly use other means of power (typically Diesel Engines), and wind power plays a secondary role to the propulsion. Generally, these systems may be attractive for slow speed vessels (< 15 knots). For modem vessels, the only viable solution for wind assisted propulsion is for fully automated systems. Moreover, additional structural effort for mast support on the ships with sails can be considerable. Kites and Flettner rotors are generally more efficient than sails per surface area. Optimum solutions depend on the operational profile of the vessel and the type of vessel. Schenzle (2010) analysed various advanced sail-assistance options for a Panamax Bulk Carrier.

### 2.5.4 Improvements in the propulsion machinery

De-rating is one of the available options to reduce the specific fuel oil consumption of Diesel engines. It is also known as 'economy' rating. This means that the operation of the engines takes advantage of the maximum cylinder pressure for the design continuous service rating (CSR), while the mean effective pressure and shaft speed is lower, at an operational point lower of the propeller normal operating curve. Fuel efficiency is improved when the ratio of Mean Effective pressure and the maximum pressure is increased (Woodyard, 2009). In combination with de-rating and in order to uncouple the injectors and the valve timing with the rotational speed of the engine through a camshaft (camshaft controlled engines), the installation of electronically controlled M/E is proposed. The main purpose of switching to electronic control is to ensure fuel injection timing and rate, as well as exhaust valve timing and operation, exactly when and as desired according to the engine load. As a result, fuel injection, exhaust valve actuating and starting air systems are controlled electronically and are optimised for all operation loads. NOx emission can be reduced and smokeless operation can be achieved (Woodyard, 2009).

Although the operation of the engine can be controlled either by the camshaft or by electronic control systems, the engine speed is crucial in terms of fuel efficiency. Nowadays it is proposed to install an electronic governor instead of its mechanical counterpart. The purpose of the governor is to regulate the amount of fuel supplied to the cylinders so that a predetermined engine speed will be maintained despite variations in load. Based on ship-board measurements for the purpose of this study, it was found that fuel savings can be as high as 9% per day in laden condition and 7.5% per day in ballast condition.

Despite the efforts to improve fuel efficiency at low loads using electronic control, more radical solutions are needed, especially when vessels are designed to operate at full load, but the volatile state of the market has forced the shipping companies to operate the vessels at very low loads. The Turbocharger Cut-out system is designed to lower the fuel oil consumption and improve the main engine performance during part-load operation by isolating one, two or three turbochargers, depending on the total number installed.

Another measure to increase the fuel efficiency of a Marine Diesel engine in low loads is the introduction of the Cylinder cut-out system. The cylinder cut-out system should be used at RPM below 40% of MCR RPM, allowing the engine to operate with only half of the cylinders, resulting in increased load on the operating cylinders with improved operating conditions for the fuel system. As a result, it ensures stable running conditions down to 20-25% of the nominal RPM.

A potential solution to reduce PM and $NO_x$ emissions are slide fuel valves. The latter have also shown significant savings, lower emissions and lower fuel consumption. The slide fuel valves both optimise the combustion of the fuel and ensure a cleaner engine. The spray pattern of the fuel is further optimised and therefore leads to an improved combustion process (Woodyard, 2009).

However, not every measure can be retrofitted to the existing vessels, nor be applied in combination with others. The following Table 2.4 presents the compatibility of each hydrodynamic device with each other for potential combination of these technologies (Carlton, 2008).

**Table 2.4: Compatibility of hydrodynamic devices amended from Carlton (2008) and based on previous work by the author performed during training for new-building projects in shipping company**

| Compatibility of Technologies C- Fully Compatible N - No compatibility PC- Partly Compatible | Mewis Duct | Propeller Boss Cap | Pre Swirl Stator | Propeller Nozzle | Contra Rotating | Propeller Rudder | Rudder Profile | Wake Equalising | Propellers with | Grim van wheel | Rudder bulb fins | Additional thrust |
|---|---|---|---|---|---|---|---|---|---|---|---|---|
| Mewis Duct | | PC | N | N | N | PC | C | N | N | N | N | N |
| Propeller Boss Cap Fins | | | P | C | N | C | C | N | PC | N | N | C |
| Pre Swirl Stator | | | | PC | N | PC | C | N | C | N | C | C |
| Propeller Nozzle | | | | | N | C | C | N | C | N | N | PC |
| Contra Rotating Propeller | | | | | | N | C | N | N | N | N | N |
| Propeller Rudder transition bulb | | | | | | | C | N | PC | N | N | C |
| Rudder Profile | | | | | | | | C | C | C | C | C |
| Wake Equalising Duct | | | | | | | | | C | N | N | N |
| Propellers with end-plates | | | | | | | | | | C | N | N |
| Grim van wheel | | | | | | | | | | | N | N |
| Rudder bulb fins | | | | | | | | | | | | N |
| Additional thrust fins | | | | | | | | | | | | |

Furthermore, a classification attempt of the operational and technical measures is attempted with respect to implementation ease, initial cost and whether or not the selected measure is appropriate for retrofitting. The results are presented in Table 2.5 and Table 2.6. The classification of Energy saving practices and measures in terms of cost is considered as:

- 'Low' when the annual corresponding amount is between 1 $ and 50,000 $
- 'Medium' when the annual corresponding amount is over 50,000 $ and less than 100,000$
- 'High' when the annual corresponding amount is over 100,000 $

**Table 2.5: Synopsis of operational practices aiming to energy efficiency and emission reduction amended from Fathom Shipping (2011), VLCC workgroup (2009) and based on author's previous work in marine consultancy company**

| Measure | Claimed Savings up to: | Cost | Implementation Feasibility | Payback period | Suitable for Retrofitting |
|---|---|---|---|---|---|
| Slow steaming | 36% | zero | Easy | 0 | Yes |
| Virtual port arrival | 6% | zero | Easy | 0 | Yes |
| Propulsion efficiency monitoring | 5% | medium | Moderate | < 24 months | Yes |
| Weather routing/ software | 10% | Low/ medium | Moderate | < 12 months | Yes |
| Port turn-around time | 10% | zero | Easy | 0 | Yes |
| Optimization of ballast & trim | 6% | Low | Moderate | 0 | Yes |
| Speed optimization | 5% | zero | Moderate | 0 | Yes |
| Autopilot upgrade/ adjustment | 1% | Low | Moderate | < 16 months | Yes |
| Optimised Voyage planning | 5% | zero | Easy | 0 | Yes |
| Optimum use of fans and pumps | 0.1% | zero | Easy | 0 | Yes |
| Optimum use of bow-thruster | 0.1% | zero | Easy | 0 | Yes |
| Efficiency control of HVAC system | 10% | zero | Moderate | 0 | Yes |
| Speed/ Power Control Units for Pumps, Fans and other Electrical Equipment | 0.7% | low | Moderate | < 12 months | Yes |
| Cargo Heating and Temperature Control Optimisation | 10% | zero | Hard | 0 | Yes |
| Optimum Lighting Operation Management | 0.1% | zero | Easy | 0 | Yes |
| Usage of Fuel Oil Additives | 5% | Low | Easy | < 12 months | Yes |
| Ballast Water exchange | 2% | zero | Moderate | 0 | Yes |
| Even main engine / e-load operation | 1.5% | zero | Moderate | 0 | Yes |
| Fuel Oil Homogenisers | 0.25% | Medium | Moderate | < 36 months | Yes |
| On-shore Power supply (Cold Ironing) | 10% | High | Moderate | < 60 months | Yes |
| Proper use of fuel oil purifiers | 0.2% | Zero | Easy | 0 | Yes |
| Improved Machinery Maintenance[1] | 4% | Medium | Moderate | <24 months | Yes |
| Energy Management | 1% | Medium | Hard | <36 months | Yes |

Concerning the technical measures, specific measures marked with * depend on the vessel specifications. The item marked with ** requires the existence of Dual Fuel M/E and/or A/E. Finally, the fuel saving potential of the item marked with *** is compared to the non-optimised sizing of the equipment. The payback period was calculated for a

[1] Minimisation of Air System Leakages, Proper insulation of steam distribution network, Electrical insulation of Electric Network and overhauling of M/E and A/E at specified by the manufacturer intervals.

baseline VLCC vessel with expected operational life of more than 25 years. Furthermore, savings should be added by multiplying the reduced power consumption. With this method, the implied error in the case of simple addition is negligible (VLCC workgroup, 2009).

The adoption of energy efficiency measures leads to a total reduction of fuel oil consumption under favourable conditions for each measure. However, the operational practices and hull modification target is to decrease the energy demand and not to improve the production of energy, which leads to the fuel efficiency. For the practices and measures that minimize the demand, the proposed Hybrid Power system is suitable for installation as it is aimed at improving the energy production.

When the installed machinery comprises of Diesel Engines, the Hybrid Power topologies aim to increase the thermodynamic efficiency of the prime movers for the given operational scenario. However, it must be taken into account that the cost of Hybrid machinery is considered high, as will be shown in Chapter 3, and the outcome of the Hybrid Power system might be compensated by cheaper solutions of the current market.

This statement is valid only when the vessel is designed for a specific purpose. This means that when the ship is designed for ultra-slow steaming, then a better engine propeller match will be performed at the early design stages and the fuel efficiency will be tuned by the manufacturer in order to serve the specific operational scenario. The hybrid system is not recommended for these cases. Nonetheless, when the vessel is designed for a broad operational range, as the entire fleet that was examined in this study, energy saving potentials such as turbocharger cut-out, cylinder isolation or engine de-rating maybe proved very hard or even impossible to implement during specific voyages, as they require dry-docking or modification to be performed by a special service team dispatched by the engine manufacturer. Consequently, the Hybrid potential is attractive in terms of real time applicability. Moreover, due to the optimisation of the Hybrid power plant and the existence of the proposed smart Hybrid controller, the engine operation may not be affected if the solution yields to a zero hybridisation degree. Thus, the existence of the hybrid system on-board does not affect other energy saving measures of the propulsion machinery while they are in place.

Therefore, it can be concluded that the Hybrid Power system is suitable in combination with many energy saving options, and is fully compatible with operational practises, although saving percentages are affected by the vessel operation.

**Table 2.6: Synopsis of technical practices aiming to improve energy efficiency and reduce emissions amended from Fathom Shipping (2011), VLCC workgroup (2009) and based on author's previous work in marine consultancy company**

| Measure | Claimed Savings up to: | Cost | Implementation Feasibility | Payback period | Suitable for Retrofitting |
|---|---|---|---|---|---|
| Rudder Surf Bulb | 5% | High | Moderate | < 36 months | Yes |
| Rudder Surf Fins | 1.3% | High* | Moderate | < 132 months | Yes |
| Propeller Boss Cap Fins | 5% | Medium | Moderate | < 14 months | Yes |
| Contra Rotating Propellers | 3% | High* | Hard | ~ 132 months | No |
| Mewis Duct | 5% | High* | Moderate | ~14 months | Yes |
| Propeller Duct | 3% | High* | Moderate | < 24 months | Yes |
| Wake Equalising Ducts | 3% | High* | Hard | < 18 months | Yes |
| Pre Swirl Fins | 1.5% | Medium* | Hard | < 30 months | Yes |
| Pre Swirl Stator | 4% | Medium* | Moderate | < 18 months | Yes |
| Silicon Anti-fouling paints | 9% | High | Moderate | ~ 9 months | Yes |
| Propeller Polishing | 3% | Low | Easy | < 6 months | Yes |
| Hull Cleaning | 21% | Low | Easy | < 1 months | Yes |
| Ax – Bow Shape | 6% | High* | Hard | < 72 months | No |
| Air lubrication | 4% | High | Hard | < 60 months | Yes |
| De-rated M/E | 6% | High* | Easy | < 60 months | No |
| Electronic controlled M/E | 6% | High* | Easy | < 60 months | No |
| Fuel Injection Slide Valves | 0.5% | Medium | Easy | < 36 months | Yes |
| Electronic Governors | 2% | Medium | Easy | <12 months | Yes |
| Part Load Optimisation | 3% | No* | Easy | 0 | No |
| Turbocharger Isolation | 3.5% | No* | Easy | 0 | Yes |
| Cylinder Isolation | - | No* | Easy | 0 | Yes |
| Waste Heat Recovery with PTI/PTO | 12% | High* | Hard | < 72 months | No |
| Shaft Generator | 1.5% | High | Moderate | < 60 months | No |
| Installation of optimum sized Auxiliary Boilers*** | 1% | High* | Hard | 0 | No |
| Replacement of Incandescent bulbs with CFLs and TFLs | 0.01% | Low | Easy | <2 months | Yes |
| Fuel Cells for Main Propulsion | - | - | - | - | No |
| Use of LNG fuel | 20% | Medium** | Moderate | ~ 12 months | No |
| Replacement of Incandescent bulbs with TFLs or CFLs | 0.01% | Low | Easy | < 2 months | Yes |
| Solar Panels for auxiliary loads | 0.5% | High | Easy | <60 months | Yes |
| Kites and Sails | 35% | High | Hard | < 60 months | Yes |
| CLT or Kappel Propellers | 6% | Medium | Moderate | < 4 months | Yes |
| Grim Vane Wheel | 5.5% | High | Moderate | ~ 36 months | Yes |
| Asymmetric Hull Aft Body | 3.5% | High | Hard | < 72 months | No |
| Minimisation of Wind Resistance | 0.8% | High | Moderate | < 96 months | No |
| Bare Hull Optimisation | 5% | High | Hard | < 4 months | No |
| Minimisation of Resistance Appendages | 0.2% | High | Hard | > vessel's life | Yes |
| Reduction of HVAC Energy | 0.2% | zero | Moderate | < 48 months | No |
| Design for 10% lower speed | 27% | High | Hard | <30 months | No |

Moreover, there is full compatibility with vessel hydrodynamic improvements. Nonetheless, the modification of engine components may compromise the effectiveness of the Hybrid system without reducing the fuel efficiency, as the system is decoupled when the fuel optimisation solution yields no zero hybridisation degree.

## 2.6 Chapter summary

This chapter identified the basic pollutants of the operation of Diesel engines. In addition, a detailed comparison of the fuel power factors and power based factors was performed. It was found that the fuel based factors are not inferior to the power based factors as the introduced error is negligible. However, it can be concluded that the fuel based factor should correspond with the engine fuel efficiency at the optimised operational point.

Moreover, a presentation of the accepted methods to measure emissions was made. Based on the accuracy of the 'bottom-up' approach, this method was selected and modified accordingly. Furthermore, the trade-offs between fuel efficiency and $NO_x$ formulations have been discussed. In addition, a connection between the policy and the energy efficiency was made. In order to assess the Hybrid power potential, a detailed comparison of up to date fuel efficiency measures was presented and the combination of these technologies with the proposed solution was demonstrated.In the next chapter, the Hybrid power system will be presented.

# 3 Hybrid Power Systems

This chapter demonstrates the implementation of Hybrid power system layouts. Suitable components such as prime movers, energy storage media and electrical components are identified, compared and selected for the proposed power system. This chapter also explains in depth the adopted methodology in order to assess whether the Hybrid Power systems are suitable for slow speed vessels, and to compare the fuel consumption of the simulated system with the 'as measured' values. For the proposed Hybrid Power layouts, efficiency figures and static efficiency tables for each of the components are given. So that to demonstrate conceptual feasibility, a case scenario was formed based on actual vessel operations.

The feasibility assessment is based on actual reported data, and the machinery operation identification is based on interpolation curves given by the component manufacturer. The interpolation accuracy relies on the reported values in the 'noon reports' forms transmitted to the company by the crew. The sizing of the battery system is based on the regression analysis of the energy requirements of the fleet, based on the actual engine load fluctuations. For the adoption of the Hybrid Power system, two layouts were examined.

Although fuel savings have been noted, the installation of the batteries reduces the available vessel free space and alters the Deadweight. Therefore, the technical and design parameters have been investigated. The approximation of the engine room volume is made by an accepted formula (SNAME, 1990) and the remaining free/void spaces of the vessels are based on the acquired vessel drawings. Finally an initial economic assessment of the Hybrid Power system is made based on a comparison of the actual fuel consumption and the simulated Hybrid system consumption.

## 3.1 Implementation of Hybrid Power Systems

Among the shipping industry, it is a common mistake to treat the power problems as M/E RPM problems. Most of sea-going and shore based personnel, relate the M/E RPM with power consumption in every voyage condition. The ship due to the constantly changing environment requires different propulsive power for the same RPM while the ship speed differs. As a result, it is a typical misunderstanding between the crew and shipping company that the constant RPM setting the majority of the time leads to higher fuel consumption than the expected. This is explained by the operational principle of the governor. This equipment controls the fuel injection to the engine cylinders so that the engine rotates at the defined speed setting. This is depicted by Figure 3.1. Due to this power difference, which leads to an increase of fuel consumption, Hybrid systems are

investigated in order to reduce a percentage of fuel consumption by maintaining at the highest possible point the thermodynamic efficiency.

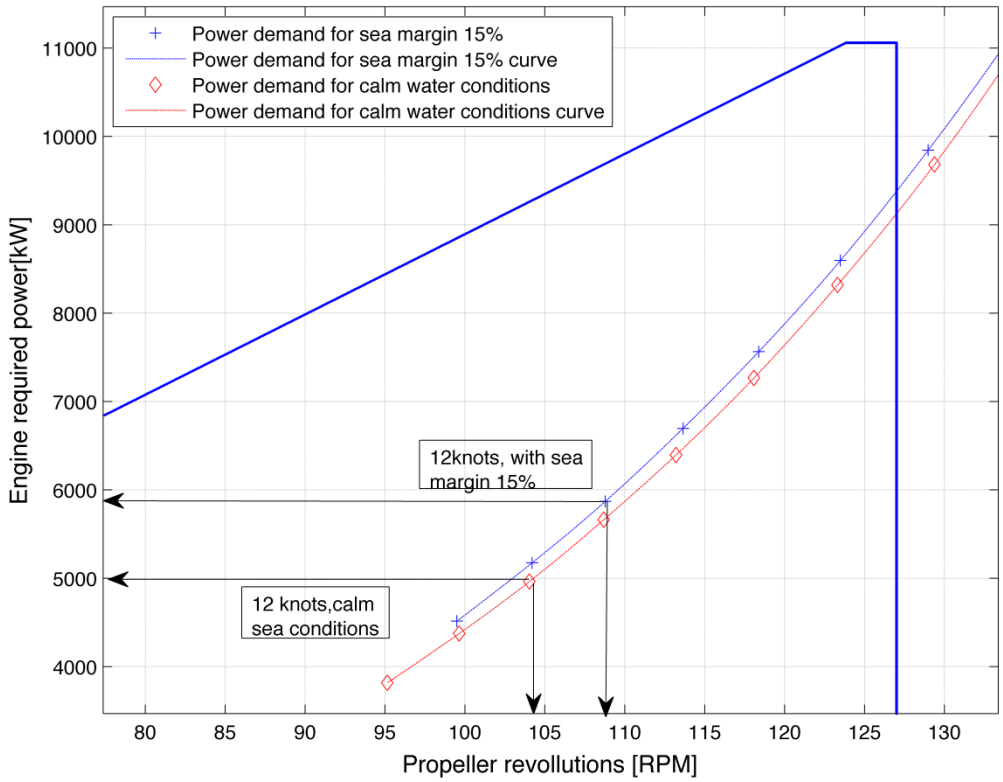


Figure 3.1: Required propulsive power and propeller RPM for resistance profiles

### 3.1.1 Selection of suitable prime movers

The purpose of this section is to identify the technologies available for propulsion, underline the key facts, present the advantages and disadvantages of their operation and using a systematic approach, detect their effect on the propulsion system energy flow. The ultimate goal is to define for the Hybrid Power system, the prime mover and it's tuning with the rest propulsion system, as it is recognised as the key component for the successful implementation of the concept. The prime mover objective is to deliver mechanical energy by generating torque. It can be a Diesel Engine, a gas turbine or a steam turbine. The torque is developed due to energy conversion that takes place during combustion of Hydrocarbons, where chemical energy contained in the fuel is transformed into a force that moves a moveable component, which can be either blades or a piston.

The Diesel Engine is a reciprocating internal combustion engine. It is installed on board vehicles, ships, shore generators, etc. It is the most frequently used prime mover in the marine industry (Kyrtatos, 1993). Marine Diesel engines can be separated into Low speed (60 – 180RPM), Medium speed (400 – 800RPM) and High speed (>800RPM). The high speed Diesel engines are not suitable for slow speed vessels as gearbox is required, high quality fuel (MDO) is required while the SFOC ranges from 170 to 220g/kWh. Their

thermal efficiency is low. Thus, despite the existence of attractive specific $NO_X$ emission characteristics, this engine solution is rejected because of the high running costs and high SFOC.

Medium speed engines have compact dimensions as are built in V or in Line cylinder configuration. Nonetheless, they require they require 1 hour to start from cold so in the marine applications where nowadays are always on standby the need continuous preheating. This solution will be investigated for Hybrid power system as it is already applied in shipping for auxiliary applications. They can have optimised tuning for all electric ship concept (propulsion) or normal electric generation (auxiliary loads). In electric propulsion, medium speed engines are coupled with an alternator. Each engine occupies significantly less space and weighs less than a similar output two-stroke diesel, although the total mass of required engines and motors may be greater than a single two-stroke diesel engine. These generator sets can operate across a broad range of loadings, but it is extremely inefficient to run them at loads less than 50% of MCR, where the production of $NO_x$, $SO_x$ and soot is high and the mechanical efficiency is low. Hence, in the cases where Diesel generators operate at the design load significant lower $NO_x$ emissions in terms of kg/tonne compared to the two-stroke of the equivalent output are observed due to shorter combustion time span (Woodyard, 2009). Smaller engines do operate in lower combustion temperatures as the total power output is less than a larger engine, therefore lower pressure and temperature are developed inside the cylinders. In the Hybrid power concepts, smaller engines can be fitted to achieve a scalable power output, while the remaining peaks and fluctuations can be covered by the energy storage device. However, exhaust heat recovery is difficult, because exhaust boilers are more efficient at high exhaust mass flow and in order to prevent back-flow when not all engines are in operation, complex valve or flaps need to be installed at the exhaust piping before the composite boiler.

Slow speed Diesel engines are dominant in shipping due to their high thermal efficiency which dependent on the thermal recovery systems can reach 55%. In addition, the slow rotation of the shaft, using very high torque (power output can reach 80MW) enable the use of large Diameter propellers which have high open water efficiency resulting in increased propulsive efficiency (Shi et al., 2010). Moreover, the SFOC can be reduced to 150g/kWh which is the best among the reciprocating machines, thermal efficiency. Nonetheless, at low loads there is fuel-air mismatch at the T/C and the fuel efficiency is low. Due to non-optimised calibration of exhaust valves, smoke is also visible something that imposes the use of light and expensive fuels in the ports of EU, USA, Australia and New Zeeland. Furthermore, because of increased combustion span, which is affected by the engine speed as combustion is connected to the crank angle (Dedes, 2009), $NO_x$

formulation is increased (Heywood, 1988). Furthermore, waste heat recovery is low and Scrubber technology operates at higher loads, where exhaust mass flow is significantly higher. The specific $NO_x$ emissions limits are dictated by regulations and means to reduce and control emissions were discussed in Chapter 2.

Gas turbines can be considered as rotating machines because they consist of solely rotating components. Nowadays their main application on board vessels is found in military ships in combined installations along with marine diesel engines. The combined systems are known as combined Diesel or gas (CODOG) and combined Diesel and gas (CODAG). The gas turbine is used as an extra energy supplier. The purpose of both layouts is to increase ship speed or, when propulsion system requirements demand, more power for constant speed. Although the system has a fast response, as a gas turbine starts within a minute and can be loaded almost directly, the thermal efficiency is low (31%) and fuel consumption is high when compared to Diesel engines. On the other hand, they exhibit high reliability and maintainability (Hockberger, 1976), as they are less prone to gas leakages. They have higher power density than diesel but they cannot be repaired on site due to the fact that components are designed to be replaced for maintenance (Klein Wood and Stapersma, 2002). In addition, in partial load their efficiency is extremely low.

Steam turbine propulsion is not a prime solution nowadays because it has low power density, is less fuel-efficient than diesel engines and involves a higher initial cost.
Taking into account all the above using the information regarding the differences between the Diesel topologies of Appendix Table 2, the Hybrid Power concept involves a two-stroke Diesel Engine and auxiliary four stroke Diesel Generator Sets as prime movers. Due to the fact that four-stroke Diesel Engines have reduced efficiency in low output powers, as the basis of the optimisation scenario, a regular Diesel Generator is used.

### 3.1.2 Selection of suitable energy storage medium

The sea is a dynamic changing environment, driven by stochastic phenomena. Consequently, this phenomena behaviour implies a dynamic and rapid load change in power requirements in order to maintain the desired vessel speed (Molland et al., 2012). The environment-ship interaction is equivalent to the interaction of sustainable energy equipment with solar emissivity or wind gust. Several storage technologies can be categorised by their operational mission and by the type of storage. Based on the mission profile, capacitor and super-capacitors, flywheels and SMES are considered as storage media oriented to system stability and system reliability. Baker (2008) performed a general overview of energy storage media. Divya and Østergaard (2009) performed an evaluation of energy storage media to ensure and improve the stability and performance of the sustainable energy system. In addition, McDowall (2007) reviewed different types

of electric storage. The combination of storage media (creation of hydrogen and use of flywheels) for more efficient application is proposed by Wang et al. (2008).

Batteries are oriented to applications for power handling and load levelling and their operational feasibility has been proven in numerous land based large scale energy storage projects. Rodriguez (1989) discussed the operational experience of the 40MWh lead acid storage plant at Chino. Cole (1995) and Wagner (1997) reviewed the developed state of play and demonstrated that regulated lead acid batteries are suitable for large energy storage banks and the market is emerging for that application. Sutanto and Lachs (1998) validated that battery energy storage device is possible and proposed an equivalent system for Southern Asia. According to the type of stored energy, each device can be categorised as a mechanical, electrical, chemical or thermal storage medium. Consequently, in order to apply the aforementioned goals, battery technology that is mature for these applications and is proved to be applicable for load levelling using battery only arrays is selected. In addition, the Efficiency issues of batteries installed in this type of applications are known and regarding the lead acid batteries, which are considered as low efficiency systems and can form a worst case scenario application are discussed in Parker (2001). The main reason of rejecting every other potential, except the use of flywheels, is that the energy production comes from the operation of the Diesel engine constantly and without any normal disruptions, something that differs the system significantly from sustainable energy topologies (e.g. solar panel arrays, wind turbines etc.). Moreover, because this type of systems involves use of electrical components and electrical energy many conversions are avoided. The conversion refers to the transformation of kinetic energy from the Diesel engines to electric energy in the case of flywheels Moreover, in cases of boosting electric power demand, a double transformation of electric to kinetic and vice versa exists. Hence, by using battery as energy storage medium, the transformation losses are reduced. The existence of chemical to electrical and vice versa transformation is still present thought. Thus, the identification of battery chemistry and of the Coulombic efficiency is crucial for the battery selection.

Besides, the energy availability to the system is determined by the engine operation, the amount of stored energy has to be set according to statistical analysis of the voyage and extreme amounts are not required. Judging from the work of Bršlica (2009) for plug in Hybrid vehicles and in combination with cold ironing facilities, as discussed in Khersonsky et al. (2007), it can be said that a Hybrid ship containing battery storage devices can charge the system, offering green operation while entering and exiting the ports, even inside the ECA zones, dependent on the vessel speed and energy capacity of the storage system.

Nonetheless, the question to be raised is if the battery as energy storage system is financially feasible (investment cost), efficient, safe, reliable and can be recycled. In automotive industry, the cycle efficiency of the batteries determines the feasibility of Hybrid applications and the percentage of GHG emissions that can be reduced (Shiau et al., 2009). How their efficiency determines the feasibility of Hybrid vehicles was initially discussed in Chalk and Miller (2006). Previous studies of Fontaras et al. (2008) and Alvarez et al. (2010) demonstrated that recuperated kinetic energy can lead to reduced emissions by regaining vehicle breaking power. The efficiency of the storage system determines the amount of reoccupied energy and thus the reduction level of $CO_2$ emissions. As a result, higher efficiency than lead acid batteries had to be investigated primarily as a result of the unique parameters which apply to marine applications. Secondly, because there is no reoccupied energy that can be stored but efficient production of energy from the prime mover. Thirdly, due to volume and weight limitations that exist also in naval applications due to the large amount of required energy compared to hybrid vehicle. Thus, lighter and higher energy density batteries had to be identified. In order to assess the battery types that are suitable or not for large scale marine applications, the following Table 3.1 summarises the energy density and the cost.

**Table 3.1: Energy density and cost per battery type (Linden and Reddy, 2002; Galloway and Dustmann, 2003)**

| Type | Wh/kg | Cost [$/kWh] |
|---|---|---|
| Lead Acid | 35 | 90 |
| Vanadium - Bromine | 50 | 300 |
| Silver Cadmium | 70 | - |
| Zinc - Bromine | 70 | - |
| Sodium/nickel chloride | 115 | 110 |
| Lithium Ion | 150 | 600 |

From Table 3.1 it is observed that Lithium Ion batteries have by far the highest energy density. The additional advantages of Lithium Ion cells are the flat characteristic curve of voltage drop during most of the discharge period, the absence of memory effects and a superior life, but there are possible environmental and human health implications (Divya and Østergaard, 2009). The principal disadvantage of Lithium Ion batteries in this application is their large cost which exceeds 600$/kWh. Lead acid batteries appear to be a more economical solution. However, the low material resistance in the marine environment, corrosive failures and the short life period of 400 complete charges and discharges, make them more expensive in the life cycle of the ship. Lead acid batteries suffer from a quick voltage drop and in a long period of storage from self-discharging

(Linden and Reddy, 2002). The Sodium Nickel Chloride batteries have a cost that ranges from 72 -110$/kWh (Galloway and Dustmann, 2003) and they keep demonstrating cycles over 3500 and at least 11 years life time while the thermal insulation is stable for more than 15 years (Dustmann, 2004). In addition, the attractive characteristics in terms of power density, energy density and charging efficiency of sodium Nickel-Chloride (commercially known as ZEBRA) batteries make this type of battery a suitable candidate for Hybrid ship propulsion. Manzoni et al. 2008 discuss about the application of such type of batteries in hybrid vehicles and conclude about their feasibility as they demonstrate remarkable round cycle efficiencies and 100% Coulombic efficiency. Moreover, the Sodium Nickel Chloride batteries are considered as maintenance-free batteries which improve the return on investment (ROI) financial coefficient. Furthermore, Sudworth (2001) states that they are tested and successfully implemented in the marine environment for submarine propulsion. He concludes that a wide range of battery types can be constructed, matching almost every application requirement. Dustmann (2004) validated Sudworth's results and in his conclusions mentions that a 40MWh array has demonstrated cost reductions and makes life cycle costs less than those of lead-acid batteries. In terms of material recyclability, the Sodium Nickel Chloride batteries are consisted of nickel powder that can be converted to a constituent re-melt alloy which can be used in stainless steel industry. Moreover, the ceramic and slat contained in the cells, the slag can be used as replacement for limestone which is used in road construction (Galloway and Dustmann, 2003). These Life cycle characteristics are attractive when compared to the LCA analysis performed for other batteries suitable for Hybrid vehicles (Gaines and Singh, 1996; Van de Bosshe et al., 2010).

In terms of safety, Sodium Nickel Chloride Batteries have been tested for rapid vertical accelerations, impacts and penetration. In application for the automotive industry, this type of battery has passed all the safety tests imposed by the European Automotive industry. The laboratory tests showed remarkable durability in cases of gasoline fire, immersion in water (Bohm and Sudworth, 1994). The durability of that type of battery is owned to the fact that has four barriers to safety, a barrier by chemistry, barrier by the cell case, barrier by the thermal enclosure, and a barrier by the battery controller (Dustmann, 2004). Based on the above, it is allowed to conclude that there are no constraints on the installation in terms of safety and robustness in marine applications where the risk of flooding (immersion), collision (impact) or fire is probable.

In terms of battery system redundancy, in cases of small cracks in the β" alumina the salt and aluminium closes any crack. In cases of large cracks or break of the aluminium form by chemical reactions shorts the current path, so the cell goes to low resistance. It has been

noted that even the 10% of cells fails; the battery can continue operation (Dustmann, 2004).

Sodium Nickel Chloride batteries are high temperature batteries that operate at near 300$^{o}$C (Sudworth, 2001). In order to exploit the full energy and power density of these batteries, this temperature must be kept constant and in the range of 280 – 360 degrees Celsius to keep the electrodes in a liquid state (Dustman, 2004). The battery consumes energy in order to maintain the minimum temperature when the battery array is not in operation. The thermal losses though are very small around 0.1% due to the very good heat conductivity and due to the BMI control unit that accompanies the battery packs (Jarushi, 2010). Nevertheless, the cooling of this type of batteries is more energy consuming. According to Bohm and Gutmann (1996) and Daniel and Besenhard (ed), (1999), each battery cell needs approximately up to 10W of cooling power, something that corresponds to up to 14% of power per installed MWh of energy capacity. Nonetheless, it is observed that based on the application, the cooling power ranges from 9-13.5%. The cooling occurs by forced air flow and the system is self-regulating (Sullivan et al., 2006). Nonetheless, there are applications of oil cooling, but this solution was considered as more expensive (Gurche (ed), 2009). However, alternatives in marine applications should be investigated, as the fluid heat exchange (central, sea and fresh water coolers) is very common solution to high temperature heat exchange problems (e.g. Main engine, auxiliary engines etc).

Ponce de Leon et al. (2006) and followed by work of Mohamed et al. (2009) investigate the performance of redox flow cells for Hybrid electric vehicles. The potential of this technology is high and worth further investigation in the marine sector. There are three types of redox flow batteries. Each type is described by the reactant type. These types are the Chromium – Iron (Fe/Cr) and Bromine –polysulfide and the vanadium – vanadium. According to Ponce de Leon et al. (2006), Vanadium – Vanadium type is investigated for automotive applications. The most efficient in terms of energy efficiency, output power capability and energy density are the Bromine polysulfide redox flow cells. The latter are suitable for large scale load levelling which reaches 120MWh with power output less than 15MW. Furthermore, the reported cycles to date exceed 10000. Thus, in terms of design energy storage capacity, these are suitable for marine Hybrid power systems. In addition, these flow cells are not self-discharging, and the reactants are fluids that can be pumped out of the system for rapid charging, by replacing the electrolytes and the energy production and storage is possible to occur in different areas. Moreover, the used fluids do not contain substances considered harmful to the marine environment. The Vanadium Redox flow batteries store the two reactants in different containers and the flow of the latter is performed using pumps (Ponce de Leon et al., 2006). The pumping of reactants though increase the cost of operation and a proportion of the storage energy can

be assumed that it is lost in order to maintain the chemical reaction process. Regarding the storage of the reactants, in automotive applications, the polypropylene tanks are considered suitable for safe storage. In marine applications, due to the inexistence of such application to this date, the construction parameters have to be carefully considered. Design and construction parameters for the storage of batteries are discussed in section 3.3.3.3. Finally, a vital component for the feasibility of redox flow batteries is the proton exchange membrane. This component has reduced life cycle. To this date, investigation on different types of membranes is underway, so to reduce the associated cost and the replacement interval.

### 3.1.3 Selection of miscellaneous electrical components

The majority of ocean going merchant ships is powered by two-stroke slow speed Diesel engines and four-stroke medium speed engines to cover the auxiliary load demand. However, there are vessel types which use an All Electric Ship concept. Therefore, because the hybrid system combines traditional power production and also electric energy storage, the following have to be taken into account.

Full Electric Propulsion (FEP) uses electric motors that transform the electric energy produced by dedicated-to-propulsion generator sets and rotate propellers. Similar to the All-Electric Ship (AES) and FEP concepts, the Integrated Full Electric Propulsion (IFEP) system is found, where the same electric generators cover the auxiliary loads too. However, the difference in an AES concept is that the latter feeds every single operation of the ship by the electric distribution network. Nevertheless, these systems have difficulties in coupling through differing component requirements for AC voltages/frequencies or DC, as well as transmission issues.

The electrical output is a direct current (DC) flow. In order to couple batteries with the rest of the energy production system, converters which consist of inverters and rectifiers are needed. A converter (power electronic) is fulfilling the requirement of transforming the current of the storage medium to a form that can be coupled with the rest of the system (DC to AC). Apart from DC to AC coupling and control it is a fast and accurate controller for both speed and torque of electric motors and an inverter from DC to AC and is used for controlling the electric motors, in order to achieve the requested rotational speed. Details about converter technology can be found in Adnanes (2003) and Prousalidis et al. (2005). Regarding the AC/DC and vice versa conversion, an overview of converter technology is presented in (Steigerwald, 2001). According to Steigerwald (2001), in higher voltage areas that the Hybrid power system runs (557VDC battery, 440VAC main generators), the gate turnoff thyristors (GTOs), insulated gate bipolar transistors (IGBTs), and integrated gate-commutated thyristors (IGCTs) are the most suitable converter

devices for AC/DC/AC conversion. Steigerwald (2001) states also that the trend is to take advantage of the already state converter devices and implement DC/AC inverters using hard switching, something that reduces the cost and complexity of higher power inverters. However, the soft switching is more difficult to implement in PWM inverters since the current in a switching pole does not inherently reverse each cycle (as in most DC/DC converters) so that it is not always in the proper direction to allow soft switching.

Connection from DC grid to AC grid or vice-versa is typically accomplished by means of a Voltage Source Converter VSC. AC motors up to 2500kW which describe the Hybrid propulsion topology require VSC IGBT converter type. The use of a VSC allows bidirectional power flow and offers a more sophisticated protection and control system. This means that in the Hybrid topologies, the power electronic converter combines the energy transfer control and component protection function, (e.g. protection equipment in separated switchboards are now not necessary). The minimum external protection acts for faults in the power electronic module, because in normal operation mode the power electronic unit limits the over-current to a desired and adjustable level. This approach reduces the size and weight of the total electrical distribution system compared with usual solutions. (Fratta et al, 2000) taking into account the advantages of DC/DC conversion, have proposed a unique topology to DC/AC converter which controls an AC motor. The results are promising and the efficiency of the conversion system when compared to other converter types is higher. In addition Lee et al. (2009) also proposed a system for AC/DC charging of batteries for plug in Electric vehicles. However, the Bidirectional AC/DC with DC/DC converter was applied in lower voltage applications, thus the application for marine propulsion can be questioned. On the other hand, regarding the coupling of batteries with the electric motor, elaborating on the work of Nilsen and Sofronn (2008) DC feeding of DC motor should be further investigated. The DC motor capability of producing high torque at low speed, the feasibility of varying the characteristic by adjusting the excitation, and easy reversing of the direction of rotation. A Full-bridge thyristor rectifier (Silicon Controlled Rectifier (SCRe)) feeds the DC motor with a controlled armature (rotor winding) current. The field winding (stator) is excited with a regulated field current. The latter technology is mature and the SCR can reach up to 98% efficiency (Radan, 2004; Adnanes 2003). However, the DC motor can reach up to 94% efficiency, so there is a trade-off to compensate before selecting the DC options. Nevertheless, when selecting converter for the propulsion motor or the battery DC/AC discharging/charging conversion, the following parameters of inverter/ converter devices should be taken into account.

Furthermore before implementing them in an electric topology they should be optimised so to have limited effect on the operation:

- Heat issues (currently there is a limit on the maximum temperature)
- Conduction losses
- Complexity
- Fault redundancy (number of components)
- Weight/ Volume
- Voltage Polarity, Current Noise, and Switching Stress
- Applicability range (type dependent)
- Cost at high power levels
- Efficiency drop due to large scale application

Transformers are used to change the voltage of the subsystem and sometimes to provide a phase shift. The latter application can be used to feed frequency converters for variable speed propulsion drives, in order to reduce distorted currents by cancelling the dominant harmonic currents that result in problems in the electric network (Chatzilau et al., 2006; Tarasiuk, 2009).

The distribution of electrical energy is achieved through switchboards. These receive control signals and distribute electrical energy. The most dominant technologies are the SF6 and vacuum breaker technologies. A ship has multiple switchboards. The main switchboards receive electric energy directly from the generator sets and, in cases where 'cold ironing' facilities exist, from the shore power station. Another use of the switchboards is the prevention of short circuits. They also tolerate the consequences of one section failing. In stricter redundancy requirements, one switchboard should withstand failure due to fire or flooding.

The final, but most important, component of the electric propulsion is the electric motor. Typically, up to 90% of the load is fed to some type of electric motor. However, in the scope of this paper only the dominant electric motor technologies for propulsion will be mentioned.

Asynchronous (induction) motors are most frequently used in conventional applications. Their main attractive characteristic is their low cost and simple design, which assures long lifespan, minimisation of breakdown risk and low maintenance Chatzilau et al. (2006). Main constructional and operational characteristics can be found in Fitzgerald et al. (2002).

The dominant category type of propulsion electric motors (PEM) is the synchronous motor type whose efficiency, depending on the excitation method, can reach up to 98.5%. The nominal voltage varies from 3.3 to 6.6kV and can reach 11kV depending on the power output of the motor. Synchronous motors are not used for propulsion motors for power outputs less than 5MW, as asynchronous ones are more cost effective.

### 3.1.4 Hybrid power system layouts

In this section the Hybrid Power system layouts are modelled. The terminology of the Marine Hybrid Power system is explained in order to separate this conceptual design from the applied systems in the automotive industry. A connection of the Hybrid layouts with the applicable operational scenarios will be made. The energy storage and the prime movers that are necessary of the implementation systems were described before. . Finally, the efficiency of each Hybrid layout component is presented just after the presentation of the topologies.

#### *3.1.4.1 Parallel Hybrid Power layout*

In a parallel hybrid, both the electric motor and the Main Diesel engine operate together to cover the propulsion power demand. A controller, which takes into account the results of the optimisation algorithm, decides when to operate the electric machine and when to absorb stored power from the energy storage medium or when to switch off or maintain the Main Engine Operation. The energy storage medium is charged by the excess production of energy from the prime mover and only when the charging criteria specified by the designer are met.

#### *3.1.4.2 Series Hybrid Power layout*

In a series hybrid, the electric motor is solely responsible for producing torque in order to rotate the propeller. The energy storage medium is charged by the four-stroke Diesel Generator set, and meanwhile it supplies electricity to the electric motors. No direct coupling of the Engines to the propulsion shaft takes place. Although this scenario is commonly used in the automotive industry, this configuration can only be used by the shipping sector with AES concepts. The main reasons are the low efficiencies of the electric components and the transformation of electric energy to mechanical and vice versa. Thus, in AES applications where the trade-off between conversion losses and the remaining operational benefits yields to the electrification of the propulsion, this layout is applicable. A controller, which takes into account the optimisation algorithm results, determines the optimum power split between the produced energy by the Diesel Generator sets and the stored power of the battery system. The controller can progressively scale down or up the number of running generators in order to increase the fuel efficiency.

#### *3.1.4.3 Series - Parallel Hybrid Power layout*

In the case of marine Hybrid Power topologies, the term series-Parallel Hybrid layout is altered. In the case of electric vehicles, the Series-Parallel Hybrid system has both the

internal combustion engine (ICE) and the electric motor connected to the transmission. The ICE is connected to a gearbox and clutch, and a generator shaft can be rotated by the ICE. Due to the existence of the clutch, ICE can be switched off and the motor can provide the vehicle power, absorbing power from batteries. The engine can either operate as a generator only, or it can be connected to the transmission. The power demand can be covered by the optimum power split between the motor and the engine. In marine propulsion, due to high power demands, which, in ocean going ships, exceed 7MW, the Series-Parallel Hybrid Power system is separated into the following scenarios, as depicted in Figure 3.2, Figure 3.3 and Figure 3.4.

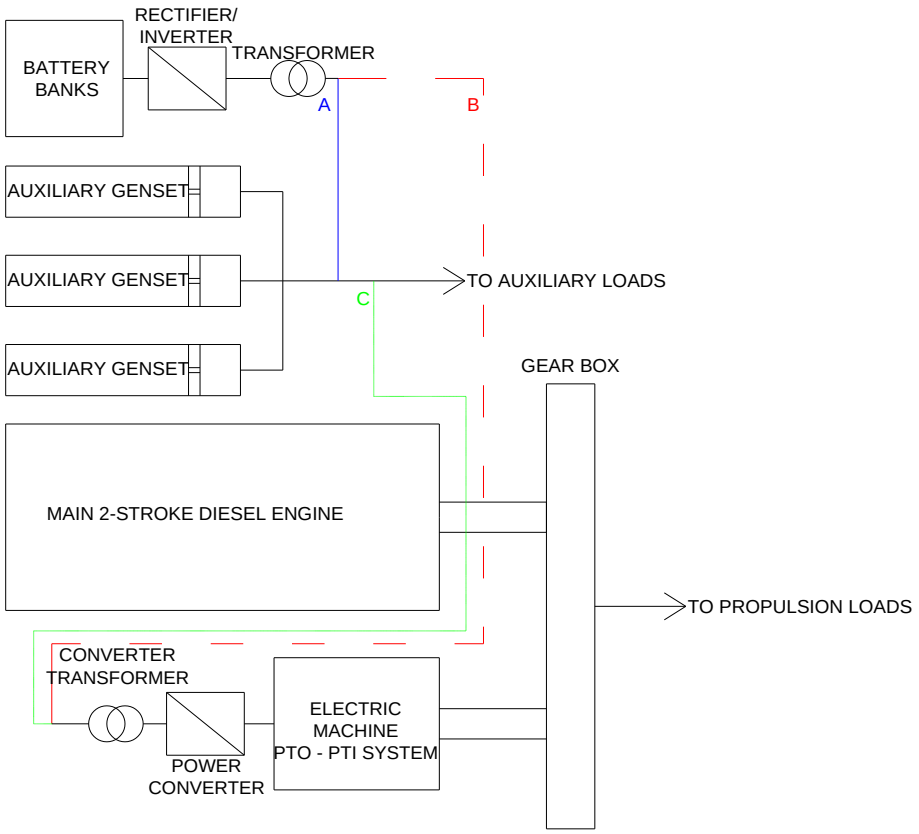


Figure 3.2 Hybrid Diesel-Mechanical System, layouts D-A, D-B or D-C

### Layout Diesel – A1 (D-A1):

Main propulsion is powered by the two-stroke Diesel Engine only. The auxiliary loads are covered by the Diesel Generator sets and/or by the energy storage system applying load levelling strategy.

## Layout Diesel – A2 (D-A2):

This layout refers to an All Electric Ship concept. No gearbox exists, the generators supply energy to the electric motors to cover propulsion. The propulsive energy can be fully covered by the generator sets or can be absorbed by the energy storage medium. Generators can be either switched off when there is no need for excessive power, or can charge the battery system. This layout is not suitable for slow speed vessels, as the direct propulsion has been proven more energy efficient (Molland et al., 2012).

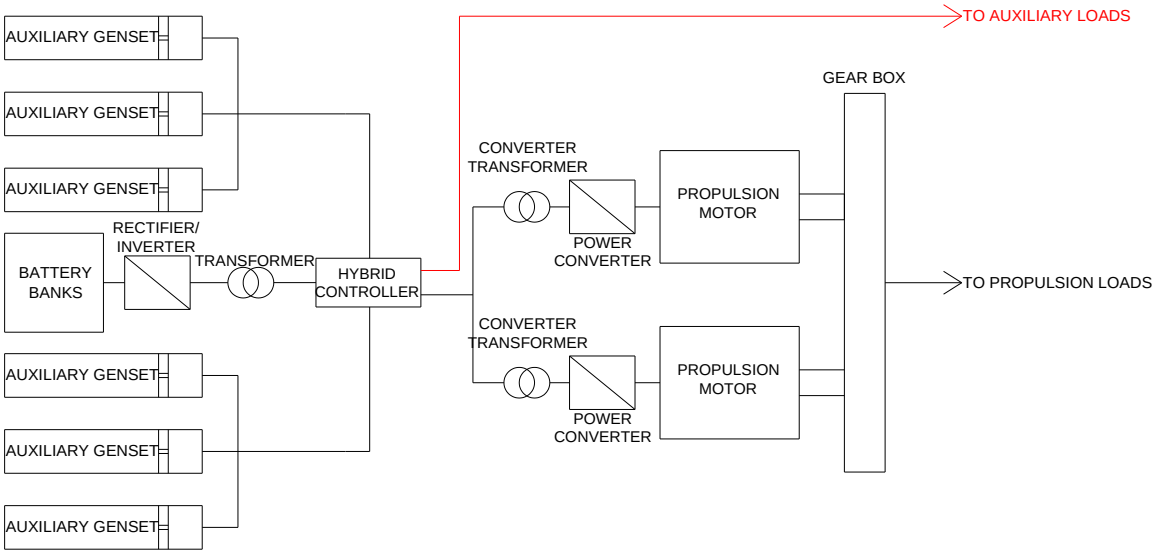


Figure 3.3: Hybrid- All Electric Ship Propulsion layout (D-A2 concept)

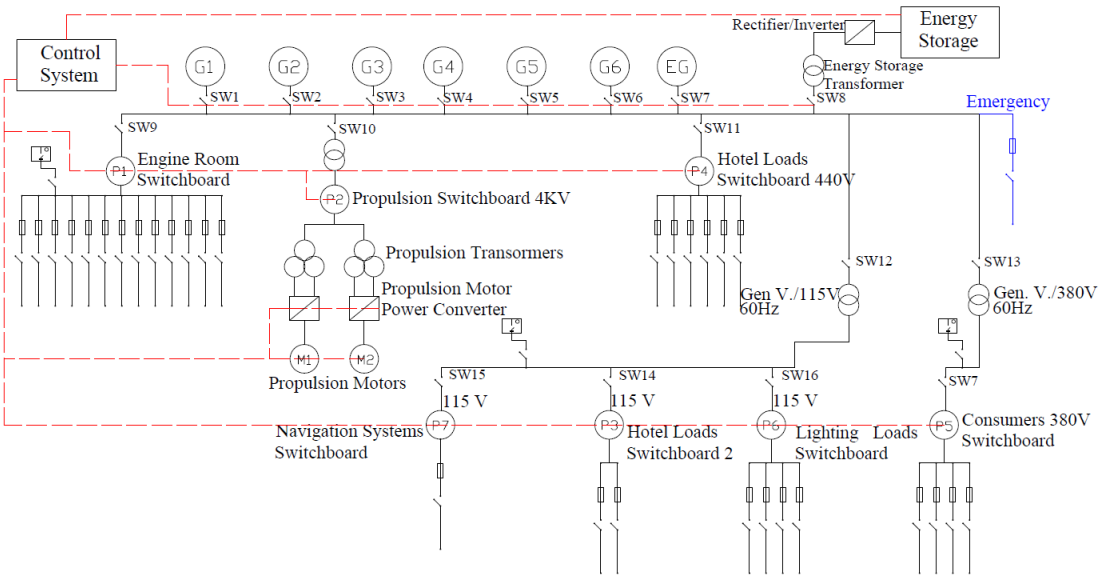


Figure 3.4: Line Diagram of the proposed D-A2 concept

**Layout Diesel – B (D-B):**

Auxiliary loads are covered by the Auxiliary Generator sets only. The main propulsion loads are covered by the optimum power split between the main two-stroke diesel engine and by the energy supplied though the electric motor via a gearbox clutch to the propeller shaft. The electric machine can operate as an electric motor or as an electric generator to store energy to the battery system for future use by the main propulsion only. No coupling with the auxiliary loads is possible. This layout has an important constraint. When the Main engine speed (or load) is less than 60%, the electric machine cannot operate as a shaft generator (PTO system) (Klein Wood and Stapersma, 2003).

**Layout Diesel – C (D-C):**

This layout is an extension of Layout D-B. Both auxiliary and propulsion loads are covered by an optimum power split between the main Diesel engine, the electric machine which operates as electric motor or as a shaft generator, by the Diesel Generator sets that can supply energy to the motor to cover the propulsion loads instead of absorbing from the batteries and the latter to apply load levelling either to the main propulsion and/ or to the auxiliary loads. Layout D-C has the same restrictions as the Layout D-B.

For scenarios D-B and D-C, the voyage is split into two phases. The first phase is considered as ocean going, where the propulsion system can store or absorb energy from the battery banks and the second phase, where the ship is in manoeuvring condition, and the electric machine can operate as electric motor only, due to the low Main Engine speeds. Furthermore, the 'at berth condition' (or phase three) is enclosed in layout D-A1, as no propulsion occurs.

### 3.1.5 Hybrid power system component efficiency

The following Table 3.2 denotes the efficiency of each sub-component of the hybrid power train. Efficiencies are of great importance in the power split of the system, as minimum fuel cost is not connected to the minimum required energy but is related to the higher efficiency of energy production. The tabular representation contains two sets of efficiency values. The first set is break down in detail, so to apply sensitivity analysis. The second set uses average efficiency figures, round-trip efficiency for the batteries and is used only to demonstrate concept potential feasibility. The positive outcome of this preliminary analysis is demonstrated in section 3.3.

The efficiency is either expressed in terms of non-dimensional factor or in terms of specific fuel oil consumption. To estimate the engine thermodynamic efficiency, equation (3.1.1) should be used.

$$\eta_{eng} = \frac{P}{Q_F} = \frac{3,6 \cdot 10^6 \cdot P}{\Theta_u \cdot m_f} = \frac{3,6 \cdot 10^6 \cdot P}{\Theta_u \cdot P \cdot b_e} \Rightarrow \frac{3,6 \cdot 10^6}{\Theta_u \cdot b_e} \quad (3.1.1)$$

where,

P : Engine output power [kW]

$Q_F$ : Chemical output power of fuel [kW]

$\Theta_u$ : Low calorific value of fuel [kJ/kg]

$b_e$ : Specific fuel consumption of Diesel engine [g/kwh]

The problem of propulsive efficiency is complex, as the engine speed has significant influence over the efficiency of the propeller (constant pitch) and the thermodynamic efficiency of the engine. Based on (3.1.1), it is clear that the decreased engine speed leads to higher SFOC, resulting in lower fuel efficiency.

**Table 3.2: Hybrid System component efficiencies (Chatzilau et al. 2006, Prousalidis et al. 2003, Greig and Bucknall, 2012)**

| Component Description | Necessary in layout | Simulation use Efficiency | Conceptual use Efficiency |
|---|---|---|---|
| Battery Converter and Transformer | All layouts | 98% | Total conversion efficiency 92% |
| Transmission losses | All layouts | 99.5% | |
| Gearbox efficiency | A1, B, C | 98% | |
| Motor Converter Transformer | B, C | 99% | |
| Electric Machine Power Converter | A2, B, C | 96% | |
| Electric Machine | A2, B, C | Figure 3.7 | |
| Electric generator | All layouts | Figure 3.8 | |
| Sodium Nickel Chloride Battery | All layouts | Figure 3.5 Figure 3.6 | Round trip 92% |
| Redox Flow Batteries | All layouts | - | Round trip 85% |
| Two-stroke Slow Speed Diesel Engine | A1, B, C | Figure 3.9 | Minimum SFOC 175g/kWh |

The second key component of the Hybrid system is the energy storage medium. This system consisted solely of batteries. Therefore, in order to implement the behaviour of the battery to the calculations, the terms open voltage, closed voltage and nominal voltage have to be explained. Thus, the theoretical voltage is dependent only on the materials of anode and cathode, the composition of the electrolyte and the temperature Linden and Reddy (2002). This means that it is independent of the operational profile of

the storage system. The open circuit voltage in the battery voltage under no-load is greater than the nominal voltage, which is the typical operating voltage of the battery. During discharge, the battery voltage is lower than the theoretical voltage.

This difference arises as electric current passes through the electrodes and polarisation occurs, which accompanies the electrochemical reactions (Linden and Reddy: Broadhead and Kuo, 2002). The losses include the activation polarisation, which is an inevitable process in order to start the reaction at the electrode surface, and concentration polarisation, which occurs due to the difference in concentration of the reactants. The product of these effects is waste heat. However, the waste heat is also increased by the internal impedance of the battery and is referred to as Ohmic polarisation. To summarise, the useful energy that can be drained out of the battery is given by the following equation (Linden and Reddy: Broadhead and Kuo, 2002):

$$E = E_0 - \left[\left(\eta_{ct}\right)_a + \left(\eta_c\right)_a\right] - \left[\left(\eta_{ct}\right)_c + \left(\eta_c\right)_c\right] - i \cdot R_i = i \cdot R \qquad (3.1.2)$$

where,

$E_o$ : electromotive force or open-circuit voltage of cell

$(\eta_{ct})_a$, $(\eta_{ct})_c$ : activation polarisation or charge-transfer overvoltage a at anode/cathode

$(\eta_c)_a$, $(\eta_c)_c$ : concentration polarisation at anode and cathode

$i$ : operating current of battery on load

$R_i$ : internal resistance of the battery

The Sodium Nickel Chloride discharge and charge behaviour was presented in Dustman (2004). The equivalent Ohmic Resistance of equation (3.1.2) can be acquired. However, for the purpose of this project, detailed laboratory measurements have been supplied. The battery discharge efficiency had been measured in the laboratory environment of a 557V, 32Ah battery for a set of discharge currents. The voltage drop had been measured until the state of Charge (SoC) reached zero (fully depleted battery pack) (Manzoni et al., 2008). By applying equation (3.1.2), the Resistance is then approximated. The voltage drop describes the energy losses of the battery, thus the discharge efficiency is calculated and Figure 3.5 is introduced. It can be extracted from Figure 3.5 that the discharge efficiency is very high when the discharge current is less than 2 A. However, the efficiency drop is significant because of the interpolation between the measured value at 2A discharge current and the theoretical value at 0A discharge current which is 100%.

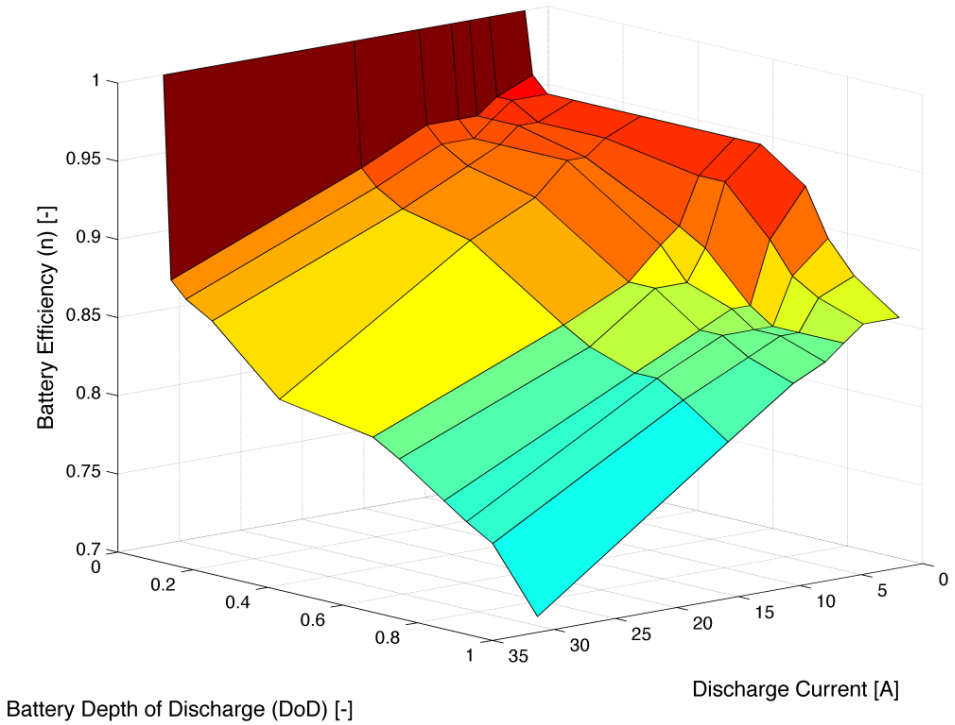


**Figure 3.5: Experimental Sodium Nickel-Chloride battery efficiency mesh versus Depth of Discharge and Discharge Current**

Based on the observed high efficiency bellow 2A, the sizing of the battery system should be made in a way that the operational discharge current per battery string is less than this value. Moreover, the reference State of Charge, where the battery system will maintain its charging, should be in areas where the discharge efficiency exceeds 94%. Manzoni et al. (2008) state the cycling should occur around 50% of the battery SoC for cycling purposes. For load leveling needs, the cycle should be around 100% and 20% of the SoC.

In order to estimate charging efficiency versus charge current, an energy approach was used and measurements were obtained in the laboratory environment. Moreover, the charging current was varied from 2A to 15A. Nonetheless, the charging voltage was set at 2.67V/cell, while the open circuit voltage ($V_{OC}$) is 2.58V. Therefore, accounting only for the voltage difference, it can be estimated that the efficiency is around 97%. Theoretically, the charge efficiency reaches 100% when it occurs in ultra- low currents. Consequently, in order to estimate the charge efficiency in less than 2A, an interpolation spline between 100% and the measured 97% is proposed. By taking into account energy losses in charging, Figure 3.6 is introduced.

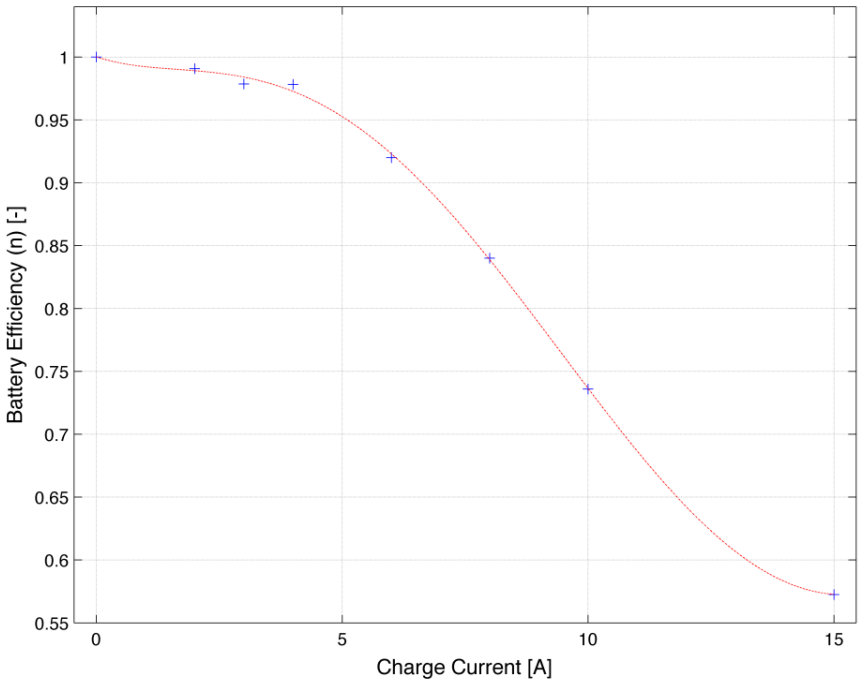


**Figure 3.6: Experimental curve of Sodium Nickel-Chloride battery efficiency versus charge current**

Based on the laboratory findings, the State of Charge has negligible effect on the efficiency and, for simplicity purposes, it can be assumed that the connection between SoC and charge efficiency is linear. Thus the latter can be implemented as a single curve versus the discharge current.

The electric machine that is present in Conventional Diesel Hybrid layouts D-B and D-C has an efficiency that is dependent on the operating load and on the rotational speed. Assuming that the rotational speed, which is controlled by the converter, remains practically at the most efficient area, the total motor/generator efficiency is considered dependent only on the load. As a result, Figure 3.7 is introduced. This curve was acquired from on board measurements by the author during a shipboard energy audit. However, it has to be stated that it was expected that the efficiency curve shape between the 75% and 100% would be flatter, increasing the overall motor efficiency. Nevertheless, changes in efficiencies are crucial for the feasibility of the system and it was for this purpose that a sensitivity analysis was performed.

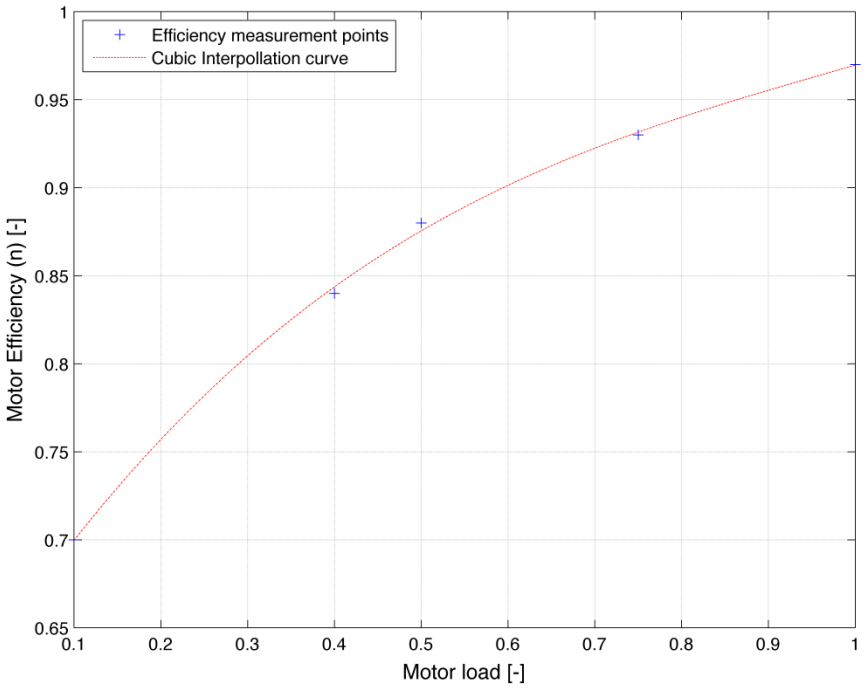


Figure 3.7: Electric Motor/ Generator efficiency versus loading

Figure 3.8 presents the fuel efficiency of four auxiliary generator sets intended to cover auxiliary load only. It can be extracted from this figure that the SFOC curve has a minimum at 100% of their MCR.

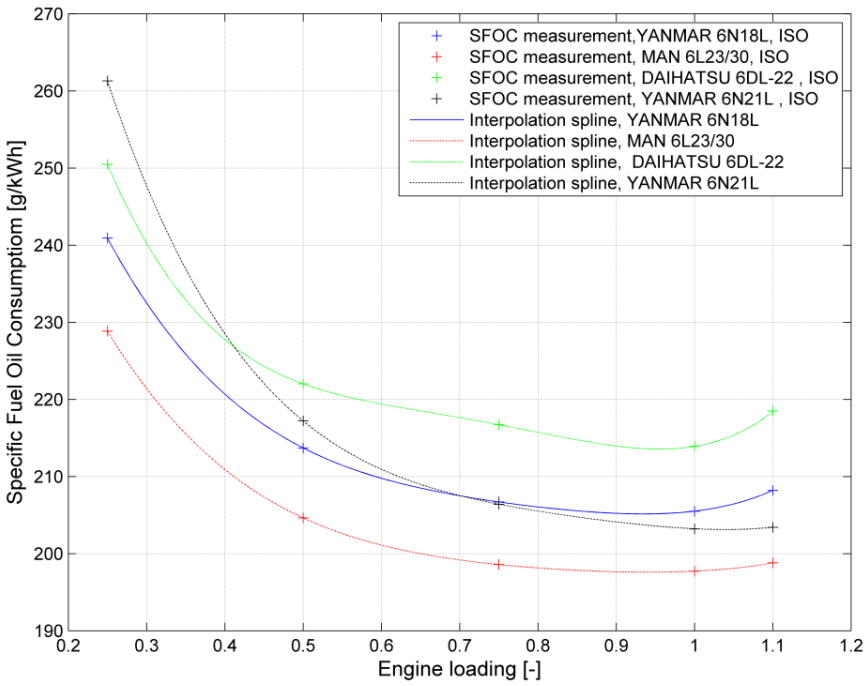


Figure 3.8: Specific Fuel Oil Consumption of Auxiliary generator sets

The nominal characteristics of the generator set that are involved into the Hybrid Power assessment can be found in Table 3.3.

**Table 3.3: Auxiliary Generator set characteristics**

| Model | Yanmar 6N18L | Yanmar 6N21L | Daihatsu 6DL-22 | MAN 6L23/30 |
|---|---|---|---|---|
| Output Power | 475 KWe | 600 kWe | 650 kWe | 730 kWe |
| Rotational speed | 720 RPM | | | |
| Frequency | 60 Hz | | | |
| Generator efficiency | ~95% | ~95.5% | ~96% | ~97% |

For the basic study of the Hybrid system, the Post-Panamax vessel that was used in the preliminary feasibility study was applied. This vessel is equipped with a 7S50MC-C7 type MAN Diesel engine with MCR at 11060 kW. For the purposes of the simulation and to estimate the effect of the shape and steepness of the curve to the Hybrid feasibility check, three tunings were implemented and are presented in Table 3.2. The line depicted in blue is the normal setting and describes the main engine operation to this date. This engine is optimised for normal sea going operation; consequently there is a flat area in a broad range of loads. The green curve depicts the SFOC curve of the same engine, if variable turbine blades were installed in the T/C (MAN Diesel 2007, 2012). According to the manufacturer, that option is recommended if the vessel regularly sails in slow or ultra-slow steaming modes. Finally the last setting is for full load optimisation, where the engine normally operates in high loads resulting in a SFOC penalty in low and normal loads. What is more attractive, however, in terms of the Hybrid system, is that SFOC is lower in a range of loads, but the most important factor is that the steepness of the curve is high, penalising any fluctuations in engine loading. However, this is not a trade-off between the fuel efficiency and the Hybrid system as with the part-load or full load SFOC curves and, given an examined voyage profile, the total consumption is lower compared to the normal optimised engine in any case. The hybrid system is investigated in terms of whether or not it increases fuel savings.

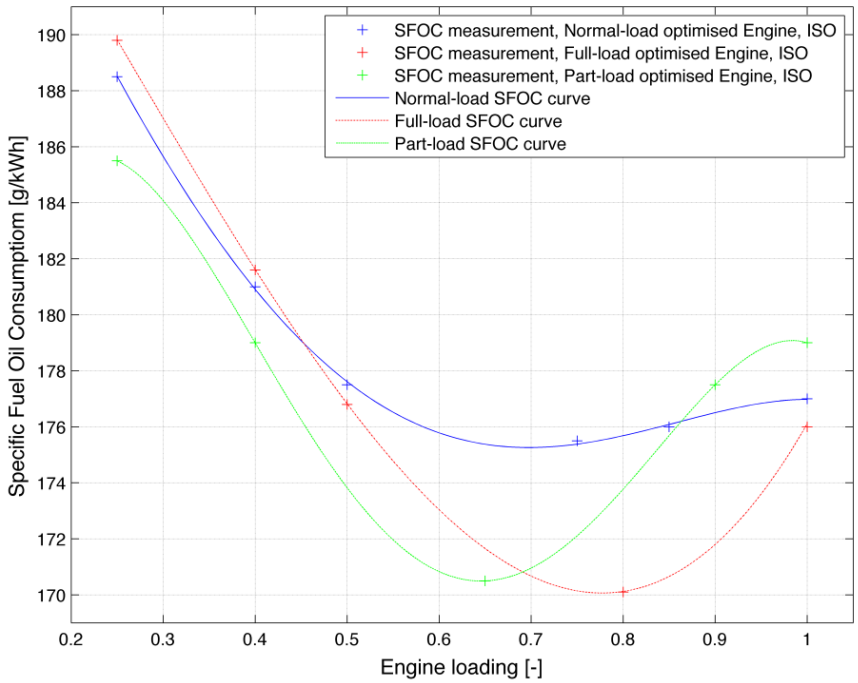


**Figure 3.9: Specific Fuel Oil Consumption curves for Full load, Part Load and Normal Load optimised Main Engine (MAN 7S50MC-C) (MAN Diesel 2007: 2009a: 2009b)**

In order to finalise the investigation of the prime mover fuel efficiency effect on the Hybrid system, a set of up-scaled and downscaled Main Engines was implemented. Table 3.4 summarises the Engine characteristics. It has to be noted that the SMCR of each engine is made for specific engine RPM. In order to couple these engines with the examined vessels, it has to be assumed that these are 'parent' engines and the actual engine to be installed should be set with the speed limit at 127 RPM but with a different output than the 7S50MC-C7. Its SFOC should follow the same curve as the 'parent' engine.

**Table 3.4: Characteristics of examined 'parent' Main Engines.**

| Engine Type | 6S70MC-C6 | 6S70MC-C6 | 6S50MC-C | 7S50MC-C | 7S50MC-C7 |
|---|---|---|---|---|---|
| Engine Output | 22920PS | 19380 | 12870PS | 14100 PS | 14825PS |
| Engine max Speed | 91 RPM | 83 RPM | 127 RPM | 119.3 RPM | 127 RPM |
| Installed at | Capesize | Capesize | Handymax | Panamax | Post-Panamax |

For the preliminary assessment of the hybrid module, static discharging/ charging efficiencies for the battery module have been used. When compared to the actual laboratory data, the static values are lower than the observed ones during the full battery

simulation. Thus, the most of the performance aspects are not captured but it valid to assume that fir at least these static efficiency values, the system is feasible and operational.

It is assumed that the operation of an equivalent Diesel-Electric system has the minimum SFOC of each vessel's current propulsion engine. Although the engine shop test curve shows that the SFOC curve is almost flat near the optimum area, the actual measured consumption differs significantly due to HFO operation and due to actual engine ship interaction. In addition, based on shipboard energy audit measurements, the SFOC curve shape may differ from the one supplied at the engine shop tests. However, when air and sea and air temperatures are not globally available, no correction is assumed that introduces error to the calculations. The overall battery performance cycle efficiency (charging/discharging) is considered constant for a broad range of discharge currents that the system is likely to operate, and equal to 85% for redox flow batteries (Mohamed et al., 2009) and 92% for Sodium Nickel Chloride (Dustmann, 2004). These values for high instantaneous discharge currents will drop, but over an overall cycle (which is denoted as a battery operation with both discharging and charging modes during the examined time frame) it should adequately represent the battery behaviour. Moreover, a 4% extra energy loss is applied to the total battery operation, because the electric current has to be transformed to mechanical energy at the electric motor and vice versa. In addition to the hybrid part, the conversion losses from electrical to mechanical energy are typically 8% - 12%. The achieved efficiency values range from 95-97% for generators, 96% for frequency converters and 95-97% for electric motors with the potential to be increased in the future. Thus, the overall system efficiency from the diesel engine's shaft to the propeller varies from 85-92% dependent on the system load. For the D-A2 conceptual case, the electromechanical conversion losses are taken equal to 8%.

## 3.2 Conceptual case based on voyage statistical analysis

The following procedure is based on actual fleet data for various laden and ballast voyages for Handysize, Handymax, Panamax, Post-Panamax and Capesize bulk carriers. A complete Hybrid Power system is proposed based on the average discharging/ charging efficiencies of the battery system.

### 3.2.1 Statistical power analysis

Daily ship performance data was collected from the technical department of a Greek Maritime Corporation. Each technical form includes the daily maintenance and monitoring logs, together with operational orders for ship routing. These forms are commonly known as 'noon reports' and an example is shown in Table 3.5. Although these forms contain important information about the ship's performance, unfortunately, errors made by the Chief Engineer or captain, due to the rush and repetition of measurements, do exist and there are cases where values do not represent the actual voyage characteristics. Thirty-one separate voyages across five vessel types and for a variety of laden and ballast conditions were collected.

The engine loading, as a percentage of the maximum continuous rating of the engine (MCR), was calculated by correlation of direct and indirect influence factors with the shop tests of the propulsion engine. Direct influence parameters are the engine RPM, the Fuel Admission Lever, the exhaust temperature (which should be corrected for engine RPM as well) and the rotational speed of the turbochargers. Secondary parameters are the slip of propeller, the ship's speed, the wind direction and force, the sea conditions, and the current strength and direction. These parameters have an indirect influence on the correlation with the shop tests, but are the main reason why the engine loading varies. In order to estimate the engine loading, the direct influence factors are interpolated into the performance curves of the engine [2]. Based on the fuel admission lever, an initial approximation of the loading is obtained. The fuel admission lever shows the actual petroleum that is injected per cycle. The estimated load is then compared to the calm water engine loading, which is described by the load indicator values. The latter shows the desired engine loading, which displays the percentage of the MCR that the engine should be operating at. If it is assumed that the engine Turbocharger is operating at the designed operational envelope, meaning near the surge line, its rotational speed is unique in every engine load. This actually defines the actual power loading of the engine, because the rotational speed of the turbocharger is defined by the exhaust gas mass flow and from the

[2] Data available at Fluid Structure Interaction research group at University of Southampton.

temperature difference between the cylinder exhaust manifold and the inlet of the economiser (accounting for a temperature difference due to the piping system).

**Table 3.5: Sample of Daily performance report ('noon report')**

| Vessel/ Voyage day | PPVSL1 | 1 | 2 | 3 | 4 |
|---|---|---|---|---|---|
| No. of Voyage/ Date | *2* | 08-Nov | 09-Nov | 10-Nov | 11-Nov |
| Condition | *LADEN* | | | | |
| Fuel Type | *HFO* | | | | |
| Ship Speed: | *Knots* | 14.67 | 13.88 | 13.67 | 13.33 |
| Slip (max measured): | - | -0.7 | +2.4 | +4.7 | +7 |
| Engine speed: | *RPM* | 115 | 117.7 | 118.6 | 118.6 |
| Activity Time: | *Hours* | 7.5 | 24 | 24 | 24 |
| Weather Type: | *Wind* | Quarter | Abeam | Abeam | Ahead |
| | *State* | 5 | 5 | 4 | 4 |
| | *Condition* | Rough | Rough | Moderate | Moderate |
| | *Current* | Abeam | Bow | Ahead | Ahead |
| | *Knots* | 0.5 | 0.6 | 0.4 | 0.4 |
| Distance Covered: | *Sea miles* | 110.03 | 333.12 | 328.08 | 319.92 |
| Daily Consumption: | *Tonnes* | 12.9 | 41.4 | 42.5 | 42 |
| Load Indicator | - | 66 | 66 | 66 | 66 |
| Fuel Admission Lever | - | 64 | 64 | 64 | 64 |
| Turbocharger speed | *RPMx10²* | 133 | 133.5 | 134 | 135 |

Thus, because exhaust mass flow and exhaust temperature are defined by the engine loading, the actual engine load can be acquired by reversing the above-mentioned process. Exceptions do exist in the cases of low loads, where an air blower is required to achieve the required compression ratio.

Figure 3.10 depicts the estimated engine loading for three Post-Panamax bulk carriers for both laden and ballast conditions. The above-mentioned process can be followed in every sea going voyage where no blowers are in operation (ultra-slow steaming voyages should not be taken into account).

Typically, while sizing the propulsion unit, a margin is left so that the engine will operate near 85% of MCR in calm sea conditions at the service speed. The margin accounts for up to 100% and covers increased energy demands due to rough sea conditions and the progressive fouling of the ship hull (Molland et al., 2012). However, this point is not always the optimum point of operation of the engine. The latter point can be obtained from the project guide of the installed two-stroke engine on the Post-Panamax vessels (MAN Diesel, 2007). Their optimum set is at 75% MCR.

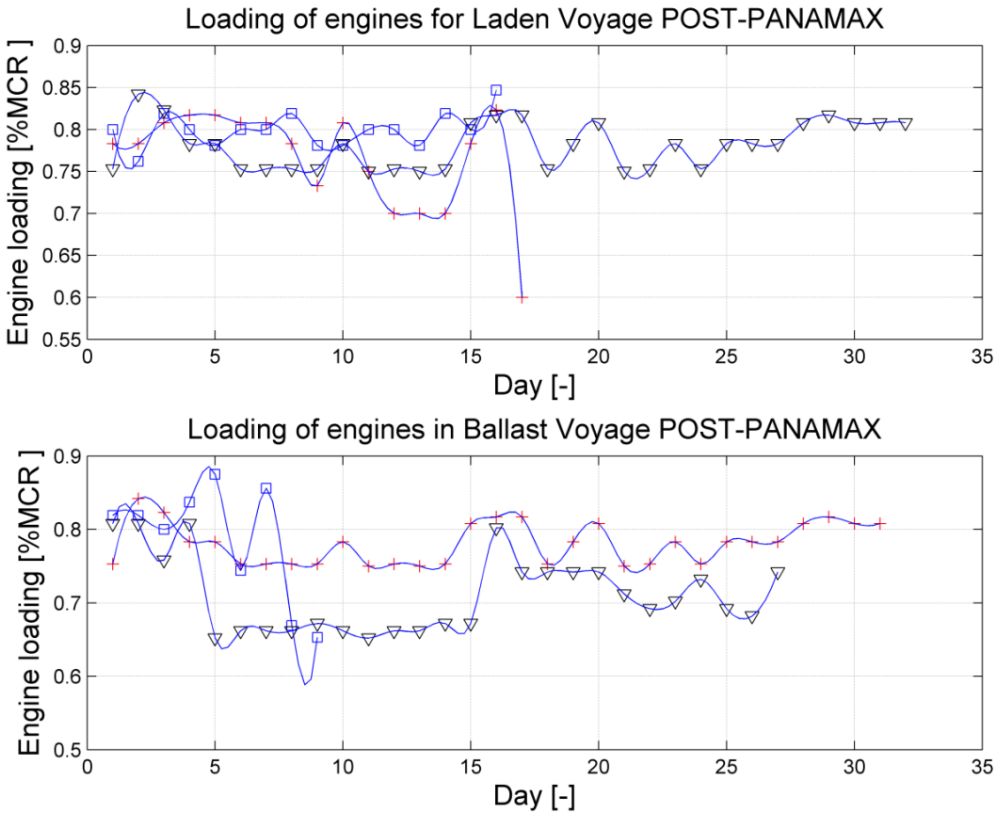


**Figure 3.10: Estimated engine loading for laden and ballast voyages of Post-Panamax ships**

From Figure 3.11 it can be observed that in every voyage of the Post-Panamax vessels within the fleet, the engine mean load varies from 70% to 80% of the MCR. It can also be observed that the 9-day voyage in ballast condition (marked with blue boxes in Figure 3.10) has the largest fluctuations in the daily engine loading. Based on the reports from that voyage, the ship faced extreme weather exceeding sea state 6, attempting, however, to maintain a speed of 13 knots. However, the vessel voluntary reduced speed on the 6$^{th}$, 8$^{th}$ and 9$^{th}$ day. Based on the obtained reports, it can be extracted that small length voyages have consistency in their reports, something that is not the case in long voyages such as the 32-day voyage denoted with the black reversed triangle. For that reason, it was attempted to regain the consistency mainly by altering the vessel speed, which normally is calculated by the crew by dividing the distance by the voyage time without accounting for the weather conditions, the propeller slip and the underwater current.

During the observation period of the fleet, the vessels were frequently cleaned underwater during port stay to minimise the frictional resistance due to fouling. This approach was implied directly by the management of the company. The aim was to maximise the vessel speeds in order to increase the number of charters per year.

Taking into account the operational envelope, the equivalent Hybrid Power system should have the main propulsion engine (in case of conventional Hybrid) optimised

near the loads depicted in Figure 3.11. The appropriate sizing of the energy storage medium in cases of load variations will lead to a zero net energy demand, as in this system the engine is constantly operating into a single point. The selection of this point is crucial as it reduces the capacity of installed energy, thus the initial cost of the system. Concerning the efficiencies of the battery system, it has already been stated that these are taken as constants and lower than the expected.

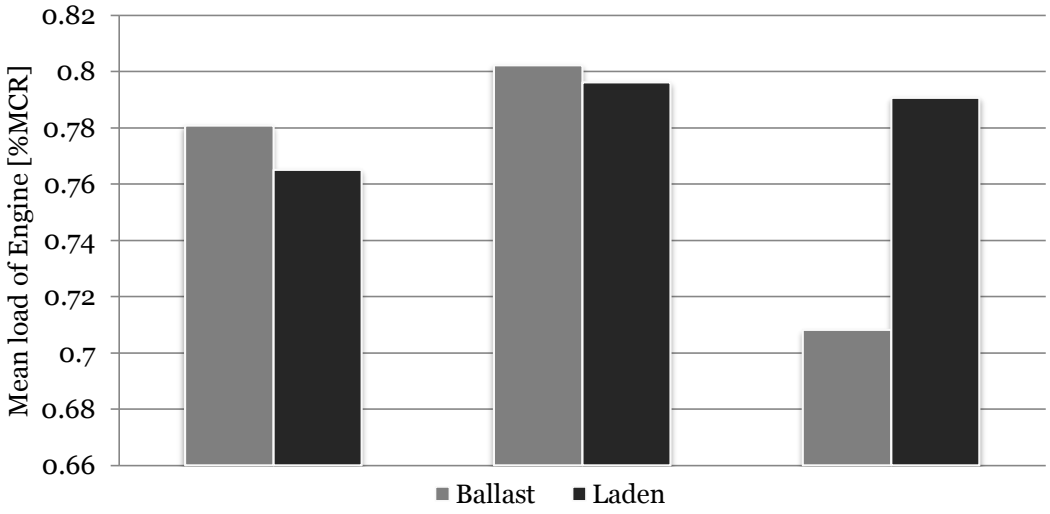


**Figure 3.11: Mean engine loading for three Post –Panamax sister ships for laden and ballast voyage**

Using the reported power requirements shown in Figure 3.10, the equation (3.2.1) is introduced, as from now; the Hybrid system is examined from an energy approach.

$$\text{Energy} = \int_{t_1}^{t_2} P \cdot \Delta t \tag{3.2.1}$$

Thus, the energy requirements (integration results) are presented in Figure 3.12 for three Post-Panamax ships used to illustrate the methodology.

The Hybrid system sizing utilises multiple diesel generator sets with different electrical output and energy storage devices, such as batteries. The operational point of the Hybrid system is taken as equivalent to the two stroke conventional plant predicted by average loading in similar routes or by a 'smart' controller. The latter will interpret data such as the state of charge of batteries, number of generators currently in operation, fuel efficiency of each engine, estimated time of arrival (ETA) at destination port and the sea state forecast. The decision constraints are the operation with the minimum number of generators and the likely demanded energy availability at the end or beginning of the voyage. The mathematical modelling of this controller is performed in Chapter 4.

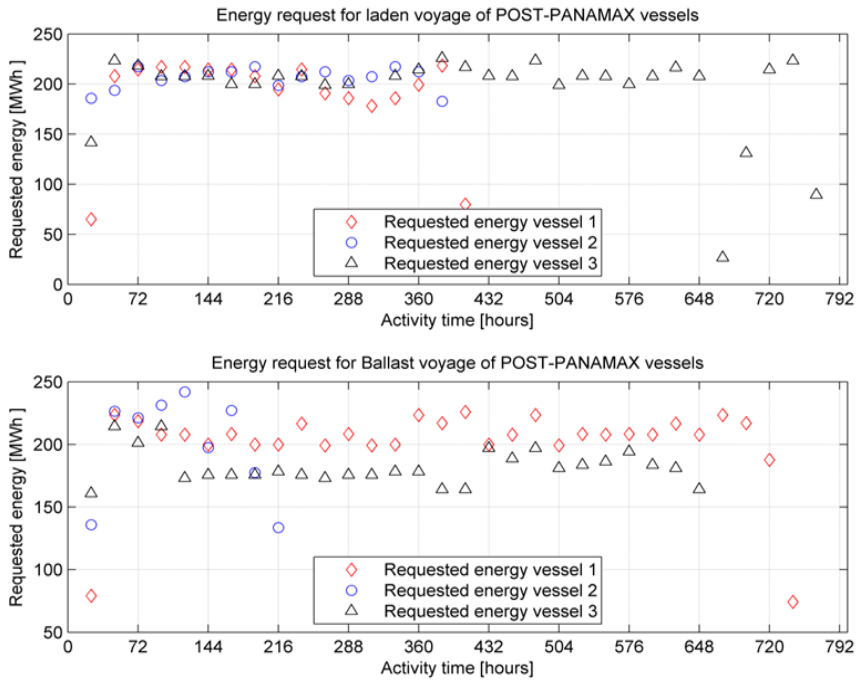


**Figure 3.12: Requested energy per day for every vessel and voyage type**

The operation of the Hybrid system is initially considered to function at discrete loads of the equivalent conventional propulsion engine. For the D-A2 concept, the total power output is formed by the algebraic sum of the optimum power output of each generator in operation. As a result, the energy production is made having the lowest possible SFOC not for a single load, but for every combination of maxima power outputs. These are referred to as the 'working points' of the Hybrid system. Table 3.6 represents the closest working point to the mean value of each voyage. Thus, the energy produced by the power output of the working point is considered to cover the average propulsion energy demand for the examined period. Nevertheless, it should be noted that, usually, generators intended for propulsion follow a SFOC curve similar to the two-stroke engine. On the contrary, generator sets oriented for auxiliary power have their optimised load near 100% of their MCR. Thus, for this purpose it is imperative for the generators to be optimised for the 100% of the power output. The investigation involves the worst-case scenario of prime mover selection, therefore the selected generator sets should be considered as propulsion generators which follow a normal cubic SFOC curve with the minimum value around the 75% of the MCR. Nonetheless, this assumption increases the initial cost of the system as the 25% of the power output is useless.

Table 3.6: Working Point of equivalent propulsion system to cover the mean power requirements for the three Post-Panamax sister ships

| Vessel: | Laden Voyage | Ballast Voyage |
|---|---|---|
| 1 | 80% | 80% |
| 2 | 80% | 80% |
| 3 | 80% | 70% |

Importing the values from Table 3.6 and combining them with the results of Figure 3.12, the energy distribution over the examined voyage duration is depicted in Figure 3.13.

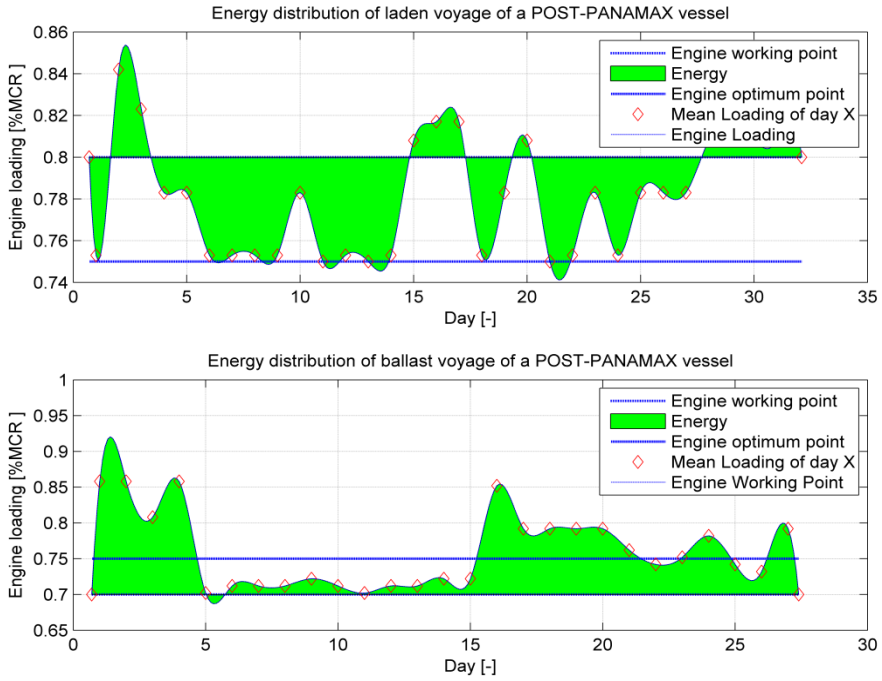


Figure 3.13: Example of energy fluctuation difference for laden and ballast Voyage of a Post-Panamax vessel (optimum point of operation is 75% of MCR) per day

This figure depicts the daily fluctuation of energy requirements for the vessel, if the Hybrid Power system was in operation. The in operation generators produce a power output equal to 80% of the conventional two-stroke engine MCR. However, the requirements of propulsion vary with time, and the working point differs from the actual energy demand. It should be noted that the working point comes from the statistical analysis of similar voyages and denotes an operational point that minimises the need for a large amount of installed energy. This minimisation occurs because the energy production is made around that point instead of the optimum which can be located even 20% off the actual operational point. Thus the standard deviation of the power demand is lower than before, therefore the required energy capacity of the storage medium is reduced accordingly. Judging from Figure 3.12, the energy storage medium, in order to meet the propulsive requirement, is forced to supply energy when there is an excess of demand. In

the opposite scenario, where the system has an excess of production, two potentials are identified. In the first potential, the system has either to decide to reduce the number of working generators, thus altering the working point and absorbing or storing energy. In the second potential, when the fluctuation does not permit the first option, yields to store energy to the energy storage medium without altering the engine loading. Option two is applicable to conventional Hybrid system. Therefore, in the ideal operation of the system, with no conversion losses and assuming a steady state time domain model, the green areas above and below each working points should be equal. This implies that, after a voyage, the system will have run in optimum condition and the storage medium will be fully charged. When battery charge/discharge conversion losses exist, these areas have to be equal with respect to the conversion losses. This means that the charging area (above the operational point) is greater that the area below. This difference is equal to the loss of power times the hours of operation.

Immediate conclusions for the energy storage installation and for the power output can be extracted. It can be observed from Figure 3.13 that the amount of energy that is available for storage, or is required to be supplied for the propulsion needs, is closely related to the working point of the engine as it was previously defined. The selection of this point can be further optimised and adjusted. Moreover, the installation of a Hybrid Power unit potentially allows the main engine to be smaller, since in the event of rough weather the extra amount of energy required for propulsion can be covered by the stored energy.

### 3.2.2 Sizing the Hybrid power system

The original ship design is assumed to remain constant so that the hull form and the propeller are unaltered. Further fuel savings by subsequent modification of the hull form were thoroughly discussed in Chapter 2. Hence, the overall system power delivered to the propeller remains the same. Potential reductions in the installed power will be a result of optimised selection of both engines and storage medium.

#### *3.2.2.1 Sizing the Diesel prime movers*

The installed engine on-board the examined Post-Panamax vessels is an MAN 7S50MC-C7 engine with specified Maximum continuous Rating (SMCR) of 11060kW at 127 RPM. The optimum point of operation is at 75% of the SMCR (MAN Diesel, 2007). In order to size the Hybrid Power system, two potential layouts will be investigated. The first concept includes six generator sets. With these six generators, 60% of the power will be supplied by two identical engines and the remaining 40% by four identical diesel generators. This selection is made in order to have larger engines which consume less fuel and for which heat recovery is better. This enables the system to cover the working points as efficiently

as possible, because the power combinations cover discrete points of 10% with the maximum efficiency. Hence, in cases of ultra-slow steaming, the SFOC of all engines is at the minimum value and the fuel efficiency remains high. Marine generator sets from two major manufactures suitable for the D-A2 Hybrid system are presented in Table 3.7.

**Table 3.7: Suitable Diesel generator sets (Tier II)**

| Manufacturer | Wärtsilä | MAN diesel |
|---|---|---|
| Type: 4 stoke Diesel generators and No | 2sets 9L32<br>4 sets 8L20 | 6L32/44<br>6L21/31 |
| Engine Output | 2x 4500kW<br>4x 1480kW | 4480kW<br>1320kW |
| Generator Output | 2x 4320kWe<br>4x 1405kWe | 4323kWe<br>1254kWe |
| Generator Efficiency | 96% | 96.5% |
| SFOC85% ISO conditions, dependent on number of cylinders | 2x 174-185g/kWh<br>4x 185-194g/kWh | 177g/kWh<br>188g/kWh |

#### *3.2.2.2 Sizing the energy storage medium*

The loading difference, as was previously explained, was multiplied by the MCR and the voyage time, in order to give the energy difference between production and requirement. These daily values are depicted in Figure 3.14 with the + symbol.

In order to estimate the actual storage capacity of the system during voyages, a regression algorithm was created by importing the statistic values of every vessel of a given type within the examined fleet. Based on the values marked with +, the pink regression curve is obtained.

The diamond symbol represents consecutive charging or discharging of the system with unaltered engine working point. As a result, the time difference between the diamond symbols is roughly 48 hours and may reach 96 hours of uninterrupted discharging or charging of the equivalent system. The spread of diamond symbols is validated by the fact that the reported average severe sea state can last to up to 3 days, although the sea description is valid up to 2 hours. Based on the diamond symbol, the second regression curve is obtained. In Figure 3.14, the everyday energy report model is found to be more accurate in the prediction of energy requirements than the total area energy model (diamond symbols), which overestimates the required energy due to the small sample of values and inserts uncertainty in the determination of the second regression curve. With the aim of determining the required energy storage capacity, the propulsion designer has to define the vessel autonomy time. Autonomy time is set as the time (hours) before battery energy is depleted.

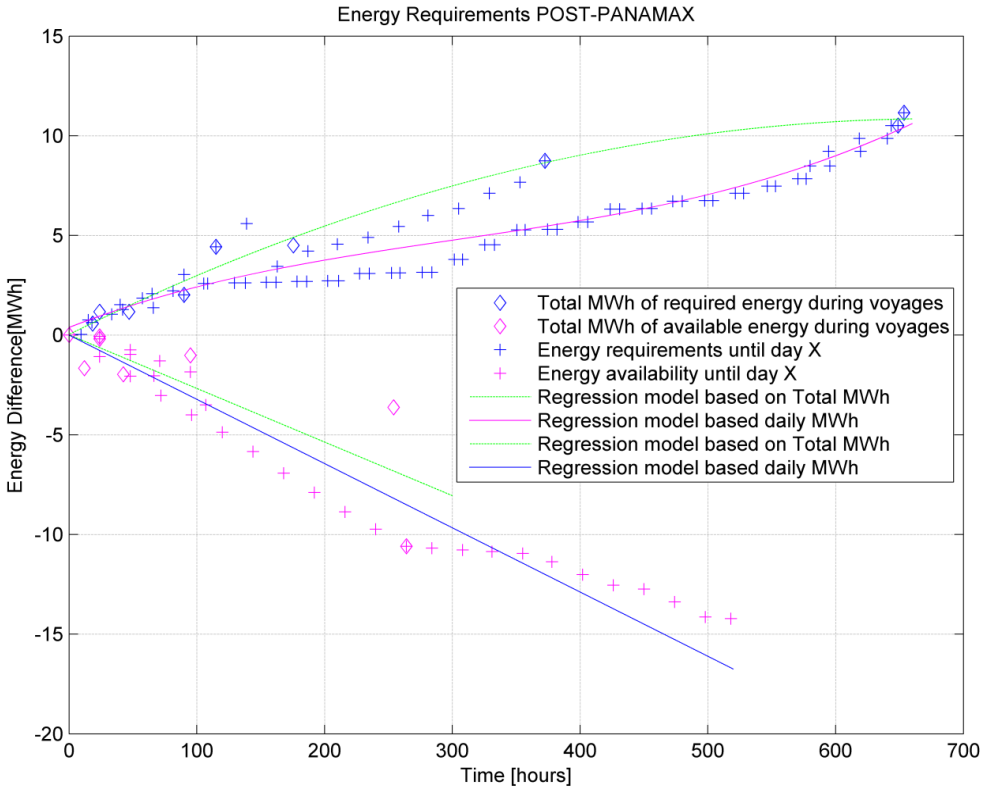


**Figure 3.14: Energy charging/discharging during at sea operation, from voyage's working point and application of regression analysis**

It can be extracted that the data presented with the diamond symbols is related to the 'autonomy radius' of the system. For the Marine Hybrid system, 96 hours autonomy time of the system is considered sufficient for bulk carrier applications. The results for 'at sea operation' for the bulk carrier fleet are summarised in Table 3.8, while the sizing graphs can be found in Appendix III.

**Table 3.8: Storage medium required energy capacity and maximum power output per vessel type for 'at sea' operation**

| Type of Vessel: | Installed MWh: | Power Output [kW] |
|---|---|---|
| Handysize | 8 | 1 |
| HandyMax | 8 | 1 |
| Panamax | 15 | 2 |
| Post-Panamax | 5 | 2 |
| Capesize | 4 | 1 |

Although the size of the energy storage medium is presented in Table 3.8, more aspects of energy availability have to be considered. It was previously mentioned that the energy storage medium at the end of the voyage has to be fully charged. This requirement is justified so the storage system has enough energy for sailing inside the Emission Control

Areas (ECAs). In these zones, an 'emission free' battery only operation is ideal, something which increases significantly the amount of stored energy and is dependent on the sailing speed and distance until the pilot station. Moreover, in certain sizing scenarios, sufficient stored energy has to be available for departure without engine operation while the cargo handling had also been performed without ship engine operation. The latter potential is possible when harbours are equipped with 'cold ironing' facilities. More energy demand scenarios can be identified, however, only some of them can be implemented without applied case specific storage capacity optimisation. Notwithstanding these variations, this project the sizing is concentrated on the voyage phase and it is assumed that the battery system is fully charged at the beginning and end of each voyage and these implications can be solved by optimally increasing the storage medium in future work.

## 3.3 Feasibility analysis

The feasibility check of the Hybrid system is made for an AES Hybrid (scenario D-A2) and a conventional Hybrid (D-B) system. A schematic representation of the investigated layouts is made in Figure 3.2 and Figure 3.3. Layout D-A2 has as basis the AES concept. The second scenario can be identified as a two-stroke Hybrid system with gearbox and electric motor similar to Power Take Off/In (PTO-PTI). The latter systems are constantly gaining ground in marine propulsion due to advantages in terms of safety and fuel consumption (Griffiths, 2006). The efficiency of each subcomponent was presented in section 3.1.5.

### 3.3.1 Operational feasibility based on voyage analysis

The voyage fuel consumption reported by the actual vessel is compared to the simulated consumption of the Hybrid Diesel Electric system. The introduced uncertainty regarding the on board fuel measurements and how the effect in this thesis is reduced was discussed in Chapter 2.

The system is using the batteries to apply load levelling in propulsion demands, hence discharge and charge are determined by the same operating loading profile of the examined voyage. This system was simulated with the constraint of fully charged batteries at the end of 'at sea' operation. Thus extra electricity, hence more fuel, is produced in order to charge the system, if the net value of energy production is positive at the end of the time period. The savings in terms of fuel using the Hybrid system are summarised in Table 3.9. The likely annual fuel savings in terms of total emission contribution to global savings from the bulk carrier shipping sector are presented in Table 3.10 for the maximum emission savings related to fuel consumption only and operation of medium speed engines in scenario D-A2. These values are the result of the projection of the acquired sample over

the global number of vessels of the same type, and exclude the likely numbers of days in port. It is clear that the number of vessels plays a significant role in the produced amount of exhaust gasses (Eyring et al. 2005).

**Table 3.9: Potential fuel savings, for D-A2 and D-B layouts per vessel type and for static efficiencies**

| Type of Vessel: | Number of Vessels in world fleet | Voyage Type: | Daily fuel savings [tonnes/Day] | | Voyage fuel savings [%][3] | | Single ship fuel savings/year (Fuel: 520$/t) up to [m. USD/year]: | |
|---|---|---|---|---|---|---|---|---|
| | | | D-A2 | D-B | D-A2 | D-B | D-A2 | D-B |
| Handysize | 1,774 | Laden | 0.065 | 1.6 | 0.3% | 7.7 % | 0.27 | 0.50 |
| | | Ballast | 3.7 | 4.7 | 22.6% | 28% | | |
| HandyMax | 1,732 | Laden | 0 | 0.2 | 0% | 0.7% | 0.00 | 0.03 |
| | | Ballast | 0 | 0.13 | 0% | 0.5% | | |
| Panamax | 1,383 | Laden | 2.6 | 4.6 | 8.6% | 15% | 0.50 | 0.80 |
| | | Ballast | 2.8 | 4.8 | 9.6% | 16% | | |
| Post-Panamax | 98 | Laden | 5.3 | 8 | 12.3% | 19% | 0.80 | 1.30 |
| | | Ballast | 3.4 | 5.9 | 8.8% | 15% | | |
| Capesize | 722 | Laden | 0 | 3.6 | 0% | 7.2% | 0.00 | 0.60 |
| | | Ballast | 0 | 3.3 | 0% | 7.5% | | |

In order to calculate the emissions from the projected decrease in fuel consumption through the application of Hybrid technology, the latter values were multiplied by the corresponding fuel based factor, to give a global projected result of emission savings per vessel category. As a subsequent step, the emissions savings were multiplied by the percentage of vessels making up that category in order to give the emission reduction results for the complete bulk carrier sector.

Finally, these values are multiplied by the percentage that this sector represents of the world fleet, giving the extrapolated result of a 14% decrease in emissions that could be achieved in the bulk carrier sector, using the maximum values of savings from the voyage data analysed. This corresponds to a 1.8% reduction in the emissions of world shipping. These projected savings are dependent on the voyage type, encountered weather and desired speed of the vessel and thus represent an upper limit on the likely emissions reductions that may be achieved through the adoption of Hybrid technology in this sector. Nonetheless, a larger sample of voyage data should be investigated in order to verify the projected values.

[3] Voyage dependent savings

Likewise, due to the fact that bulkers operate at low speeds and usually the fluctuation of loading is considered small, faster ships and especially containerships that share the largest $CO_2$ emission percentage (depicted in Figure 1.1) benefit the most from the Hybrid Power systems. Hence, if the proposed system is installed on these ships, the reduction percentage for the global shipping could increase more significantly.

**Table 3.10: Extrapolated for the global bulker fleet potential emission savings [m. tonnes/year] assuming 60% laden and 40% ballast voyages**

| Emission Gas: | $CO_2$ [m. tonnes/year] | | $NO_x$ [m. tonnes/year] | | $SO_x$ [m. tonnes/year] | |
|---|---|---|---|---|---|---|
| Voyage Type: | Laden | Ballast | Laden | Ballast | Laden | Ballast |
| D-B | | | | | | |
| HandySize | 1.800 | 3.500 | 0.050 | 0.098 | 0.030 | 0.060 |
| HandyMax | 0.230 | 0.095 | 0.006 | 0.003 | 0.004 | 0.002 |
| Panamax | 4.100 | 2.900 | 0.110 | 0.080 | 0.070 | 0.050 |
| Post-Panamax | 0.510 | 0.250 | 0.010 | 0.007 | 0.009 | 0.004 |
| CapeSize | 1.600 | 1.000 | 0.046 | 0.028 | 0.030 | 0.018 |
| D-A2 | | | | | | |
| HandySize | 0.070 | 2.800 | 0.210 | 0.220 | 0.001 | 0.050 |
| HandyMax | 0.000 | 0.000 | 0.250 | 0.130 | 0.000 | 0.000 |
| Panamax | 2.300 | 1.700 | 0.320 | 0.210 | 0.042 | 0.030 |
| Post-Panamax | 0.330 | 0.140 | 0.028 | 0.014 | 0.006 | 0.003 |
| CapeSize | 0.000 | 0.000 | 0.180 | 0.120 | 0.000 | 0.000 |

### 3.3.2 Financial feasibility based on voyage analysis

The type of storage system determines the economic feasibility of the Hybrid ship concept. As seen in Dedes, et al. (2010) and described in section 3.1.2, the Vanadium Bromine redox flow cell and the Sodium Nickel Chloride batteries are suitable candidates for Hybrid power systems. Redox flow cells are reported to have a life period of more than 10000 cycles (Divya and Østergaard, 2009), while Sodium Nickel Chloride batteries have reported life cycles of over 4000 (Dustman, 2004). Based on the reported estimated engine loading and operating engines as described in Figure 3.10, ship operations are unlikely to exceed 2500 cycles (full charging/discharging) over a 25 year period. As a result, no cost for replacing the storage medium will be assumed. However, sets of complete voyage simulations will define a mean number of cycles per voyage, which can be extrapolated to identify vessel life time cycles.

The cost of the equivalent propulsion unit is increased compared to the conventional two-stroke diesel. Aside from the storage medium cost, a difference in price exists between large two-stroke diesel engines and smaller Diesel generators. The cost of a propulsion system using this system is estimated by the Benford equation (3.3.1)

$$C_{OTM} = A_M \cdot SHP^{0.7} \tag{3.3.1}$$

where, $A_M$ is a constant and taken as equal to 2050$/kW (Mulligan, 2008).
The man hours of labour are given by equation (3.3.2)

$$MHS_M = 20000 \cdot \left(\frac{SHP}{1000}\right)^{0.30} \tag{3.3.2}$$

Where,

SHP : Shaft horse power [kw]

The total cost of the working labour is given by

$$C_{MW} = K_{KHRM} \times MHS_M \tag{3.3.3}$$

where, $K_{MHRM}$ = 30$ which is the man hour cost, (average ship yard labour cost, China is excluded from the calculation (Mulligan, 2008)).

Such calculations indicate that the cost of the main engine is approximately 250$/kW. However, the typical cost of diesel generator engines is significantly higher than the main engine. A typical price per kW of diesel generators is 350$/kW (Fragkopoulos, 2007). Although the initial cost of such engines is higher, the advantage of prefabrication

and the modular application of the machinery components leads to savings in construction man-hours by shortening the overall construction time of the vessel. Thus, the total construction costs are potentially reduced (Prousalidis et al., 2003), although this statement is not investigated further here. Furthermore, cost difference exists due to the installation of electric motors, cabling and other components of the electrical installation. An overall 6% increase in machinery cost will be assumed as the cost of the electrical components. The machinery cost is taken to be 30% of the total cost of the ship (Papanikolaou, 1991). Thus the extra machinery cost represents a 2% increase in the overall price of the vessel. The market value of the vessels is taken according to the current market state (Cotzias Shipping Group, 2010). Concerning the fuel price market, an average value for the year is taken equal to 520$/tonne (Petromedia LTD, 2010). However, the trend of fuel prices shows that its price is likely to increase in future years. As a result, a rate of price increase of 10% each year is assumed. It is further assumed that after 25 years the storage system can be sold for 10% of the original cost.

For an initial evaluation of the economics of the Hybrid concept, the dynamic index of Internal Return Rate (IRR) is adopted. The income of the investment is that calculated as fuel savings per year multiplied by the dynamically changing fuel prices.

$$\sum_{j=0}^{n} \frac{FS_j}{(1+IRR)^j} = Cost_{HYBRID} + \sum_{J=1}^{n} \frac{C_j}{(1+IRR)^j} \tag{3.3.4}$$

where, $FS_j$ is considered as 'income' of the investment and is equal to the calculated and projected fuel savings per year per vessel and $C_j$ are the maintenance costs as follows:

$$\begin{aligned} C_1 &= OM_{hybrid} \\ C_j &= C_{j-1} \cdot e \end{aligned} \tag{3.3.5}$$

Table 3.9 shows the simulated fuel savings obtained by the optimisation of energy flow and using the Hybrid technology on-board ships. Hence,

$$FS_j = FS_{j-1} \cdot e_1 \cdot e_2 \tag{3.3.6}$$

where, $OM_{Hybrid}$ is equal to 0.08$/kWh for the Sodium Nickel Chloride batteries. For the redox flow cell batteries, it is equal to 0.0008$/kWh.

The investment will be funded by a fixed interest rate bank loan. The rate ($R_L$) is equal to 8% and the loan payback period ($N_L$) is 10 years. Every instalment amount is given by the equation (3.3.7):

$$A_{Lt} = L_{FF} \cdot \frac{r_L}{1-(1+r_L)^{-N_L}} \tag{3.3.7}$$

A Post-Panamax vessel ideally operates for 340 days per year on average and spends 60% of the time in laden and 40% of the time in ballast condition (Psaraftis and Kontovas, 2008). A five-day period per month on average for charging/discharging is assumed as port time. As a result maximum 280 days remain for voyages.

The Internal Rate of Return value provides a means to assess whether the initial investment is worthwhile. A suitable threshold value of IRR is considered to be 10% (Osborne, 2010). Every scenario above this value is considered worthwhile from a purely economic perspective. In alternative cases, either the scenario is judged economically unfeasible or potential improvements in technology, relative to the current state, will improve the economic criterion of the investment. It should be noted that IRR values depend on the fluctuating market costs of materials.

It is likely, as the market for large-scale energy storage systems increases, that there will be corresponding reductions in costs. Table 3.11 presents calculated values of IRR for each vessel type within the fleet examined and for the two storage media considered. The results suggest that a system based on Sodium Nickel-Chloride batteries is economically feasible in most vessel types and the payback period is very attractive. Vanadium redox flow batteries, on the other have, seem to have potential in the future.

**Table 3.11: Internal Rate of Return for conceptual Hybrid power layout**

| Type of Vessel: | Installed MWh: | Storage System: | Internal Rate of Return: | |
|---|---|---|---|---|
| | | | Scenario 1: | Scenario 2: |
| Handysize | 8 | Sodium Nickel-Chloride | 11.5% | >100%[4] |
| | | Vanadium Bromine | 2.0% | 25.1% |
| Handymax | 8 | Sodium Nickel-Chloride | 0% | 0% |
| | | Vanadium Bromine | 0% | 0% |
| Panamax | 15 | Sodium Nickel-Chloride | 20.0% | >100%[4] |
| | | Vanadium Bromine | 1.4% | 16.6% |
| Post-Panamax | 5 | Sodium Nickel-Chloride | 71.7% | >100%[4] |
| | | Vanadium Bromine | 33.0% | >100%[4] |
| Capesize | 4 | Sodium Nickel-Chloride | 0% | 61.6% |
| | | Vanadium Bromine | 0% | 27.6% |

[4] The value is >100% because in Handysize, Panamax, Post-Panamax, the payback period is 8, 19, 3 and 1 years respectively instead of 25 in other cases.

### 3.3.3 Technical feasibility assessment

This section investigates the technical feasibility of energy storage devices installed on bulk carriers through use of a systematic concept design variation. Likely values of energy losses due to conversion are also considered. Through observation of engine variations and the operational curves of the engine, the potential fuel savings of the Hybrid system are compared to the conventional propulsion system. The Hybrid system assumes a scenario of constant speed operation. Any variance in loading and any peak requirements will be supplied from the storage system by applying load levelling to the system. Thus, diesel engines are either switched off to reduce the total fuel consumption or are operated at constant load resulting in the engine to be always loaded at the optimised consumption point so to have the minimum Specific Fuel Oil Consumption (SFOC). In order to achieve significant fuel savings, the variance should exceed a certain percentage determined from the SFOC curve of the engine. The amount of fuel saving is dependent on the observed fluctuations.

A system engineering approach is applied (Elliot and Dearsley, 2007), which is holistic in its attempt to improve the Energy Efficiency Design Index (EEDI) of ships both in terms of design and operation, although Hybrid ships are currently excluded from the calculation of IMO. This requires an understanding of the trade-off between system complexity and resultant new build cost against reductions in operational through-life cost and exhaust emissions. The adopted methodology is presented and, through this, the constructional and technical feasibility of the concept are demonstrated. The latter is examined for new-builds based on a proposed and non-developed concept design together with an investigation for retrofitting current designs for new-buildings, or on newly built ships with a short operational life, with the Hybrid technology. In assessing the technical feasibility, the calculation of engine room volume is critical and is performed first, along with a record of all free spaces on board existing vessels. In addition, the weight calculation and distribution are noted so that that any trim issues that might arise can be inserted in the calculation of major loading conditions of the examined ship type. Finally, the energy storage devices and the electric components are introduced and their weights and volumes are inserted in calculations affecting the trim and filling of the free spaces. The new components and the battery system have known volume and have to fit into the current compartments as well as maintaining the Ship's lightweight and with a minimal impact on cargo capacity and hence economic viability of the initial vessel.

### *3.3.3.1 Estimation of volume requirements*

Whilst Hybrid diesel electric propulsion may appear a promising means of emissions reduction, its technical viability needs to be assessed against the requirement of not increasing the size of the engine room or by reducing the areas reserved for cargo. The components that absorb the largest volume are the battery storage medium and the prime movers. The installed capacity for the two battery candidates and the four stroke Diesel prime movers is found in Table 3.12.

**Table 3.12: Hybrid energy requirements according to ship type (Dedes et al., 2010), required installation volume per battery type and generator type for the conceptual case**

| Ship Type | HandySize | HandyMax | Panamax | Post - Panamax | Capesize |
|---|---|---|---|---|---|
| Required Energy [MWh] | 8 | 8 | 15 | 5 | 4 |
| Required Battery Volume $m^3$ | | | | | |
| 1) Sodium Nickel Chloride 190Wh/L | 42 | 42 | 79 | 26 | 21 |
| 2) Vanadium Redox Flow 30Wh/L | 267 | 267 | 500 | 167 | 133 |
| Engine Room Volume [$m^3$] | 3800 | 4530 | 4900 | 5150 | 9600 |
| Free volume in current engine room: 35% of total volume | 1300 | 1580 | 1650[5] | 1760[3] | 3350 |
| Added Volume due to electric components: 1040$m^3$<br>Additional Engine Volume: 2x100.4$m^3$ + 4x59.30$m^3$ = 438$m^3$ | | | | | |
| Suitable for installation only in ER for 1): | no | yes | partially | yes | yes |
| Suitable for installation only in ER for 2): | no | no | no | partially | yes |

Thus, it is crucial to estimate the available volume of the engine room. An estimate of engine room volume may be obtained by using SNAME (1990),

$$V_E = 21.6 \cdot f_6 \cdot f_7 \cdot f_8 \cdot \left( 9.55 \cdot \frac{bkW}{RPM} \right)^{0.83} \tag{3.3.8}$$

where,

$f_i$ : Volume coefficients defined in SNAME (1990) [-]

bkW : Break horse power [kW]

RPM : Engine rotational speed [RPM]

[5] Denotes measured values

On account of the fact that equation (3.3.8) does not describe modern designs, a direct measurement was performed using vessel drawings. By this means, the actual volume of the engine room for a Panamax type bulk carrier is 88% of that estimated by equation (3.3.8). For a Post-Panamax type, the corresponding figure is 90%. These figures reflect the more compact engines installed in modern designs. The volume used in subsequent calculations is thus taken as 5150 $m^3$.

In Appendix Table 3 of Appendix II, the volume of each engine room component in a conventional two-stoke installation in a bulk carrier (Panamax and Post-Panamax types) is presented. Where available, the weights of the components are cited. It can be seen from this table that many items are not connected to the type of propulsion system used and are associated with the operation of the vessel. These items are thus accounted for in equivalent propulsion systems. Concerning the existence of pumps and other hydraulics, a separation was attempted with the intention of justifying those that can be replaced in an electric propulsion system, or even neglected.

Appendix Table 1 presents components representative of those installed in a modern cruise ship with integrated full electric propulsion, equipped with conventional propulsion shafts instead of podded propulsion units. The power output for propulsion of such a vessel is four times the power required by a bulk carrier. The examined cruise vessel is equipped with two Synchronous motors of 21MW rated power. Each one weighs approximately 150 tonnes. Using this information, an approximation can be made for a bulk carrier installation.

Recent technological improvements indicate that the weight for the same nominal output (20MW) could be reduced to only 89 tonnes and with more compact dimensions (Lewis, 2007). In subsequent calculations, the weight of an electric motor rated at 10MW is taken as 75 tonnes. Although the extra volume for electric components is presented in Appendix Table 1, the dimensions of rectifiers, inverters, transformers and other parts of the circuits are relative to the number of generator sets. A general overview of the dimensions and weights is given for the equipment list of the fleet of cruise ships that were examined. The weight of the generator sets is lower that the weight of a conventional two-stroke diesel. However, for large power outputs and depending on the propulsion system design, more than two generator sets have to be installed. Hence the total weight of the engines including the appropriate electrical motor can vary from -10% to +10% of the equivalent conventional engine weight.

For the examined Post-Panamax type ship, the increase in weight is 1.7% and is connected to the number of generator sets. The added weight for the propulsion system also has to account for the added mass of the storage medium. Using the preliminary sizing

for the energy storage system, the final added weight to the Hybrid vessel is given as a percentage of lightweight in Table 3.13.

**Table 3.13: Added weight to the vessel due to propulsion system retrofitting and installation of energy storage medium**

| Ship Type | HandySize | HandyMax | Panamax | Post-Panamax | Capesize |
|---|---|---|---|---|---|
| Required Energy [MWh] | | | | | |
| | 8 | 8 | 15 | 5 | 4 |
| Required Battery weight [tonnes] | | | | | |
| Sodium Nickel Chloride 150Wh/kg | | | | | |
| | 70 | 70 | 130 | 43 | 35 |
| Vanadium Redox Flow 50Wh/kg | | | | | |
| | 160 | 160 | 300 | 100 | 80 |
| Final Added weight to the vessel (propulsion system + storage) | | | | | |
| | 323 | 323 | 384 | 297 | 288 |
| | 414 | 414 | 554 | 354 | 334 |
| Increase in Lightweight [%] | | | | | |
| | 4.1% | 3.4% | 3.2% | 2.0% | 1.2% |
| | 5.2% | 4.3% | 4.7% | 2.4% | 1.4% |

### *3.3.3.2 Estimation of hydrostatics and cargo loss*

The construction of the engine room greatly affects the ship design from the hydrodynamic, aerodynamic, trim and stability points of view. It is fundamental to allocate the weight of the lightship such that when the ship is loaded, the trim of the vessel is as close as possible to zero. According to research performed in (IMO, 2009), achieving optimal trim of the vessel can result in fuel savings of up to 2%. Table 3.14 presents the most probable loading scenarios of this ship type in operation. The vessel trim is described by,

$$Trim = \frac{(LCB - LCG) \cdot \Delta}{MTC \cdot 100} \tag{3.3.9}$$

Due to changes in the total machinery weight, the proposed retrofitting of the machinery arrangement and the installation of energy storage devices and electric components for electrified propulsion should be performed in respect of the trim values. Design issues arise if the vessel is designed to have zero trim while no cargo is present. The case of zero ballast water and zero trim has to be further investigated. However, the design is mainly performed for the full load departure and full load arrival conditions, where cargo is present. The current form of bulk carriers, where the LCB is located forward of the amidships section, is directed at achieving this aim. Fore and aft asymmetry to the cargo holds does not permit any drastic change of weight distribution. It can be observed from

the Table 3.14 that the full load departure condition has no trim. On the contrary, every other condition has trim and, most of the time, ballast water. Any future weight distribution of the current design requires a compromise between the full load departure condition and the remainder of conditions in order to optimise trim and reduce the amount of required ballast water.

**Table 3.14: Loading Conditions of examined Post-Panamax bulk carrier**

| Condition | Cargo [tonnes] | Cargo Loss % | Ballast [tonnes] | LCB [m] | LCG [m] | MTC [tm] | Trim [m] |
|---|---|---|---|---|---|---|---|
| Normal Ballast Departure | 0 | 0.00 | 23414.3 | 117.126 | 117.189 | 1040.2 | 2.08 |
| Normal Ballast Arrival | 0 | 0.00 | 26061.1 | 114.757 | 114.855 | 1068.1 | 3.045 |
| Heavy Ballast Departure | 16487.1 | 0.00 | 23411.7 | 115.991 | 116.059 | 1226.5 | 2.667 |
| Heavy Ballast Arrival | 16487.1 | 0.00 | 24476.8 | 116.88 | 116.682 | 1191.4 | 2.265 |
| Grain Departure SF65 | 60188.4 | 0.00 | 2250.7 | 116.664 | 116.702 | 1346.4 | 1.674 |
| Grain Arrival SF65 | 60188.4 | 0.00 | 2250.7 | 118.866 | 118.879 | 1298.4 | 0.514 |
| **69990 tonnes DWT cargo Departure** | **65152.1** | **0.54** | **0** | **115.448** | **115.501** | **1364.5** | **2.323** |
| 69990 tonnes DWT cargo Arrival | 65152.1 | 0.54 | 0 | 117.517 | 117.548 | 1331.3 | 1.205 |
| Homogenous Design Departure | 67858.4 | 0.52 | 0 | 115.656 | 115.702 | 1364.6 | 2.09 |
| Homogenous Design Arrival | 67858.4 | 0.52 | 0 | 117.668 | 117.693 | 1336.3 | 0.983 |
| Grain Departure SF42 | 87866.1 | 0.40 | 0 | 116.837 | 116.841 | 1392 | 0.335 |
| Grain Arrival SF42 | 87866.1 | 0.00 | 939.4 | 117.483 | 117.482 | 1384.9 | 0 |

Table 3.14 highlights the minimal cargo loss associated with the additional weight and volume of the necessary equipment for the proposed Hybrid power installation, expressed as a percentage of the cargo carried. The extra weight may be subtracted from the ballast water, as added lightweight reduces this amount and when no ballast is present, this weight reduces the cargo capacity. The worst case scenario is depicted in bold letters and considered to be the minimum cargo capacity, with zero ballast, 100% filled fuel and fresh water tanks, full provisions and minimum trim. The cargo loss is expressed as a percentage of the initial loaded cargo.

It can be determined from Table 3.14 that cargo loss is related to the cargo transported and to the presence of ballast water. The lower the cargo capacity of the vessel, the higher the percentage cargo loss and vice versa (e.g. in Post-Panamax the cargo loss is 0.54% and reaches 0.78% for Panamax in Homogenous Loading).

### *3.3.3.3 Design and construction parameters*

In order to install the Hybrid power system components in existing ship designs, typical general arrangements, profile and decks plans and structural drawings have to be studied. The extra volume of the battery system and components of the fully electrified propulsion system are given in Table 3.12. A proportion of this volume can be installed in the engine room (E/R) if there is sufficient space. The major contributors to the required volume are the components for the electrified propulsion system. It is important that these be installed inside the engine room. An approximation of the engine room volume following installation of the components is also presented. If the final available volume is insufficient, other free and void spaces have to be selected in order to install the energy storage system. For the battery arrays, the battery volume can be a significant proportion of the total required volume. For example, in the case of a 15 MWh installation (Panamax vessel), the required battery volume is almost 25% of the total volume required. A void space is an enclosed space, with access and/or ventilation below the main bulkhead deck, astern and forward of the cargo length of bulk carriers excluding spaces for dedicated water ballast, carriage of cargo, storage of substances (e.g. HFO, provisions), installation of machinery and space used by crew. This compartment is suitable for energy storage devices since, being located at the fore peak it improves the zero trim condition. The volume in certain designs approaches 1200$m^3$. The space is accessible through manholes from the Bosun's store and the height of the compartment is sufficient for easy handling and removal of components and inspection. However, the bow section of the vessel suffers from movement and slamming, hence the behaviour of batteries subject to such motions requires further investigation. Nevertheless, Common Structural Rules (CSR) and flooding scenarios set high standards for the longitudinal strength of the ship in specific damage conditions. This implies restrictions in weight allocation in forward and aft void or ballast compartments, as in certain scenarios the calculated bending moments exceed the maximum allowed value for the structural integrity.

Another potential void space is the lower stool of bulkheads above the double bottom. The preferable selections have to be made as close to the forward perpendicular (between cargo holds 5, 6, 7) as possible, in order to create a constant lever around the amidships point. This space is accessible while cargo is present through manholes or weather tight hatches on the main deck. However, the manhole openings are located inside the involved or adjacent cargo hold, something that does not allow any repairs that involve equipment removal. For the case of Sodium Nickel Chloride batteries, due to the increased temperature, natural or mechanical ventilation of the energy storage areas should be available. At the lower or upper stools, mechanical ventilation can be achieved using high

speed electric motors that drive a fan. The heat exchange is proportional to the air mass flow. Hence, a large number of air changes per hour is required. In bulk carriers that are certified to carry dangerous goods, mechanical ventilation which is able to change 8 times the capacity of the hold is installed with success. Thus, it is believed that heat exchange can be made using this way and the location of the fans to be in mushroom type ventilators located on top of the mast houses. Cases such as water or oil cooled battery packs can be achieved mainly in double bottom areas in Forepeak tank and in lower stools. In smaller vessels, such as handysize and handymax bulkers, a pipe tunnel at the centreline exists. This pipe duct accommodates the bilge and ballast lines. There is free space to install a 3rd pipe that will be responsible for energy storage cooling.

However, for maintainability, repair and regular visual control of the system, potential spaces have to be well thought out. Each compartment has to be easy to inspect and maintain without any cargo removal. In case of failure, or flooding, a manual shutdown of the electric system has to be implemented. Meanwhile, each array of batteries should have the capability of isolation in case of damage. The access of the battery arrays though the pipe duct enable the inspection capability during the voyage. Moreover, the access through man holes and the existence of a wagon inside the duct permit excessive repairs and transfer of spares easily from the E/R.

On the other hand, the already mentioned forepeak void space should be examined. Unfortunately, a cooling installation can increase the cost of the system and, above all, limit the space reserved for battery equipment. Moreover, depending on the for peak design, ventilation ducts may be difficult to install. It should be mentioned though that additional space is required for the secondary circuits and systems of the battery. In addition, for protection purposes, it is advisable to have a switchboard panel installed in every compartment that stores a significant amount of energy, for minimisation of the short circuit risk and the possibility of overall storage system failure. In addition, the length of power cables that will run through pipes located on top of the main deck increase also the cost. Moreover, dependent on the voltage and current, proper screen type cables should be installed, so to decrease potential interference with the electronic remote control and sensors of the ship. However, this problem is already covered by classification society's rules.

In the case of Redox flow batteries storage can be achieved in a similar manner as with Heavy Fuel Oil (HFO). Tanks allocated in the double bottoms can be used. However, these areas are mainly reserved for HFO storage in built vessels. According to the new MARPOL regulations concerning the storage of heavy fuel oil, the wing side tanks will be used instead of double bottom tanks. The regulation (Annex I regulation 12A) applies to all new-buildings delivered after the 1st of August 2010. Thus, the double bottom space will

be reserved for ballast water. As a result, the designs of new ships with minimum water ballast influence the storage of the reactants, because these designs with a V shape hull under the design waterline minimise the void spaces and limit the potential storage areas. Though a reduction in fuel oil consumption was statistically demonstrated with the Hybrid system, hence, the requirement to carry more HFO in tanks can be altered and space reserved for HFO can now be used for the electrolyte reactants allowing a flexible determination of storage areas. The largest environmental impact of Redox flow batteries is the polypropylene tanks, the flow frames and the steel stacks (Rydh, 1999). Thus, additional tank retrofitting should be made, in order to accommodate the reactants. Given the industrial progress in marine paints, the coating of these tanks does not pose problems. In addition, the location of the wing tank reserved for HFO is between the cargo hold and the ballast water top side tank, so in cases of collision, the HFO or the battery reactant has a penetration protection of a couple of meters. Hence, the risk of damage is significantly reduced. Nonetheless, energy is required to pump the reactants towards the proton exchange membrane. The latter should be always positioned inside the E/R so to be easily monitored and maintained. Thus, area close to the E/R should be ideal positions in terms of secondary energy loss. For both battery media, an existence of a deep tank forward of the E/R bulkhead could be the best solution. If the volume of the deep tank would be reserved for the energy storage system, then the access to this compartment can be made using watertight doors, simplifying the access problem significantly. Nonetheless, the weight distribution should be carefully studied.

Given that the allocation of the weight can be performed in an optimum way, a selection of proposed compartments for housing the systems has to be performed. However, before discussing these potential arrangements in detail, the following design constraints affecting the overall ship design have to be examined.

The location and type of propulsor have to be selected, as does the location of the superstructure. The superstructure and its associated air drag contribute to the overall resistance of the vessel. Meanwhile, an optimum location of the bridge deck can allow better navigation if it is located near the bow. In the case of a propeller, a shaft system is required. The weight and the length of the shaft system are associated with the volume and compartment arrangement at the stern. It is not optimum to have large shafts and this is one of the reasons why a conventional two-stroke diesel engine is located as close as possible to the stern. In that case, the engine room compartment has to be located at the stern to house the main engine and the exhaust piping, which usually requires the superstructure to be located on top of the engine room and astern. Therefore, there is no capability to alter the design and allocate the weights differently.

The potential of electric propulsion allows a different approach in the design of the stern and overall layout of the ship. Electrified propulsion uses electric cables as the medium for power transfer instead of mechanical connections, and this allows alternative locations of the prime movers to be considered, with subsequent optimisation of the hull form at the stern. However, the location of one or multiple engine rooms must be combined with the constraints of available space for cargo holds. As a result, the bow and stern are the most suitable spaces for machinery allocation. For a conventional electric propulsion system, electric motors and a shaft system are required. Due to the small dimensions of electric, motors the housing compartment can have limited dimensions in length.

The combination of diesel electric and energy storage devices permits the use of the void space above the electric motors for the installation of a part of the storage system, while housing the steering gear system in the adjacent room. Prime movers can be vertically installed in a bow compartment, while a boiler room and/or turbine generators can exploit the rest of the space. Concerning the electric equipment (summarised in Appendix Table 1), it is recommended that it be located in different rooms, preferably in separate watertight compartments. For example, electric motors and control inverters should be in the same watertight compartment. The converters, located in a dedicated room, have to be situated as close as possible to the motors to reduce the length of the cables. On the other hand, generators can be placed wherever the ship design allows it. Concerning the superstructure decks, they can have the same use as before, while the construction and the design should take into account the aerodynamic drag and the wave spraying in case of slamming events.

An alternative approach with electric propulsion is the use of podded drives that combine steering and propulsion capabilities and do not require any space for electric motors inside the hull. However, a dedicated compartment for steering the pods is essential. Any free space can be covered by a set of batteries, if an energy storage device is applicable. On top of this compartment, mooring equipment and bosun store can be constructed. The rest of the machinery, along with the rest of the battery storage system, can be installed in the bow section. The discussion on the modifications in existing ship designs has been presented in Dedes et al. (2013a).

## 3.4 Chapter summary

This chapter presented the statistical analysis of a set of laden and ballast bulk carrier voyages. The adopted energy approach formed the basis of the Hybrid Diesel layouts and of the appropriate sizing of the Hybrid machinery components. The sizing of the system is dependent on the statistical sample. It was found that an every-day mean analysis is suitable for sizing the energy storage medium and the prime movers. Moreover, the sizing of the battery system is defined by the operational point of the prime movers. For this reason a detailed table with the proposed energy capacity and the maximum battery power output was presented. Nonetheless, the statistical analysis revealed the need of a detailed ship voyage simulation for accurate estimation of power demand. This simulator is implemented mathematically in Chapter 4 while its representation in computer environment is made in Chapter 5.

The examined Hybrid scenarios proved to be financially viable with high IRR, constructively feasible, in terms of added volume and added mass to the vessel displacement and lightweight respectively. A set of void spaces was considered for the installation of the battery equipment such as the forepeak void space, the double bottom tanks and areas inside the engine room. It was proved that the payload reduction is negligible compared to the overall fuel savings and the vessel trim is reduced in many of the important loading conditions. In the worst case scenario, the payload capacity was reduced by 0.54% and the vessel was sailing even-keel during departure condition.

This chapter also demonstrated the complete Hybrid – Diesel. The energy storage medium which inserts the hybridization degree in the power train is consisted of batteries. The proposed battery technologies which were demonstrated as feasible for the Hybrid layouts are the Sodium Nickel Chloride battery type and the Redox flow batteries which is a novel battery type for Hybrid electric vehicles. Both technologies offer significant advantages which were described. However, due to the maturity of Sodium Nickel Chloride batteries and the durability in the marine environment, is used for the further analysis.

A set of auxiliary and propulsion 'parent' engines was selected for sizing purposes. In addition, the machinery component efficiencies were presented in a tabular or graphical way, in order to form the mathematical models which are presented in Chapter 4.

Parts of this analysis where published in Energy Policy Journal (Dedes et al., 2012a) and in Transactions of RINA (Dedes et al., 2013a).

# 4 Mathematical Modelling

This chapter presents the governing equations that describe the Hybrid Power module and the ship simulator. The mathematical modelling is separated into two logical parts. The first part describes the governing equations of the Simulink® environment blocks which are presented in Chapter 5, while the second part defines the governing equations of the optimisation algorithm. The latter is responsible for the operation or not of the Hybrid module. The results of the simulation and optimisation are described in Chapter 6. The applied models in this thesis are proposed by the literature for this type of studies (Molland et al. 2012; Schneekluth and Betram, 1998). When applicable, the original publication is cited. Furthermore, IMO in the second green-house emission studies (IMO, 2009) accepts the applicability of these models for accurate approximation of ship calm water and added resistance.

## 4.1 Ship – Environment interaction modelling

This part defines the governing equations of the ship with the fluids around its hull. This interaction entails a level of complexity and it is imperative to model the calm water resistance, the added resistance, the hydrodynamic induced loads, the wind resistance, and the propeller model. Finally, in order to simulate the marine environment, the simulator can either import mean reported data, or a generation of environmental parameters is required. Models and assumptions for the parameter generation are described.

### 4.1.1 Calm water resistance approximation

In order to simulate the calm water resistance of a ship, a set of resistance approximation methods was investigated. The reviewed resistance prediction methods are expressed by means of a tabular and/or a graphical and/or a mathematical model. The mathematical model contains the regression analysis equations. Resistance prediction methods using regression analysis can be directly used for simulations. The other two formats can be indirectly implemented in a computer environment. Typically, tabular data can be suitably transformed using statistical methods to derive one or more equations from the data, which are then utilised in the simulation code. In addition, tabular data can be represented by interpolation. Graphical data can be treated in the same way as the tabular; however, the precision depends on the quality of the graph and the number of selected key points. Data handling is achieved by using interpolation methods such as linear interpolation, Taylor's 2$^{nd}$ order interpolation (Aughey, 1968) and Thrilheimer cubic spline (Versluis, 1977). At the higher and lower speed ranges, the resistance curves characteristically tend

to flatten out. Therefore, when extrapolating beyond the bounds of the speed range of any method, linear extrapolation is assumed to best approximate this trend (Moody, 1996).

The methods examined for simulation are a combination of graphical and tubular, and one method is based on regression analysis. Each method has restrictions in applicability. Table 4.1 summarises the applicability of each method and its publication date in order to determine whether that method is still valid for modern ship forms.
The first method was developed by Hoof and Nicholson (1948), and is intended for fast vessels with prismatic coefficient lower than 0.80 ($C_P$<0.80).

In 1954, Lap developed a calm water resistance method applicable to single screw merchant vessels. The method was based on model testing of modern – for that period – hull forms. Keller, in 1973, updated the method for application in large vessels with a high block coefficient ($C_B$). This method can be used for most normal and full ships in full load condition, but with less accuracy for ships in light load condition (Journee, 1976).

In 1940, SSPA published a resistance method not directly applicable to bulk carriers. It was based on a series of vessels with U hull form. The results were intended for $0.525 < C_B < 0.725$.

Another method intended for bulk carriers is the Japanese single screw vessel series, developed by the Shipbuilding Research Association of Japan in 1964. It was based on 35 model tests in a testing basin. This method has been developed for fast slender ships with $C_B \leq 0.84$ and the length to beam ratio should be less than or equal to 6.17 ($L/B \leq 6.17$).

Todd (1963) published a graphical method for resistance approximation for single screw merchant ships. Adequate data can be derived from the series '60' to calculate the residual Resistance $R_R$. Restrictions in block coefficient apply, and the applicability of the method is dependent on the position of the LCB together with the Beam to Draft ratio (B/T).

Guldhammer and Harvald (1974) published a graphic method that correlated the data of Taylor, series 60, SSPA and NPL methods. The parent hull form that was used to export results had no bulbous bow, destroyer stern type and normal shaped form. Due to its limited applicability because of the 'parent' form, the results are corrected in order to describe modern vessels. The method is intended for $0.15 \leq Fn \leq 0.45$, $4 \leq L/V^{1/3} \leq 8$ and $0.5 \leq C_P \leq 0.85$.

BSRA is a standard method of analysing speed trial results, published in 1964. The shaft power curve is the basis for corrections, where resistance is added using a derivative of the power curve (ITTC, 2002). The BSRA series was formed by independent model sets, which were formed using a geometrically altered 'parent' form. To extend its applicability and in order to interpolate different forms, four series where considered as

basic. In order to apply the method and correlate the examined vessel to one of the 'parent' forms, the block coefficient should range from $0.65 \leq C_B \leq 0.875$ (Schneekluth and Bertram, 1998).

Hollenbach analysed model tank tests during the period of 1980 to 1995. A total of 433 model tests took place in the Vienna Ship Model Basin with the aim of improving the reliability of performance prediction of modern cargo ships at the design stage. Hollenbach's method gives an envelope of resistance. This envelope gives a minimum resistance that can be achieved after optimisation, as well as the regular resistance. Ballast and Laden conditions are separated. The method can be easily computerised. The output of the method is the residual resistance.

The total resistance is given by:

$$R_T = R_F + R_R \tag{4.1.1}$$

The residual resistance is given by:

$$R_R = C_R \cdot \frac{\rho}{2} \cdot V^2 \cdot \left( \frac{B \cdot T}{10} \right) \tag{4.1.2}$$

where,

B : Ship's Breadth [m]
T : Ship's Depth [m]
V : Ship's surge speed [m/s]
ρ : Water density [kg/m³]

The determination of Coefficient CR can be found in Schneekluth and Bertram (1998).The frictional resistance is approximated by the ITTC 1957 formula. Thus,

$$R_F = \frac{0.075}{\left(\log Rn - 2\right)^2} \cdot \frac{\rho}{2} \cdot V^2 \cdot S_{total} \tag{4.1.3}$$

where,

Rn : Reynolds number [-]
$S_{total}$ : Wetted surface area approximation [m²]
The wetted surface area is approximated by:

$$S_{total} = k \cdot L \cdot \left( B + 2 \cdot T \right) \tag{4.1.4}$$

Where, L is the equivalent length and is defined in (Schneekluth and Bertram, 1998). The coefficient k is given by:

$$k = a_0 + a_1 \cdot \frac{L_{OS}}{L_{WL}} + a_2 \cdot \frac{L_{WL}}{L} + a_3 \cdot c_B + a_4 \cdot \frac{B}{T} + a_6 \cdot \frac{L}{T} + a_7 \cdot \frac{(T_A - T_F)}{L} + a_8 \cdot \frac{D_P}{T} + k_{Rudd} \cdot N_{Rudd} + k_{Brac} \cdot N_{Brac} + k_{Boss} \cdot N_{Boss} \quad (4.1.5)$$

where,

$k_{Rudd}$ : Rudder coefficient [-]
$k_{Brac}$ : Bracket coefficient [-]
$k_{Boss}$ : Boss coefficient [-]
$N_{Rudd}$ : Number of rudders [-]
$N_{Brac}$ : Number of brackets [-]
$N_{Boss}$ : Number of bosses [-]

The polynomial coefficients can be found in Schneekluth and Bertram (1998).

A statistical method to determine the vessel calm resistance was developed by Holtrop and Mennen (1982). This method is accurate for a broad range of vessels and is based on regression analysis. Some coefficients of the method were updated by Holtrop (1984). However, some vessels have unique block and prismatic coefficient combinations, along with length and beam that may lead to a slightly inaccurate approximation of the resistance. The total resistance of the ship can be subdivided into:

$$R_{total} = R_F \cdot (1 + k_1) + R_{APP} + R_W + R_B + R_{TR} + R_A \quad (4.1.6)$$

where,

$R_F$ : Frictional resistance according to ITTC 1957 formula
$1+k_1$ : Viscous resistance form factor in relation to $R_F$
$R_{APP}$ : Appendage resistance
$R_W$ : Wave-making and wave-breaking resistance
$R_B$ : Additional pressure resistance of bulbous bow near the water surface
$R_{TR}$ : Additional pressure resistance of immersed transom stern
$R_A$ : Model-ship correlation

The mathematical expression of the components that form the total Calm water resistance using the Holtrop and Mennen (1982) method is given in Appendix I.

**Table 4.1: Applicability range of calm water resistance approximation methods**

| Method | Publication date | Restrictions |
|---|---|---|
| Guldhammer-Harvald | 1965, 1974 | $0.5< C_{P,WL} < 0.8$<br>$0.15 \leq Fn_{WL} \leq 0.44$<br>$4 \leq L_{WL}/\nabla^{1/3} \leq 0.44$ |
| Taggart | 1954 | $0.56< C_P < 0.68$<br>$0.18 \leq Fn \leq 0.42$ |
| Danckwardt | 1969 | $50\leq L_{PP} \leq 280$<br>$6 \leq L/B \leq 8$<br>$0.14 \leq Fn \leq 0.32$<br>$0.525 \leq C_B \leq 0.825$<br>$2\leq B/T \leq 3$ |
| Taylor-Gertler | 1910, 1954, 1964 | Fast Cargo Ships, warships<br>Influence of bulb not taken into account<br>Constant $C_M$ |
| Hoof – Nicholson | 1948 | Fast vessels with $C_P<0.80$ |
| Lap – Keller | 1954 updated in 1973 | Large slow ships with high $C_B$ |
| SSPA | 1948-1959 | $1.5\leq B/T \leq 6.5$<br>$0.525< C_B < 0.75$<br>$0.18 \leq Fn \leq 0.32$ |
| Japanese single screw series | 1964 | $C_B \leq 0.84$<br>$L/B \leq 6.17$ |
| Todd (Series 60) | 1963 | $0.6 \leq C_B \leq 0.80$<br>$1.5\%\leq LCB\leq 2.5$ from MidShip<br>$2.5 \leq B/T \leq 3$ or<br>$0 \leq B/T \leq 3.5$ |
| Formdata method combining Todd and Guldhammer-Harvald | 1974 | $0.15 \leq Fn \leq 0.45$<br>$4 \leq L/V^{1/3} \leq 8$<br>$0.5 \leq C_P \leq 0.85$ |
| BSRA | 1964 | $0.65 \leq C_B \leq 0.875$ |
| Hotrop and Mennen | 1982 | - |
| Hollenbach | 1997, 1998 | - |

On the basis of method-implied restrictions, ease of programming into a computerised environment and publication date, the Hollenbach and Holtrop-Mennen methods are selected for simulation modelling.

### 4.1.2 Added resistance due to wind and waves

Ships operate in a changing environment driven by stochastic phenomena, and, in most cases, they operate in rough conditions. The calm water resistance does not represent the actual induced resistance due to wind and waves. Studies to estimate this effect were performed and then continued mainly for tanker vessels. Maruo (1957; 1960; 1963) attempted the first approach to added resistance estimation due to the motion of the ship in waves. His method was used with the addition of the force created due to wave reflection. Numerous studies on ship performance were performed and published by Aertssen (1963; 1966), Aertssen et al. (1967), Aertssen and Van Sluys (1972), and detailed speed performance monitoring using ship logs and satellite data was performed later by Townsin et al. (1975). Aertssen (1969) introduced an approximate formula for the calculation of ship speed loss in bad weather conditions. This formula was implemented for the head weather case only. The formula is only dependent on Beaufort number, length between perpendiculars, ship speed and constants dependent on Beaufort number.

Gerritsma and Beukelman (1972) used the general idea of Maruo's approach, introducing, however, the radiated energy approach for the calculation of the added resistance of the ship in longitudinal waves. Salvensen et al. (1974) used the seakeeping strip theory and radiated energy approach to produce more accurate results for the hull designs. Townsin et al. (1975), after analysing a generalised system for speed performance and monitoring, presented a simple formula for the speed loss of the vessels in head weather. The formula was derived by monitoring the performance of large tankers. Fujii and Takahashi (1975), Faltinsen et al. (1980), and Kwon focused on the issue of added resistance due to wave reflection.

The Towsin and Kwon (1983) formula for speed loss due to added resistance was updated by Kwon (2008) for a broader range of block coefficients ($C_B$=0.55-0.85) and Froude number ($F_N$=0.05-0.30).

An alternative approach to the Kwon (2008) model was made by Grigoropoulos et al. (2001), who published data of mean added resistance in a tabular form for a set of seventy-two series 60 models in order to extrapolate the results to vessel specific designs. The first attempt at tabular representation was made by Shintani and Inoue (1984). The interpolation to the results is made using the L/B and B/T ratios, the $C_B$ the longitudinal centre of buoyancy concerning the examined hull geometry. The sea condition during the experiments was described by a two-parameter Bretchshneider spectrum (modal period and significant wave height required). The results are given for wave angles and are non-dimensional for the significant wave height.

Faltinsen et al. (1980), using a direct pressure integration approach, came up with very interesting results, as well as setting a simple added resistance formula for the short

waves added resistance due to the lack of efficiency of the generalised one. An improved formula of Faltinsen et al. (1980) was published by Ohkusu (1984), which focuses on blunt bow full hull forms while travelling at low speed. An overview of the methods for added resistance in seaways was published by Wilson (1985). Naito (2008) calculated the added resistance based on an improved version of Maruo's approach, by using the Kochin function. Kashiwagi (2009) took this further by inserting an enhanced unified theory.

The most recent studies have been performed by Liu et al. (2011), employing a 3D frequency domain panel and a new Hybrid time domain Rankine source-Green function method, and based on Mauro's approach to calculate the added resistance of ship in waves.

Although models of added resistance contain the wind parameter in total resistance, as in Aertssen (1967) and Towsin and Kwon (1983), dedicated studies have been performed since the 60s. Shearer et al. (1960) have taken model testing measurements and compared them to previous works of on-board measurements that were published to that date. The effect of type and location of the superstructure was highlighted. Moreover, they underlined that the absence of true wind experiments may lead to an underestimated effect of wind resistance; hence the experimental setup differs from the real voyage. Isherwood (1974) reviewed these published methods and proposed a set of coefficients for roe and aft forces, lateral force and yawing moment. The data was analysed by multiple regression techniques from model tests. This work was originally submitted for written discussion; however, these coefficients describe with accuracy modern designs up to the present day. The investigation of the wind effect was continued, and van Berlekom et al. (1974) published equations that describe the forces of wind in large tankers and large bulk carriers for laden and ballast voyages. Model tests were carried out and the Norrbin mathematical model that described the simulations was used. In this paper, the effect of rudder movements to keep the course straight was highlighted, as it increases the total resistance. Furthermore, the rudder propeller interaction was inserted in the calculations. The wind effect on the overall performance of the ship was later updated by Willem and van Berlekom (1981). This approach was similar to the publication of 1974, but contained model tests in modern hull and superstructure geometries, thus a different set of equations was published. Blendermann (1994) published equations based on twenty-eight model tests of present-day geometries. With respect to the aerodynamic loading, there are only three basic ship types classified as rectangular cubes (car carriers, ferries etc.), multiform shapes (containerships, cargo vessels etc.) and longitudinally unsymmetrical shapes (supply vessels, tugs etc.). It is believed that these equations accurately represent the wind effect on modern vessels.

### *4.1.2.1 The Aertssen model*

Aertssen proposed a simple formula for approximation of the speed loss due to wind and waves. By rearranging the proposed formula, the added resistance percentage is given by equation (4.2.1)

$$\frac{\Delta R}{R} = \left( \frac{\Delta V}{V} + 1 \right)^2 - 1 \tag{4.2.1}$$

where,

ΔR : Added Resistance [N]

ΔV : Speed loss due to added resistance [m/s]The speed loss is determined by equation (4.2.2)

$$\frac{\Delta V}{V} = \frac{m}{L_{pp}} + n \tag{4.2.2}$$

where,

$L_{PP}$ : Ship's length between perpendiculars [m]

m, n : Constants defined in Table 4.2 [-]

**Table 4.2: Aertssen (1967) values for m and n coefficients**

| | Head sea | | Beam sea | | Following sea | |
|---|---|---|---|---|---|---|
| BN | m | n | m | n | m | n |
| 5 | 900 | 2 | 700 | 2 | 100 | 0 |
| 6 | 1300 | 6 | 1000 | 5 | 200 | 1 |
| 7 | 2100 | 11 | 1400 | 8 | 400 | 2 |
| 8 | 3600 | 18 | 2300 | 12 | 700 | 3 |

Aertssen considers the speed loss percentage constant in Beaufort numbers less than 5 and equal to 10%.

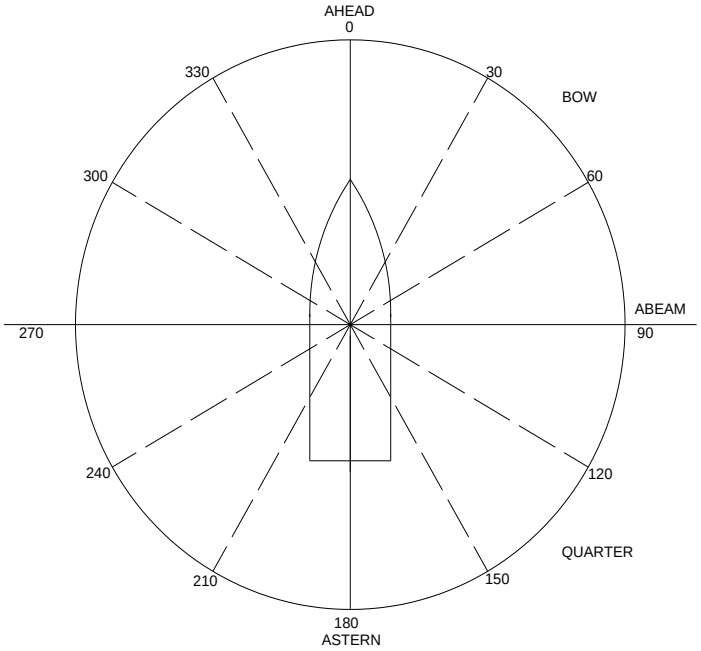


**Figure 4.1: Wave and wind angles of attack in degrees and description terminology**

#### *4.1.2.2 The Towsin and Kwon model*

In 1982, Towsin and Kwon updated the Aertssen formula. Constants have been chosen so that the suggested formulae can closely represent the results of wind resistance by van Berlekom (1981), wave reflection by the Kwon method, and ship motion resistance by Maruo's (1963) method. Thus the formulae intended to provide an estimate of the percentage speed loss are given by equations (4.2.3) for tankers in laden, (4.2.4) and for tankers in ballast and for containerships by equation (4.2.5), updated by Kwon (2008) for larger range of $C_b$ and $F_n$. The proposed formulae consist of two parts. The first part denoted the effect of wind in added resistance and the second the effect of waves. In the event that a mathematical model to represent the wind is present in the calculations, the wind effect part must be omitted (Kwon, 2008).

$$\alpha \cdot \mu \cdot \frac{\Delta V}{V} \cdot 100\% = 0.5 \cdot BN + \frac{BN^{6.5}}{2.7 \cdot \nabla^{2/3}} \tag{4.2.3}$$

$$\alpha \cdot \mu \cdot \frac{\Delta V}{V} \cdot 100\% = 0.7 \cdot BN + \frac{BN^{6.5}}{2.7 \cdot \nabla^{2/3}} \tag{4.2.4}$$

$$\alpha \cdot \mu \cdot \frac{\Delta V}{V} \cdot 100\% = 0.7 \cdot BN + \frac{BN^{6.5}}{22 \cdot \nabla^{2/3}} \tag{4.2.5}$$

where,

BN : Beaufort number which is defined by Henschke (1965) shown in Table 4.3

$\nabla$ : Volume of displacement in [m³]

α : Correction factor for $C_B$ and Froude number given in Kwon (2008) [-]

μ is the correction coefficient of the wind and wave direction. The coefficient is given by the set of equations described in (4.2.6).

$$\begin{aligned} 2\cdot\mu_{bow} &= 1.7 - 0.03\cdot(BN-4)^2 && 30^0 - 60^0 \\ 2\cdot\mu_{beam} &= 0.9 - 0.06\cdot(BN-6)^2 && 60^0 - 150^0 \\ 2\cdot\mu_{following} &= 0.4 - 0.03\cdot(BN-4)^2 && 150^0 - 180^0 \end{aligned} \qquad (4.2.6)$$

**Table 4.3: Henschke (1965) sea description and correlation with Beaufort number and sea scale**

| Sea Scale | Beaufort Number (BN) | Wind speed range [m/s] | Sea Description |
|---|---|---|---|
| 0 | 0 | 0 - 0.2 | Smooth sea |
| 1 | 1 | 0.3 - 1.5 | Calm rippling sea |
| 2 | 2-3 | 1.6 – 5.4 | Gentle sea |
| 3 | 4 | 5.5 - 7.9 | Light sea |
| 4 | 5 | 8.0 - 10.7 | Moderate sea |
| 5 | 6 | 10.8 - 13.8 | Rough sea |
| 6 | 7 | 13.9 -17.1 | Very rough sea |
| 7 | 8-9 | 17.2 – 24.4 | High sea |
| 8 | 10 | 24.5 – 28.4 | Very high sea |
| 9 | 11-12 | 28.5 – 36.9 | Extremely high sea |

In cases where on-board observations are present (usually reported in 'noon reports'), the recorded sea description is converted to Beaufort number using the correlation of Table 4.3.

### *4.1.2.3 Detailed added resistance model*

The application of the seakeeping methods discussed above produce response amplitude operators (RAOs) (or transfer functions) for the examined vessels. As a result, when running the seakeeping code, the RAO for the added resistance for a given angle of attack can be acquired. Moreover, in order to produce a loading from the sea, the behaviour of the latter can be described by a spectrum. The most commonly used sea spectra are the JONSWAP, Bretschneider and the single parametric spectrum proposed by Pearson and Moskovich. In order to obtain the response of the vessel to the given spectrum, the following transformation should be made:

$$S_{AR}(\omega) = \left|RAO_{AR}\right|^2 \cdot S_{\eta\eta}(\omega) \tag{4.2.7}$$

The sea spectrum $S_{\eta\eta}(\omega)$ is corrected for the encounter frequency. The relationship is valid for deep water (depth> 90m) and is given by the following equation:

$$S_{\eta\eta}(\omega) = S_{\eta\eta}(\omega_0) \cdot \left(1 - \frac{2 \cdot \omega_0 \cdot V}{g} \cdot \cos\beta\right)^{-1} \tag{4.2.8}$$

where,

$\omega_o$ : Encounter frequency [rad/s]

For simulation purposes, it is essential to produce a time series of added resistance given the ship's speed, the sea spectrum and the wave angle of attack. The model by Pierson (St Denis and Pierson, 1953) and Longuet-Higgins (1952) is commonly used in the literature. It is based on the idea that random cosine wave is expressed by a large number of different amplitude cosine waves of random phase.

$$R_{AR}(t) = \sum_{n=1}^{N} A_n \cdot \cos\left(\omega_n \cdot t + \xi_n\right) \tag{4.2.9}$$

where,

$A_n$ : Wave amplitude [-]
t : Time [s]
$\xi_n$ : Uniformly distributed random variables between [0, 2π] [-]

The amplitudes are obtained for each encounter frequency by calculating the slice area under the added resistance response spectrum $S_{AR}(\omega)$ :

$$A_n = 2 \cdot \sqrt{S_{AR}(\omega_n) \cdot \Delta\omega_n} \tag{4.2.10}$$

For seakeeping purposes, it is acceptable to create segments greater than 100 and smaller than 500.

### *4.1.2.4 Medium complexity added resistance model*

In cases where there is no information regarding the added resistance RAO, and when the simulation entails the usage of fluctuating added resistance, wave forecasting techniques are adopted. The purpose is to acquire a fluctuated profile of the significant wave height and the modal period. Subsequently, the tabular data of the added resistance given by Grigoropoulos et al. (2001) can be used. This approach is valid, as the duration of the sea state is dependent on the geographical area of the voyage, and can be up to two hours (Ochi, 2005). This approach defines the simulation time step, as the usage of the mean added resistance model should be made once each time the modal period or the significant wave height is altered.

The forecasting techniques are classified into two types: the simplified or parametric and the elaborate or numerical. Parametric methods explicitly give wave height and period, having information about the wind speed, the fetch distance and the duration of the wind phenomenon. The numerical methods are far more accurate, but require a number of oceanographic and meteorological parameters that make the simulation process very demanding. However, they are correct when the speed and direction vary considerably into the examined area for a given time period. On the contrary, when the wind field is assumed stationary and when accurate wind data is not available, the simplified parametric empirical relationships are proposed by the literature. The Sverdrup-Munk and Bretschneier equations are based on dimensional analysis considerations, which are valid for deep water cases (US Army, 1984). Hence, the wind that blows over a fetch distance will be responsible for a significant wave height and modal period according to the following empirical formulae:

$$H_s = \frac{0.283 \cdot \tanh\left[0.0125 \cdot \left(\frac{g \cdot F}{u_w^{\,2}}\right)^{0.42}\right]}{g} \cdot u_w^{\,2} \tag{4.2.11}$$

and for the modal period:

$$T_s = \frac{2.4 \cdot \pi \cdot \tanh\left[0.077 \cdot \left(\frac{g \cdot F}{u_w^{\,2}}\right)^{0.25}\right]}{g} \cdot u_w \tag{4.2.12}$$

where,

g : Acceleration of gravity [m/s²]
F : Fetch [m]
$u_w$ : Wind speed [m/s]

The aforementioned formulae are valid if the duration of the phenomenon is greater than a minimum value, which is approximated by the following equation:

$$t_{\min} = \frac{68.8 \cdot \left( \frac{g \cdot F}{u_w^{\,2}} \right)^{0.67}}{g} \cdot u_w \tag{4.2.13}$$

In cases where the time duration of the phenomenon is less than the $t_{min}$ value, equation (4.2.13) is solved as F:

$$F = \frac{u_w^{\,2}}{g} \cdot 0.67 \sqrt{\frac{t_{\min} \cdot g}{68.8 \cdot u_w}} \tag{4.2.14}$$

Consequently, the fluctuation of added resistance due to waves is dependent on the fluctuation of the wind speed over the examined period. Given the modal period and the significant wave height, which are obtained by the aforementioned formulae (4.2.11) and (4.2.12), mean added resistance data can be acquired using the tables presented in Grigoropoulos et al. (2001).

### 4.1.3 Hydrodynamic induced forces

When the ship is sailing under favourable conditions, e.g. sea state less than 4, the ship is experiencing lateral and yawing forces that can be neglected due to their small effect. The rudder movement occurs only to alternate the vessel course. Nonetheless, when the ship is sailing in sea state higher than 4, and when the relative wind direction is in a position other than on the bow or stern, the lateral force and a yawing moment can be described by the equations presented at the wind resistance model. According to Van Berlekom (1981), if it is assumed that for the examined time step steady wind conditions exist, counteracting hydrodynamic forces are induced in order to compensate the drift and yaw forces and moments, respectively, so as to maintain the ship's heading. These hydrodynamic forces are expressed as a constant drift angle and a constant rudder angle.

Concerning the drift induced resistance, Van Berlekom (1981) states that $X_{vv}$ motion can be evaluated from model tests for small drift angles. The applicability of the

initial study varied for conventional tankers and bulk carriers with deadweight range of 100,000 – 500,000 tonnes (Van Berlekom et al., 1974). The aforementioned study consisted of model tests in wind tunnels, and results in the following expression, which is also adopted here.

$$X_{vv} \cdot v^2 = R_{drift} = 10^{-3} \cdot 0.1 \cdot \rho \cdot L_{pp} \cdot T \cdot v^2 \tag{4.3.1}$$

The lateral ship velocity (v) can be approximated by (4.3.1), that the reported speed is always in the surge axis and the wave angle is always given relatively to the bow. Thus,

$$v = \tan(\delta) \cdot V \tag{4.3.2}$$

Assuming that velocity at the rudder is unaffected by the propeller operation, the rudder resistance can be expressed according to Norrbin (1972), as follows;

$$R_{Rudder} = f(AR) \cdot \frac{1}{2} \cdot V^2 \cdot A_R \cdot \delta^2 \tag{4.3.3}$$

where,

$A_R$ : Rudder area [m²]
f(AR) : Function of rudder area which can be assumed equal to 1
δ : Rudder angle [deg]

However, this simplification implies errors in the calculation of rudder resistance. According to Molland and Turnock (2007), the velocity in a propeller slipstream may be made using axial momentum theory

Thus, (4.3.3) can be re-determined using the equations presented in Appendix I:

$$R_{Rudder} = f(AR) \cdot \frac{1}{2} \cdot V_{RR}{}^2 \cdot A_R \cdot \delta^2 \tag{4.3.4}$$

where,

$V_{RR}$ : Relative rudder velocity [m/s²]

For rudders with aspect ratio 1.5-3.0, the function *f* (AR) equals to 1 (Van Berlekom, 1981). The rudder angle δ is given by the following equation in a non-dimensional form:

$$\delta = \frac{C_N - \xi_\beta \cdot C_Y}{Y''_{cc\delta} \cdot \left(\xi_\delta - \xi_\beta\right)} \cdot \frac{L^3}{2 \cdot \nabla} \cdot \frac{\rho_a}{\rho} \cdot \left(\frac{V_R}{V}\right)^2 \tag{4.3.5}$$

where,

$C_N$ : Non-dimensional Yaw coefficient [-]

$C_Y$ : Non-dimensional Sway coefficient [-]

$\nabla$ : Displacement volume of the ship [$m^3$]

$Y'_{uv}$ : Static force coefficient [-]

$Y'_{uv\,\delta}$ : Vessel Hydrodynamic coefficient [-]

$V_R$ : Wind relative speed [m/s]

$\xi_\delta$ : $N'_\delta / Y'_{cc\delta}$

$\xi_\beta$ : $N'_{uv} / Y'_{uv}$

If the non-dimensional coefficients for the examined vessels are not known, the estimates presented in Table 4.4 are valid for merchant ships (Van Berlekom et al., 1974; Van Berlekom, 1981). Van Berlekom et al. (1974) proposed the following simplification of the δ angle if no vessel hydrodynamic coefficients are known:

$$\delta = 0.18 \cdot \frac{L^3}{\nabla} \cdot \left(0.5 \cdot C_Y - C_N\right) \cdot \left(\frac{V_R}{V}\right)^2 \tag{4.3.6}$$

**Table 4.4: Static and rudder force and yawing moment coefficients estimates for merchant ships (Van Berlekom et al., 1974; Van Berlekom, 1981)**

| Coefficient name | Coefficient value range |
|---|---|
| $Y'_{uv}$ | -1.5 ~ -1.1 |
| $Y'_{cc\delta}$ | 0.2 ~ 0.3 |
| $\xi_\delta$ | -0.5 ~ -0.4 |
| $\xi_\beta$ | 0.3 ~ 0.6 |

A similar process to account for rudder resistance when correcting the vessel heading due to induced waves should be followed when the rudder angle is known. However, due to the absence of reported data, the rudder added resistance movement can be neglected from the calculation. The implied error to the total resistance determination is negligible, as the added resistance models incorporate the rudder effect into the calculations.

### 4.1.4 Wind induced resistance

This section defines the mathematical equations that describe two statistical models of wind resistance applicable to modern vessels. The first approach is by Isherwood (1974), which has been proven accurate. The second by Blendermann (1994) is a more detailed statistical correlation of data of modern hull forms. The resistance is calculated for the surge (x-axis) movement. However, in manoeuvring condition, the movement effects in all the vessel's degrees of freedom are significant; nonetheless any contribution of these factors during a sea voyage will be neglected. Nonetheless, non-dimensional coefficients for yaw and sway movements have been approximated in order to make use of the values at the rudder and drift resistance. It is proposed to use the Isherwood model in designs before 1985 as the superstructure form was significantly altered after 90s; hence the statistical analysis of Blendermann is believed to be more accurate for the modern hull forms that this project is based on.

#### *4.1.4.1 The Isherwood wind model*

This method calculates with adequate accuracy the effect of wind in added resistance. It is based on a statistical analysis of one hundred and seven complete model tests. It is applicable to various hull superstructure forms for various ship types, such as tankers, bulk carriers, cargo vessels, passenger ships and ferries, tug boats and stern trawlers. The published paper includes a table with values of independent variables for the suggested equations according to ship type, if vessel superstructure information is unavailable. Although this work has full access to the design characteristics of the examined fleet, the coupling of the project with the global fleet is possible using this approach. Thus the equation of the x-axis force is given by:

$$F_X = C_X \cdot 0.5 \cdot \rho \cdot A_T \cdot V_R^2 \tag{4.4.1}$$

The $C_X$ coefficient is given from the multiple regression polynomial equation (4.4.2):

$$C_X = A_0 + A_1 \cdot \frac{2 \cdot A_L}{L_{OA}^2} + A_2 \cdot \frac{2 \cdot A_T}{B^2} + A_3 \cdot \frac{L_{OA}}{B} + A_4 \cdot \frac{S_p}{L_{OA}} + A_5 \cdot \frac{C}{L_{OA}} \tag{4.4.2}$$

where,

C : Distance from bow of centroid of lateral projected area [m]

$S_p$ : Length of lateral projection of vessel excluding waterline, slender bodies [m]

$L_{OA}$ : Ship's overall length [m]

The non-dimensional sway coefficient is determined by:

$$C_Y = B_0 + B_1 \cdot \left( \frac{2 \cdot A_L}{L_{OA}{}^2} \right) + B_2 \cdot \left( \frac{2 \cdot A_T}{B^2} \right) + B_3 \cdot \left( \frac{L_{OA}}{B} \right) + \\ + B_4 \cdot \left( \frac{S}{L_{OA}} \right) + B_5 \cdot \left( \frac{C}{L_{OA}} \right) + B_6 \cdot \left( \frac{A_{SS}}{A_L} \right) \tag{4.4.3}$$

The non-dimensional Yaw coefficient is given by:

$$C_N = C_0 + C_1 \cdot \left( \frac{2 \cdot A_L}{L_{OA}{}^2} \right) + C_2 \cdot \left( \frac{2 \cdot A_T}{B^2} \right) + C_3 \cdot \left( \frac{L_{OA}}{B} \right) + C_4 \cdot \left( \frac{S}{L_{OA}} \right) + C_5 \cdot \left( \frac{C}{L_{OA}} \right) \tag{4.4.4}$$

where,

$A_{ss}$ : Lateral projected area of superstructure

$A_L$ : Lateral projected area of the ship [m²]

$A_T$ : Transverse projected area of the ship [m²]

### *4.1.4.2 The Blendermann wind model*

Blendermann (1994) published a recent study for wind loads on ships using state of-the-art methods of wind tunnel testing, and treating the data in statistical terms. The analysis was based on twenty-eight test results, and it is accepted that they sufficiently cover present-day ship geometries. The equations that have been suggested by Blendermann rely on basic ship geometry characteristics. The wind force on x-axis is given by (4.4.5):

$$F_x = CX_{AF} \cdot q \cdot A_F \tag{4.4.5}$$

where dynamic pressure of the apparent wind (q) is given by

$$q = 0.5 \cdot \rho \cdot u_w{}^2 \tag{4.4.6}$$

The coefficient $CX_{AF}$ is given from the following equation:

$$CX_{AF} = -CD_l \cdot \frac{A_L}{A_F} \cdot \frac{\cos \varepsilon}{1 - \frac{\delta_B}{2} \cdot \left( 1 - \frac{CD_l}{CD_t} \right) \cdot \sin^2 2 \cdot \varepsilon} \tag{4.4.7}$$

$CD_l$ is calculated using the linearly interpolated data of $CD_{1AF}$ for 0 and π angles of attack from Blendermann (1994). Thus,

$$CD_l = CD_{1A_F} \cdot \frac{A_F}{A_L} \tag{4.4.8}$$

The non-dimensional sway coefficient is determined by:

$$C_Y = CD_T \cdot \frac{\sin(\varepsilon)}{\left(1 - \frac{\delta_B}{2} \cdot \left(1 - \frac{CD_1}{CD_T}\right) \cdot \left(\sin(2 \cdot \varepsilon)\right)^2\right)} \tag{4.4.9}$$

The non-dimensional Yaw coefficient is given by:

$$C_N = \left(\frac{S_L}{L_{OA}} - 0.18 \cdot \left(\varepsilon - \frac{\pi}{2}\right)\right) \cdot C_Y \tag{4.4.10}$$

where,

ε : Wind angle of attack [rad]
$\delta_B$ : Cross-force parameter [0-1]
$S_L$ : Position of the lateral-plane centroid with respect to the main section [m]

### 4.1.5 The Propulsor and Governor models

The behaviour of the machinery operation is defined by requirements in torque and rotational speed. Journee (1976) states that the relation of the engine speed at constant setting and the increased loading in a seaway is also important. As a result, the mathematical implementation of the forces acting on the ship due to the operation of the propeller is necessary and the coupling between the propeller operation and engine is essential.

#### *4.1.5.1 The Propeller model*

The main force that the propeller produces is the thrust, which is always along the x-axis. Apart from the thrust, another interesting expression of the propeller's operation is the torque acting on the main shaft. In practical terms, part of the force due to propeller-hull hydrodynamic interaction is lost. The percentage of this coefficient is dependent on the geometry of the hull and the appendages. This is expressed through the thrust-deduction factor *t* and the propeller force is given by:

$$T = T_0 \cdot (1 - t) \tag{4.5.1}$$

In order to have a self-propelled ship (sum of forces equal to zero), T should be equal to the total ship resistance ($R_T$). Thus by taking into account the thrust deduction due non open water propeller conditions:

$$T_0 = \frac{R_T}{(1-t)} \tag{4.5.2}$$

where,

$T_o$ : Open water developed thrust [N]
t : Thrust deduction factor [-]

The method that was followed by Oosterveld and Oossanen (1975) to calculate the thrust and torque is based on the Wageningen B-screw series data. The open-water characteristics are obtained from open-water test results, for about one hundred and twenty propellers. They are given in a conventional way, in the form of thrust and torque coefficients $K_T$ and $K_Q$, respectively. However, if detailed propeller model tests are available, the following equations (4.5.3) - (4.5.5) should not be used and the non-dimensional thrust and Torque coefficients are supplied directly by the $K_T$, $K_Q$, and $\eta_o$ graph. In the case of the Wageningen B-screw series:

$$K_T = \frac{T_0}{\rho_w \cdot n^2 \cdot D_p^4} \tag{4.5.3}$$

$$K_Q = \frac{Q_0}{\rho_w \cdot n^2 \cdot D_p^5} \tag{4.5.4}$$

where,

n : Propeller revolutions per second [rps]
$D_p$ : Propeller diameter [m]
$Q_o$ : Open water developed torque [Nm]

In order to calculate the thrust and the torque, coefficients should be defined. Oosterveld and Oossanen (1975) have published a polynomial form of the coefficients using non-dimensional propeller data, such as the number of blades, the expanded blade ratio, the pitch to diameter ratio and the advance coefficient. The polynomials in the following equations are valid for Reynolds number, $Re=2x10^6$ at 75% of the propeller radius.

$$K_T = \sum_{n=1}^{39} C_n \cdot J^{s_n} \cdot \left(P / D_p\right)^{t_n} \cdot \left(A_E / A_0\right)^{u_n} \cdot z^{v_n}$$
$$K_Q = \sum_{n=1}^{47} C_n \cdot J^{s_n} \cdot \left(P / D_p\right)^{t_n} \cdot \left(A_E / A_0\right)^{u_n} \cdot z^{v_n} \quad (4.5.5)$$

where,

Cn, Sn, un, vn are coefficients determined in (Oosterveld and Oossanen, 1975)

J : Advance speed and given by equation (3.57)

Z : Number of blades

The advance speed is given by:

$$J = \frac{V_A}{n \cdot D_p} \quad (4.5.6)$$

Where $V_A$ is the advance velocity given by:

$$V_A = V \cdot \left(1 - w\right) \quad (4.5.7)$$

In order to determine the $K_T$ and $K_Q$ coefficients for other than Reynolds number equal to $2x10^6$, corrections have to be made as described in Oosterveld and Oossanen (1975).

The shaft horsepower (SHP) in kW required by the prime mover is given by equation (4.5.8)

$$P = \frac{\left(10^{-3} \cdot K_Q \cdot \rho_w \cdot n^2 \cdot D_p^5\right) \cdot \left(2 \cdot \pi \cdot n\right)}{\eta_{tr} \cdot \eta_R} \quad (4.5.8)$$

where,

$\eta_{tr}$ : Shaft losses between the prime mover and the propulsor [-]

$\eta_R$ : Relative rotative efficiency [-]

w : Wake friction [-]

### *4.1.5.2 The Governor and Bridge Commands models*

The purpose of the Engine Governor is to regulate the fuel consumption so to maintain a predefined engine speed. In Diesel Engines, due to the excess air that is always present in combustion, the consumption without the presence of the governor would increase and the engine speed would not have a limit. As a result, in order to control the engine speed, a governor regulates the injected fuel (Woodyard, 2009). Consequently, the regulation of fuel and engine speed defines the ship's speed, as the available power to the propulsor is controlled.

The coupling of the propeller is defined mathematically by the following principle: in the case of desired vessel speed, the torque needed by the propeller must be in equilibrium with the engine delivered torque and the thrust delivered by the propeller must be in equilibrium with the total resistance of the ship (Molland et al, 2012: Journee, 1976). As a result, the rotational speed of the propeller is defined by equalising the developed thrust with the total ship resistance. According to the three-parameter theorem (Politis, 1991), when there is information regarding the propeller and its operation, the remaining information can be determined using the $K_T$, $K_Q$ graph. In the propulsion problem, the thrust, the propeller diameter and the desired vessel speed are known. Thus, the revolutions per second and the power requirement are defined. In the simulation, the determination of the propeller rotational speed was found by the trial and error method, which was optimised using numerical analysis techniques (midpoint method) with a tolerance equal to $10^{-7}$. The determination of engine speed and power can be characterised as an engine governor.

The different application of the simulated engine governor is to maintain constant power. The controller is now responsible for altering the engine speed in order to meet the constant power setting when the total ship resistance changes due to added resistance, imposed by wind and waves. In terms of simulation modelling, the method adopted in the simulator is trial and error. The algorithm is altering the vessel speed until it reaches the defined power setting with respect to the resistance thrust equilibrium. The resistance thrust match is different in each trial step, since the resistance component is mainly dependent on the vessel speed and has a unique power requirement.

### 4.1.6 Main Engine simple model

The Diesel engine was modelled using the manufacturer's engine operational maps. The acquired data provided information for the complete engine operation, in terms of temperatures, pressures, turbocharger operation, power-RPM curves for normal loading and specific fuel oil consumption versus power output. The latter value is corrected according to the manufacturer. Due to the existence of lube oil pumps, different than ISO conditions in air temperature and cooling water temperature, the SFOC is increased. Furthermore, the HFO operation of lower calorific value significantly alters the SFOC (MAN Diesel, 2007). Thus, the following corrections should be made:
There is a 0.6% increase in fuel consumption due to different than ISO inlet temperature for every 10°C:

$$CR_1 = 6 \cdot 10^{-4} \cdot \Delta T \tag{4.6.1}$$

For different lower calorific value fuel ($\Theta_u \neq 42700$kJ/Kg):

$$CR_2 = \frac{42700}{\Theta_u} - 1 \tag{4.6.2}$$

For marine gas oil (MGO) consumption:

$$CR_3 = 0.02 \tag{4.6.3}$$

For lube oil pump operation, the losses leading to $CR_4$ are dependent on engine load. Hence,

$$SFOC_{\text{corrected}} = SFOC_{\text{ISO}} \cdot \left(1 + \sum_{1}^{4} CR_i\right) \tag{4.6.4}$$

The equations outlined above must be combined with the engine efficiency curves, which were presented in Figures 3.15 and 3.16.

### 4.1.7 Miscellaneous calculations

This section covers mathematic transformations and coefficient calculations that are present on the developed simulation block library.
The kinematic viscosity and water density respectively are given by:

$$\mu_{sw} = \frac{\left(1.023379273 \cdot 0.001787 \cdot 10^3\right)}{\left(1 + 33.408772 \cdot T_w + 0.1681570669 \cdot T_w^2\right) \cdot 10^{-9}} \tag{4.7.1}$$

$$\rho_{sw} = \left(\left(-0.48033168167 \cdot T_w^2 - 7.6223076145 \cdot T_w\right) \cdot 10^{-3} + 104.83\right) \cdot g \qquad (4.7.2)$$

where,

$T_W$ : Water temperature [C]
g : Acceleration of gravity [m/s]
$T_{air}$ : Air temperature [C]

The air density is given by:

$$\rho_{air} = 360.7782 \cdot T_{air}^{-1.00336} \qquad (4.7.3)$$

The wake, thrust deduction and relative rotation propulsion coefficients are essential for calculation. The thrust deduction factor is approximated using the following the expressions of Holtrop and Mennen (1981) and SSPA laboratory, which have better accuracy versus the actual coefficients of other approximations found in the literature.

For single screw cargo vessels:

$$t = \frac{0.25014 \cdot \left(\frac{B}{L}\right)^{0.28956} \cdot \left(\sqrt{\frac{B \cdot T}{D}}\right)^{0.2684}}{\left(1 - C_P + 0.0225 \cdot lcb\right)^{0.01762}} + 0.0015 \cdot C_{stern} \qquad (4.7.4)$$

$$t = w \cdot \left(1.57 - 2.3 \frac{C_B}{C_{WP}} + 1.5 \cdot C_B\right) \qquad (4.7.5)$$

The wake coefficient is approximated by Holtrop and Mennen (1981) and Kruger (1976), respectively.

For single screw cargo vessels:

$$w = 0.3 \cdot C_B + 10 \cdot C_V \cdot C_B - 0.1 \qquad (4.7.6)$$

$$w = 0.75 \cdot C_B - 0.24 \qquad (4.7.7)$$

The relative rotation efficiency is calculated by the formula proposed by Holtrop and Mennen (1981).

For single screw cargo vessels:

$$\eta_R = 0.9922 - 0.05908\frac{A_E}{A_0} + 0.07424\cdot\left(C_P - 0.0225\cdot lcb\right) \tag{4.7.8}$$

where,

D : Ship's Drought [m]
$C_P$ : Prismatic coefficient [-]
$C_B$ : Block coefficient [-]
$C_{WP}$ : Water plane coefficient [-]
$C_{stern}$ : Stern type as described in Holtrop and Mennen (1981) [-]
lcb : Longitudinal centre of buoyancy expressed in percentage from amidships [%]
$A_E/A_o$ : Propeller expanded blade area ratio [-]
P/D : Propeller pitch to diameter ratio [-]

### 4.1.8 Generation of environmental parameters

The wind speed changes continuously and, in order to obtain long-term estimations, statistical methods are used. In marine applications these areas can be sea areas of large fetch distance and can be described by geographical coordinates. Hatziargyriou et al. (1993) state that the Weibull probability density function has been widely used to describe variations of wind speed for an examined area. The Weibul model is given by the following relationship:

$$f\left(V\right) = \frac{a_w}{\beta}\cdot\left(\frac{u_w}{\beta}\right)^{a-1}\cdot e^{\left(-\left(\frac{u_w}{\beta}\right)^a\right)} \tag{4.8.1}$$

where,

$u_w$ : wind speed [m/s]
a : shape factor of Weibul probability density function [-]
b : scale factor of Weibul probability density function [-]

a, β coefficients can be obtained using the following two expressions:

$$\overline{u_w} = \int_0^\infty u_w\cdot f\left(u_w\right)dv = \beta\cdot\Gamma\left(1+\frac{1}{a_w}\right) \tag{4.8.2}$$

where,

Γ : Gamma function

The variance of the wind measurements is given by:

$$\sigma^2 = \int_0^{\infty} \left(u_w - \overline{u_w}\right) \cdot f\left(u_w\right) dv = \beta^2 \left\{ \Gamma\left(1 + \frac{2}{a_w}\right) - \Gamma^2\left(1 + \frac{1}{a_w}\right) \right\} \tag{4.8.3}$$

The mean wind speed value is given by (4.8.4):

$$\overline{u_w} = \frac{1}{N} \cdot \sum_{i=1}^{N} u_{wi} \tag{4.8.4}$$

where,

N : Total number of wind speed measurements [-]

The standard deviation (σ) can be found using:

$$\sigma = \frac{1}{N} \cdot \sqrt{\sum_{i=1}^{N} \left(u_{wi} - \overline{u_w}\right)^2} \tag{4.8.5}$$

Equations (4.8.2) and (4.8.3) can be solved simultaneously to obtain a, β coefficients. However, this process is considered complex and slow, hence the Justus (1978) approach is used, which defines a as:

$$a_w = \left( \frac{\sigma}{\overline{u_w}} \right)^{-1.086} \tag{4.8.6}$$

Thus, the β coefficient can be obtained using (4.8.2).

Hatziargyriou et al. (1993) also proposed a random generation wind model using the Weibul coefficients obtained from the long-term statistical model. The inverse transformed method consists of:

$$F\left(V\right) = 1 - e^{\left( -\left( \frac{u_w}{\beta} \right)^{a_w} \right)} = R \tag{4.8.7}$$

Solving (4.8.7) for R, the pseudo-random number generator is defined:

$$F(R)^{-1} = \beta \cdot \left(-\ln(1-R)\right)^{\frac{1}{a_w}} = u_w \tag{4.8.8}$$

The Rayleigh distribution is a simplified version of the Weibul distribution. It is globally accepted that a Normal distribution can accurately describe the wind direction, given the mean angle value and the standard deviation.

For the approximation of the Wind velocity, the α coefficient of the Rayleigh distribution should be defined. Usually, in a vessel noon report, only the mean relative wind speed is reported. Thus, using a Rayleigh random number generator, a statistical sample of N values can be acquired. Hence,

$$a_w = \frac{\bar{u}_W}{\sqrt{\pi/2}} \tag{4.8.9}$$

A third model, which is suitable for application in a ship simulator, is defined by Anderson et al. (1983). This model can properly simulate the spatial effect of wind behaviour, including gusting, rapid changes and background noises. Consequently, the wind model is a four-component model and is given by the following equation:

$$V_M = V_{WB} + V_{WG} + V_{WR} + V_{WN} \tag{4.8.10}$$

The mathematical equation set of the (4.8.10) wind model subcomponents is given in Appendix I.

## 4.2 Energy storage system

More than 90% of the world's fleet is powered by Diesel Engines. The majority of ocean-going ships are propelled by a two-stroke slow speed Diesel Engine directly coupled to the propulsion shaft. In high Froude number vessels, the propulsion system is broken down into multiple four-stroke Diesel Engines or into multiple Diesel Generator sets, which power electric motors that are coupled to the propeller shaft(s) (Klein Wood and Stapersma, 2003; Bose, 2008).

The hybrid module, as discussed in the previous chapters, consists of a specific number of battery banks that fulfil two basic requirements. The first is battery voltage, which is constrained by the battery manufacturer, and the second is the required Capacity, as found in Table 3.4. In this study, the battery banks are treated as a one, formed by the appropriate number of strings and parallel units.

### 4.2.1 Sizing of battery banks

The energy storage system capacity is determined by the vessel type and autonomy radius of the ship, as it was estimated by correlation of voyage energy requirements. The required voltage is determined by the designer and is constrained by the transformer capability of altering voltage. Usually, the propulsion system runs from 0.4 – 13.8kV and alternations of the voltage are determined by the on-board applications, which can be 220V for hotel loads, 380V for auxiliary equipment and, dependent on the motor type, up to 1kV for propulsion.

The total number of batteries ($n_{bs}$) that should be connected in series in order to implement one battery string is dictated by the DC-bus voltage ($V_{op}$) and the nominal battery voltage ($V_{bat}$). The DC-bus nominal voltage is equal to the DC/AC converter DC input nominal voltage (Koutroulis et al., 2009). Thus,

$$n_{bs} = \frac{V_{op}}{V_{bat}} \tag{4.9.1}$$

The total nominal capacity ($C_{nom}$) of the battery bank [MWh], $Q_{nom}$ depends on the nominal capacity of each battery $Q_{batmax}$ (Ah) and the total number of strings forming the battery bank ($N_{BB}$). Hence,

$$C_{nom} = N_{BB} \cdot Q_{bat_{\max}} \tag{4.9.2}$$

The battery manufacturer denotes that sixteen parallel units of Sodium Nickel Chloride can be connected, offering a nominal voltage of 557V and 0.285 MWh energy density.

Transforming equation (4.9.2) and by constraining the result (value has to be rounded to the next integer), the number of the Battery Banks is given by:

$$N_{BB} = \frac{\text{Energy}_{req.}}{0.285} \tag{4.9.3}$$

In addition, given that the discharge/charge current is one of the most important parameters of battery efficiency, the current should remain as low as possible. In testing facilities, these sixteen parallel units that form a large battery bank offer 0.5MW maximum power. Moreover, with the appropriate connections and converters, multiple banks can be connected, increasing the energy storage medium capability. Hence, due to the parallel connection of the batteries, the discharge/charge current is found using the following relationship:

$$I_{\text{discharge/ Charge}} = \frac{\frac{P_{\text{demand}}}{V_{\text{nominal}}}}{\left(N_{BB} \cdot 16\right)} \tag{4.9.4}$$

where,

$P_{demand}$ : Demanded power by the propulsion and/ or auxiliary loads [W]
$V_{nominal}$ : Battery Nominal Voltage [V]
$N_{BB}$ : Number of Battery Banks [-]

However, the total number of DC/AC converters ($N_c$) required to implement the Hybrid system is calculated by the guaranteed power value ($P_G$) and the nominal AC power rating of the selected converter. Consequently,

$$N_C = \frac{F_0 \cdot P_G}{P_0} \tag{4.9.5}$$

where,

$F_o$ : Oversizing factor and is determined by the designer.

### 4.2.2 Battery models

This thesis proposes the use of two models that sufficiently describe battery behaviour. The experimental model requires laboratory measurements that are often not available to the designer. The second model is a modified version for a quasi-steady condition dynamic model for the battery operation. This model requires significantly less information regarding the battery type. However, the battery coefficients are available in the literature for a range of commercial batteries.

#### *4.2.2.1 Battery experimental model*

The model makes use of the information provided by the manufacturer (Manzoni et al., 2008). Detailed efficiency calculations had been presented in Chapter 3. The following equation is used to estimate the available energy in the battery per simulation time step.

$$SoC_{\Delta t} = \frac{\left(V_{OC} \cdot i \pm i^2 \cdot R\right) \cdot \Delta t}{Q_{nom} \cdot V_{oc}} = \frac{\left(V_{OC} \cdot i \pm dV \cdot i\right) \cdot \Delta t}{Q_{nom} \cdot V_{oc}} \tag{4.9.6}$$

For the charging and discharging efficiencies, respectively:

$$\eta_{ch.} = \frac{\left(V_{OC} \cdot i + i^2 \cdot R\right)}{V_{oc} \cdot i} = \frac{\left(V_{OC} \cdot i + dV \cdot i\right)}{V_{oc} \cdot i} \tag{4.9.7}$$

$$\eta_{dis.} = \frac{V_{OC} \cdot i}{\left(V_{OC} \cdot i + i^2 \cdot R\right)} = \frac{V_{OC} \cdot i}{\left(V_{OC} \cdot i + dV \cdot i\right)} \tag{4.9.8}$$

Using (4.9.6) and (4.9.7), Figures 3.12 and 3.13 are constructed.

where,

$V_{OC}$ : Open circuit voltage [V]
i : battery current [A]
dV : Voltage drop [V]

### *4.2.2.2 Kinetic Battery Model*

The Kinetic batery model (KiBaM) model is called kinetic because the approach is developed on the basis of a chemical kinetics process (Manwell et al., 2005). Although this model is dynamic, it can be transformed to a quasi-steady model under appropriate conditions. The model of the battery charge is distributed in two wells. The first well is the available-charge and the second is the bound-charge. The first describes the available energy ready for system supply. The second determines the amount of energy that is processed in order to fill the available energy well. The rate at which charge flows between the wells depends on the difference of height of the two wells, defined by parameter k. Parameter c gives the fraction of the total charge in the battery that is part of the available-charge well (Manwell et al., 2005). The procedure is described by two differential equations (4.9.9) and (4.9.10).

$$\frac{dy_1}{dt} = -I + k \cdot \left(h_2 - h_1\right) \tag{4.9.9}$$

$$\frac{dy_2}{dt} = -k \cdot \left(h_2 - h_1\right) \tag{4.9.10}$$

The initial conditions are:

$$\begin{aligned} y_1\left(0\right) &= c_{KB} \cdot Q_{\max} \\ y_2\left(0\right) &= \left(1 - c_{KB}\right) \cdot Q_{\max} \end{aligned} \tag{4.9.11}$$

The solution is given by applying Laplace transformation (4.9.12-4.9.13)

$$y_1 = y_{1,0} \cdot e^{-k' \cdot t} + \frac{\left(y_0 \cdot k' \cdot c - I\right) \cdot \left(1 - e^{-k' \cdot t}\right)}{k'} - \frac{I \cdot c \cdot \left(k' \cdot t - 1 + e^{-k' \cdot t}\right)}{k'} \tag{4.9.12}$$

$$y_2 = y_{2,0} \cdot e^{-k' \cdot t} + y_0 \cdot \left(1 - c\right) \cdot \left(1 - e^{-k' \cdot t}\right) - \frac{I \cdot \left(1 - c\right) \cdot \left(k' \cdot t - 1 + e^{-k' \cdot t}\right)}{k} \tag{4.9.13}$$

where

$y_{i,o}$ is the amount of available and bound charge respectively at the start of each time step. For t=0 the values are equal to the initial conditions of the problem.

$k'$ is defined as

$$k' = \frac{k}{c \cdot \left(1 - c\right)} \tag{4.9.14}$$

In the energy approach of the Hybrid system, however, the demand of electrical power and energy from the batteries is described by Power and Capacity and not by

current. Hence, equations (4.9.12), (4.9.13) can be transformed to energy by being multiplied by the Voltage (Vrettos and Papathanassiou, 2011). If the voltage curve is not known, it can be assumed as constant until a specific state of charge (SoC) is reached. However, this procedure introduces errors, as it does not take into account the different charge or discharge currents. Nonetheless, a proper sizing and a charge-discharge controller could apply constant current to the battery arrays without affecting the performance of either the battery or the model.

$$E_1 = E_{1,0} \cdot e^{-k' \cdot t} + \frac{\left(E_0 \cdot k \cdot c - P\right) \cdot \left(1 - e^{-k' \cdot t}\right)}{k'} - \frac{P \cdot c \cdot \left(k' \cdot t - 1 + e^{-k' \cdot t}\right)}{k'} \quad (4.9.15)$$

$$E_2 = E_{2,0} \cdot e^{-k' \cdot t} + E_0 \cdot \left(1 - c\right) \cdot \left(1 - e^{-k' \cdot t}\right) - \frac{P \cdot \left(1 - c\right) \cdot \left(k' \cdot t - 1 + e^{-k' \cdot t}\right)}{k} \quad (4.9.16)$$

The KiBaM approach offers a voltage model. However, in order to apply curve fitting and to export a curve that depicts the voltage drop versus current (Manwell et al., 2005), it requires experimental data from the battery.

$$V = V_{OC} + A \cdot X + C \cdot \frac{X}{\left(D - X\right)} \quad (4.9.17)$$

Where, the A coefficient is a parameter reflecting the initial linear variation of internal battery voltage with state of charge. Typically, it is negative when discharging and positive when charging. C is a parameter that reflects the decrease/increase of voltage when batteries are progressively discharged/charged. It is negative when discharging and positive when charging. D is a parameter reflecting the decrease/increase of battery voltage when the battery is progressively discharged/charged. D is positive and is normally approximately equal to the maximum capacity. However, the nature of the fitting process will usually be such that it will not be exactly equal to that value.
X is a normalised maximum capacity at the given current and is defined as follows:

$$X = \frac{q}{Q_{\max}} \quad (4.9.18)$$

and for discharging X is defined as:

$$X = \frac{\left(Q_{\max} - q\right)}{Q_{\max}} \quad (4.9.19)$$

The percentage of the energy that the Hybrid system can absorb or give to the energy storage medium is dependent on the excess or lack of the propulsion energy requirement in every time step. Thus,

$$I_{demand} = \frac{P_{demand}}{V} \tag{4.9.20}$$

$$I_{excess} = \frac{P_{excess}}{V} \tag{4.9.21}$$

In order to check that the storage medium has sufficient energy to export/import to and from the Hybrid system, the maximum discharging/charging current has to be calculated. As a result,

$$I_{demand,\max} = \frac{k \cdot q_{1,0} \cdot e^{-k' \cdot t} + q_0 \cdot k \cdot c \cdot \left(1 - e^{-k' \cdot t}\right)}{1 - e^{-k' \cdot t} + c \cdot \left(k \cdot t - 1 + e^{-k' \cdot t}\right)} \tag{4.9.22}$$

$$I_{charging,\max} = \frac{k \cdot c \cdot Q_{\max} + k \cdot q_1 \cdot c \cdot \left(1 - e^{-k' \cdot t}\right)}{1 - e^{-k' \cdot t} + c \cdot \left(k \cdot t - 1 + e^{-k' \cdot t}\right)} \tag{4.9.23}$$

The energy equations can be found by multiplying constant Voltage with equations (4.9.22) and (4.9.23), which that introduces error to the calculations, as previously explained.

According to the kinetic battery model approach, the capacity of the battery is preserved and any losses during charging/discharging are caused by the voltage change during these phenomena. In order to calculate the losses, the voltage at each time step is compared to the nominal voltage of the battery. The value of battery voltage can be found if the current and State of Charge (SoC) are known. When battery capacity is almost depleted (Depth of discharge ~100%), the current is ~0A, thus the battery voltage is equal to the E of the empty battery. During charge, when the battery reaches its nominal capacity, the current is high and the terminal voltage is different than battery's E, hence the losses are high. The losses are given by the equation (4.9.24):

$$L_{ch} = I \cdot \left(V(I,t) - V_{nom}\right) \tag{4.9.24}$$

In cases where actual experimental data or manufacturer curves of the battery are not available, equation (3.25) is not used. Consequently, in order to take into account the energy losses, the round-trip efficiency can be used instead.

## 4.3 Optimisation of Machinery Operation

The hybrid configuration implies the existence of an energy management strategy that will choose the optimum power split between the operation of combustion engines and the usage of electricity drained out of the batteries. The strategy is developed to achieve system level objectives, such as fuel economy, low emissions of $CO_2$ and particulate matter, and battery charge sustenance. According to Xu et al. (2010), the energy management strategies can be classified into two categories: the rule-based, in combination with fuzzy logic control if applicable (Schouten et al., 2002), and the optimal. A rule-based strategy is feasible and can be implemented in real time application based on heuristic methods. The optimal strategies differ from each other in each time step, e.g. the fuel consumption is minimised during this time step. A more global solution can be extracted using Dynamic Programming (DP), which relies on the principle of optimality, where the optimal policy can be built step by step. This can be achieved by building an optimal control of the tail sub-problem. It involves the last step and then progresses it towards the front time series steps by iterating and by involving the last two stages during each control (Rousseau et al., 2008). For automotive applications, Lin et al. (2001) and Musardo et al. (2005) proposed the usage of DP, which is well suited to multistage processes, instead of the fuzzy based approach. Nevertheless, the problem with the application of DP is that the operational profile of the vessel is not known in advance, as the chartering commands may alter the speed or, due to unexpected weather change, the forecasted situations may not be encountered during the voyage. In addition, if the vessel operates at constant speed, it is not possible to acquire *a-priori* the propulsor loading, because sea behaviour is stochastic. In literature, two implementations for describing the power train in combination with the operator commands are found. The forward facing implementation has as an input the desired propulsive power, thus the M/E provides the equivalent torque to the propeller and the vessel speed is subsequently determined. This approach is more complex than the backward facing model. The latter approach uses a speed profile (in the marine case, the master speed command), and afterwards the model calculates backward the corresponding operating point of the M/E (Musardo et al., 2005). The backward approach is selected and is also proposed by Van Kessel (2007) for the simulation of submarine battery operation. Thus, the energy strategy has to anticipate a future power demand at the next simulation time step (Grimmelius et al., 2011). To deal with this problem, Guzzella and Sciarretta (2005) proposed the implementation of a cost function in combination with the optimisation routine. ECMS treats the combustion engines as prime cost factors, while the energy storage system is a secondary cost factor, which costs fuel in the future but is inserted into the optimisation algorithm in the examined step. Moreover, during charging,

the cost of fuel to charge is reduced from the fuel bill because this will eventually save fuel in the future. This approach involves a comparison of charging and discharging solutions, and the optimal one is the minimum of the two. This approach was adopted and implemented in this project. However, a different pseudo multi-objective optimisation is also given for reduction of not only of $CO_2$ but of PM. The second approach will be described firstly in this chapter as it is more complex than the ECMS.

The optimisation algorithm selected in this study is a non-linear medium scale optimisation algorithm based on a sequential programming method (Hock and Schittkowski, 1983; Fiacco and Mc Cormick, 1990), which updates the Hessian of the Lagrangian by applying the Broyden, Fletcjer, Goldfarm and Shanno (BFGS) method (Shanno, 1985). It is a single objective optimisation, where the selection of the objective function in all stages of a ship's voyage is the fuel consumption. This optimisation algorithm was selected between the Trust region reflective, active set and internal point algorithms. These algorithms are also proposed by Mathworks® for solving that type optimisation problems. The main reasons for this adoption are that this algorithm converges rapidly to the optimal solution, identifies rapidly the local minima and given the different start points it converges to the global minimum, while active set for example fails. The algorithm principles and the programming process are presented in Nocedal and Wright (2006).

For each of the Hybrid Power layouts, an objective function was formed and the linear and non-linear constraints (equalities and inequalities) were implemented. The set of equations is separated into two parts because of the fact that, due to layout constraints, the electric machine can operate either as an electric motor, hence boosting the propulsion, or act as a shaft generator, thus absorbing energy from the two-stroke Diesel engine in loads more than 60% of maximum continuous rating (MCR) and producing electricity. Concerning the global restrictions applied to each scenario, the following variable limits have been employed. The shape of the objective function has great influence on the successful identification of the global minimum solution. The non-convex form of the objective function has many local minima. To guarantee that the solution is for the global minimum, a commonly suggested method is to change the starting value vector and re-run the optimisation in order to skip each time the already identified solution of this local minimum. Once this process is made several times, where the number is denoted by the degree of the polynomial objective function (e.g. it is a polynomial of n degree, then the local minima can be up to n-1), the outputs are compared and the minimum is the global minimum solution.

### 4.3.1 Pseudo multi-objective optimisation algorithm

During each simulation step, the optimisation algorithm is called up in order to estimate if the hybrid system should run using stored energy. The criterion is the equivalent cost penalty of running the battery system in parallel with the normal energy production, which comes from the auxiliary engines and the main engine. The equivalent cost penalty is found by assuming that the power to charge the battery bank is made with the minimum SFOC and the efficiency of the battery is dependent on the discharge current and not of the charge current. This assumption is validated at a later stage, where the algorithm is called up again to decide how to charge the battery system. This will be described in detail later in this section.

For the implementation of ECMS, a lambda coefficient and a SoC reference value are inserted into the objective function of charging mode. The simplified lambda coefficient is the absolute difference of the SoC at the given time step minus the SoC reference value. Although, for electric vehicles, lambda exist in both discharging and charging (Musardo et al. 2005), this project avoids constraining the discharge operation using a battery cycling constrain coefficient, in contrast to similar studies such of Grimmelius et al. (2011) which applied a similar optimisation to hybrid tug vessels. Primarily, this happens because the battery discharge operation should be an output of the optimisation algorithm without user constraints in battery depletion using the lambda coefficient, which determines when to start charging the battery due to extreme difference between actual SoC and SoC reference. The SoC reference value is proposed by the designers in the automotive industry to be around 50 - 60% (Grammatico et al., 2010). According to Grimmelius et al. (2011), if the lambda coefficient is small, the optimisation algorithm will not use the battery aggressively. Based on that statement, the optimisation algorithm loses a degree of freedom, thus, in this project, due to the unconstrained nature of the optimisation problem, lambda will be used only as a trigger to start charging (inevitably) when SoC reaches 90%. Moreover, due to the fact that the obvious solution to the optimisation leg of charging is not to charge the battery as more energy is required instead of the desired load, lambda will be inserted in order to fulfil the minimum charging requirement. In this case, the designer should define the time period when the battery would be round the SoC reference value e.g. at the end of the day. Hence the modified lambda coefficient will be given by:

$$\lambda = \frac{\left| SoC_t - SoC_{ref} \right|}{t_{ref} - t_{el.}} \cdot \Delta t_{sim} \tag{4.10.1}$$

where,

$SoC_t$ : Battery State of Charge at simulation time t [%]
$SoC_{ref}$ : Reference Battery State of Charge, user defined [%]
$t_{ref}$ : Reference time where the $SoC_t$ must be equal to $SoC_{ref}$ [h]
$t_{ref}$ : Simulation elapsed time [h]
$\Delta t_{sim}$ : Simulation time step [h]

Based on equation (4.10.1), it can be extracted that when the simulation time approaches the time reference value, the charging will be more aggressive than in early simulation steps. When simulation time exceeds the reference value, the $t_{el.}$ variable is set again to zero and the process is restarted. Although, this equation maintains the SoC at the desired level, it is not guaranteed that the charging occurred in an optimum manner. To solve this problem, instead of producing a Dynamic Programming Code, as no future loading is 100% known in advance, the following propositions are made:

If the battery SoC is not equal to zero, it is different than the $SoC_{ref}$ and at the current simulation step the $P_{bat}$ = 0 based on the optimisation algorithm, the following criteria are applied:

a) Constrain charging if charging current is more than 5A. It can be extracted from Figure 3.13 that charging efficiency drops significantly in high charging currents.
b) In layouts B and C charging is not possible if engine speed is less than 60% of the nominal value.
c) The optimisation objective should be changed to operate the engine with the minimum SFOC. This requirement leads to a pseudo-multivariable optimisation problem, where, in particular cases, the two objectives are transformed again into a single objective problem, which is the $SFOC_{min}$ instead of the min*f*. When applying that type of optimisation, a set of assumptions and project-defined solutions should be applied. Firstly, the optimisation algorithm is programmed to identify the number of engines operating at low non-zero loads. It also counts the number of engines that operate at the same low load. Moreover, the algorithm is programmed to divide the equivalent extra loading by the number of generators, in order to increase the load of each of these engines into higher efficiency points. The $SFOC_{min}$ algorithm is driven by the fact that a parallel goal of this study is to reduce exhaust emissions. By increasing the load of the engines, the amount of Particulate Matter is reduced (Wright, 2000).
d) In cases where engine is loaded at a percentage higher than its optimum value, the c) criterion is not valid, since the engine needs to reduce the load to meet the

$SFOC_{min}$ and, as a result, no charging will occur. In addition, if the optimisation algorithm yields to no hybrid discharge mode, then the required charging will be defined by equation (4.10.1), simplifying the problem. Furthermore, this limit, maintains the $NO_x$ in low levels. This operation yields to a lower engine $NO_x$ cycle as the amount of operational time spent in high loads is reduced (Heywood, 1988; MAN Diesel, 2009).

e) In all cases where the objective is transformed to minimum SFOC, an extra linear inequality constraint is applied and given by the equation (4.10.2). Operating the engine at the optimum point might give a solution where the optimum storage power is higher than the storage capability, leading to non-feasible results.

$$\frac{x_i}{E_{Bat}} \cdot \Delta t_{sim} - DoD_{t-1} \leq 0 \tag{4.10.2}$$

where,

$x_i$ : Optimum charge power in order to have best engine SFOC [kW]

$E_{bat}$ : Installed Battery Energy Density [kWh]

$DoD_t$ : Battery Depth of Discharge at simulation time t [%]

In layouts D-B and D-C, if at the examined simulation step the solution of the optimisation algorithm results in absorbing energy from the battery and the SoC is different than the $SoC_{ref}$, then a comparison of the minimum fuel consumptions of running the electric machine as a motor (battery discharging) and running the electric machine as a generator (battery charging or in layout D-C electricity might provide energy for the auxiliary demand (optimisation output)) should be performed. However, in order to compare equivalent fuel consumptions, the power to be stored in the energy storage device should be equal to the value to be absorbed by the battery. This problem is solved by the appropriate logic criteria defined by the designer. For this strategy, it is proposed to check the optimisation algorithm output in terms of battery discharging. If the power output equals zero kW, then the system should charge because either the batteries are depleted, hence charging is imperative, or there is already a divergence between the SoC and its reference value, which should be covered. However, this strategy implies much cycling over battery when there are periods of repeated favourable conditions for the operation of the hybrid module. Nonetheless, the sizing of the Hybrid system is performed in a way that enables it to withstand up to 96 hours of consecutive discharging, as it was stated in Chapter 3.

#### *4.3.1.1 Layout D-A1*

The objective is to minimise fuel consumption of the Auxiliary engines for given electric loads, either as reported by the Chief Engineer, or taken directly from an energy audit performed on-board, or by simulating a random profile for the auxiliary loads containing energy demanding operations, such as ballast water exchanging, port loading/unloading, etc. The objective function is given by equation (4.10.3).

$$\min f = \left( \sum_{i=1}^{3} g\left(x_i\right) \cdot x_i \cdot MCR_{A/E} + \frac{SFOC_{\min}}{\eta_{T/F,inv} \cdot w\left( \frac{x_4}{N_{BB} \cdot V_{bat}} \right)} \cdot x_4 \right) \cdot \Delta t_{sim} \cdot 10^{-6} \qquad (4.10.3)$$

where,

g(x) : Specific Fuel Oil Consumption curve as extracted from Figure 3.8 [g/kWh]

w(x) : Battery Charge efficiency curves as obtained from Figure 3.6 [-]

$MCR_{A/E}$ : Maximum Continuous Rating of Auxiliary Diesel Engine [kW]

$SFOC_{min}$ : Minimum SFOC of Auxiliary Engine [g/kWh]

$\eta_{T/F,inv}$ : Battery Transformer and inverter efficiency, as given in Table 3.2[-]

$\Delta t_{sim}$ : Simulation time step [h]

The objective vector X is given by the following relationship:

$$X = \begin{bmatrix} x_1 \\ x_2 \\ x_3 \\ x_4 \end{bmatrix} = \begin{bmatrix} \text{Load}_{A/E1} \\ \text{Load}_{A/E2} \\ \text{Load}_{A/E3} \\ P_{battery} \end{bmatrix} \qquad (4.10.4)$$

where,

$x_1$-$x_3$ : Auxiliary Engine Loading [-]

$x_4$ : Power absorbed from battery banks [kW]

The optimisation problem contains lower and upper bounds and non-linear constraints. For the given optimisation problem, the lower bound and upper bound limit vectors are given below:

$$lb = \begin{bmatrix} 0 & 0 & 0 & 0 \end{bmatrix} \tag{4.10.5}$$

$$ub = \begin{bmatrix} 1 & 1 & 1 & \left(1 - DoD_{t-1}\right) \cdot \dfrac{\text{Bat}_{\text{cap.}}}{\Delta t_{sim}} \end{bmatrix} \tag{4.10.6}$$

where,

$DoD_{t-1}$ : Battery Depth of Discharge at previous time step [%]

$Bat_{cap}$ : Battery Energy Capacity, defined at the design stage or by Table 3.8 [kWh]

This non-linear optimisation problem has a linear inequality for the discharge current. The linear inequality has to be in the following form:

$$AX \leq b \tag{4.10.7}$$

Thus,

$$\frac{1}{\left(16 \cdot N_{BB}\right) \cdot V_{Bat}} \cdot x_4 \leq \max_{d.c.} \tag{4.10.8}$$

where,

$V_{Bat}$ : Battery Voltage [V]

$Max_{d.c.}$ : Battery Maximum Discharge current, as presented in Figure 3.5 [A]

The non-linear equality regarding how the hybrid system will meet the power requirements is given by the following equation:

$$\sum_{i=1}^{3}\left(x_i \cdot MCR_{A/E} \cdot \eta_{gen}\right) + \eta_{T/F,inv} \cdot w\left(\frac{x_4}{N_{BB} \cdot V_{Bat}}\right) \cdot x_4 = \frac{P_{req.}}{\eta_{loss}} \tag{4.10.9}$$

where,

$\eta_{gen}$ : Auxiliary Engine generator efficiency, as given in Table 3.2 [-]

$\eta_{loss}$ : Transmission losses, as given in Table 3.2 [-]

$P_{req.}$ : Required Power [kW]

For the charging scenario, the number of running generators is known in advance. The algorithm selects the number of the worst loaded engines and increases their load in order

to minimise their specific fuel oil consumption. Hence, the following non-linear optimisation constraint has to be satisfied by the process:

$$\sum_{i=1}^{3}\left(x_i \cdot MCR_{A/E} \cdot \eta_{gen}\right) - \eta_{T/F,inv} \cdot w_2\left(\frac{x_4}{N_{BB} \cdot V_{Bat}}\right) \cdot x_4 = \frac{P_{req.}}{\eta_{loss}} \qquad (4.10.10)$$

### *4.3.1.2 Layout D-A2*

The only difference between Layout D-A1 and Layout D-A2 is that Layout D-A2 will probably not have identical generator sets. Based on the preliminary study that was described in Chapter 3, the principle of switching generator sets on and off and running them at near optimum loading points covering all the demands of the vessel, is investigated by this optimisation algorithm. Based on the initial analysis, two types of Diesel Generator Sets will be used. Consequently, the optimisation algorithm of D-A1 layout is altered in specific parts. The equations describing this system are given bellow:

$$\min f = \left( \begin{array}{l} \sum_{i=1}^{n} g\left(x_i\right) \cdot x_i \cdot MCR_{A/E1} + \sum_{i=1}^{m} h\left(x\right) \cdot x_i \cdot MCR_{A/E2} \\ + \dfrac{SFOC_{\min}}{\eta_{T/F,inv} \cdot \eta_{loss} \cdot w\left(\dfrac{x_4}{N_{BB} \cdot V_{Bat}}\right)} \cdot x_4 \end{array} \right) \cdot \Delta t_{sim} \cdot 10^{-6} \qquad (4.10.11)$$

where,

g(x) : Specific Fuel Oil Consumption curve for type I Diesel Generator Set obtained from the manufacturer [g/kWh]

h(x) : Specific Fuel Oil Consumption curve for type II Diesel Generator Set obtained from the manufacturer [g/kWh]

The non-linear equality constraint that defines how the hybrid system will meet the power requirements is given by the following equation:

$$\begin{array}{l} \sum_{i=1}^{n}\left(x_i \cdot MCR_{A/E\ I} \cdot \eta_{gen\ I}\right) + \sum_{i=1}^{m}\left(x_i \cdot MCR_{A/E\ II} \cdot \eta_{gen\ II}\right) + \\ + \eta_{T/F,inv} \cdot w\left(\dfrac{x_{n+m+1}}{N_{BB} \cdot V_{Bat}}\right) \cdot x_{n+m+1} = \dfrac{P_{req.}}{\eta_m\left(P_{prd.}\right) \cdot \eta_{loss} \cdot \eta_{T/F} \cdot \eta_{Conv.}} \end{array} \qquad (4.10.12)$$

For the charging scenario, the (4.10.12) is transformed to:

$$\sum_{i=1}^{n}\left(x_i \cdot MCR_{A/E\ I} \cdot \eta_{gen\ I}\right)+\sum_{i=1}^{m}\left(x_i \cdot MCR_{A/E\ II} \cdot \eta_{gen\ II}\right) - \\ -\eta_{T/F,inv} \cdot w\left(\frac{x_{n+m+1}}{N_{BB} \cdot V_{Bat}}\right) \cdot x_{n+m+1} = \frac{P_{req.}}{\eta_m\left(P_{prd.}\right) \cdot \eta_{T/F} \cdot \eta_{loss} \cdot \eta_{Conv.}} \tag{4.10.13}$$

where,

$P_{req.}$ : Required Power [kW]

$P_{prd.}$ : Produced Power [kW]

$\eta_m$ : Electric motor efficiency curve, as depicted in Figure 3.7 or supplied by the motor manufacturer

$\eta_{T/F}$ : Propulsion motor transformer efficiency, as given in Table 3.2[-]

$\eta_{conv.}$ : Propulsion converter efficiency, as given in Table 3.2 [-]

#### *4.3.1.3 Layout D-B*

This layout describes a Hybrid system where the existence of the battery aids only the main propulsion. The electricity is supplied to an electric motor, which is coupled to a gearbox-clutch. This motor provides the extra power for the propulsion when needed. Charging occurs only when the electric machine operates as a generator. In order for the latter to operate as a generator, constraints apply as described previously. In the simulation, the voyage phase is a user input. In this case, the controller understands how to treat the hybrid system. Moreover, in every simulation time step, the propulsion power is divided by the engine MCR, in order to define the initial operational point of the engine, thus deciding which optimisation algorithm to apply. The objective is to minimise fuel consumption. Hence the objective function is given by equation (4.10.14).

$$\min f = \left(\begin{array}{l} d\left(x_1\right) \cdot x_1 \cdot MCR_{M/E} + \\ +\dfrac{SFOC_{\min}}{\eta_{T/F,inv} \cdot \eta_{loss} \cdot \eta_g \cdot \eta_{conv.} \cdot \eta_m\left(x_2\right) \cdot w\left(x_2\right)} \cdot x_2 \end{array}\right) \cdot \Delta t_{sim} \cdot 10^{-6} \tag{4.10.14}$$

The optimisation vector X is given by the following relationship:

$$X = \begin{bmatrix} X_1 \\ X_2 \end{bmatrix} = \begin{bmatrix} \text{Load}_{\text{M/E}} \\ P_{battery} \end{bmatrix} \tag{4.10.15}$$

where,

$x_1$ : Main Engine Loading [-]

$x_2$ : Power absorbed from battery banks [kW]

The optimisation problem contains lower and upper bounds and non-linear constraints. For the given optimisation problem, the lower bound and upper bound limit vectors are given below:

$$lb = \begin{bmatrix} 0 & 0 \end{bmatrix} \tag{4.10.16}$$

$$ub = \begin{bmatrix} p(rpm) & \min\left(MCR_m, \quad (1 - DoD_{t-1}) \cdot \mathrm{Bat}_{\mathrm{cap.}}\right) \end{bmatrix} \tag{4.10.17}$$

Layout D-B has the same constraints as described by equations (4.10.7) - (4.10.8).

The non-linear equality regarding on how the hybrid system will meet the power requirements is given by the following equation (4.10.18):

$$\eta_g \cdot \left(MCR_{M/E} \cdot x_1 + \eta_C \cdot \eta_{T/F} \cdot \eta_{loss} \cdot \eta_{T/F,inv} \cdot \eta_m\left(x_2\right) \cdot w\left(x_2\right) \cdot x_2\right) = P_{req.} \tag{4.10.18}$$

Although equations (4.10.14) - (4.10.18) outline the hybrid controller behaviour for the main propulsion when the electric machine operates as a motor, for the majority of the operational period, due to conversion losses, the system is running as a shaft generator, hence the electric machine acts as generator and the batteries are either charging, or are decoupled from the system and the propulsion machinery behaves conventionally. The optimisation objective is once again changed to that of minimum SFOC. The lambda coefficient is introduced again without any modifications to the equation (4.10.1) and charging constraints remain intact. However, because this study refers to vessels equipped with a single propulsion engine (except the AES concept), there is no capability of optimising the engine with the worst operational loading, as is the case with the Diesel Generators. The non-linear constraints that the optimisation has to satisfy are given below:

$$\eta_g \cdot \left( MCR_{M/E} \cdot x_1 - \eta_C \cdot \eta_{T/F} \cdot \eta_{loss} \cdot \eta_{T/F,inv} \cdot \eta_m \left( x_2 \right) \cdot w\left( x_2 \right) \cdot x_2 \right) = P_{req.} \quad (4.10.19)$$

where,

$x_1$ : Main Engine loading [-]

$x_2$ : Optimum battery charging power in order to minimise Main Engine's SFOC value [kW]

#### *4.3.1.4 Layout D-C*

This layout describes the fully Hybrid vessel. The total power demand (auxiliary loads and main propulsion) is managed by the controller. The scope of the optimisation algorithm is set to minimise the total fuel oil consumption of the vessel. The optimisation algorithm is run for two operational scenarios during sea passage. The first is when the electric machine operates as an electric motor and the second as an electric generator. The two solutions of the optimisation algorithm are compared to each other, and the lower of the two yields to the global optimum solution (Grimmelius et al., 2011). In manoeuvring and in slow steaming (<60% Main engine load), the problem is covered by the first scenario. Thus, for the motor condition in discharging mode:

$$\min f_{\text{m-dis.}} = \left( \begin{array}{l} d\left( x_1 \right) \cdot x_1 \cdot MCR_{M/E} + \\ + \sum_{i=2}^{4} \left( g\left( x_i + x_{i+4} \right) \right) \cdot \left( x_i + x_{i+4} \right) \cdot MCR_{A/E} + \\ + \dfrac{SFOC_{\min\ M/E} \cdot \left( x_5 + x_9 \right)}{\eta_{T/F,inv} \cdot \eta_{conv.} \cdot \eta_m \left( x_5 + x_9 \right) \cdot w\left( x_5 + x_9 \right)} \end{array} \right) \cdot \Delta t_{sim} \cdot 10^{-6} \quad (4.10.20)$$

For the scenario where the hybrid system is charged during the motor condition, the objective is to minimise the SFOC of the Auxiliary engines. The process was described in layout D-A1.

In cases where the electric machine operates in generator mode, the objective functions are given by:

$$\min f_{\text{gen-dis.}} = \left( \begin{array}{l} d\left(x_1 + x_2\right) \cdot \left(x_1 + x_2\right) \cdot MCR_{M/E} + \\ + \sum_{i=3}^{5} g\left(x_i\right) \cdot \left(x_i\right) \cdot MCR_{A/E} + \\ + \dfrac{SFOC_{\text{min M/E}} \cdot x_6}{\eta_{T/F,inv} \cdot \eta_{conv.} \cdot \eta_m\left(x_6\right) \cdot w\left(x_6\right)} \end{array} \right) \cdot \Delta t_{sim} \cdot 10^{-6} \qquad (4.10.21)$$

$$\min f_{\text{gen,charg.}} = \left( \begin{array}{l} d\left(x_1 + x_2\right) \cdot \left(x_1 + x_2\right) \cdot MCR_{M/E} + \\ + \sum_{i=3}^{5} g\left(x_i\right) \cdot \left(x_i\right) \cdot MCR_{A/E} \end{array} \right) \cdot \Delta t_{sim} \cdot 10^{-6} \qquad (4.10.22)$$

The non-linear constraints for the scenario where the electric machine operates as an electric motor are defined by equations (4.10.23) -(4.10.26).

For the propulsion load demand it can be extracted that:

$$\begin{array}{l} x_1 \cdot MCR_{M/E} + \eta_g \cdot \eta_m\left(P_{A/E} + x_5\right) \cdot \eta_C \cdot \eta_{T/F} \cdot \eta_{loss} \cdot \sum_{i=2}^{4} x_i \cdot MCR_{A/E} + \\ \eta_g \cdot \eta_m\left(P_{A/E} + x_5\right) \cdot \eta_C \cdot \eta_{loss} \cdot \eta_{T/F,inv} \cdot w\left(x_5 + x_{10}\right) \cdot x_5 = P_{shaft} \end{array} \qquad (4.10.23)$$

For the auxiliary loads in discharging mode, it can be written that:

$$\sum_{i=6}^{9}\left(x_i \cdot MCR_{A/E}\right) + \eta_{loss} \cdot \eta_{T/F,inv} \cdot w\left(x_5 + x_{10}\right) \cdot x_{10} = P_{aux.} \qquad (4.10.24)$$

For the propulsion load demand in charging mode, it can be extracted that:

$$\eta_g \cdot x_1 \cdot MCR_{M/E} = P_{shaft} \qquad (4.10.25)$$

For the auxiliary loads in charging mode, it can be said that:

$$\sum_{i=2}^{4}\left(x_i \cdot MCR_{A/E}\right) - \eta_{T/F\,inv.} \cdot x_5 = P_{aux.} \qquad (4.10.26)$$

The optimisation vector X along with the lower and upper bounds is given by the following matrix expression:

$$\begin{bmatrix} 0.6 \\ 0 \\ 0 \\ 0 \\ 0 \\ 0 \\ 0 \\ 0 \\ 0 \end{bmatrix} \leq X = \begin{bmatrix} X_1 \\ X_2 \\ X_3 \\ X_4 \\ X_5 \\ X_6 \\ X_7 \\ X_8 \\ X_9 \end{bmatrix} \leq \begin{bmatrix} p(rpm) \\ 1 \\ 1 \\ 1 \\ \min\left(MCR_m, \left((1-DoD_{in})\cdot \mathrm{Bat}_{\mathrm{cap.}}\right)\right) \\ 1 \\ 1 \\ 1 \\ \left((1-DoD_{in})\cdot \mathrm{Bat}_{\mathrm{cap.}}\right) \end{bmatrix} \tag{4.10.27}$$

where,

$x_1$ : Main Engine load [-]

$x_2 - x_4$ : Auxiliary load intended for propulsion [-]

$x_5$ : Battery power intended for propulsion [kW]

$x_6 - x_8$ : Auxiliary load intended for hotel loads [-]

$x_9$ : Battery power intended for hotel loads [kW]

The problem consists of linear inequality constraints following the expression (4.10.28)

$$A \cdot X \leq b \tag{4.10.28}$$

The A vector is given by:

$$A = \begin{bmatrix} 1 & 0 & 0 & 0 & 0 & 0 & 0 & 0 & 0 \\ 0 & 1 & 0 & 0 & 0 & 1 & 0 & 0 & 0 \\ 0 & 0 & 1 & 0 & 0 & 0 & 1 & 0 & 0 \\ 0 & 0 & 0 & 1 & 0 & 0 & 0 & 1 & 0 \\ 0 & 0 & 0 & 0 & 1 & 0 & 0 & 0 & 1 \\ 0 & MCR_{A/E} & MCR_{A/E} & MCR_{A/E} & 1 & 0 & 0 & 0 & 0 \end{bmatrix} \tag{4.10.29}$$

The ***b*** vector is given by:

$$\boldsymbol{b} = \begin{bmatrix} 1 \\ 1 \\ 1 \\ 1 \\ (1 - DoD_{in}) \cdot \text{Bat}_{\text{cap.}} \\ MCR_m \end{bmatrix} \tag{4.10.30}$$

The linear constraint expressions (4.10.29) and (4.10.30) constrain the variables that refer to the engine loads and to the battery discharge power. Due to the complexity of the problem, each engine load and battery power was divided into two. The first goes to the propulsion demand and the second goes to the auxiliary demand. The result of the summation of each 'sub-loading' set has to be lower than 100% of the engine's MCR and for the battery power, lower than the maximum power capability at the examined simulation time step.

The non-linear constraints for the scenario where the electric machine operates as an electric generator are outlined by the following equations.

For both the discharging and charging mode of the battery bank, the propulsion demand is described by (4.10.31).

$$\eta_g \cdot x_1 \cdot MCR_{M/E} = P_{shaft} \tag{4.10.31}$$

The non-linear constraints for the scenario where the electric machine operates as an electric generator and the Hybrid system is run in discharging mode, can be expressed as follows:

$$\begin{aligned} &\eta_g \cdot \eta_m(x_2) \cdot \eta_C \cdot \eta_{T/F} \cdot \eta_{loss} \cdot x_2 \cdot MCR_{M/E} + \eta_{gen} \cdot \eta_{loss} \cdot \sum_{i=3}^{5} x_i \cdot MCR_{A/E} + \\ &+ \eta_{loss} \cdot \eta_{T/F,inv} \cdot w(x_6) \cdot x_6 = P_{aux.} \end{aligned} \tag{4.10.32}$$

The non-linear constraints for the scenario where the electric machine operates as an electric generator and the Hybrid system is run in charging mode, for the auxiliary and charging loads, can be expressed as follows:

$$\eta_g \cdot \eta_m\left(x_2\right) \cdot \eta_C \cdot \eta_{T/F} \cdot \eta_{loss} \cdot x_2 \cdot MCR_{M/E} + \eta_{gen} \cdot \eta_{loss} \cdot \sum_{i=3}^{5} x_i \cdot MCR_{A/E} -$$
$$- \frac{1}{\eta_{loss} \cdot \eta_{T/F,inv}} \cdot w\left( \frac{\lambda \cdot \frac{E_{Bat}}{\Delta t_{sim}}}{N_{BB} \cdot V_{Bat}} \right) \cdot \lambda \cdot \frac{E_{Bat}}{\Delta t_{sim}} = P_{aux.} \tag{4.10.33}$$

The optimisation vector X along with the lower and upper bounds is given by the matrix expression (4.10.34):

$$\begin{bmatrix} 0 \\ 0 \\ 0 \\ 0 \\ 0 \\ 0 \end{bmatrix} \leq X = \begin{bmatrix} X_1 \\ X_2 \\ X_3 \\ X_4 \\ X_5 \\ X_6 \end{bmatrix} \leq \begin{bmatrix} p\left(rpm\right) \\ \frac{MCR_m}{MCR_{M/E}} \\ 1 \\ 1 \\ 1 \\ \left(1 - DoD_{in}\right) \cdot \mathrm{Bat}_{\mathrm{cap.}} \end{bmatrix} \tag{4.10.34}$$

where,

$x_{1,2}$ : Main Engine Load [-]

$x_{3\text{-}5}$ : Auxiliary Engine Load [-]

$x_6$ : Power to charge battery [kW]

The problem consists of linear inequality constraints following, once again, the expression (4.10.28) where the vector A is given by (4.10.35) and the $\boldsymbol{b}$ by (4.10.36).

$$A = \begin{bmatrix} MCR_{M/E} & MCR_m & 0 & 0 & 0 \end{bmatrix} \tag{4.10.35}$$

The $\boldsymbol{b}$ vector is given by:

$$\boldsymbol{b} \leq \begin{bmatrix} MCR_{M/E} \end{bmatrix} \tag{4.10.36}$$

When the system is charging the battery banks, the following constraints and bounds are applied to the optimisation algorithm.

The lower and upper bounds are given by the following equations, respectively.

$$lb = \left[ 0 \quad 0 \quad 0 \quad 0 \quad 0 \quad \min\left( DoD_{in} \cdot \mathrm{Bat}_{\mathrm{cap.}}, \lambda \cdot \frac{E_{Bat}}{\Delta t_{sim}} \right) \right] \tag{4.10.37}$$

$$ub = \left[ 1 \quad \frac{MCR_m}{MCR_{M/E}} \quad 1 \quad 1 \quad 1 \quad DoD_{in} \cdot \mathrm{Bat}_{\mathrm{cap.}} \right] \tag{4.10.38}$$

The linear inequality matrix is given by:

$$A = \left[ MCR_{M/E} \quad MCR_m \quad 0 \quad 0 \quad 0 \quad 0 \right] \tag{4.10.39}$$

And the inequality vector ***b*** by:

$$\boldsymbol{b} = \left[ MCR_{M/E} \right] \tag{4.10.40}$$

### 4.3.2 Equivalent Cost Minimisation Strategy (ECMS)

For the purpose of identifying actual and future fuel savings, the aforementioned layouts have been transformed using the ECMS strategy. The identified differences are found in the objective functions, where an equivalent fuel saving replaces the objective function, which minimises PM emissions. In practical terms, the constraints and the bounds of the variable vector remain as they have been presented in 4.3.1. To further clarify this procedure, the following equations outline the ECMS strategy for each scenario.

#### *4.3.2.1 Layout D-A1*

When the Hybrid system is in operation, two operational modes are identified. The first when the batteries are in discharging mode, where their operation has an equivalent fuel penalty and the second where the batteries charge and their operation has an equivalent fuel saving. Thus:

**Discharging mode:**

The objective function while the system is discharging is given by:

$$\min f = \left( \sum_{i=1}^{3} g\left(x_i\right) \cdot x_i \cdot MCR_{A/E} + \frac{SFOC_{\min}}{\eta_{T/F,inv} \cdot w\left( \frac{x_4}{N_{BB} \cdot V_{bat}} \right)} \cdot x_4 \right) \cdot \Delta t_{sim} \cdot 10^{-6} \tag{4.11.1}$$

The non-linear equality regarding how the hybrid system will meet the power requirements is given by the following equation:

$$\sum_{i=1}^{3}\left(x_i \cdot MCR_{A/E} \cdot \eta_{gen}\right) + \eta_{T/F,inv} \cdot w\left(\frac{x_4}{N_{BB} \cdot V_{Bat}}\right) \cdot x_4 = P_{req.} \qquad (4.11.2)$$

The lower and upper bounds of the optimisation vector is given by:

$$\begin{bmatrix} 0 \\ 0 \\ 0 \\ 0 \end{bmatrix} \leq \begin{bmatrix} x_1 \\ x_2 \\ x_3 \\ x_4 \end{bmatrix} \leq \begin{bmatrix} 1 \\ 1 \\ 1 \\ \left(1 - DoD_{t-1}\right) \cdot \dfrac{\mathrm{Bat}_{\mathrm{cap.}}}{\Delta t_{sim}} \end{bmatrix} \qquad (4.11.3)$$

where,

$x_1$-$x_3$ : Auxiliary Engine Loading [-]

$x_4$ : Power absorbed from battery banks [kW]

**Charging mode:**

However, the objective function in charging conditions is presented by:

$$\min f = \begin{pmatrix} \sum_{i=1}^{3} g\left(x_i\right) \cdot x_i \cdot MCR_{A/E} \\ -\eta_{T/F,inv} \cdot w\left(\dfrac{x_4}{N_{BB} \cdot V_{bat}}\right) \cdot SFOC_{\min} \cdot x_4 \end{pmatrix} \cdot \Delta t_{sim} \cdot 10^{-6} \qquad (4.11.4)$$

The non-linear equality regarding how the hybrid system will meet the power requirements is given by the following equation:

$$\sum_{i=1}^{3}\left(x_i \cdot MCR_{A/E} \cdot \eta_{gen}\right) + \eta_{T/F,inv} \cdot w\left(\frac{x_4}{N_{BB} \cdot V_{Bat}}\right) \cdot x_4 = P_{req.} \qquad (4.11.5)$$

Hence, the following non-linear optimisation constraint has to be satisfied by the process:

$$\sum_{i=1}^{3}\left(x_i \cdot MCR_{A/E} \cdot \eta_{gen}\right) - \eta_{T/F,inv} \cdot w_2\left(\frac{x_4}{N_{BB} \cdot V_{Bat}}\right) \cdot x_4 = P_{req.} \qquad (4.11.6)$$

The lower and upper bounds of the optimisation vector is given by:

$$\begin{bmatrix} 0 \\ 0 \\ 0 \\ 0 \end{bmatrix} \leq \begin{bmatrix} x_1 \\ x_2 \\ x_3 \\ x_4 \end{bmatrix} \leq \begin{bmatrix} 1 \\ 1 \\ 1 \\ DoD_{t-1} \cdot \dfrac{\text{Bat}_{\text{cap.}}}{\Delta t_{sim}} \end{bmatrix} \tag{4.11.7}$$

Usually, the global solution is found by comparing the fuel consumption of (4.11.1) and (4.11.4). However, the non-existence of the λ coefficient, which constraints the cycling over battery, leads to the implication of two more logic criteria. The first criterion is when the optimisation yields to zero cycling over battery because the optimised solution is for the system to act as a non-hybrid system. At that point, the system is forced to charge the battery with a minimum fuel denoted by the time step value of the λ coefficient. Moreover, a charging forcing criterion is applied when the battery SoC is lower than 20% but higher than 10%. When, the DoD of the battery reaches 80%, the algorithm imposes a charge current. The comparison of the solutions is again overwritten and the battery is charged.

### *4.3.2.2 Layout D-A2*

The objective function while the system is discharging is given by (4.10.11). However, for the objective function in charging conditions:

$$\min f = \begin{pmatrix} \sum_{i=1}^{n} g(x_i) \cdot x_i \cdot MCR_{A/E1} + \sum_{i=1}^{m} h(x) \cdot x_i \cdot MCR_{A/E2} - \\ -\eta_{T/F,inv} \cdot w\left(\dfrac{x_4}{N_{BB} \cdot V_{Bat}}\right) \cdot SFOC_{\min} \cdot x_4 \end{pmatrix} \cdot \Delta t_{sim} \cdot 10^{-6} \tag{4.11.8}$$

The same logic criteria as in 4.3.2.1 are applied.

### *4.3.2.3 Layout D-B*

This layout describes a Hybrid system where the existence of the battery aids only the main propulsion. The electricity is supplied to an electric motor, which is coupled to a gearbox-clutch. This motor provides the extra power for the propulsion when needed. Charging occurs only when the electric machine operates as a generator.

The objective is to minimise fuel consumption.

**Discharging mode:**

The objective function is given by equation (4.11.9).

$$\min f = \left( \begin{array}{c} d\left(x_1\right) \cdot x_1 \cdot MCR_{M/E} + \\ + \dfrac{SFOC_{\min}}{\eta_{T/F,inv} \cdot \eta_{loss} \cdot \eta_g \cdot \eta_{conv.} \cdot \eta_m\left(x_2\right) \cdot w\left(x_2\right)} \cdot x_2 \end{array} \right) \cdot \Delta t_{sim} \cdot 10^{-6} \quad (4.11.9)$$

The non-linear equality regarding on how the hybrid system will meet the power requirements is given by the following equation (4.11.10):

$$\eta_g \cdot \left( MCR_{M/E} \cdot x_1 + \eta_C \cdot \eta_{T/F} \cdot \eta_{loss} \cdot \eta_{T/F,inv} \cdot \eta_m\left(x_2\right) \cdot w\left(x_2\right) \cdot x_2 \right) = P_{req.} \quad (4.11.10)$$

where,

$x_1$ : Main Engine Loading [-]

$x_2$ : Power absorbed from battery banks [kW]

The lower and upper bounds of the optimisation vector is given by:

$$\begin{bmatrix} 0 \\ 0 \end{bmatrix} \le \begin{bmatrix} x_1 \\ x_2 \end{bmatrix} \le \begin{bmatrix} p\left(rpm\right) \\ \min\left(MCR_m, \left(1 - DoD_{t-1}\right) \cdot \mathrm{Bat}_{\mathrm{cap.}}\right) \end{bmatrix} \quad (4.11.11)$$

**Charging mode:**

The objective function in charging conditions:

$$\min f = \left( \begin{array}{l} d\left(x_1\right) \cdot x_1 \cdot MCR_{M/E} - \eta_{T/F,inv} \cdot \eta_{loss} \cdot \eta_g \cdot \\ \cdot \eta_{conv.} \cdot \eta_m\left(x_2\right) \cdot w\left(x_2\right) \cdot SFOC_{\min} \cdot x_2 \end{array} \right) \cdot \Delta t_{sim} \cdot 10^{-6} \quad (4.11.12)$$

The non-linear constraints that the optimisation has to satisfy are given below:

$$\eta_g \cdot \left( MCR_{M/E} \cdot x_1 - \eta_C \cdot \eta_{T/F} \cdot \eta_{loss} \cdot \eta_{T/F,inv} \cdot \eta_m \left( x_2 \right) \cdot w\left( x_2 \right) \cdot x_2 \right) = P_{req.} \tag{4.11.13}$$

where,

$x_1$ : Main Engine Loading [-]

$x_2$ : Power absorbed from battery banks [kW]

The lower and upper bounds of the optimisation vector is given by:

$$\begin{bmatrix} 0 \\ 0 \end{bmatrix} \leq \begin{bmatrix} x_1 \\ x_2 \end{bmatrix} \leq \begin{bmatrix} p(rpm) \\ \min\left( MCR_m, DoD_{t-1} \cdot \mathrm{Bat}_{\mathrm{cap.}} \right) \end{bmatrix} \tag{4.11.14}$$

### *4.3.2.4 Layout D-C*

For the Layout D-C scenario, two conditions are identified. The first is when the electric machine operates as a motor and the second when it acts as a shaft generator.

**Motor condition – Discharging mode:**

The objective function is depicted by:

$$\min f_{\text{m-dis.}} = \left( \begin{array}{l} d\left( x_1 \right) \cdot x_1 \cdot MCR_{M/E} + \\ + \sum_{i=2}^{4} \left( g\left( x_i + x_{i+4} \right) \right) \cdot \left( x_i + x_{i+4} \right) \cdot MCR_{A/E} + \\ + \dfrac{SFOC_{\min\ A/E} \cdot \left( x_5 + x_9 \right)}{\eta_{T/F,inv} \cdot \eta_{conv.} \cdot \eta_m \left( x_5 + x_9 \right) \cdot w\left( x_5 + x_9 \right)} \end{array} \right) \cdot \Delta t_{sim} \cdot 10^{-6} \tag{4.11.15}$$

The lower and upper bounds of the optimisation vector is given by:

$$\begin{bmatrix} 0.6 \\ 0 \\ 0 \\ 0 \\ 0 \\ 0 \\ 0 \\ 0 \\ 0 \end{bmatrix} \leq X = \begin{bmatrix} x_1 \\ x_2 \\ x_3 \\ x_4 \\ x_5 \\ x_6 \\ x_7 \\ x_8 \\ x_9 \end{bmatrix} \leq \begin{bmatrix} p(rpm) \\ 1 \\ 1 \\ 1 \\ \min\left(MCR_m, \left((1-DoD_{in})\cdot \mathrm{Bat}_{\mathrm{cap.}}\right)\right) \\ 1 \\ 1 \\ 1 \\ \left((1-DoD_{in})\cdot \mathrm{Bat}_{\mathrm{cap.}}\right) \end{bmatrix} \tag{4.11.16}$$

where,

$x_1$ : Main Engine load [-]
$x_2 - x_4$ : Auxiliary load intended for propulsion [-]
$x_5$ : Battery power intended for propulsion [kW]
$x_6 - x_8$ : Auxiliary load intended for hotel loads [-]
$x_9$ : Battery power intended for hotel loads [kW]

The linear constraints which are applicable to the D-C motor discharging scenario:

The A matrix:

$$A = \begin{bmatrix} 1 & 0 & 0 & 0 & 0 & 0 & 0 & 0 & 0 \\ 0 & 1 & 0 & 0 & 0 & 1 & 0 & 0 & 0 \\ 0 & 0 & 1 & 0 & 0 & 0 & 1 & 0 & 0 \\ 0 & 0 & 0 & 1 & 0 & 0 & 0 & 1 & 0 \\ 0 & 0 & 0 & 0 & 1 & 0 & 0 & 0 & 1 \\ 0 & MCR_{A/E} & MCR_{A/E} & MCR_{A/E} & 1 & 0 & 0 & 0 & 0 \end{bmatrix} \tag{4.11.17}$$

and the $\boldsymbol{b}$ vector by:

$$\boldsymbol{b} = \begin{bmatrix} 1 \\ 1 \\ 1 \\ 1 \\ \left(1-DoD_{in}\right)\cdot \mathrm{Bat}_{\mathrm{cap.}} \\ MCR_m \end{bmatrix} \tag{4.11.18}$$

The non-linear constraints for the scenario where the electric machine operates as an electric motor are defined by equations (4.11.19) – (4.11.20).

For the propulsion load demand loads in discharging mode it can be extracted that:

$$\begin{aligned} &x_1 \cdot MCR_{M/E} + \eta_g \cdot \eta_m \left(P_{A/E} + x_5\right) \cdot \eta_C \cdot \eta_{T/F} \cdot \eta_{loss} \cdot \sum_{i=2}^{4} x_i \cdot MCR_{A/E} + \\ &\eta_g \cdot \eta_m \left(P_{A/E} + x_5\right) \cdot \eta_C \cdot \eta_{loss} \cdot \eta_{T/F,inv} \cdot w\left(x_5 + x_{10}\right) \cdot x_5 = P_{shaft} \end{aligned} \tag{4.11.19}$$

For the auxiliary loads in discharging mode, it can be written that:

$$\sum_{i=6}^{9} \left(x_i \cdot MCR_{A/E}\right) + \eta_{loss} \cdot \eta_{T/F,inv} \cdot w\left(x_5 + x_{10}\right) \cdot x_{10} = P_{aux.} \tag{4.11.20}$$

**Motor condition – Charging mode:**

The objective function is given by:

$$\min f_{m-\text{charg.}} = \left( \sum_{i=1}^{n} g\left(x_i\right) \cdot x_i - x_4 \cdot \eta_{T/F,inv} \cdot w\left( \frac{x_4}{N_{BB} \cdot V_{bat}} \right) \cdot SFOC_{\min} \right) \cdot \Delta t_{sim} \cdot 10^{-6} \tag{4.11.21}$$

The lower and upper bounds of the optimisation vector is given by:

$$\begin{bmatrix} 0 \\ 0 \\ 0 \\ 0 \\ \min\left( DoD_{in} \cdot \text{Bat}_{\text{cap.}}, \lambda \cdot \frac{E_{Bat}}{\Delta t_{sim}} \right) \end{bmatrix} \leq X = \begin{bmatrix} x_1 \\ x_2 \\ x_3 \\ x_4 \\ x_5 \end{bmatrix} \leq \begin{bmatrix} p\left(rpm\right) \\ 1 \\ 1 \\ 1 \\ DoD_{in} \cdot \text{Bat}_{\text{cap.}} \end{bmatrix} \tag{4.11.22}$$

where,

$x_1$ : Main Engine load [-]

$x_2 – x_4$ : Auxiliary load [-]

$x_5$ : Battery charged power [kW]

The linear constraints which are applicable to the D-C motor charging scenario:

The A matrix:

$$A = \begin{bmatrix} 0 & 0 & 0 & \dfrac{1}{\left(16 \cdot N_{BB}\right) \cdot V_{Bat}} \end{bmatrix} \tag{4.11.23}$$

The $\boldsymbol{b}$ vector by:

$$\boldsymbol{b} = \max_{d.c.} \tag{4.11.24}$$

The non-linear constraints for the scenario where the electric machine operates as an electric motor are defined by equations (4.11.25) – (4.11.26).

For the propulsion load demand in charging mode, it can be extracted that:

$$\eta_g \cdot x_1 \cdot MCR_{M/E} = P_{shaft} \tag{4.11.25}$$

For the auxiliary loads in charging mode, it can be said that:

$$\sum_{i=2}^{4} \left( x_i \cdot MCR_{A/E} \right) - \eta_{T/F\ inv.} \cdot x_5 = P_{aux.} \tag{4.11.26}$$

**Generator condition – Discharging mode:**

The objective functions is given by:

$$\min f_{\text{gen-dis.}} = \begin{pmatrix} d\left(x_1 + x_2\right) \cdot \left(x_1 + x_2\right) \cdot MCR_{M/E} + \\ + \sum_{i=3}^{5} g\left(x_i\right) \cdot \left(x_i\right) \cdot MCR_{A/E} - \eta_{T/F,inv} \cdot \\ \eta_{conv.} \cdot \eta_m\left(x_6\right) \cdot w\left(x_6\right) \cdot SFOC_{\min\ \text{M/E}} \cdot x_6 \end{pmatrix} \cdot \Delta t_{sim} \cdot 10^{-6} \tag{4.11.27}$$

The lower and upper bound of the optimisation vector are given by:

$$\begin{bmatrix} 0 \\ 0 \\ 0 \\ 0 \\ 0 \\ 0 \end{bmatrix} \leq X = \begin{bmatrix} x_1 \\ x_2 \\ x_3 \\ x_4 \\ x_5 \\ x_6 \end{bmatrix} \leq \begin{bmatrix} p\left(rpm\right) \\ \dfrac{MCR_m}{MCR_{M/E}} \\ 1 \\ 1 \\ 1 \\ \left(1 - DoD_{in}\right) \cdot \text{Bat}_{\text{cap.}} \end{bmatrix} \tag{4.11.28}$$

where,

$x_{1,2}$ : Main Engine Load [-]
$x_{3\text{-}5}$ : Auxiliary Engine Load [-]
$x_6$ : Power to absorb from battery [kW]

The linear constraints which are applicable to the D-C generator discharging scenario:

The A matrix:

$$A = \begin{bmatrix} 1 & 1 & 0 & 0 & 0 \end{bmatrix} \tag{4.11.29}$$

and the $\boldsymbol{b}$ vector by:

$$\boldsymbol{b} = 1 \tag{4.11.30}$$

The non-linear constraints for the scenario where the electric machine operates as an electric generator and for both the discharging and charging mode of the battery bank, the propulsion demand is described by (4.11.31):

$$\eta_g \cdot x_1 \cdot MCR_{M/E} = P_{shaft} \tag{4.11.31}$$

For the auxiliary demand by:

$$\begin{aligned} &\eta_g \cdot \eta_m\left(x_2\right) \cdot \eta_C \cdot \eta_{T/F} \cdot \eta_{loss} \cdot x_2 \cdot MCR_{M/E} + \eta_{gen} \cdot \eta_{loss} \cdot \sum_{i=3}^{5} x_i \cdot MCR_{A/E} + \\ &+\eta_{loss} \cdot \eta_{T/F,inv} \cdot w\left(x_6\right) \cdot x_6 = P_{aux.} \end{aligned} \tag{4.11.32}$$

**Generator condition – Charging mode:**

The objective function is given by:

$$\min f_{\text{gen,charg.}} = \left( \begin{array}{l} d\left(x_1 + x_2\right) \cdot \left(x_1 + x_2\right) \cdot MCR_{M/E} + \\ +\sum_{i=3}^{5} g\left(x_i\right) \cdot \left(x_i\right) \cdot MCR_{A/E} \end{array} \right) \cdot \Delta t_{sim} \cdot 10^{-6} \tag{4.11.33}$$

The lower and upper bounds of the optimisation vector are given by:

$$\begin{bmatrix} 0 \\ 0 \\ 0 \\ 0 \\ 0 \\ \min\left( DoD_{in} \cdot \text{Bat}_{\text{cap.}}, \lambda \cdot \frac{E_{Bat}}{\Delta t_{sim}} \right) \end{bmatrix} \leq X = \begin{bmatrix} x_1 \\ x_2 \\ x_3 \\ x_4 \\ x_5 \\ x_6 \end{bmatrix} \leq \begin{bmatrix} 1 \\ \frac{MCR_m}{MCR_{M/E}} \\ 1 \\ 1 \\ 1 \\ DoD_{in} \cdot \text{Bat}_{\text{cap.}} \end{bmatrix} \quad (4.11.34)$$

where,

$x_{1,2}$ : Main Engine Load [-]

$x_{3\text{-}5}$ : Auxiliary Engine Load [-]

$x_6$ : Power to charge from battery [kW]

The linear constraints which are applicable to the D-C generator charging scenario:

The A matrix:

$$A = \begin{bmatrix} 1 & 1 & 0 & 0 & 0 & 0 \end{bmatrix} \quad (4.11.35)$$

The $\boldsymbol{b}$ vector by:

$$\boldsymbol{b} = 1 \quad (4.11.36)$$

The non-linear constraints for this scenario for the auxiliary and charging loads, can be expressed as follows:

$$\eta_g \cdot \eta_m\left(x_2\right) \cdot \eta_C \cdot \eta_{T/F} \cdot \eta_{loss} \cdot x_2 \cdot MCR_{M/E} + \eta_{gen} \cdot \eta_{loss} \cdot \sum_{i=3}^{5} x_i \cdot MCR_{A/E} -$$
$$- \frac{1}{\eta_{loss} \cdot \eta_{T/F,inv}} \cdot w\left( \frac{\lambda \cdot \frac{E_{Bat}}{\Delta t_{sim}}}{N_{BB} \cdot V_{Bat}} \right) \cdot \lambda \cdot \frac{E_{Bat}}{\Delta t_{sim}} = P_{aux.} \quad (4.11.37)$$

The global minimum is found by comparing charging and discharging in motor mode, yielding to the local minimum 1. The process is repeated for the generator mode, finding the local minimum 2. The global minimum is the minimum of the two local minima. Logic criteria are applied, as mentioned in 4.3.2.1, the difference being that when the system is

forced to charge, the comparison of solutions is made only between charging in motor mode (which occurs by the auxiliary Diesel generators) and the shaft generator mode. As a result, in both cases the batteries are charged having the optimal power generation for propulsion, auxiliary loads and charging of the energy storage medium.

## 4.4 Implementation example – Mathematical representation

This section demonstrates an application of the above mentioned equations to an actual performed voyage. This example will accompany Chapter 5 as well and the final results will be given in Chapter 6. At this point, the selection of the proper equations will be given and explained. The input data will be presented, explained and transformed so to fit to the mathematical models. The goal of the mathematical implementation and simulation is primarily to regenerate the voyage identify the power demand and converge the simulation results with the 'as measured' fuel consumption, which is also known. Afterwards, the question to be answered is if the Hybrid solution was applied to this ship before the examined voyage, would the fuel consumption be lower or not. Hence, after obtaining the power profile, the optimisation algorithm is involved. As a result, the following process will be followed.

### 4.4.1 Ship – Environment interaction

For this demonstration case, a 31 day voyage from Hong Kong to Brazil is selected. The ship is in ballast condition.

Primarily in order to regenerate in simulation environment the voyage, the inputs and known information should be identified. Firstly, detailed vessel particulars are known. Secondly, the speed profile and the dominant weather parameters, acquired by the analysis of daily performance reports are also available. Thus, the ship and the voyage parameters are known. Consequently, the problem can be mathematically represented.

For better understanding of the representation of the voyage, a ten day segment of the uncorrected vessel speed, the underwater current and the weather parameters are shown in Table 4.5. These values are the inputs to the mathematical models which will be explained here below. It should be noted that depended on the report system of the shipping Company, the Beaufort number might not be given but the sea description is given instead. Thus, the transformation of description to Beaufort number is made using Table 4.3. Furthermore, the direction of waves is reported using the terminology described in Figure 4.1. Hence, it is again transformed to degrees using this figure. For simplification purposes and due to lack of wave data, it is valid to assume that the average wind direction converges with the wave direction. This statement though is only valid when swell is not present. The existence of underwater current affects the ship's speed. The sea current

speed is approximated by the ship's Master by comparing the speed over ground of the vessel and the indication on the bridge panel of the speed log/ Doppler. This difference under normal external conditions gives a good estimation of the underwater current. Furthermore, in order to reduce the implied error, the values before are transmitted to the shore office are crosschecked with the sea current charts of the operating area.

**Table 4.5: Sample of data interpretation for ship voyage simulation**

| Time step | Uncorrected vessel speed [knots] | Wind Direction [deg] | Beaufort Number [-] | Underwater current speed [knots] | Corrected vessel speed [knots] |
|---|---|---|---|---|---|
| 1 | 14.84 | "abeam" = 110 | "rough"= 5 | "astern"= 0.5 | 14.34 |
| 2 | 14.46 | 110 | 5 | 0.5 | 13.96 |
| 3 | 14 | 0 | 5 | -0.5 | 14.5 |
| 4 | 14.29 | 0 | 6 | -0.5 | 14.79 |
| 5 | 14.92 | 45 | 6 | 0.5 | 14.42 |
| 6 | 13.63 | 45 | 6 | -0.5 | 14.13 |
| 7 | 15.12 | 135 | 3 | 0 | 15.12 |
| 8 | 14.79 | 135 | 5 | 0.5 | 14.29 |
| 9 | 14.83 | 135 | 6 | 0.5 | 14.33 |
| 10 | 14.24 | 135 | 6 | 0.5 | 13.74 |

In order to estimate the fuel consumption, the main engine consumption model is required. According to the mathematical implementation, the engine model demands a known power profile so to be multiplied by the corrected SFOC and the operational time. Thus, so that to identify the SFOC of the prime mover, the fuel low calorific value, the operating temperature should be known. As a result the percentage increase estimated by equation (4.6.4) can be inserted to the calculations. Nonetheless, the question to be raised is how to identify the power demand. The connection between the engine and the ship is established through the use of the propeller model which is mathematically presented in (4.1.5.1). The best method to implement the propeller is by using the Wageningen B series approximation which requires though a full set of propeller characteristics, shown in equation set (4.5.5). Consequently, if the propeller characteristics are known, this approximation is used. Nevertheless, more information regarding the vessel unique hydrodynamic parameters is required. For the propeller model the wake friction coefficient is required. These coefficients and miscellaneous coefficients can be identified using the material presented in section 4.1.7.

The propeller model in order to give power results requires the ship's speed and resistance data. The approximation of resistance is a complex problem and should be decomposed to calm water resistance, wave resistance, wind resistance, rudder and drift resistance. Hence, a total set of two (if it is assumed that wave, wind, rudder and drift resistance are denoted as "added resistance") resistance components, calm and added

should be identified. The calm water resistance should be identified first. For a given problem, the question to be answered is why the user should select Holtrop-Mennen method or Hollenbach approximation. The rule of thumb is to use the model which best describes the ship resistance if the user has access to the towing tank model tests or to sea trial measured points. Nonetheless, because in the majority of the applications, this data is classified or unknown, the following in respect of importance will be assessed so to use the suitable model:

1. Amount of vessel geometrical information
2. Age of the vessel
3. Hull form
4. Available computational time

Regarding the first parameter, the Holtrop-Mennen method requires a lot of information which make it unattractive for quick simulation for a given fleet. Nonetheless, it can describe accurately the majority of designs. However, in unique modern (parameter No 2) hull forms (parameter No 3), Hollenbach method is suggested. Thus, for the examined Post-Panamax vessel with dimensions of a regular Panamax ship but with expanded beam and block coefficient, it is believed from the early beginning that Holtrop-Mennen method might not describe the problem in laden condition. On the other hand it may better describe this problem in ballast condition as the hull form in lower drafts yields to typical hull forms. Thus, by taking into account the above, the calm water resistance will be approximated by Holtrop method; however, the results should be crosschecked at later stage with the model data if available.

For this case, the added resistance will be formed by the combination of mean added resistance models described in 4.1.2.1 – 4.1.2.2 excluding the effect of wind loads (Kwon, 2008). Aertssen model should be used with caution as it is simple approximation but yields to modest results. In addition it requires only the length between perpendiculars of the ship and direction and force of the wind and waves. Kwon model though, uses more up to date data and applies corrections according to the vessel type, sailing Froude number and block coefficient. Because the added resistance is a complex problem, the selection of the model in every case should be done by trial and error method. In case the ship power demand exceeds regularly the MCR, this means that there is a mismatch of the model and the reported speed vector or the model is not suitable for this particular simulation case. For this demonstration case the final selection will be made in Chapter 5 where the mathematical case will be transformed to Simulink environment.

For the wind resistance, the Blendermann model will be used as it is more up to date and better describes modern superstructures. Both models in terms of data needs have the

same geometrical information requirements. Thus this parameter does not play any role to the selection. The rule of thumb for selection the wind resistance is the age of the vessel and the superstructure type. Usually the age of the ship defines the superstructure form (examined vessels built in 2005 and onwards).

Concerning the added resistance method of Grigoropoulos (2001), due to the fact that the vessel coefficients do not drop near the "parent" series forms and also, because these data do not accurately represent unique designs, this method will not be used. However, because of the necessary information are known, it will be compared to the rest mean models in Chapter 5. Although the added resistance models can describe the effect of wind and waves to the vessel, the lack of sea keeping data inserts a large parameter of uncertainty. Because RAO information is impossible to be found and detailed towing test have to be performed, the 4.1.2.3 model will not be used in this thesis. However, in order to reduce this uncertainty factor, the 4.1.2.4 weather generation coupled with mean models will be used and demonstrated. This coupling will be analysed in Chapter 5 where the simulation time step parameters will be discussed.

### 4.4.2 Coupling power profile and Hybrid system Optimisation

After the mathematical implementation of the ship – environment interaction, the resistance is transformed to required torque, power and propeller speed. Vessels equipped with two-stroke Diesel engines have direct propulsion, meaning that no gearbox/ clutch exits, thus the propeller speed equals to the Diesel engine speed. Therefore, the rotational speed should remain the same, so that the propeller can maintain the speed of advance and to produce the required thrust. Furthermore, the production of power, accounting the transformation losses should be equal to the propeller demand.

For this case, the ECMS strategy will be used as the primary objective is to minimise the fuel consumption only. Based on the equation set described in 4.3.2, the D-B and D-C scenarios are applicable to this case. Consequently, before proceeding, the required information should be identified. Observing the objective functions of D-B power train, the transformation losses, the engine MCR and the minimum SFOC of the engine are required. These parameters are static, thus are inserted to the calculations. However, the battery and the engine fuel efficiencies are load dependent and are not linear. Based on the Diesel engine fuel efficiency curves of Chapter 3, these curves can be represented by polynomials of 3$^{rd}$ degree and up, thus the optimisation problem is non-linear. Therefore, data fitting should be performed and equation for SFOC versus engine load should be created (g(x) or h(x)). The same is applied to the battery charge and discharge efficiencies creating the w(x) function.

The case is now mathematically represented. The inputs and outputs are defined. What remains is how to couple the different time steps and response time for each sub-model so to form the complete simulation. This will be described in Chapter 5, where the Simulink representation will be given prior to the continuation of this example.

## 4.5 Chapter summary

In this chapter, the governing equations for the ship simulator and the optimisation algorithm were presented. Regarding the ship simulator, a set of models was implemented for each of the vessel's calm water resistance. In addition, the propeller and engine models were also implemented. Furthermore, a mathematical representation of the actual vessel operation was shown. Concerning the data entry part, environment generation models were investigated and presented in this chapter. Consequently, a large number of mathematical models is available for the construction of the simulation blocks. The description of the simulator blocks will be performed in Chapter 5.

For the Diesel configuration optimisation, two strategies were demonstrated. The first applied the ECMS strategy for fuel oil consumption reduction. The second algorithm, named as 'pseudo multi-objective' targeted primarily the fuel consumption when the system is discharging and secondly at the reduction of PM while the system was charging.

The results of the ECMS strategy for Diesel Hybrid power trains are presented in Chapter 6.

# 5 Ship Voyage Simulator

Townsin et al. (1975) underlined the importance of monitoring the speed performance of ships. Two main reasons for monitoring the ship performance are charter party conditions and studying bad weather performance. For that reason, it is of vital importance to demonstrate a non-complex, reality-based simulation tool for the ship voyage.

The identification of patterns or of operational randomness will facilitate the construction of valid test cases and simulation scenarios. The latter will assess primarily the feasibility of the mathematical modelling and, secondly, the propulsion machinery optimisation outputs in artificial conditions, based, however, on reality scenarios. Therefore, the proposed simulation tool accounts for the mathematical implementation of ship and propulsion components and of charter party agreement requirements. As a result, based on the management profiles of a large number of shipping companies, the operation of the vessel is defined by the charter type. In the event of operation in the spot market, the vessel increases its speed in order to reduce the time spent in the leg, so as to arrive early at the discharge port and probably receive a demurrage. Alternatively, it is observed that during years of economic growth when demand is high, shipping companies decide to break the charter party agreement of unloading the goods at a predefined time and unload the cargo earlier by paying a penalty, in order to catch the next freight that is far more profitable for the ship-owner. In this case, the vessel regularly operates at a predefined and high speed without accounting for the increase in power requirement (Lorange, 2005). This approach can be characterised as constant speed. When the vessel operates in time charter, only the distance is predefined and the master usually defines the vessel speed in order to arrive during the predefined time slot at the arrival port based on a three day or seven day weather forecast. Usually, the setting is for 'constant RPM' during each day, and re-adjusted accordingly if the ETA is revised. The final operation scenario that was investigated was the predefined distance to be covered during the voyage day. Actually, this scenario is a mixture of constant power and constant speed during the examined increment and relies on the master's decisions. In the simulation environment, a pseudo decision making process was inserted using two simple principles. The first principle was to set a power limit versus sea state, which is usually defined by safety standards for voluntary speed reduction due to slamming, heavy vertical accelerations forward and racing of the propeller (Journee and Meijers, 1980), and by the operations department of the maritime corporation. The second principle is to implement a negative coefficient that accounts for the 'off-target percentage', which is dependent on the elapsed time and the miles to go. A simple logical operator was inserted to switch from the constant power setting to constant speed, in order to cover the desired daily distance. It is obvious that the

vessel speed is altered significantly when the elapsed time reaches 24 hours, and still the off target percentage is not equal to zero, indicating that this is not an optimised solution as decision modelling was not attempted in this project.

## 5.1 Simulation implementation

This section presents the implementation of the mathematical equations with a graphical programming representation using the Simulink environment. The Simulink environment is offered together with the Matlab® Suite, developed by Mathworks[6]. Simulink is a software package for modelling, simulating, and analysing dynamic systems. It supports linear and nonlinear systems, modelled in continuous time, sampled time, or a hybrid of the two. Systems can also be multi-rate, i.e. have different parts that are sampled or updated at different rates. For modelling, Simulink provides a graphical user interface (GUI) for building models as block diagrams. With this interface, the models are drawn easily, with 'drag and drop', in contrast to conventional simulation packages that formulate differential equations and difference equations in a compiled language or program. Moreover, a predefined template function to write the code of the mathematical implementation is used. This template is called S-function and significantly reduces the code complexity (Mathworks, 2002).

The simulation blocks consist of logical separation of the mathematical models; for example, one simulation block represents the calm water resistance and a different the wind induced loads. With the modular, scalable and extendable technique, the simulation tool can be further improved by replacing the models with more complex ones, and can be updated if there are changes in the governing equations, i.e. to include modern hull forms similar to the updates proposed by Kwon (2008) for the mean added resistance approximation.

The input and the output of each sub-model are achieved by the block connection ports. For each block, the number of inputs and outputs is defined, thus appropriate connection points are made in order to interconnect with the remaining simulator blocks.

In the Simulink environment, the connection of the blocks is represented using signal arrows. These arrows can be grouped together into a single bus either they can be connected to a signal transmitter block. Both ways aim to reduce the graphical complexity of the simulation representation.

In order to avoid a complex diagram for the entire fleet, it is proposed to group similar blocks and form major blocks (e.g. fleet calm resistance major block). The approach using signal buses and major blocks significantly reduces the programming error.

[6] Matlab® version 2011b, www.mathworks.com

Moreover, the graphical representation of the Simulink simulation is also clear to the designer or to the operator of the simulator tool. Furthermore, to add and/or remove vessels remains relatively easy and common signalling errors such as wrong input information are avoided. A schematic overview on how the blocks can be connected in order to form the Ship voyage simulator is given in Figure 5.1 while the Simulink representation is given in Figure 6.1 of Chapter 6.

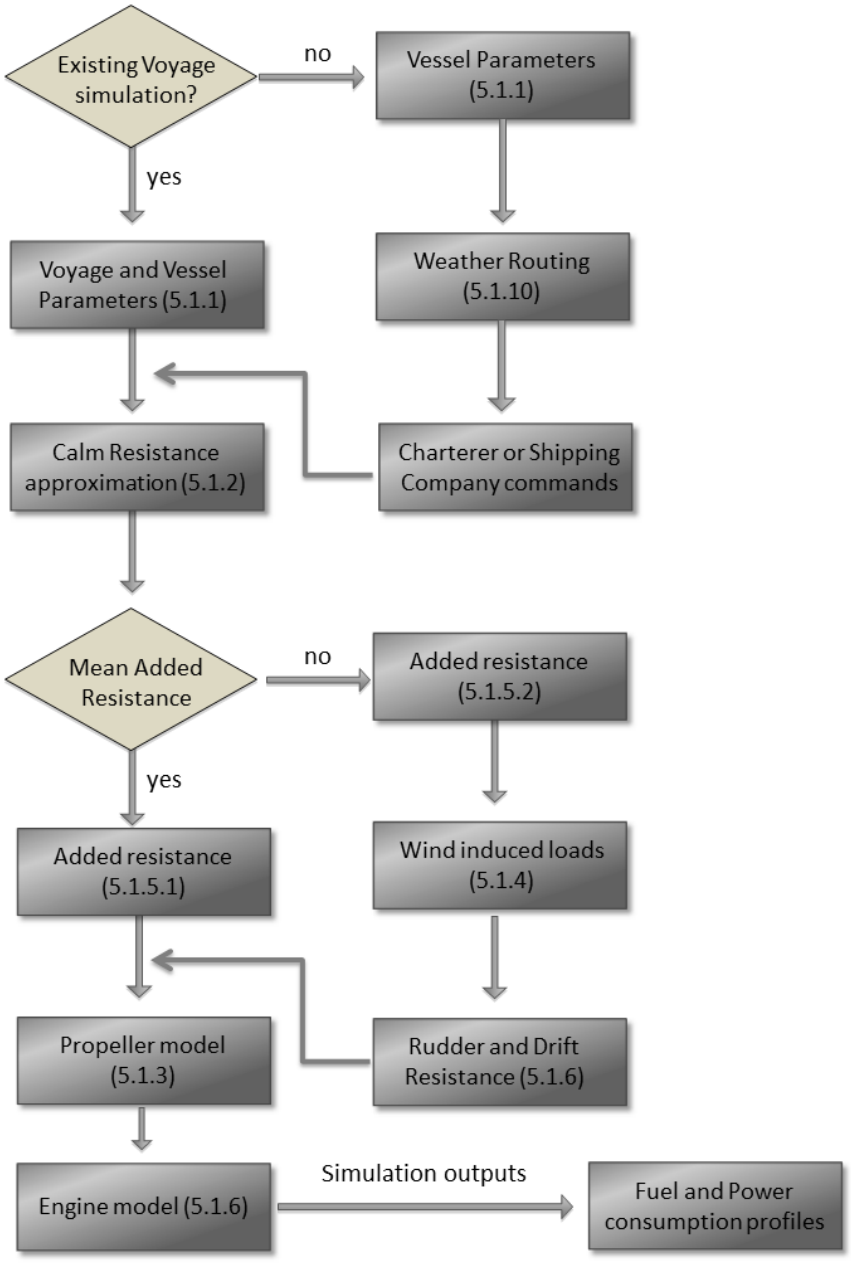


**Figure 5.1: Ship Voyage Simulator flow chart**

In order to successfully use the Ship Voyage simulator, the minimum simulation time should be defined. Simulation time step can be selected by the user however, the minimum simulation time step is dictated by each model's response time. The global simulation time step is thus defined by the largest time step of the selected blocks. For a quick overview of the minimum response time of each simulation block, which are defined in this chapter, Figure 5.2 is introduced.

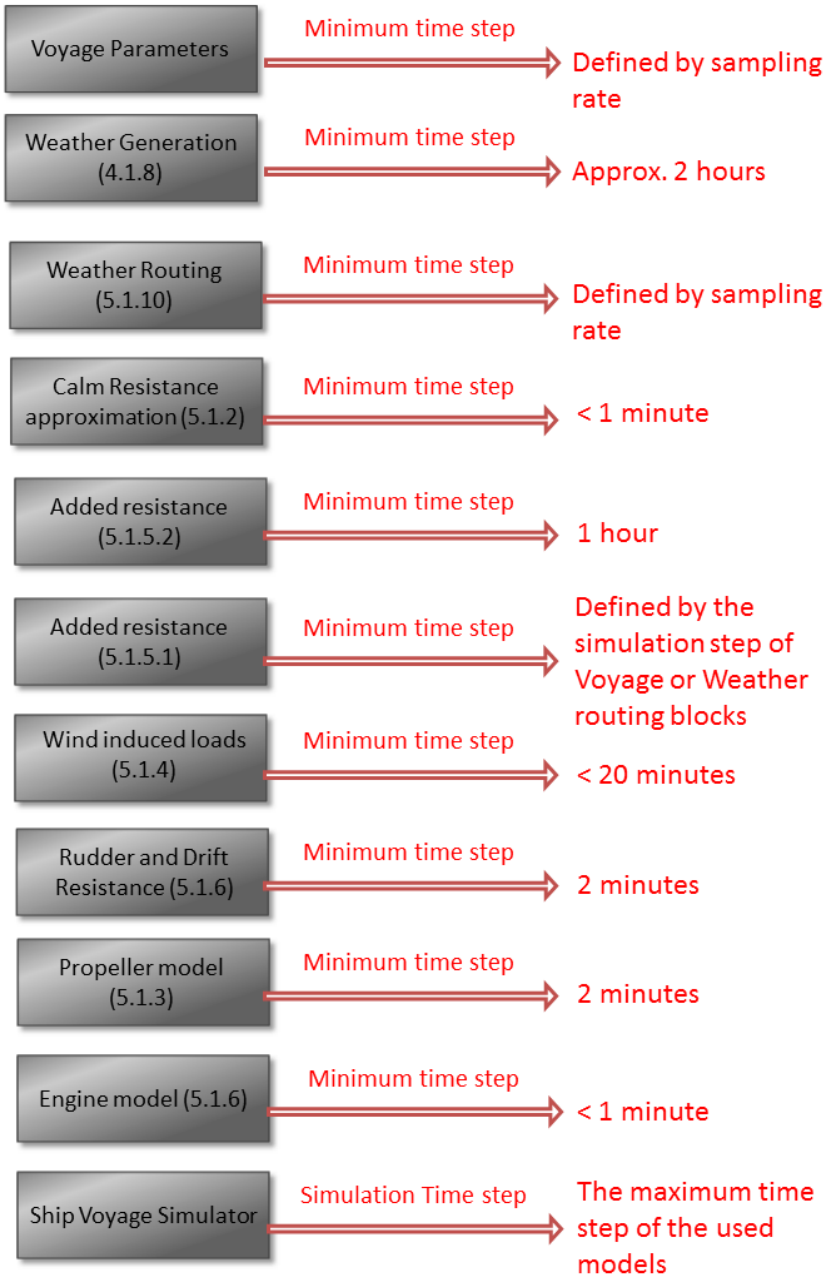


Figure 5.2: Simulation block minimum response time

For the calculation of shipping emissions using the bottom up approach based on the ship simulation findings, the optimisation was performed in a time domain. The dynamic behaviour of the vessel was not accounted for, as the selected time step is two

hours. This can be justified by the fact that emissions are quasi-static phenomena and the transient operation of the machinery does not need to be simulated. During transient phenomena, the emission calculation using fuel based or power based factors does not represent the actual emission phenomena and, in addition, no modelling of emissions during the dynamic phenomenon is accurate to this date. Thus, the dynamic approach is rejected, and a time step more than five minutes is required, as a result. However, the absence of the response amplitude operator (RAO) of added resistance in induced wind and waves (which requires detailed model basin tests and or runs of complex sea keeping codes) given a specific sea state (significant wave height and modal period) has led to the adoption of a two hour simulation time step, with the reasons for this adoption having been discussed in Chapter 4. The simulation models follow the SI unit system. When other units are required in interpolation tables, appropriate conversion is performed at a local stage.

### 5.1.1 Input data blocks

The simulations require a set of inputs in order to perform the necessary calculations and produce their outputs, which then can be used as inputs to other blocks. The basis of this process is made at the input data blocks. Their implementation is simplistic, as the variables are fed by input values by the user in a text data form. Each variable name is unique in the data form and has exactly the same name in the Simulink environment. Consequently, the values are fed to the appropriate output ports and the information can then pass to the other blocks. With this approach, the blocks are not changed within the Simulink program, but the user can modify the input file, which then re-assigns the values to the appropriate variables. Two blocks of this type are found in the developed simulator package. The first block, coloured in blue, contains the hydrodynamic and geometrical data for the examined vessel and is identified as ‘ship particulars block’. The second block, denoted in dark yellow, contains the propeller characteristics and information regarding the bulbous bow and is referred as ‘propeller data block’. The block coloured in white contains information regarding air and sea environmental conditions, such as temperatures, but not the wind velocity or the Beaufort number, which are produced by the signal generator block. The latter is fed by values produced by the process of random weather generation defined in chapter 4. Nevertheless, if the simulation is about an actual voyage, the master’s reported data included in the ‘noon report’ are inserted, along with the reported vessel speed. This process simplifies the simulation procedure as the data is not manually transformed into the Simulink but at the input stage. Using that topology, the simulation can be performed at a very short time for the complete fleet if data is available, producing a global solution.

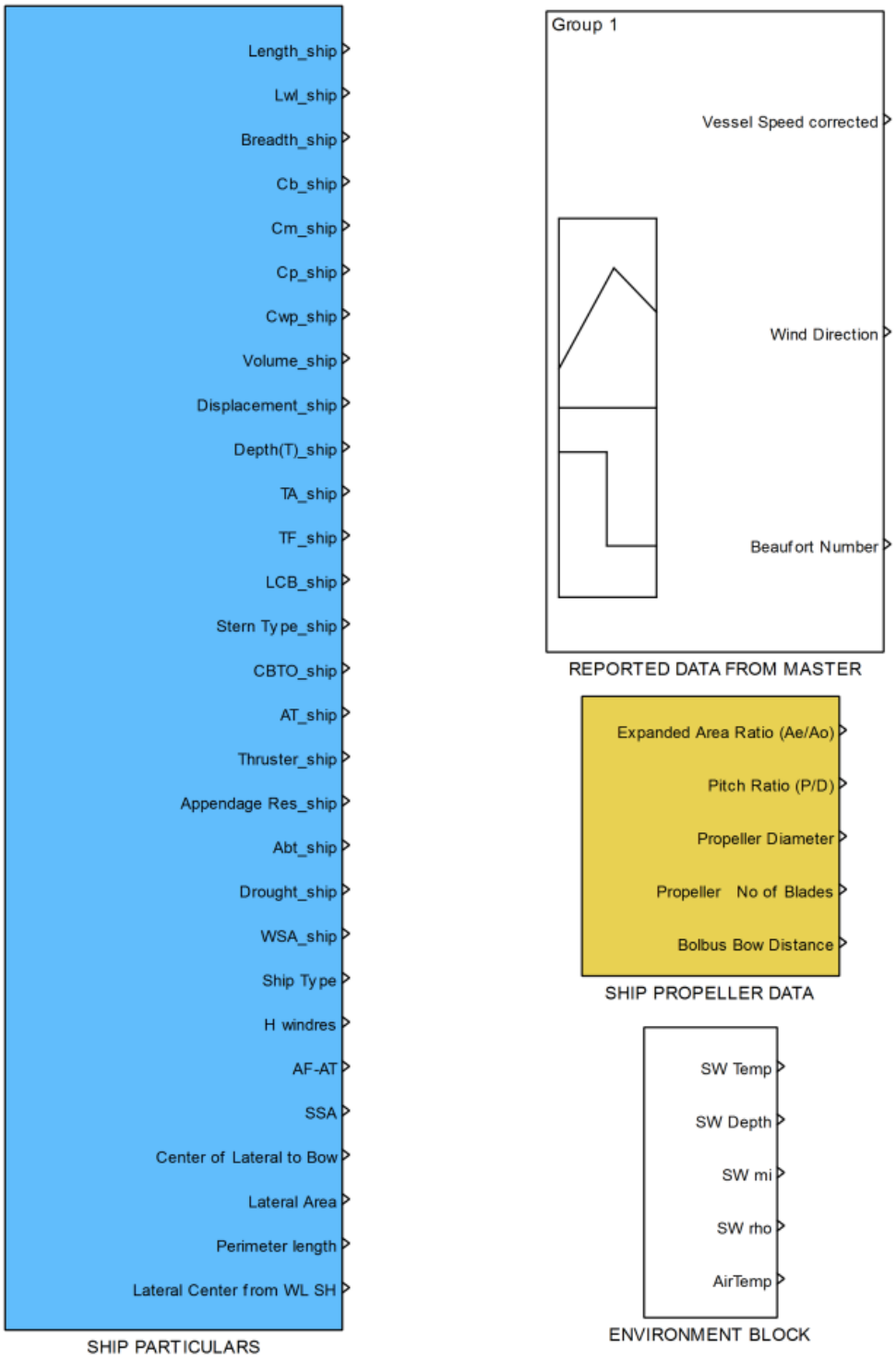


**Figure 5.3: Data input blocks and signal generators in Simulink environment**

### 5.1.2 Calm water resistance block

The simulation blocks describe the equation set of subchapter (4.1.1) for both resistance approximation methods. In addition the wake, thrust deduction and relative rotative coefficients are defined by the equation set of subchapter (4.1.7).

#### *5.1.2.1 The Holtrop-Mennen calm water approximation method*

For the approximation of calm water resistance using the aforementioned method, a large number of geometrical vessel data is required. Due to the requirement of a detailed geometry of the ship, where – in the case of a globalisation of the simulator – such information may not be available, this method should be avoided. However, the existence of this block is necessary as it is where hydrodynamic coefficients required by the propeller and engine blocks are calculated.

The Holtrop Mennen resistance block is connected to the 'ship particulars block', the 'propeller data block', which are considered as input blocks. Their definition is described later in subchapter 5.2.9. The outputs of this block, with the exception of the calm resistance, are connected to the propeller block, whether it is the B-Series approximation or the actual propeller characteristics block.

**Table 5.1: Holtrop Mennen resistance block inputs and outputs**

| Model Inputs | Model Outputs |
|---|---|
| $L_{wl}$, B, D, lcb, $C_B$, $C_M$, $C_P$, $C_{WP}$, fore and aft Draft, mean Draft, Drought, Displacement volume Wetted Surface Area, Immersed transom area, Thruster diameter, Stern type, Bolbus bow cross sectional area, Bow thruster added resistance | Calm Water Resistance |
| Appendage Resistance (Holtrop look up table) | Wake coefficient |
| Vessel's speed | Thrust deduction coefficient |
| Sea water kinematic viscosity | Relative rotation coefficient |
| Sea water density | |
| Sea water depth | |
| Expanded Blade Area ratio | |
| Pitch to Diameter ratio | |

It can be seen in the block description of Figure 5.4 that the simulator user can switch between the approximations of the hydrodynamic coefficients with Holtrop-Mennen and other methods, as found in subchapter 4.1.7.

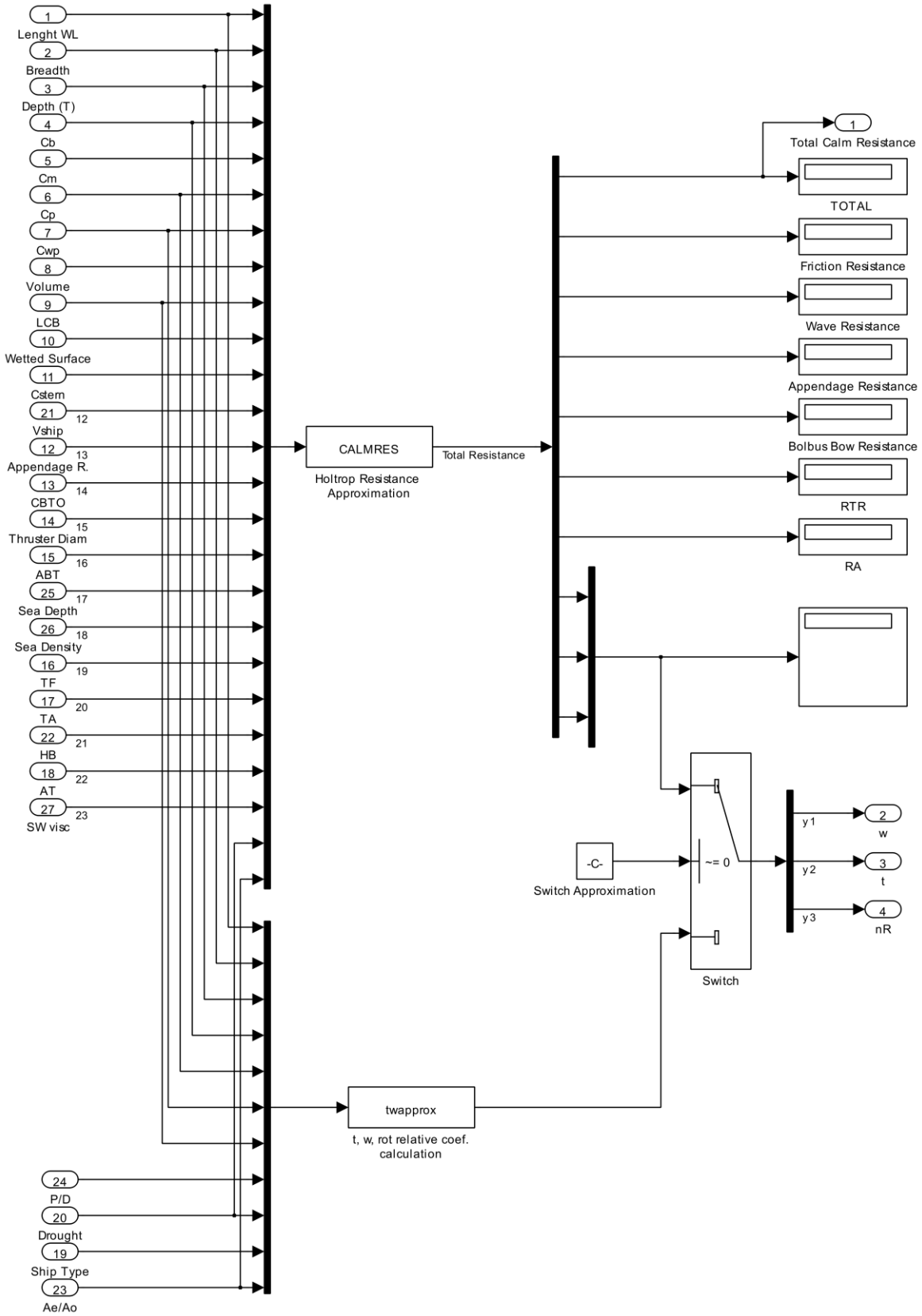


**Figure 5.4: Representation of Holtrop Mennen resistance and approximation of hydrodynamic coefficients block in Simulink**

### *5.1.2.2 The Hollenbach calm water approximation method*

The Hollenbach method requires a smaller set of data compared to the Holtrop Mennen method. This block has no wake, thrust or rotative efficiency coefficient approximation, thus it is proposed to be used in combination with the Holtrop Mennen block. Moreover, it is recommended that the resistance approximation results of the two methods be compared to each other, in order to identify the method that converges in a better way with the actual ship resistance.

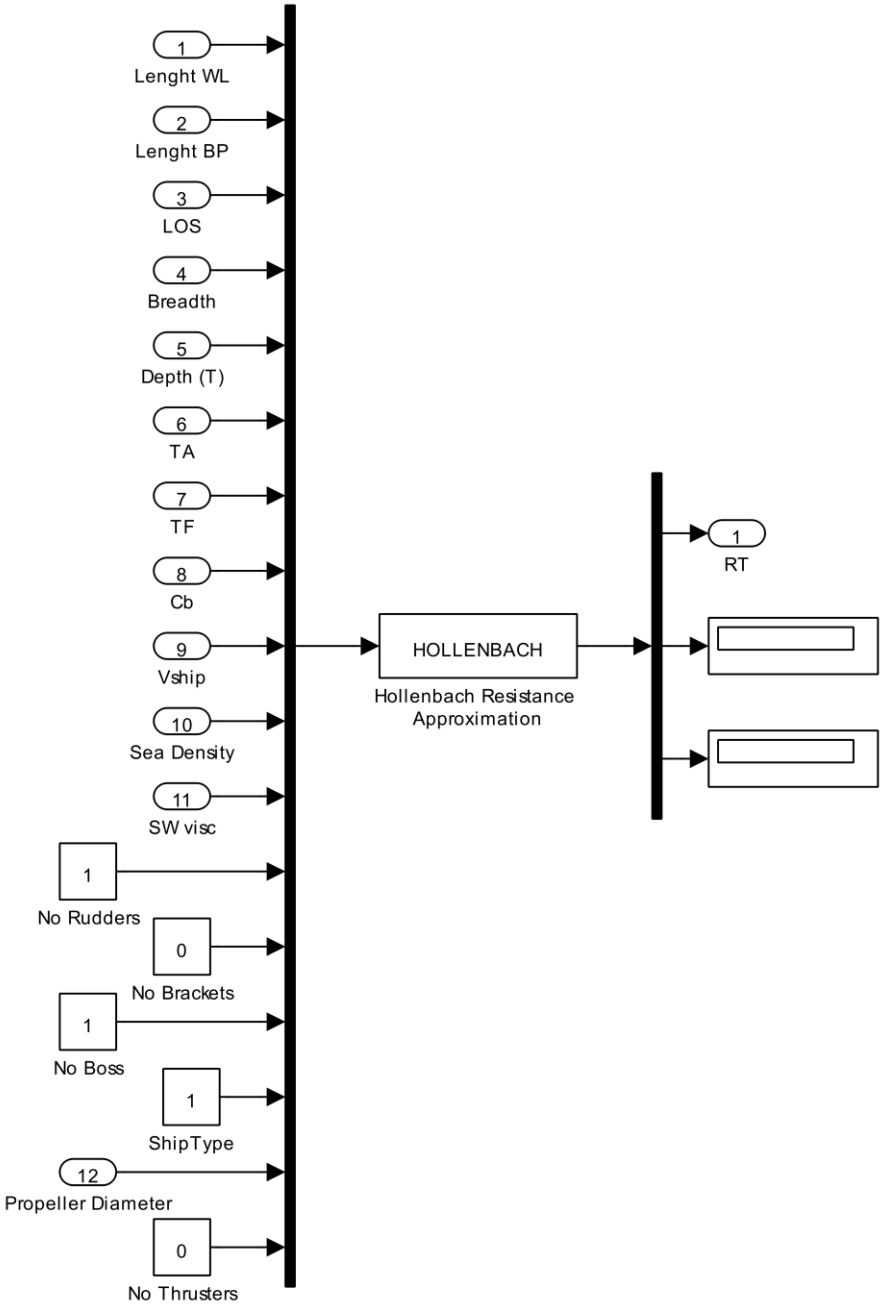


**Figure 5.5: Representation of the Hollenbach resistance block in Simulink**

The Hollenbach method approximates the residual resistance only. For the friction resistance, the method of ITTC is adopted but for a wetted surface area approximated by

the method. The friction resistance is the third output of the S-function block and the result can be checked on the screen by the display sink block.

Table 5.2: Hollenbach resistance block inputs and outputs

| Model Inputs | Model Outputs |
|---|---|
| $L_{wl}$, $L_{BP}$, $L_{os}$, B, $C_B$, fore and aft Draft, Number of Bosses, Number of bilges, Number of Rudders | Calm Water Resistance |
| Vessel's speed | |
| Sea water kinematic viscosity | |
| Sea water density | |

For simplicity purposes, the S-function block through the first port exports the total resistance, which is the sum of the friction resistance (port 3) and the residual resistance (port 2). Due to its application in bulk carriers, this particular model has as constants the number of bilges (one propeller vessels), the number of propeller boss and the number of bow thrusters, which is set to zero as the sampled vessels are not equipped with bow thrusters. The propeller shaft is not supported by brackets thus the number is set to zero.

### 5.1.3 Propeller block

This block is responsible for matching the resistance with the production of thrust, given the hydrodynamic coefficients obtained from the resistance blocks. The required information for the propeller characteristics is imported from the propeller data block. The output of the system is the propeller developed thrust, the propeller torque and the rotational speed. Finally, the required engine power to propel the vessel is estimated, given the speed request.

Table 5.3: Propeller block inputs and outputs

| Model Inputs | Model Outputs |
|---|---|
| Expanded Blade Area ratio | Propeller Thrust |
| Pitch to Diameter ratio | Propeller Torque |
| Number of propeller blades | Propeller RPM |
| Wake coefficient | Required Engine power |
| Thrust deduction coefficient | |
| Relative rotation coefficient | |
| Sea water kinematic viscosity | |
| Sea water density | |
| Propeller shaft efficiency | |
| Vessel's total resistance | |
| Vessel's speed | |

It can be seen from the schematic of the Simulink model that the user can easily switch between the actual propeller data and the B-series approximation. However, the existence of the two models increases the computer power demand, thus the simulation time. In

cases where the user requires specific models, it is proposed to delete the appropriate model.

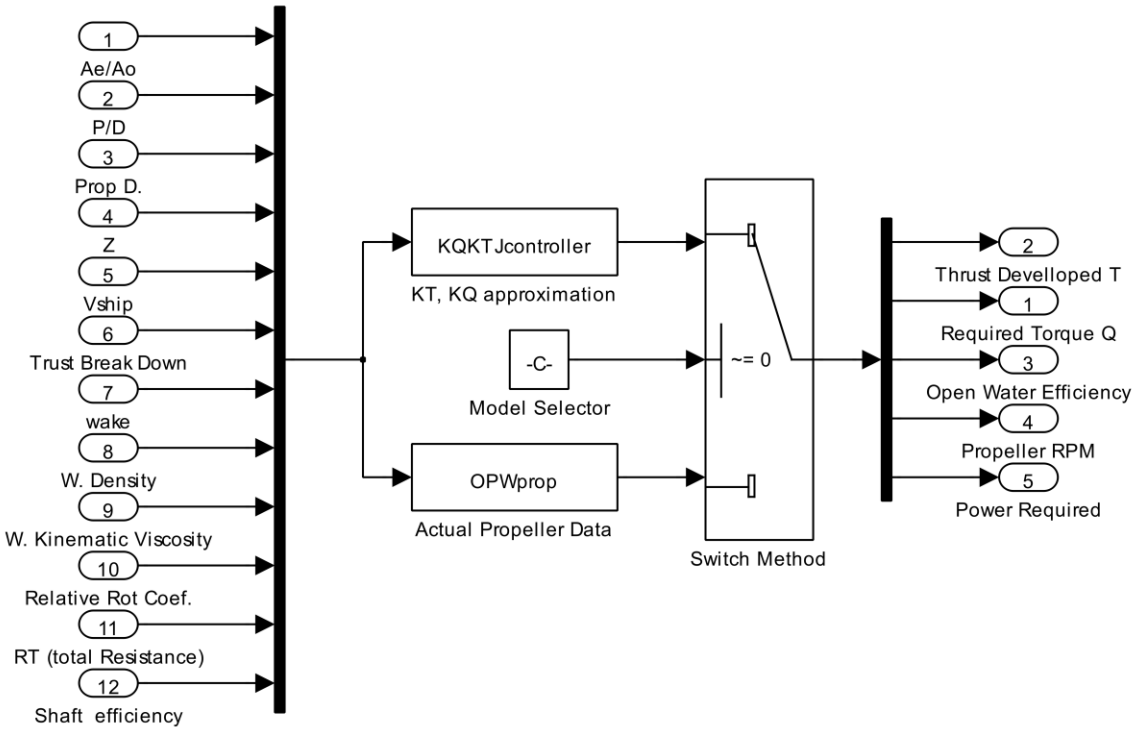


Figure 5.6: Representation of Propeller block in Simulink

### 5.1.4 Wind induced resistance blocks

This simulation block contains the approximation of the wind induced loads using the Blendermann and Isherwood models. The simulator user can switch between these two methods.

Table 5.4: Wind induced loading block inputs and outputs

| Model Inputs | Model Outputs |
|---|---|
| $L_{OA}$, B | Surge force |
| Superstructure area | Sway force |
| Lateral projected wind area | Yawing moment |
| Lateral projected area of superstructures | Sway coefficient |
| Lateral Area including Superstructures | Yawing coefficient |
| Ship's perimeter length | |
| Lateral centre distance from waterline | |
| Transverse/ Frontal area | |
| Height until top of superstructures | |
| Number of Masts | |
| Ship's speed | |
| Ship's heading | |
| Wind velocity | |
| Wind angle of attack | |

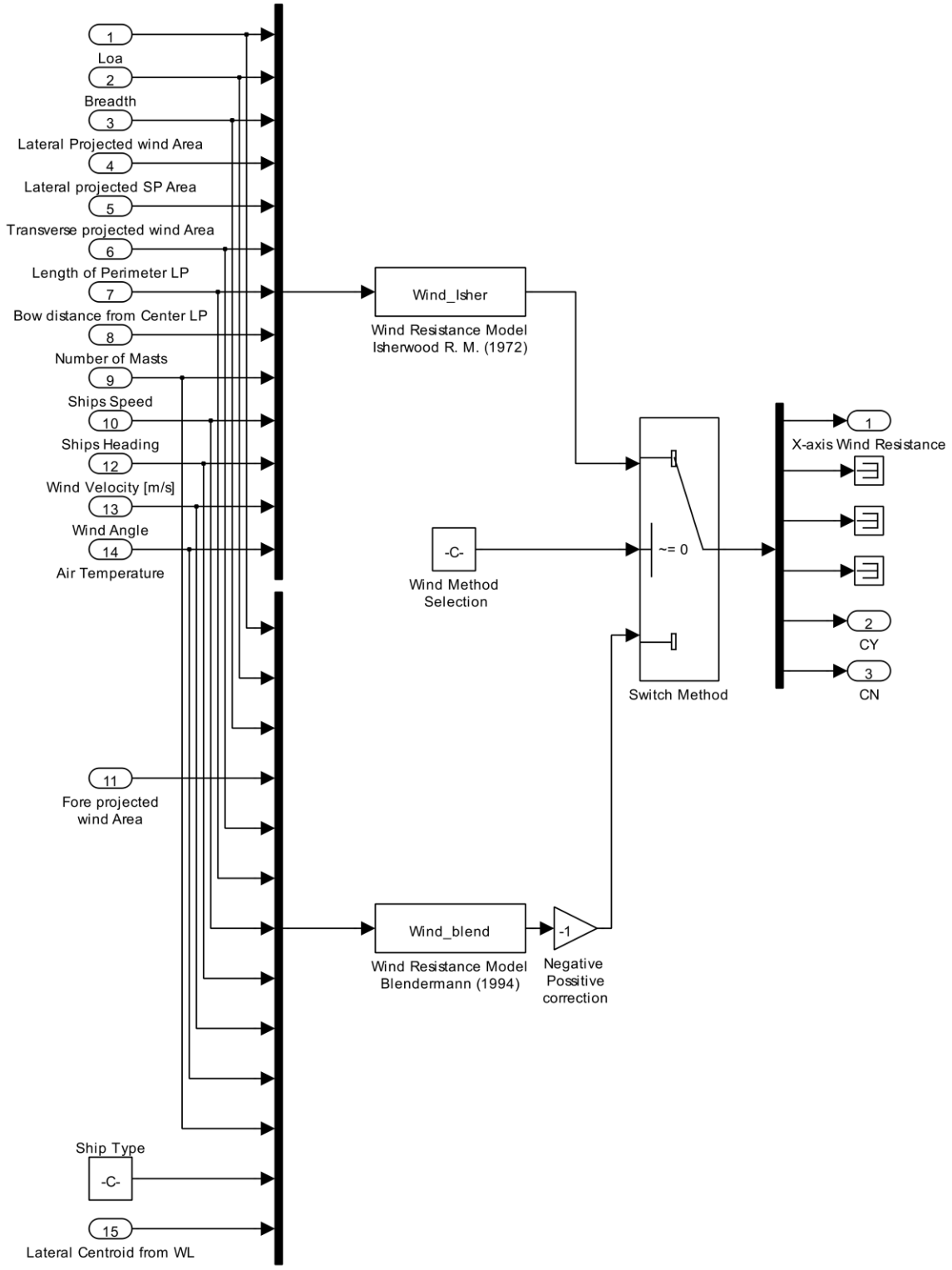


**Figure 5.7: Representation of Wind induced forces block in Simulink**

The model outputs the surge force, which is crucial in the direct approximation of the engine power requirement. In addition, for indirect power increase due to wind loads, the sway force is approximated. This model also calculates the sway and yawing static coefficients, which are required by the rudder resistance block.

This model necessitates the knowledge of various geometrical characteristics of the vessel. This information regards the area above the water line because that part of the construction is exposed to the wind. The resistance components are added together into a resistance sink in order to form the total ship resistance given the specific vessel speed and the dominating environmental parameters.

### 5.1.5 Added resistance blocks

For the approximation of added resistance, two approximation methods are proposed. For a more complex method, but with introduced uncertainty, the Series 60 added resistance with the use of interpolation tables is modelled.

#### *5.1.5.1 The Aertssen and Kwon block*

The Aertssen and Kwon methods rely on the knowledge of simple vessel characteristics and the Froude number. In addition, the simple wind wave characteristics, such as the angle of attack and the force expressed in Beaufort number, are required. This block uses an interpolation table to estimate the minimum and maximum occurrence value of wind speed given the sea state. When these two values have been identified, a random number generator produces a wind value into the range defined by the interpolation matrix.

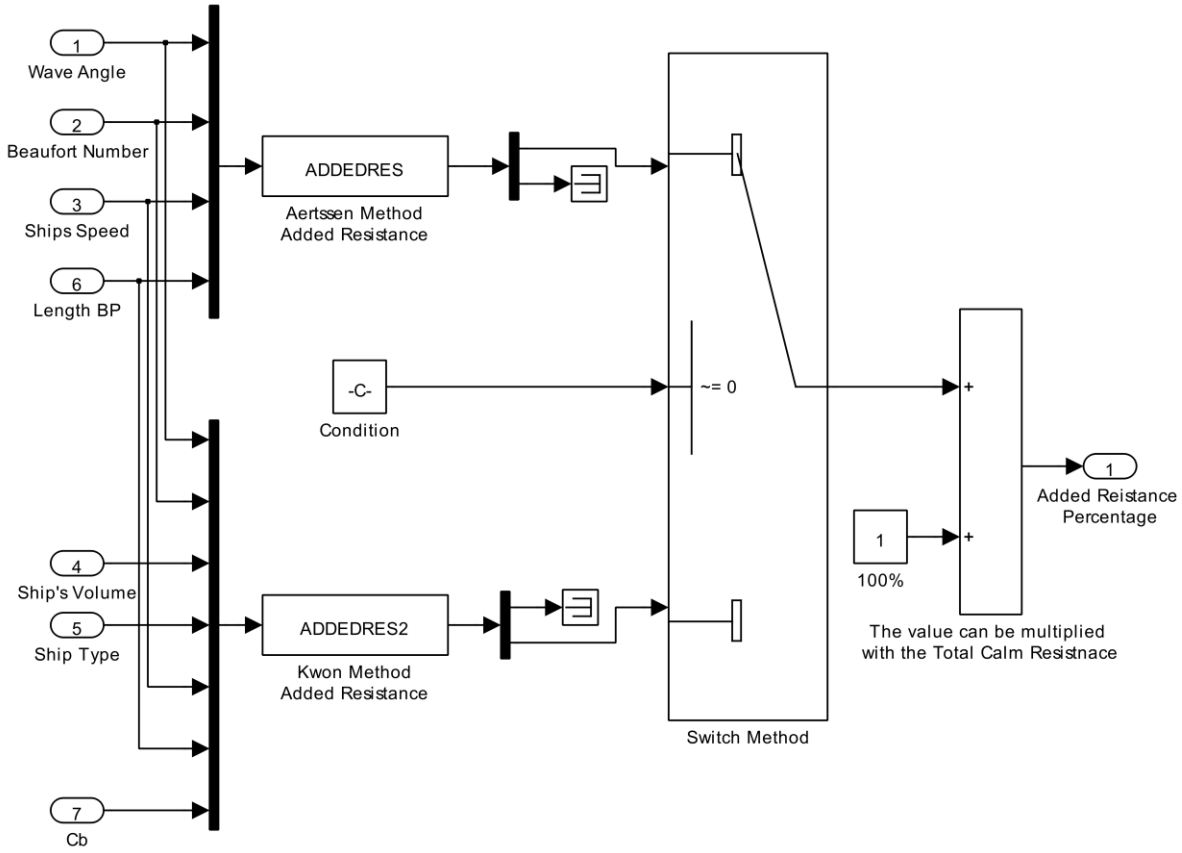


**Figure 5.8: Representation of Added resistance block in Simulink**

Table 5.5: Aetrssen and Kwon block inputs and outputs

| Model Inputs | Model Outputs |
|---|---|
| $L_{OA}$, $C_B$, Displacement volume | Surge force percentage of calm resistance |
| Beaufort Number | |
| Ship type (interpolation table for Blendermann model) | |
| Wave angle of Attack | |
| Ship's speed | |

### *5.1.5.2 Series 60 added resistance block*

This block uses a set of matrices to approximate the non-dimensional added resistance value for an equivalent vessel of the series 60 models of the same L/B and B/T ratio and $C_B$. In order to estimate the actual value of added resistance, the vessel characteristics, the wind direction and the significant wave height are inserted into the calculation and the final value of added resistance is given in algebraic form. This procedure is implemented using four-dimension interpolation data. Firstly, based on the Grigoropoulos et al. (2001) publication, the tabular data for added resistance for two B/T ratios have been utilised. The acquired set of data is for the given vessel $C_B$ and for L/B ratio as close as to the ratio of the examined vessel. In the event that there is a notable difference between the vessel L/B ratio and the Series 60 model, the recommended procedure is to perform interpolation between L/B and then B/T. Due to the fact that a five-dimension interpolation matrix does not exist in Simulink environment, this approximation technique will require two four-dimension lookup tables and then a two-dimension lookup table for the final interpolation for the examined L/B and B/T. The four-dimension matrix requires information regarding the wave peak modal period (port 1), the wave direction (port 2), the vessel sailing Froude number (port 3) and the B/T ratio (port 4).

There are cases that the modal period calculated by the environmental block outputs values that exceed the interpolation range. During the test cases it was observed that the modal period is lower than the lower range bound. Thus, a decision switch was added to the block in order to acquire the minimum interpolation value instead of the actual. Although it may argued that this adoption introduces errors into the calculations and for that reason the non-dimensional form of modal period was implemented, this assumption led to meaningful results because the insertion of lower range value outcomes strange modal periods that have no physical meaning. The final value is transformed to kN and then summed to the resistance sink through the block output port one.

Japanese shipyards were the first to identify the importance of model runs in order to define at an early design stage the appropriate engine sea margin. However, this method, compared with the actual voyage, introduces uncertainty into the calculations.

**Table 5.6: Series 60 added resistance approximation block inputs and outputs**

| Model Inputs | Model Outputs |
|---|---|
| Length between perpendiculars | Surge force |
| Breadth to Draft ratio | |
| Significant wave Height | |
| Wave modal period | |
| Wave angle of Attack | |
| Ship's speed | |
| Sea water density | |
| Acceleration of gravity | |

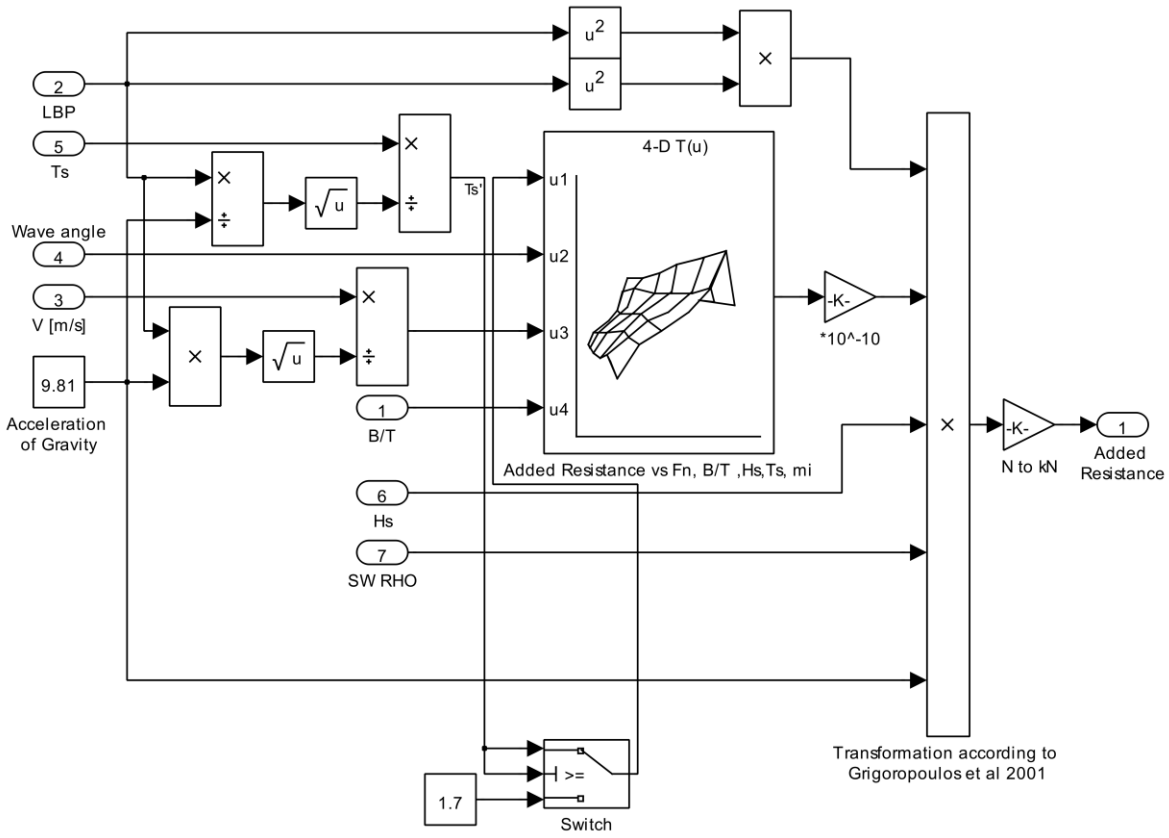


**Figure 5.9: Representation of Series 60 added resistance block in Simulink**

### 5.1.6 Rudder and Drift resistance block

This block calculates added resistance due to rudder movement only to compensate the yawing induced by the wind loads. In addition, it estimates the drift resistance. For clarification purposes, two S-function blocks that contain the algorithm have been implemented. The input information is obtained from the vessel characteristic block, the propeller block and the wind induced loads block. The vessel speed is obtained by the signal generator, which loads the simulation scenario. The output of this block is connected to the resistance sink through the block output port one.

**Table 5.7: Rudder and Drift resistance approximation block inputs and outputs**

| Model Inputs | Model Outputs |
|---|---|
| $L_{PP}$, T, Displacement volume, | Surge force |
| $Y'_{uv}$, $Y'_{cc\delta}$, $N'_{uv}$, $N'_{uu\delta}$ | |
| Yaw coefficient ($C_N$) sway coefficient ($C_Y$) | |
| Rudder Area | |
| Function of Rudder aspect ratio | |
| Ship's speed | |
| Sea water density | |
| Air density | |

For the calculation of drift resistance, the drift speed should be determined. For the calculation of this speed, the heel angle to compensate the wind loads should be estimated by the Rudder resistance block. Afterwards, it is assumed that the reported speed vector is the sum of the surge and sway speed vectors. This approximation results in the insertion of a tangent function to the rudder angle delta, which finally estimates the sway (drift) speed. Additional information required by the drift S-function is the length between perpendiculars, the ship's mean draft and the sea water density. The output of this block is connected to the resistance sink though the block output port 2.

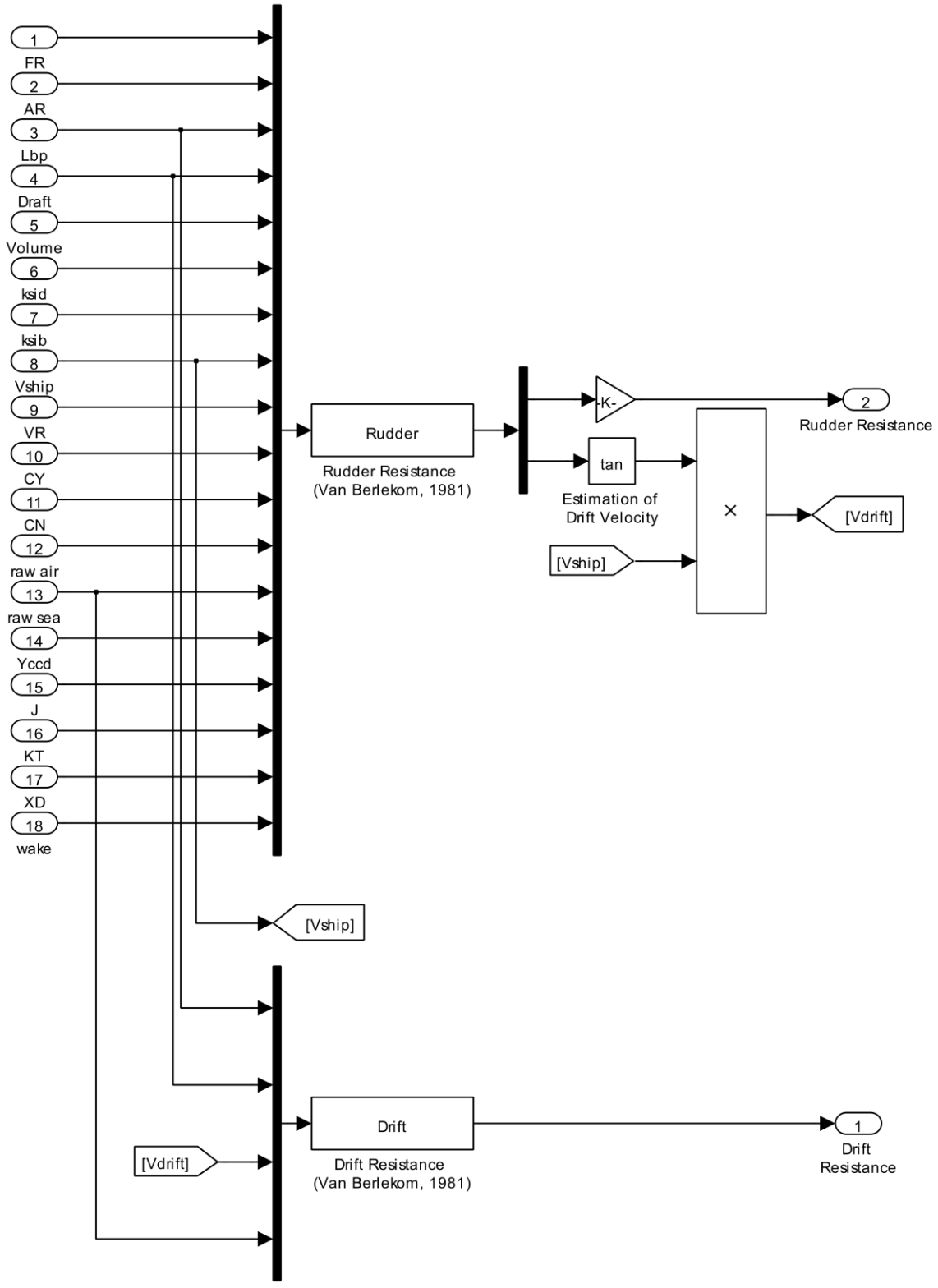


**Figure 5.10: Representation of Rudder and Drift resistance block in Simulink**

### 5.1.7 Engine interpolation block

This block estimates thermodynamic data of the Diesel engine given the engine load. The estimation process relies only on the knowledge of shop test data or data that has been obtained from an energy audit on the machinery side. For the purpose of the simulation, only the SFOC curve and the maximum developed RPM are required. The SFOC curve is corrected based on the corrections proposed by the engine manufacturer, which are described in subchapter 4.1.6. The maximum RPM are obtained from manufacturer data, which defines the engine envelope. In order to estimate the hour fuel consumption, the SFOC is multiplied by the engine loading. In case daily consumption is required, the result should be multiplied by 24 hours. The remaining information defines the thermodynamic process of the engine given its loading. This information is important to the Technical department of shipping companies, which monitor the engine deterioration versus time. In this study, this information is not required hence no output is produced and the signals are terminated until future usage.

**Table 5.8: Engine Interpolation block inputs and outputs**

| Model Inputs | Model Outputs |
|---|---|
| RPM required | Engine RPM |
| Power required | Engine Developed power |
| Air temperature | Engine RPM in calm weather |
| Sea temperature | Engine max. RPM versus load |
| Fuel lower calorific value | Cylinder maximum pressure |
| Fuel type | T/C inlet temperature |
| T/C RPM measured (not used) | T/C outlet temperature |
| Load indicator (not used) | SFOC corrected |
| Fuel admission lever (not used) | Fuel consumption per hour |

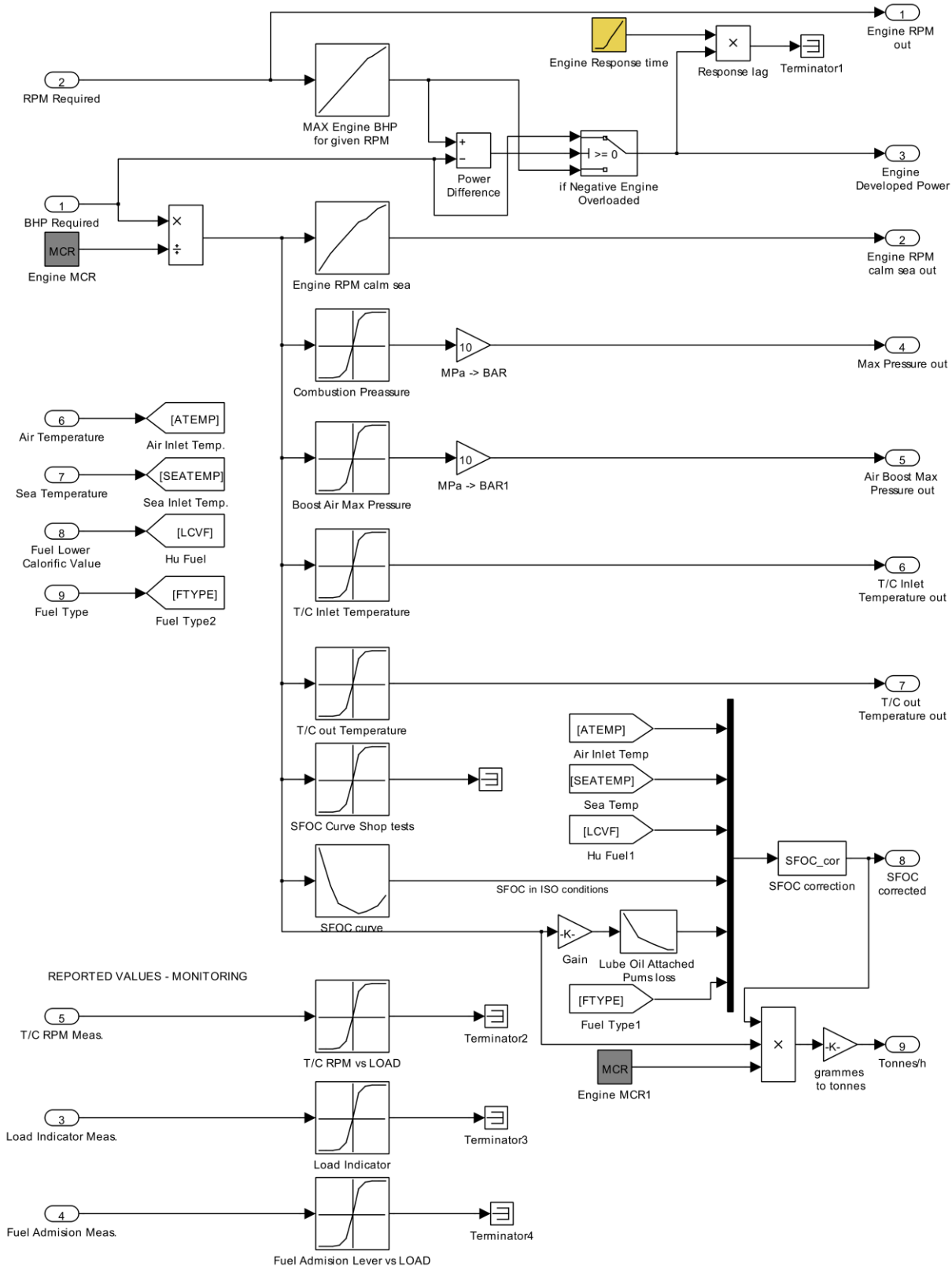


**Figure 5.11: Representation of Engine interpolation block in Simulink**

### 5.1.8 Kinetic Battery Model block

The Kinetic Battery Model is a dynamic simulation model of the battery discharging and charging. Based on the mathematical equations described in subchapter (4.2.2.2), there is an exchange of energy between the two wells (Manwell and McGowan, 1993). Due to the fact that the discharge and charge phenomena are dynamic, differential equations have to be solved. This block solves the two differential equations and supplies the derivative though a memory function, in order to proceed with the calculation of the other parameters, which is the final energy to be absorbed from each well. Nonetheless, the existence of the memory blocks significantly slows down the simulation process. For that reason, it is proposed to use the embedded differential equation solver into the S-function block in order to speed up the process. It has to be noted that in both cases the result should be the same. In order to increase the block complexity, a two-dimension lookup table is implemented that describes the cell/battery voltage drop versus the current. In case that the simulation implies extra accuracy, the lookup table output shall replace the fourth input port. The SoC and the discharge/charge current can be further calculated by the existing block outputs.

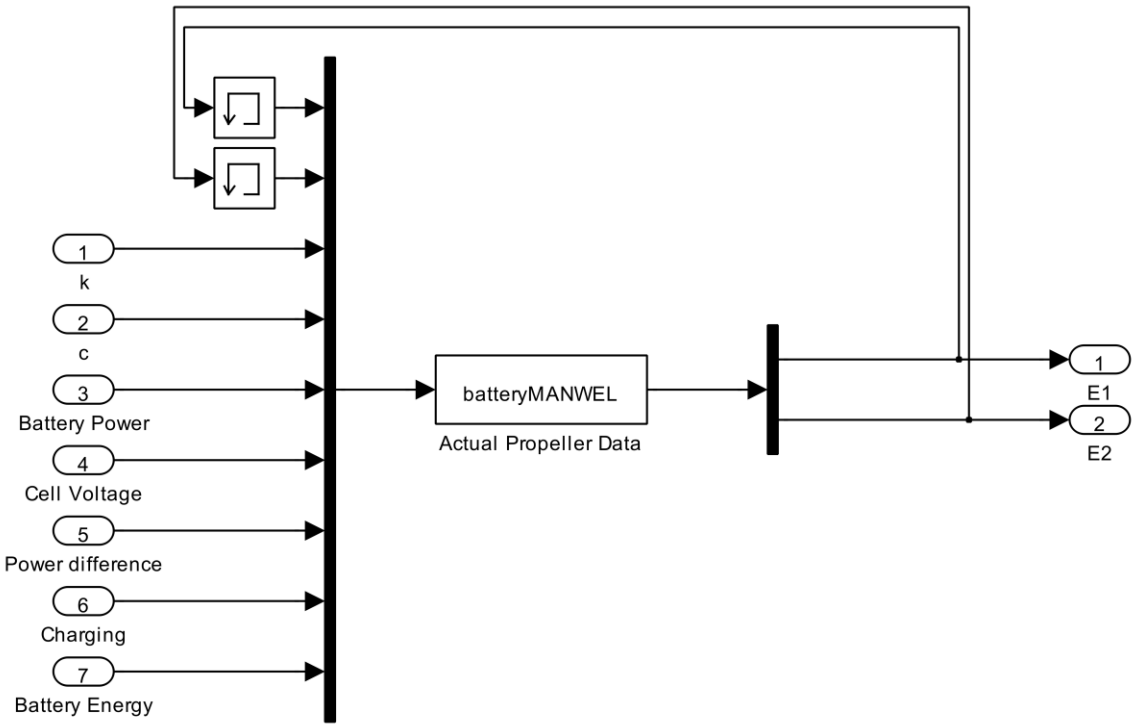


Figure 5.12: Representation of KiBaM battery block in Simulink

Table 5.9: Kinetic Battery Model block inputs and outputs

| Model Inputs | Model Outputs |
|---|---|
| C, k experimental battery coefficients | Energy of the 1st well |
| Battery required power | Energy of the 2nd well |
| Cell/ Battery Voltage | |
| Power difference | |
| Charging logical function | |
| Battery required energy | |

### 5.1.9 LP Optimisation block

This block implements the power minimisation strategy proposed by Grimmelius et al. (2011). This strategy is based on the ECMS algorithm and was originally modelled for dynamic simulation systems. In this project, for a discrete time domain and steady state simulation, modifications to the estimation of the lambda coefficient have been made as described in chapter 4.

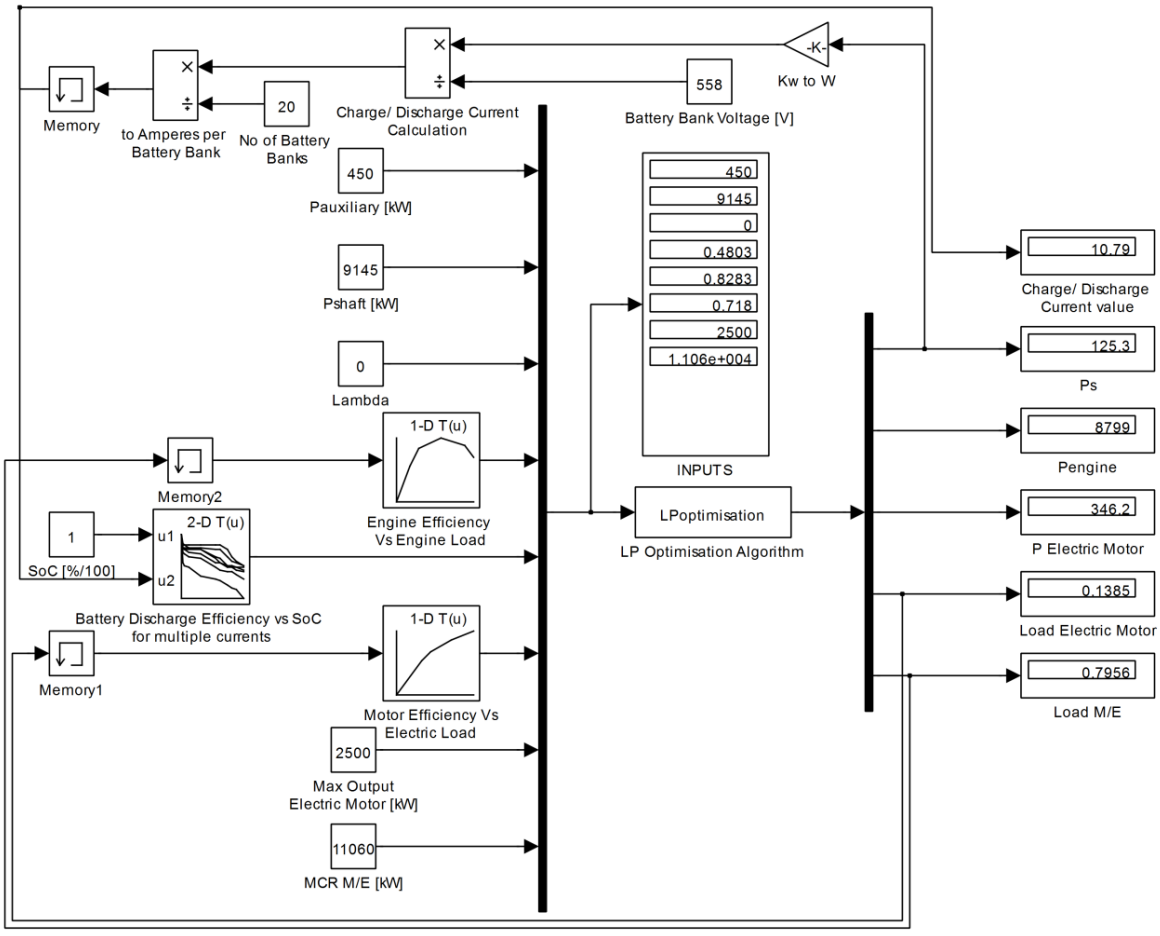


Figure 5.13: Representation of Linear Programming optimisation block in Simulink

The subcomponent efficiencies with this strategy are assumed constant at the broad operational range. However, for vessel machinery systems, this assumption is valid for a very small range of engine operations, where the efficiency remains flat. Moreover, it is

valid for battery systems that operate under constant current for a time period where the voltage drop is constant.

This block incorporates the Hybrid component efficiencies in the form of a lookup table. The engine efficiency, the electric motor efficiency is a one-dimension lookup table with engine or motor load as the interpolating vector. For the battery efficiency, the lookup table is more complex, as the battery discharge efficiency depends on the State of Charge, which is the first input, as can be seen in Figure 5.13, and the discharge current as the second input. Given the fact the LP S-function block yields to the loads of electric machine and M/E, which feed the input of the efficiency lookup tables, multiple algebraic loops are present. In order to solve this problem, memory blocks have been inserted to the model, which are responsible for supplying the previous simulation step values, enabling the system to run. Nonetheless, the simulation time is increased significantly and for large variations where the efficiencies are not constant, the outputs are not valid, thus it is suggested to run the optimisation script described in Chapter 4.

**Table 5.10: LP optimisation block inputs and outputs**

| Model Inputs | Model Outputs |
|---|---|
| Number of battery banks ($N_{BB}$) | Battery storage power exchange |
| Auxiliary required Power | M/E power output |
| Propulsive required Power | Electric machine power output |
| λ coefficient | Electric machine load |
| Battery SoC | M/E load |
| Electric machine MCR | |
| M/E MCR | |

### 5.1.10 Weather routing capability

The ship simulator can be also used for weather routing decisions as it is a non- complex fast package. The importance of routing for reduction of fuel consumption, voyage time and increased passage safety was established in the early years of ocean going shipping. In order to decrease the consumption of power due to added and wind resistance, it was necessary to identify ways to optimise the route. The first attempt, however, was made by James (1957), and Hanssen and James (1960). In their study, the use of an isochrones time-front method based on weather forecast data, which attempted to minimise the journey time, was demonstrated. James' (1957) method was based on empirical results studying the effect of the waves while the ship proceeds into them at different speeds. Haltiner et al. (1962) published a new approach with the use of calculus variations. This method was used later by Papadakis et al. (1989), who described the ship speed as a function of the significant wave height and direction. Zoppoli (1974) produced the first dynamic approach for optimisation of routing based on James' (1957) results, by setting wave height and direction as random parameters. Work on minimisation of voyage time is

performed by Bijlsma (1975) as well, who proposed alternative solutions for fuel savings and routing optimisation. Frankel and Chen (1978) used the Bretschneider wave spectrum to match sea state conditions with random wave frequency, direction and height. It was the first time that the problem was not approached with empirical curve methods, and a physics implementation was followed to simulate the wave energy and direction. Lo and McCord (1998) used global data for ocean currents with the addition of data measurements from ship voyage weather monitoring, in order to estimate state transition probabilities. Azaron and Kianfar (2003) used the directed acyclic network theory to find the shortest route. The goal was to decide for each geographical position of the vessel whether it would be optimum to change its position and towards which direction. Vlachos (2004) attempted to find the optimum solution for a weighted equation of voyage travel time and safety. To perform the optimisation he followed two separate methods: the use of an iterative optimisation algorithm, and the simulated annealing method. Speed loss in waves was described using James's results. The study was revised in 2008 and 2009 by the addition of actual experimental data. Hinnenthal and Saetra (2005) used Pareto fronts, two objective optimization algorithms, and population generation algorithms to create different routes to minimise simultaneously travel time and fuel consumption. The swell forecasts used were modelled using the Bretscheider spectrum. Padhy et al. (2007) employed optimal control theory and a dynamic programming technique to obtain a reliable optimum route in a given random sea-state. Szłapczyńska and Śmierzchalski (2008) attempted in their research to use the Isochrones method with area partitioning, combined with a weather routing system with an evolutionary approach to find alternative routes of reduced collision risk and low passage cost.

## 5.2 Simulink block and optimisation algorithm test cases

This section presents the accuracy of the Simulink models given known inputs and outputs. The algorithm's outputs were compared with by hand calculation for the specified given inputs or by comparing the simulation results with published results presented by the original authors. The Simulink representation of 5.2.1, 5.2.2 comparison is depicted in Figure 5.18.

### 5.2.1 Calm water resistance block test

The selection of the calm water resistance model was made by comparing the different approximation methods presented in Table 4.1. The selected method should best suit the experimental resistance curve which was obtained from the MOERI (KRISO) model test basin in Korea. Due to applicability constraints and due to the publication date, five resistance approximation methods have been compared. It can be observed from Figure

5.14 that the method that contains the largest error is the BSRA. This significant deviation can be explained by two reasons. The first is the publication date (1964) and the second is the approximation procedure, which is based on by hand interpolation in very small and low quality graphs. Moreover, there are cases where the designer has to extrapolate the graph results introducing uncertainties to the read values. This means that the total error significantly increases as the process approaches the end. The Lap-Keller method is known for overestimating the resistance, as it was intended for slow speed vessels with a high block coefficient. Moreover, the regression analysis performed in the early 70s is not representative of modern designs, especially the Post-Panamax vessels, which were first introduced after 2000. Based on the Lloyds list data, by 2007, only 98 Post-Panamax vessels were in service, which explains the absence of regression data for that vessel type. The Formdata method has an abnormal shape, which significantly underestimates the resistance at slow speed and overestimates the resistance at high speeds, converging with the BSRA method. The Formdata method is based on by hand interpolations, but with significantly fewer graphs of higher quality. Of all methods compared, the Holtrop-Mennen method has so far proven to be best suited to the data.

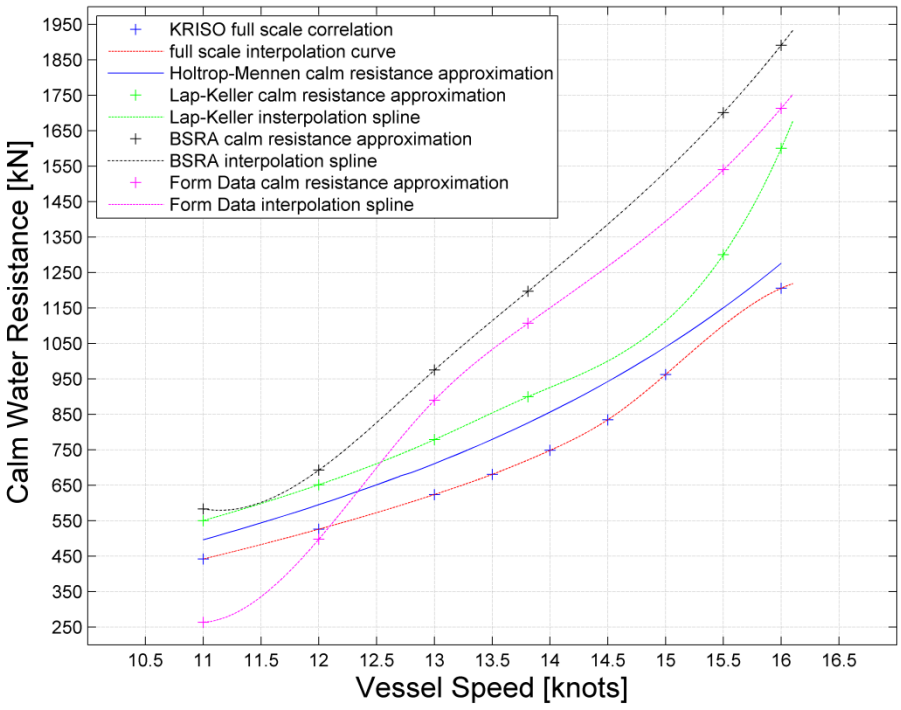


**Figure 5.14: Comparative analysis of multiple approximation methods and full scale resistance model data**

It can be extracted from Figure 5.14 that there is a difference of 14.4% in the design speed (13.8 Knots). Furthermore, the difference is ~108kN for the speed range of 13-14.5 Knots

and the prediction method follows a cubic trend, as expected. For higher speeds, when wave-breaking resistance takes place, the error decreases. The approximation curve, however, has a normal shape for the examined speed range. The last comparison will be made between the Holtrop-Mennen method and the Hollenbach method. For this purpose, Figure 5.15 is introduced. The values are corrected for air-drag, which is given for the examined speed range, and the hull roughness is neglected as the ship is on sea trials. Based on Figure 5.15, the Hollenbach method slightly overestimates the resistance from 12.5 to 14.3 knots. There is very good matching at 11-12.5 and 14.5 knots, while for high speeds of >15knots, the method underestimates the total resistance. However, the introduced error at high speed does not affect the calculations, as the vessel design speed is 13.81 knots with a maximum reported speed of 14.7 knots in both laden and ballast conditions.

Differences between this prediction method and the experimental data are due to the hull design, which has a high block coefficient and small dimensions compared to the statistical data that the method was based on. Due to the small error introduced, this method will be considered as best suited for the simulator purpose.

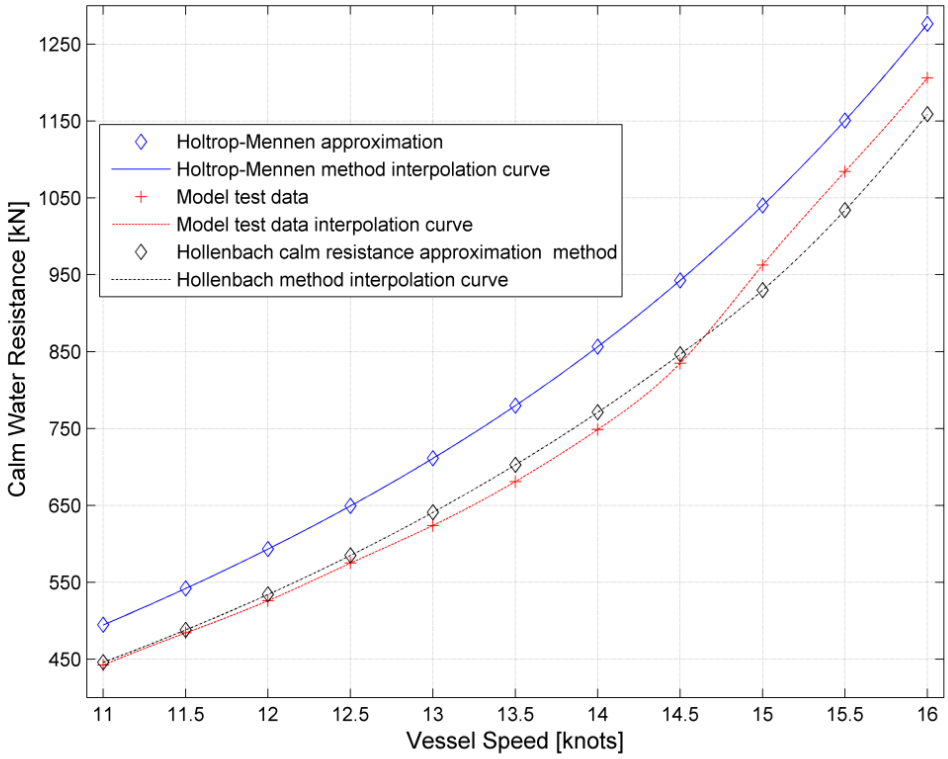


**Figure 5.15: Comparative analysis of resistance approximation and model test results for design draft and speed range of 11 – 16 knots**

### 5.2.2 Propeller block test

The second comparison will be performed for the purpose of estimating the deviation of the Wageningen B-series approximation and the actual propeller data as supplied by the KRISO model basin facility, which performed the propeller tests. The comparison was performed for ten simulation segments, which correspond to a progressive speed increase from 11 to 16 knots. It can be observed from the detail of Figure 5.16 that there is approximately 2.3% difference in the propeller open water efficiency. Nonetheless, the B-series approximation yields to a very good approach to the actual data and is considered as an acceptable method in cases where the real propeller performance characteristics are not available. In order to better understand the effect of this error, the engine propeller interaction should be evaluated. Two set of tests that couple the resistance model and the propeller performance have been completed.

Figure 5.17 presents the propeller engine interaction for two thrust resistance matches. The top figure correlates the thrust resistance match for model test resistance data.

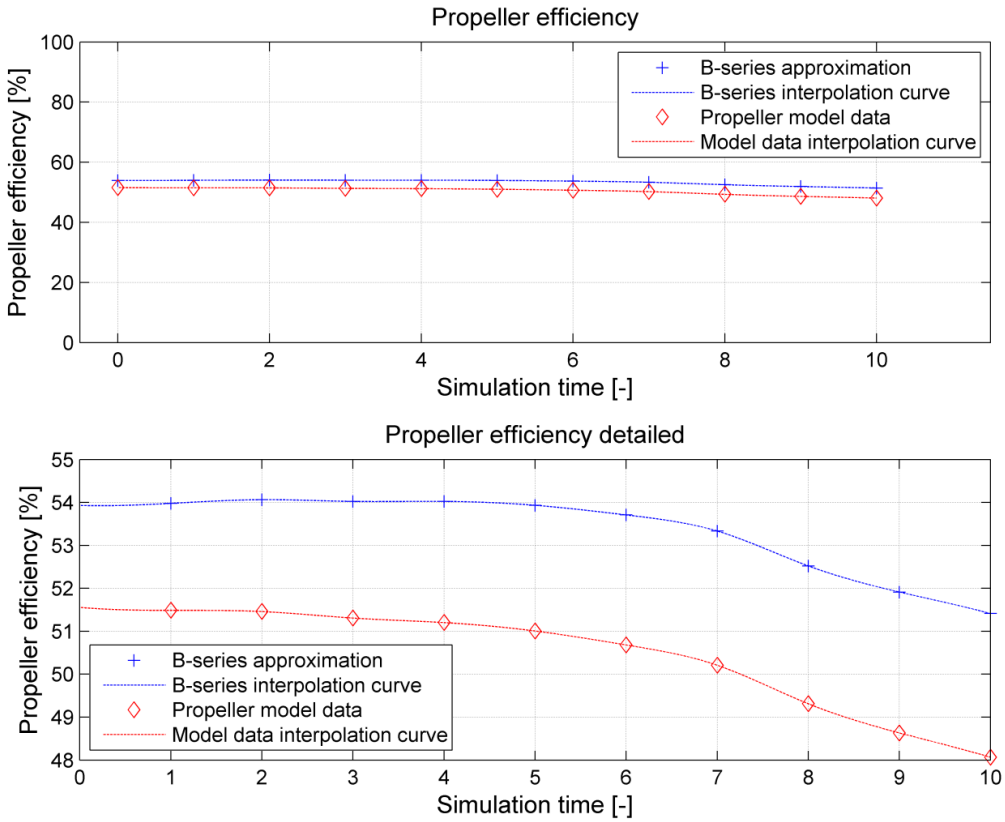


Figure 5.16: Comparative analysis of B-series approximation and actual propeller data

The curve depicted in diamond symbols represents the engine power and RPM demand to match the ship's calm resistance at the design draft, in calm sea, with clean hull and for a

speed range of 11 to 16 knots with the developed thrust. It can be observed that the propeller efficiency greatly affects the power consumption, thus the propeller is heavily loaded. In addition, the RPM demand is lower than the actual propeller. However, the engine propeller matching is not acceptable, since, with the existence of sea margin and hull foulness, the vessel is unable to absorb the full power of the engine at the maximum speed. The second figure depicts the engine propeller interaction for thrust resistance match. The resistance is approximated by the Holtrop-Mennen method. The purpose of this comparison is to identify the effect of the resistance curve on the engine power and to conclude which imposed error has greater effect on the total simulation. It can be observed from Figure 5.17 (lower subplot) that the B-series approximation, in combination with the Holtrop-Mennen resistance method, leads to a unacceptable propeller engine match. The propeller cannot absorb the maximum power of the engine, although it does not reach the speed limit. Nonetheless, the matching of the actual propeller with the Holtrop-Mennen method leads to an acceptable matching, although the maximum speed is not reached. The latter is not caused by the simulation block, but by the improper initial design of the vessel.

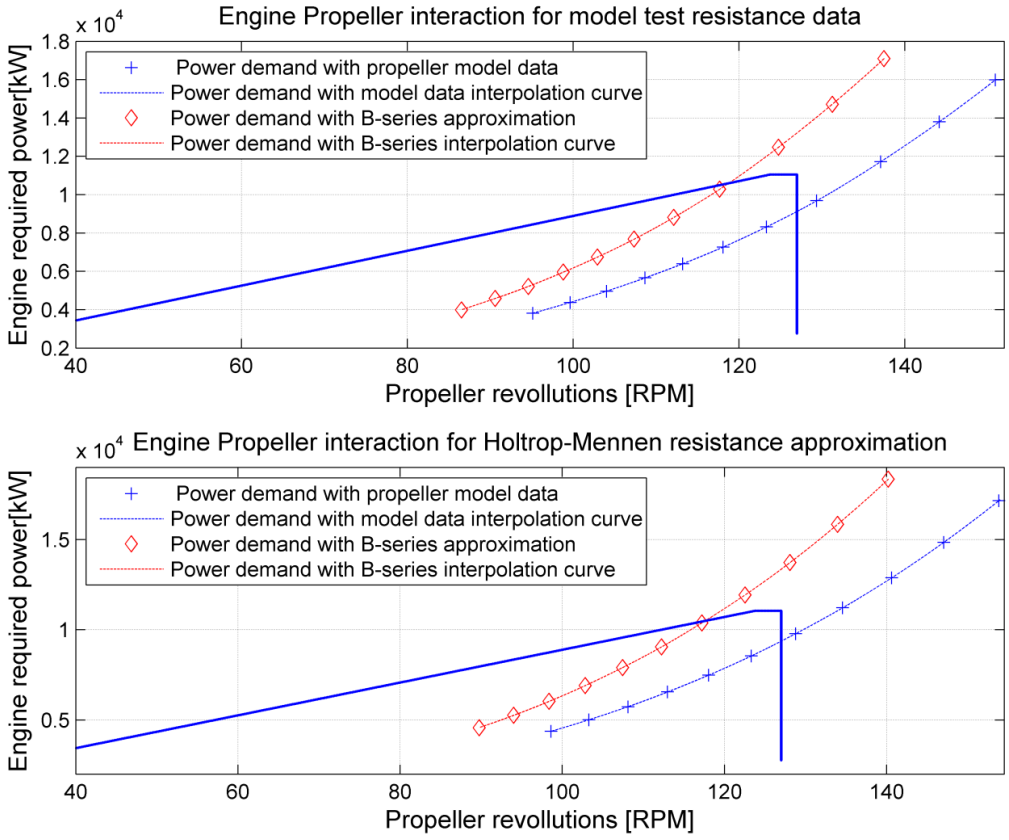


**Figure 5.17: Propeller engine interaction for 2 resistance methods and for B-series approximation compared to actual propeller performance data**

Thus, the resistance method has a slight effect on the power requirement, but it alters the propeller rotational speed by approximately 3-5 RPM. By examining Figure 5.17, it can be concluded that the effect of the resistance on the propeller engine interaction is negligible, but the approximation of the propeller characteristics greatly affect the simulator accuracy. This finding necessitates the insertion of the actual propeller data into the ship voyage simulator, in order to reduce the multiplication of error.

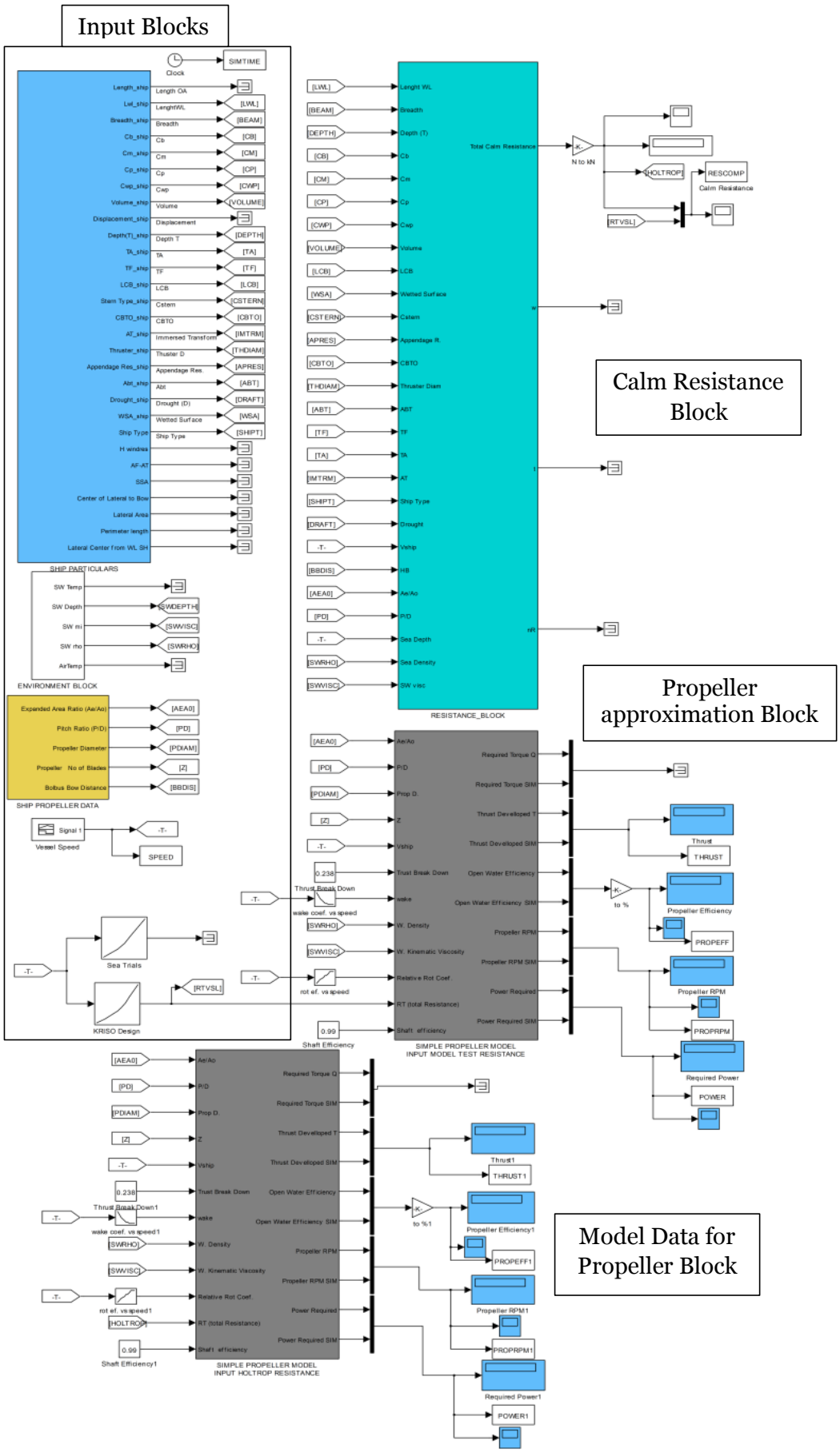


**Figure 5.18: Simulink representation for Calm water resistance, propeller and propeller-engine interaction comparative analysis**

### 5.2.3 Wind induced loads block test

The third comparison will focus on the accuracy of the wind induced loads blocks. Two methods are compared to each other and are crosschecked with by-hand calculation. The Simulink representation of the test case layout is found in Figure 5.20. The comparison test was performed for constant vessel speed of 13.81 knots (design speed) and for constant wind speed equal to 15 knots. For this test, the single varying parameter was the wind force angle of attack relative to the ship's bow.

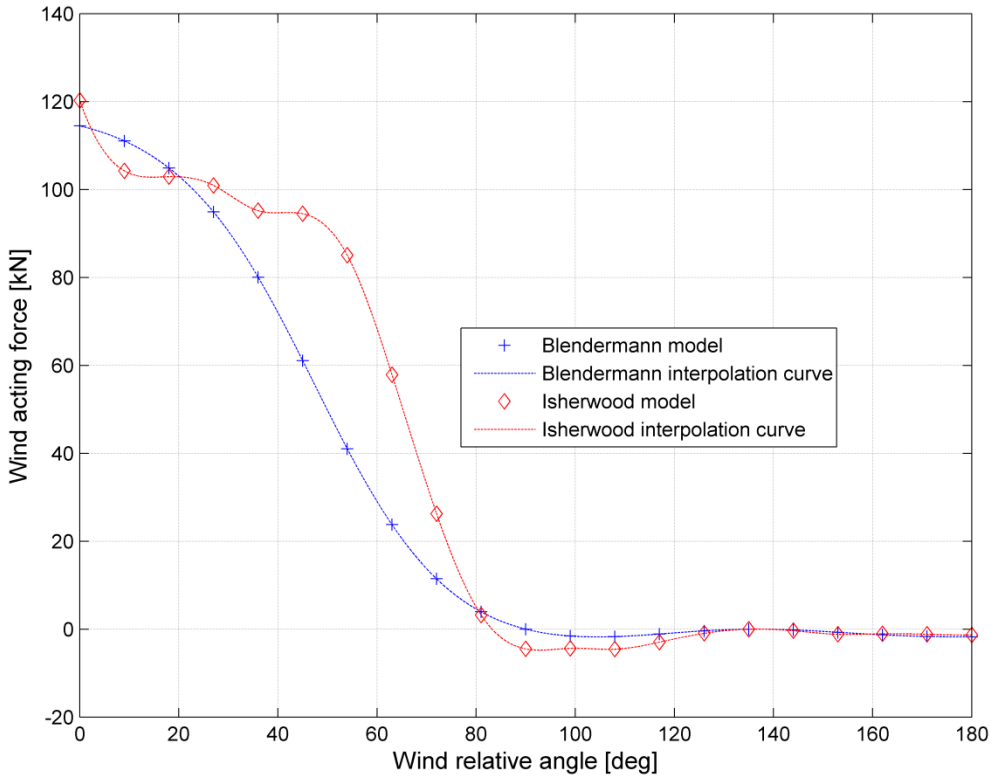


**Figure 5.19: Comparison of wind induced loads approximated by Blendemann and Isherwood methods**

The direction changes from head (0°) to astern (180°). For simplicity purposes, the vessel is considered to sail always in zero angle heading. On the examined ship, two masts exist. The ship is in laden condition and the lateral and projected areas were measured using the ship drawings supplied by the shipping company. Based on Figure 5.19, it can be extracted that both models converge to the wind induced force when the angle of attack is in excess of 120 degrees (quarter) and up to 180 (astern). The Isherwood model curve (denoted in red with diamond symbols) has no smooth results over the range of zero to 45 degrees compared to the Blendermann model curve. This behaviour can be explained by the fact

that this model is based on polynomial interpolations, which are, in turn, based on a sample of superstructure geometries on various ship models.

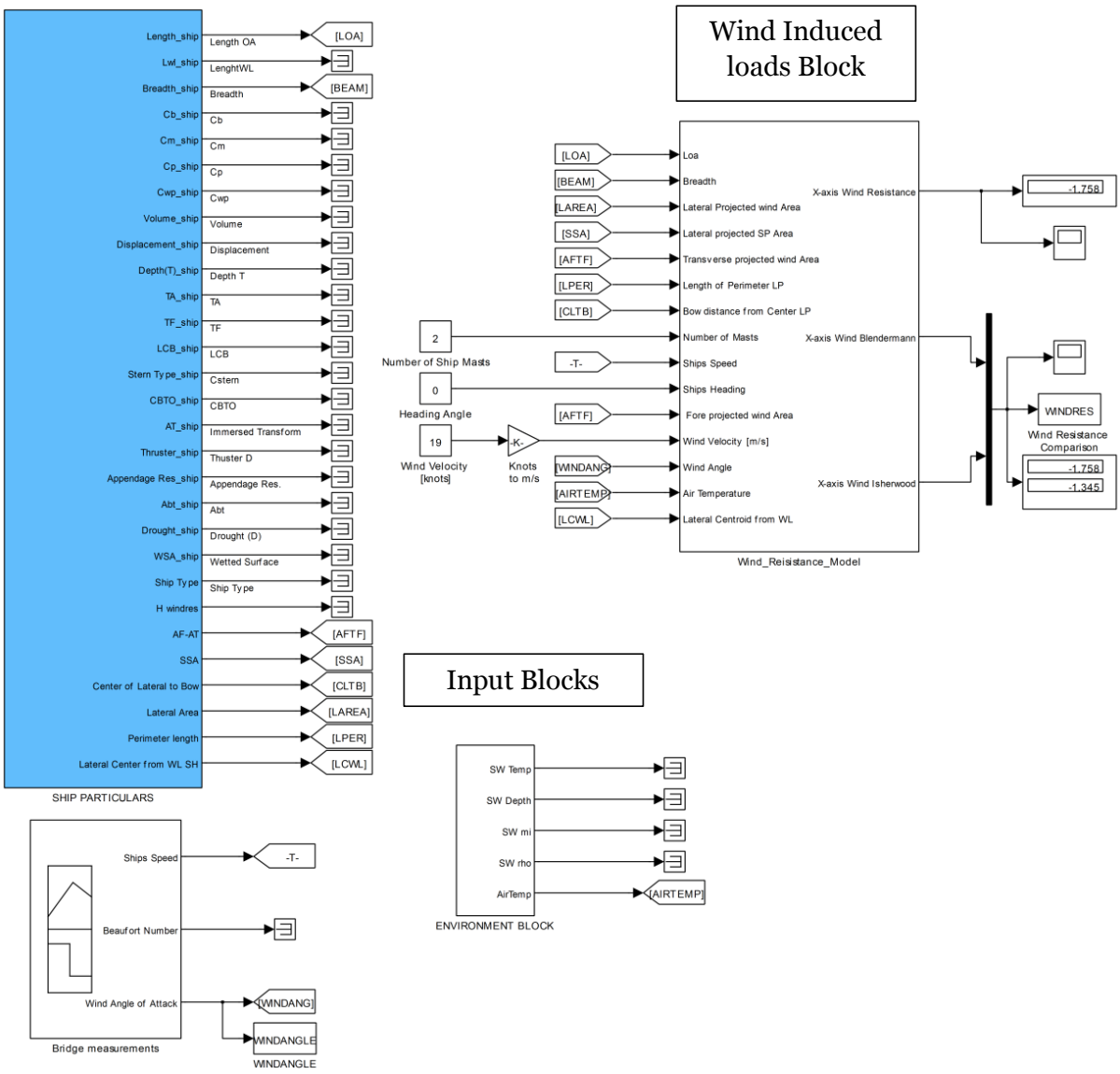


**Figure 5.20: Simulink representation for wind induced loads comparative analysis**

The Blendermann (1994) model is also based on interpolation values. However, the regression analysis that was performed incorporated modern superstructure forms, which explains the smoothness of the Blendermann model curve. Nonetheless, both models are considered accurate for simulation purposes. However, the simulator user is encouraged to decide which model to use by taking into account the examined vessel geometry and the vessel built date.

### 5.2.4 Added resistance block test

In this subchapter, the added resistance approximation models of Aertssen and Kwon will be compared, and the results, with the exception of the discussion on the trend of the two curves, will be assessed based on the published comparison in Towsin and Kwon (1983) publication. The Simulink representation of the comparison of these two models is presented in Figure 5.26.

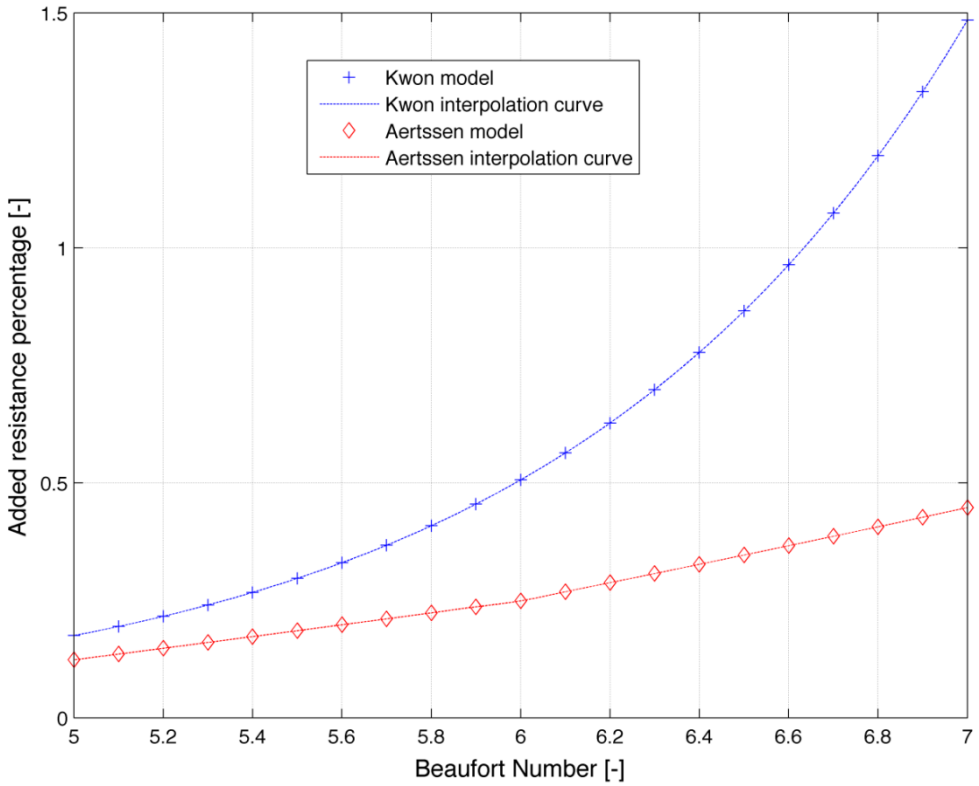


**Figure 5.21: Comparative analysis of Aertssen and Kwon added resistance models for constant speed, head waves and increasing sea state**

The first comparison is performed for constant vessel speed equal to 13.81 knots. The wind and waves have an angle of attack at zero degrees relative direction. The sea state is increased from 4 to 6 during the simulation time. Based on the published results, the behaviour of the curves is as expected. The Aertssen model (model 2) is known to underestimate the effect of high BN because the original equation is simplistic, although Aertssen himself was the first to introduce corrections to his formulae for the wind and wave direction.

A second comparison of the behaviour of the two model curves is performed and the results are shown in Figure 5.22. The simulation run was performed for the speed range of 11 knots progressively increased to 16 knots, while the Beaufort Number was increased accordingly from 5 to 8. The ship was in laden condition (design draft). However, this

approach differs from the real vessel operation as, when the vessel exceeds Beaufort number 7, the master alters vessel speed in order to avoid slamming and racing of the engine. Moreover, when the ship sails into Beaufort number 8 and higher, the master lowers the fuel admission lever in order to ease the ship motions and the deck wetness (Aertssen and Sluys, 1972).

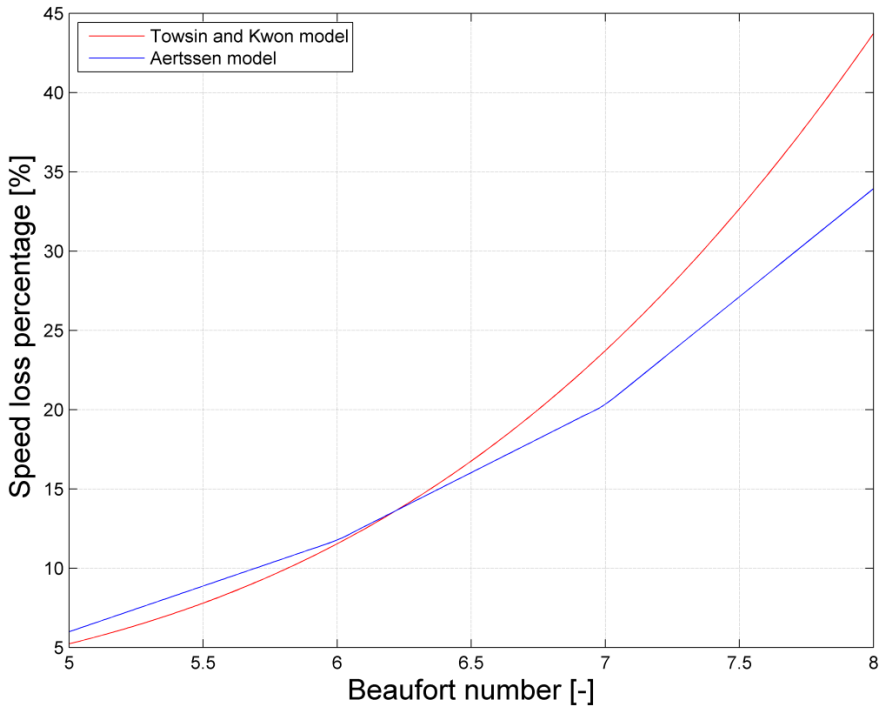


**Figure 5.22: Comparative analysis of Towsin and Kwon and Aertssen models for head waves, increasing Beaufort number and progressively increased speed.**

It can be extracted from Figure 5.22 that the two models have good accuracy when the ship sails with increasing speed up to Beaufort number 6. In higher sea states, when the ship increases its speed instead of performing voluntary speed loss, there is an equivalent speed loss which is translated into added resistance. The 33% of the equivalent speed loss in BN 8 given by model 2 is precisely what the equation implies. Model 1 value is within the expected range, allowing the conclusion that the shape and the range of added resistance and speed loss values are valid. However, the potential error in high sea states due to the uncertainty in statistical data is limited based on the time the ships spent in high sea states, as seen in Table 5.11. Nevertheless, it is advisable for the simulator user to identify which of the two models best describe the sea state by comparing with the actual total resistance if on-board measurements using torque meters exist.

In order to finalise the test cases of added resistance, one more comparison is performed to evaluate the added resistance approximation, using the Series 60 model results dimensioned for the examined Post-Panamax vessel. For this test case, a voyage of

thirty-two days is selected. The dominating weather parameters, such as the wind force, the sea state and the relative angle of attack for wind and waves, are obtained from the examination of thirty-two 'noon reports' of the examined vessel. The daily mean vessel speed and the mean daily reported Beaufort number are presented in Figure 5.23. Based on the depicted values of this figure, it can be said that there is a voluntary speed loss when the ship sailed in sea state 6 (Beaufort number 7). Concerning the values of added resistance, Figure 5.24 and the detail of the latter figure presented in Figure 5.25 are introduced.

**Table 5.11: Percentage of sailing time in specific Beaufort numbers**

| | Laden Voyage | | | Ballast Voyage | | |
|---|---|---|---|---|---|---|
| | Vessel 1 | Vessel 2 | Vessel 3 | Vessel 1 | Vessel 2 | Vessel 3 |
| BF ≤ 4 | 5.88% | 12.50% | 0.00% | 6.45% | 11.11% | 0.00%<br>6.25% |
| BF = 5 | 76.47% | 75.00% | 75.00% | 45.16% | 0.00% | 54.55%<br>25.00% |
| 6 ≤ BF ≤ 7 | 17.65% | 12.50% | 25.00% | 48.39% | 88.89% | 45.45%<br>68.75% |

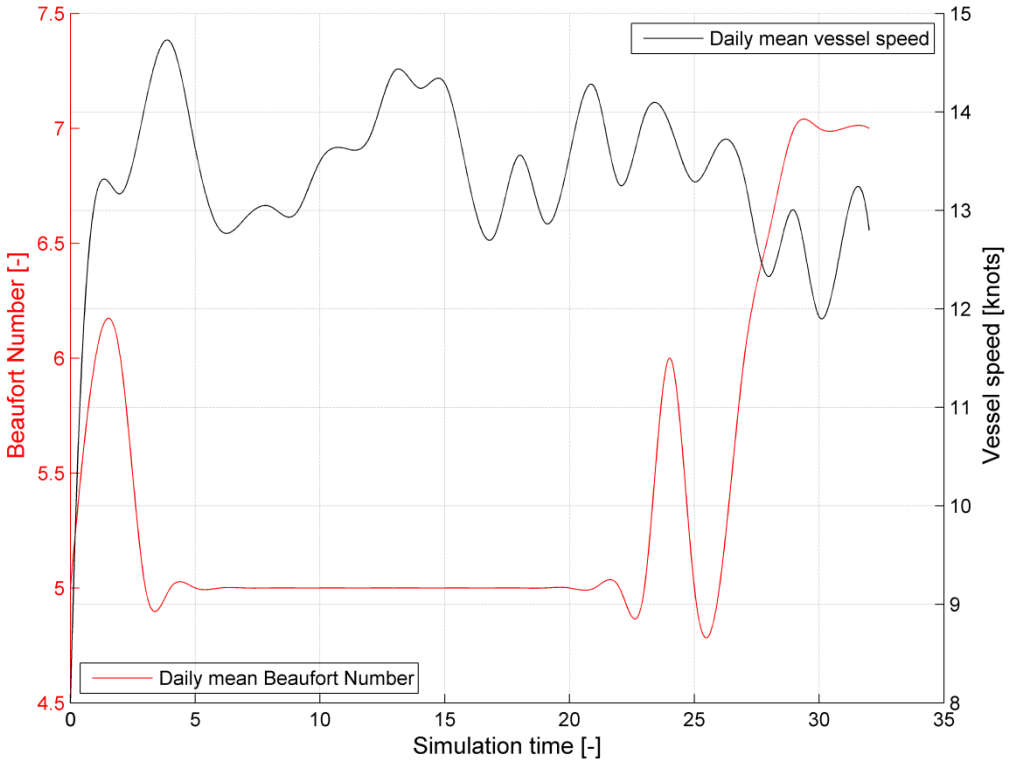


**Figure 5.23: Daily mean Beaufort Number and vessel speed versus voyage day**

It can be extracted from Figure 5.24 that there is an added resistance increase due to the increase of sea state on the second day. After the third day, there is a significant drop in

added resistance, which takes on negative values. Physically, the negative sign represents the aid in the ship's speed due to direction of the waves.

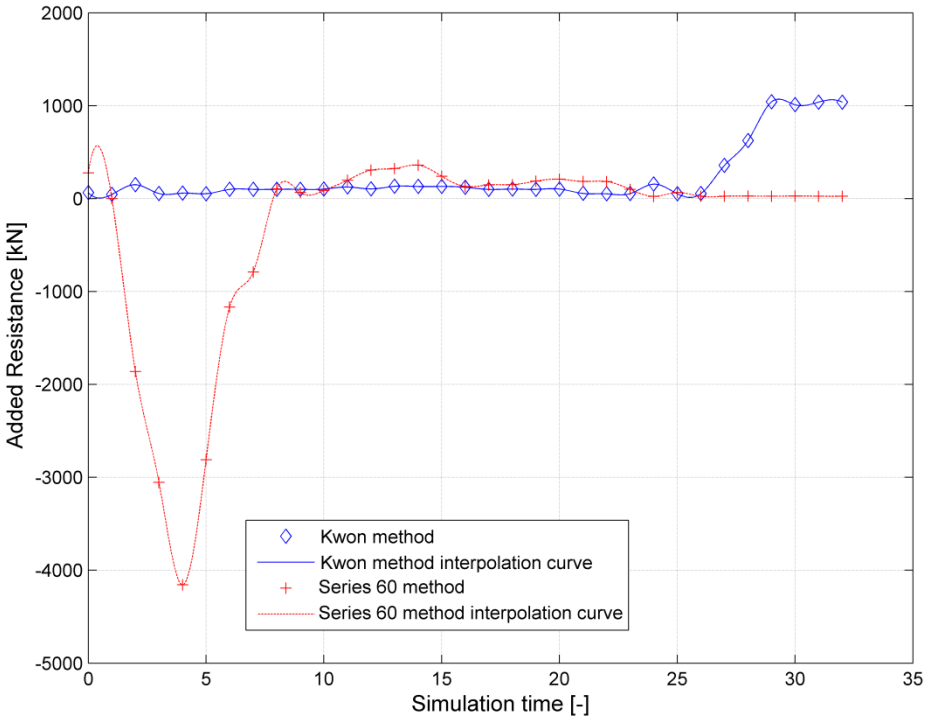


**Figure 5.24: Added Resistance comparative analysis of Kwon and Series 60 methods**

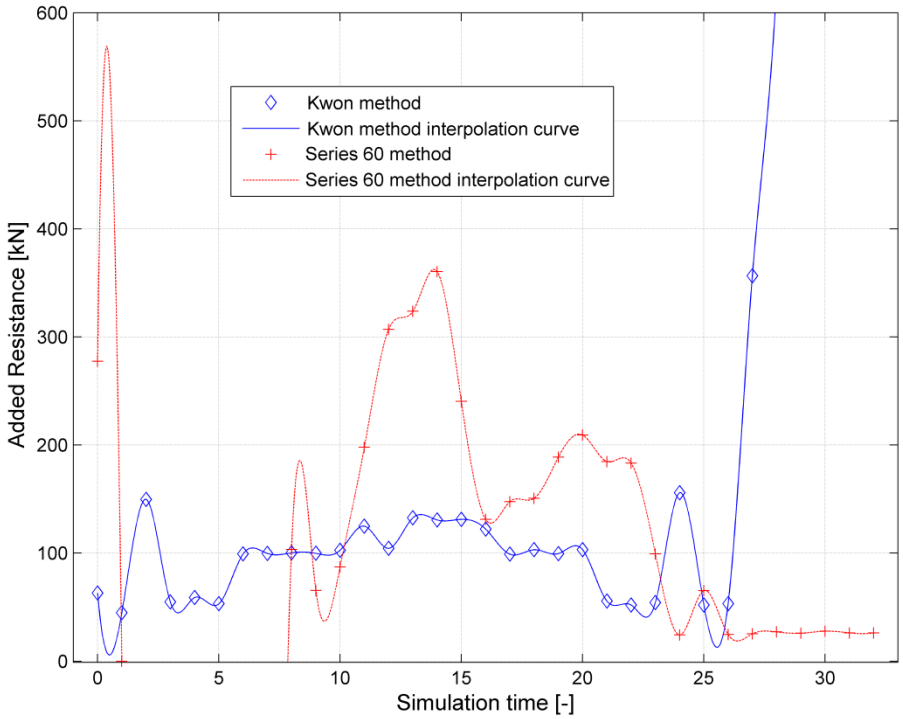


**Figure 5.25: Detail of added Resistance comparative analysis of Kwon and Series 60 methods**

On the fourth day, however, the vessel speed is increased and reaches the maximum reported value, as seen in Figure 5.23, while the added resistance takes the maximum absolute value at the same time, presenting the coherence of the reported data. The Kwon model, however, is modelled in a way that does not permit the usage of negative or positive signs, making the comparison more difficult.

Concerning the rest of the voyage, significant deviations occur on the eleventh day and up to the fourteenth, as depicted in Figure 5.25. Taking into account the extreme deviation of the Kwon model and the series 60 approximation for day twenty-seven to thirty-two, it can be concluded that the connection of the vessel speed (or Froude number) is the dominant parameter for the accuracy of the models. In addition, there is no capability to extract secure conclusions, as the Kwon model is sensitive to the Beaufort number value and to the vessel speed, while the tabular data of Series 60 approximation is sensitive to the wave angle and the Beaufort number, and not so much to the Froude number, as the model interpolates only between 0, 0.1, 0.2 Froude number values, significantly reducing the model sensitivity in speed variations.

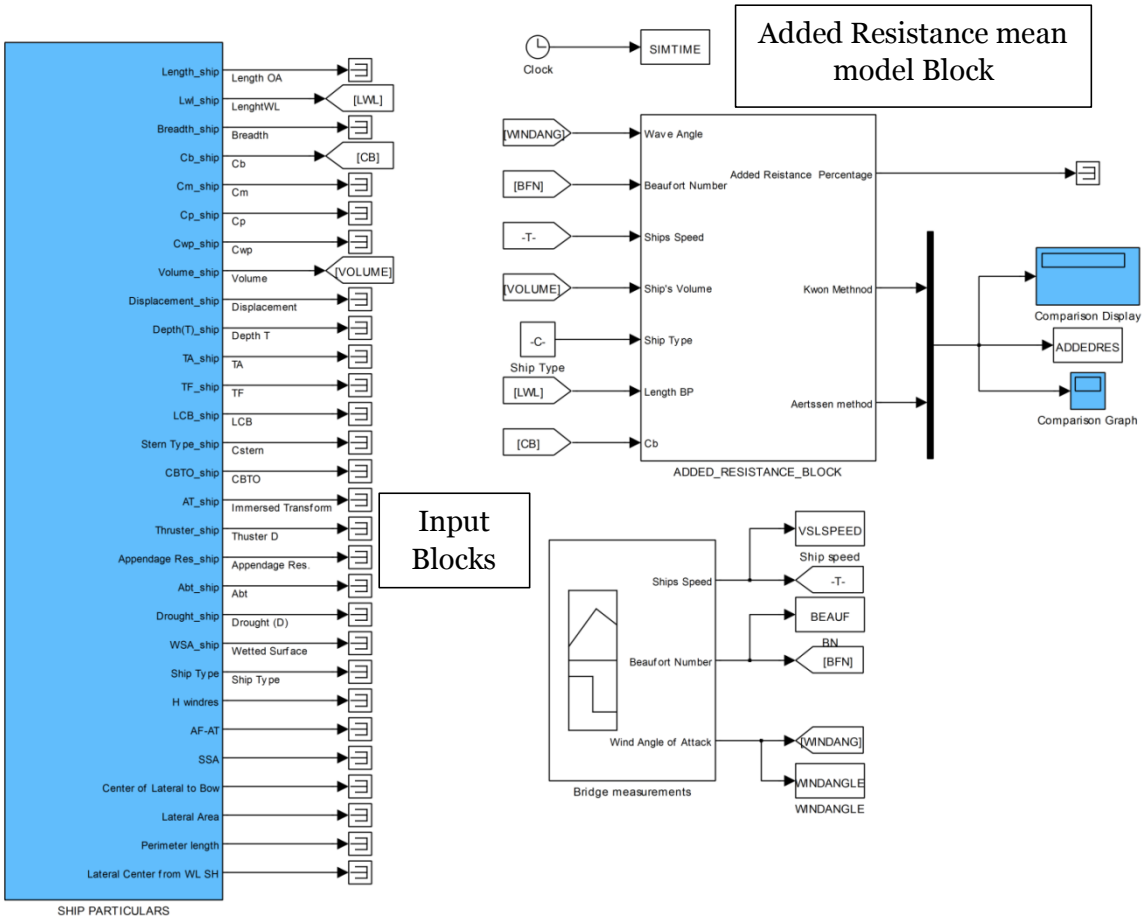


**Figure 5.26: Simulink representation for added resistance comparative analysis**

### 5.2.5 Non-linear optimisation test

The simulations were performed for the auxiliary loads of a Bulk carrier for a time period of 24 hours. Primarily, the simulator was fed by an artificial load, which remains constant for 2.4 hours, in order to validate the simulator's ability to operate with initially depleted batteries (Depth of Discharge 100%). The results are presented in a graphical way in Figure 5.27. In combination with Figure 5.28, it can be extracted that the battery is charged (because of a rule based restriction, as the system prohibits the operation with State of Charge less than 10%) and is followed by discharge and then by a charge. Meanwhile, in order to meet the power demand, the Hybrid system engine alters its load, which is depicted in blue in Figure 5.27. The percentage of this fluctuation is determined by the ECMS strategy, which optimises the system operation in order to save energy for future demand and thus minimise fuel consumption and emissions. Of crucial importance to the outcome of the optimisation and the racing over batteries percentage is the installed energy capacity. For the artificial load, the capacity was set to 2MWh. The selection energy capacity of the storage medium is dependent on the engine auxiliary output and the study of electric load analysis.

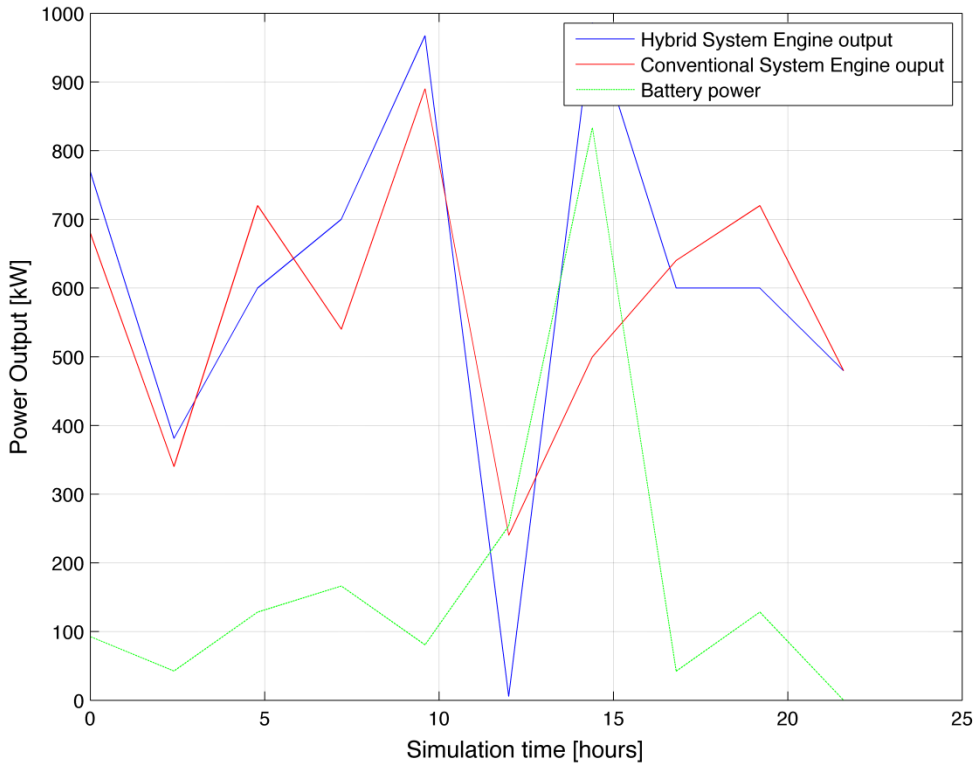


Figure 5.27: Comparison of Conventional, Hybrid engine outputs and battery power

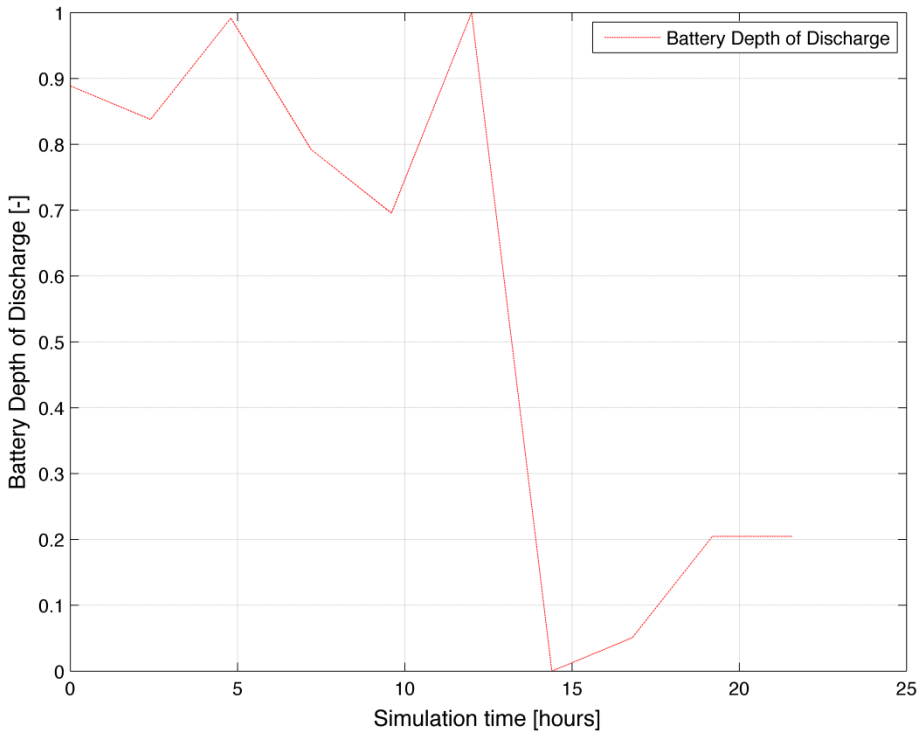


Figure 5.28: Battery Depth of Discharge versus simulation time

Figure 5.28 denotes that the hybrid system is charging for 50% of the simulation time, discharging for 40% and remains idle for 10% of the time. This graph denotes that the logic criteria that accompany the optimisation algorithm do apply and constrain the optimisation procedure in order to maintain the battery SoC close to the reference value, which is 35%. However, the SoC reference is the minimum SoC that the system should have at the end of the reference time. Based on this figure, the optimisation algorithm applied energy to the battery, reaching, at the final time step, a SoC equal to 80%.

## 5.3 Implementation example – Simulation representation

In this section, the example of section 4.4 is implemented in the Simulink environment using the blocks described in section 5.1.

The selected voyage is a 31 day ballast voyage from Hong Kong to Brazil. A data file containing the vessel geometrical information for the sailing draft, the freeboard etc. should be created and inserted to the simulator. The input data blocks are the source of information for the simulation. Every output port is connected to its unique parameter which is defined in a matrix form. As a result, the data file should provide the required information in matrix structure. A sample matrix is depicted in Table 5.12, where the information provided are the geometrical characteristics of the examined ship. Once this process is completed, the unique parameters defining the voyage should be provided. The

block which inserts these parameters to the simulation is called “Bridge measurements”. However, the time step that the parameters are fed to the simulation should be firstly identified. As a result, before programming the simulation time step, the involved models should be inserted to the simulation file.

**Table 5.12: Set of geometrical information for heavy ballast draft provided by the user**

| | | | | | |
|---|---|---|---|---|---|
| INPUT 01 = $L_{OA}$ | 229.50 | INPUT 11 = $T_A$ | 7.288 | INPUT 21 = S | 10360.30 |
| INPUT 02 = $L_{BP}$ | 225.80 | INPUT 12 = $T_F$ | 9.989 | INPUT 22 = $C_{SHIP}$ | 1.00 |
| INPUT 03 = B | 36.92 | INPUT 13 = Lcb [%] | 0.04 | INPUT 23 = h | 30.76 |
| INPUT 04 = $C_B$ | 0.8393 | INPUT 14 = Holtrop coef. | 10.00 | INPUT 24 = $A_S$ | 976.7 |
| INPUT 05 = $C_M$ | 0.9956 | INPUT 15 = Cyl. opening | 0.00 | INPUT 25 = $A_T$ | 383.94 |
| INPUT 06 = $C_P$ | 0.8594 | INPUT 16 = $A_T$ | 1.10 | INPUT 26 = C | 172.13 |
| INPUT 07 = $C_{WP}$ | 0.8713 | INPUT 17 = Thruster D. | 0.00 | INPUT 27 = $A_L$ | 2397.13 |
| INPUT 08 = Δ | 59697.90 | INPUT 18 = $A_S$ | 2.00 | INPUT 28 = $S_P$ | 552.16 |
| INPUT 09 = V | 58505.27 | INPUT 19 = $A_K$/ $A_S$ | 25.00 | INPUT 29 = $A_H$ | 10.33 |
| INPUT 10 = $T_M$ | 8.639 | INPUT 20 = D | 20.80 | | |

In order to estimate the total resistance, the decomposed model of added resistance is inserted to the simulation model. The switching between the different models for each block is made by the data file (user entry) which selects which approximation methods to use. The information such as speed and weather data is provided by the signal generator in a time step which will be defined later in this section. It can be observed from the equation set that the use of Aertssen or Kwon model gives results as portion of the calm water resistance. Thus, the output of the calm water resistance is an input to the added resistance block. Moreover, the added resistance block requires the knowledge of Beaufort number. For this voyage the use of weather generation model is selected. The weather generation model involves a routine in Matlab which is run by the user prior to the simulation. The parameters which are involved to the estimation of weather parameters are primarily the daily mean wind speed and wind direction values. Secondly it is the requested time step (≥ 2h). Once this information is defined, the Rayleigh and Normal number generators of Matlab suite are called. The output is a two column by m x n (where n is 24 derived by the time step and m is the number of simulation days) wind characteristics matrix. A part of this matrix is presented in Table 5.13.

**Table 5.13: Wind speed regeneration matrix sample using Rayleigh distribution generator**

| Time segement | Day 1 | Day 2 | Day 3 | Day 4 | Day 5 | Day 6 | Day 7 | Day 8 |
|---|---|---|---|---|---|---|---|---|
| 0-2 | 5.67 | 4.20 | 12.78 | 4.29 | 6.94 | 7.77 | 8.04 | 1.88 |
| 2 – 4 | 5.67 | 2.82 | 2.07 | 6.37 | 15.03 | 11.01 | 4.58 | 1.93 |
| 4 – 6 | 6.25 | 6.40 | 11.93 | 5.64 | 9.01 | 8.45 | 13.51 | 3.54 |
| 6 – 8 | 3.03 | 7.23 | 6.49 | 1.77 | 12.46 | 17.67 | 6.58 | 4.24 |
| 8 – 10 | 5.75 | 4.09 | 10.54 | 3.24 | 9.01 | 11.96 | 16.25 | 0.73 |
| 10 – 12 | 1.37 | 8.75 | 5.95 | 9.13 | 8.52 | 12.85 | 2.60 | 1.41 |
| 12 – 14 | 12.08 | 3.55 | 5.87 | 4.79 | 6.22 | 2.68 | 0.93 | 6.16 |
| 14 – 16 | 6.09 | 9.99 | 14.07 | 15.66 | 1.99 | 12.46 | 2.96 | 6.20 |
| 16 – 18 | 2.98 | 4.31 | 1.72 | 20.59 | 12.32 | 7.83 | 0.93 | 6.72 |
| 18 – 20 | 8.47 | 10.59 | 0.76 | 5.62 | 12.75 | 11.22 | 2.82 | 3.08 |
| 20 – 22 | 6.74 | 6.75 | 7.32 | 8.65 | 7.25 | 13.05 | 1.09 | 6.38 |

Using the mathematical representation of Chapter 4, the wind speed is transformed to significant wave height. This vector is loaded to a signal generator, along with the speed and the rest time variant user input parameters. Because the used mean added resistance models require the Beaufort number in every time step, the significant wave height during simulation is transformed to Beaufort number with a 2D lookup table (Beaufort number versus significant wave height) which is derived from Table 4.3. Thus the added resistance is estimated. The wind resistance is calculated by the dedicated block for wind induced loads. The wind speed and direction are directly fed to the block without any transformation. Moreover, the rest ship geometrical constants are also fed and the wind resistance is approximated. Because a dedicated block for wind resistance is used, the added resistance block calculates the effect of wind as well. Therefore, the added resistance output is transformed so that the portion of added resistance due to wind loads is removed. As a result, there is no double calculation of any contributing resistance factor to the total ship resistance. Nevertheless, in order to account all the resistance values, the use of a block which performes the algebraic sum of resistance components is required. The Simulink offers an embedded block for this operation. Nonetheless, the added resistance block has as output the added resistance as proportion of the calm resistance. Thus, the added resistance due to waves is transformed from percentage of calm resistance to absolute value by a simple multiplication and then is connected to the resistance combiner. The total resistance is now defined. It should be also mentioned, that in every case that algebraic summations between output values of different blocks, the use of combiners is mandatory.

Eventually the fuel engine power and fuel consumption have to be simulated. In order to connect the ship resistance with the required propulsive power, the use of Propeller block is required. The block outputs are the required engine torque and the

developed propeller thrust. This block has as inputs, the total ship resistance for given speed and the hydrodynamic coefficients which describe the examined hull. In addition a full set of propeller characteristics is required. The propeller characteristics are supplied by the "input data blocks". The dedicated input block is the "Ship Propeller Data" which is illustrated in Figure 5.3. The hydrodynamic coefficients are supplied by the input data model (user entry) or by the Holtrop-Mennen model, if the user selects this option. In case that the Hollenbach method is used, the user has to supply through the data file the hydrodynamic coefficients, otherwise the simulator cannot run. For this demonstration scenario, the hydrodynamic coefficients were obtained from the towing tank tests and are built in Simulink environment as 2D lookup tables with only input the vessel sailing speed at each time step.

The governing equations of the propeller block are implemented using the S-function format. By applying the mid-point method of numerical analysis the propeller RPM are defined. The appropriate advance coefficient J is determined so the resistance and thrust (accounting the losses) are equal, thus the ship can steam with the user predefined speed. After identifying the propeller RPM and the required thrust and torque, the main engine power is estimated prior to any transmission losses. The shaft losses are user input and are defined when implementing the initial simulation data file.

According to the mathematical implementation, when the power profile is determined by the Propeller block, the engine block is required so as to identify the fuel consumption. The SFOC curve is implemented as a 2-D lookup table. The lookup table represents the SFOC of the M/E versus engine load. Thus, the engine load should be defined at every time step. This is estimated by a simple mathematical derivation of power by the engine MCR (user entry at data file) using the mathematical basic design blocks of Simulink. The corrections are made inside the S-Function. The fuel low calorific value, the operating temperature are supplied by the user thought the input data file. Based on Figure 5.11, the engine block has many outputs which are reserved for future use. For example, when the model is used by a Technical department of a maritime company which requests information regarding the thermodynamic performance of the engine, these lookup tables will depict the thermodynamic performance of the engine versus its loading. Thus, because such information is not required in this thesis, this block will not be further analysed.

Finally, when the input and model blocks have been connected, and the appropriate information display/save blocks have been defined and connected to the appropriate block output ports, the simulation time step should be defined and so the computer's method for simulating the desired scenario.

In order to identify the simulation time step Figure 5.2 should be used. Based on this figure, the calm water resistance model has a minimum response of 1 minute. The

added resistance of 1 hour and the wind induced loads less than 20 minutes. In order to couple these models together and give correct results, the maximum response time is selected. Thus, the first simulation time can be defined and is set to 1 hour. However, in order to have a fully developed sea and the weather generator model to be valid, 2h response time is required for this model. Thus the simulation time is at least defined to 2 hours. Regarding the engine model, the response time of the engine can be less than a minute for short fluctuations or can be up to 30 minutes for progressive increase/ decrease of load which can be overwritten by the crew if necessary. For this simulation, one minute can be considered as a good average time. Regarding the propeller model two minutes response time is acceptable time. Hence, the simulation time for this examined case is two hours.

The problem is discrete and does not involve differential equations, thus a discrete state solver which is fast and accurate can solve the mathematical equations of the blocks. Regarding the total simulation time, the number of voyage hours should be divided by 12 in order to get the discrete simulation time steps. This number is deducted by 1 because the simulation starts from step zero. (t=0). Once all the above have been accomplished, the user can use sinks to have screen representation of the block outputs or use the Matlab/ Simulink integration to save the output data to matrices. Using this capability, the power profile is extracted from the Simulink environment and is saved to predefined format and name data file inside a specific directory. The data file is a two dimensional matrix which containts the power requiremernt in one row and in the second row the simulation time step. Then this matrix is imported by the Optimisation algorithm.

The optimisation algorithm was implemented in Matlab due to the non-linear form and because of the time consuming process for it to be implementeded in the Simulink environment. Furthermore, this would also allow power profiles derived from shipboard measurements or laboratory tests.

The results of the implementation example concerning the voyage simulation are presented in section 6.1.2 while the optimisation results for the acquired and simulated power profiles in section 6.2.

## 5.4 Chapter summary

This chapter presented the simulation block implementation of the mathematical equations presented in Chapter 4. The key characteristics of the simulator package and the advantages of the graphical programming have been discussed. It was found that the adoption of signal flows and major block leads to non-complex models which are more convenient for simulation expansion while maintaining a low risk of programming errors.

Furthermore, it was found that the calm water resistance in design draft is better approximated by the Hollenbach method which is more up to date and is based on the statistical analysis of a large number of modern hull forms.

Moreover, the Blendermann method was also selected to describe the wind induced loads as it is a more up to date method.

Regarding the added resistance due to wind and waves, the method of Aertssen or Kwon is selected. The latter method compared to the Grigoropoulos et al. (2001) approach was found to be more accurate in the method's applicability range. Thus, the calculations are based on Kwon (2008) model with the exception when the introduced error to the calculations is high (large power difference when comparing measured data at similar conditions with the simulated ones and when continuous overloading of M/E is present, something that is not possible to happen regurarily); hence the modest approach of Aertssen is selected.

Due to the absence of RAO data which are more accurate than a daily mean approximation procedure, this thesis demonstrated a way to regenerate environmental conditions in order to apply a mean added resistance model, resulting in fluctuating environmental parameters per day. This method regenerates the environmental parameters at two-hour intervals, using weather forecasting formulae and by applying the assumption that sea spectra, which describe the current, are only valid for up to two-hour periods. A Rayleigh statistical distribution was used for wind speed, and a Normal distribution around the reported mean value was also implemented for wind direction. This procedure resulted in more accurate than the daily mean model and introduced significant less uncertainty than the Grigoropoulos et al. (2001) proposal.

For the engine propeller interaction, the Wageningen B-series approximation has good accuracy compared to the model test data. However, because the effect in engine RPM cannot be neglected, for the simulation purposes the model test data should be used.

Concerning the test case of the non-linear optimisation, the ECMS strategy was adopted. It was found that the algorithm performs power split between the prime movers and the battery system. In addition, the logic criteria for charging conditions are always met and the algorithm converges to a global minimum, resulting in fuel savings.

On the scope of the above, the simulation blocks are considered accurate; therefore the simulator can be used in combination with the optimisation algorithm to solve powering scenarios. The results of voyage cases along with the optimisation of power vectors for both propulsive and auxiliary loads are given in the next Chapter 6.

# 6 Simulation and Optimisation Results

This chapter presents the results of voyage simulation cases and uses simulator outputs to assess the Hybrid power layouts using the implemented ECMS optimisation algorithm. The first part demonstrates the accuracy of the ship voyage simulator compared to the 'as measured' data obtained from the shipping company. Various runs have been performed at this stage and a variation of the parameters is also presented for clarification purposes. The second part of this chapter contains the optimisation outcomes concerning the Diesel Hybrid power system. Three examined layouts are presented.

## 6.1 Ship Voyage simulation

For the ship simulator test case scenarios, voyage conditions are modelled based on the vessels' daily performance reports. The total mean daily power ($P_{total}$) was calculated by the ship simulator using the models described in Chapter 4. This power is determined by the Thrust-Resistance match for self-propelled ships sailing with constant speed setting. Thus, $P_{total}$ is the required shaft power to achieve the reported speed at a specific sea state. The primary source of engine loading is obtained by the simulator, with the relevant Simulink representation is illustrated in Figure 6.1. The selection of the suitable mathematical models and simulation blocks was described in sections 4.4 and 5.3 respectively. Figure 6.1 depicts the layout of the simulation blocks, the input data and signal generator blocks and their interconnections using signal arrows in simulation environmnent. Display/ save blocks can also found in this figure. The outline of this Figure is always specific as the Simulink utilises the principles of graphical programming. Always from the left hand side the user defined information is located. To the right hand side, the simulation outputs are found.

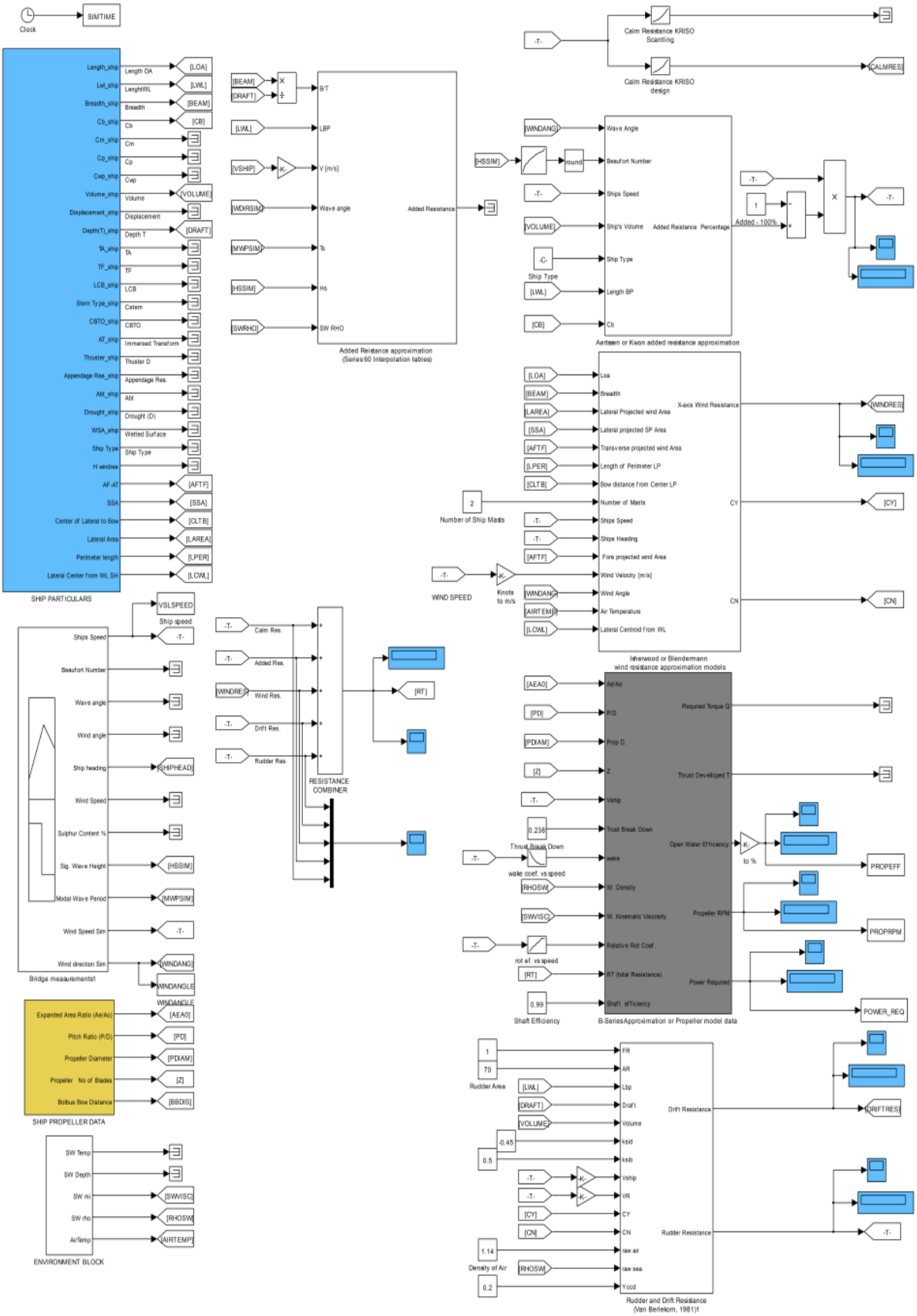


Figure 6.1: Ship Simulator representation in Simulink environment

### 6.1.1 Voyage simulation using 24 hour time step

For the conventional configuration, six voyages have been implemented in the simulation environment. For the needs of the simulation, mean 24h values are inserted to the simulator. The accuracy of reported data relies on the ship's master. However, during the sampling period, the data consistency was checked and in cases where errors exceed the 5% of the sampled data, the voyage was rejected and re-sampling was made.

Given the environmental parameters, the corrected SFOC can be determined and the total fuel consumption to be estimated. For the 6 voyages where details can be found in Table 6.1, comparison between actual fuel consumption and reported fuel consumption is made. For demonstration purposes a thirty-two day laden voyage between Australia (Dalrymple Bay coal station) and Italy (Port Taranto) is presented in detail. The ship sailed 9,535 sea miles. The 'as measured' fuel consumption for the main engine was equal to 1359.1 tonnes.

**Table 6.1: Ship Simulation examined voyages and cargo quantity present**

| Ship | Departure Port | Arrival Port | Distance (sea miles) | Cargo Type | Quantity (MT) |
|---|---|---|---|---|---|
| Vessel 1 | Rio Grande | Marin | 5168 | Soya Beans Milled | 60600 |
| | Hong Kong | Tubarao | 9435 | Ballast | 39063 |
| Vessel 2 | Tubarao | Amsterdam | 5045 | Grains | 80000 |
| | Port Talbot | Port Cartier | 2610 | Ballast | 39060 |
| Vessel 3 | Dalrymple Bay | Taranto | 9535 | Coal | 89524 |
| | Luoyan | Dalrymple bay | 3906 | Ballast | 39121 |
| | Rio Grande | Marin | 5168 | Ballast | 40500 |

For the resistance approximation in laden voyage, for increased accuracy reasons, the full scale correlated results from ship model tests were used. The runs were performed for the case that the ship sailed at constant speed in any faced sea state.

The actual propeller performance data was selected instead of the Wageningen B-series approximation, for the same reason. For the approximation of added resistance due to waves, the formulae of Aertssen instead of Kwon (2008) are selected because they insert a modest approach to the effect of added resistance and because the simulation resulted in continuous engine overload a fact that indicates that the Kwon model overestimated the added resistance significantly.

The simulated resistance breakdown is presented in Figure 6.2. It can be identified from this figure that the largest percentage of the resistance is held by the calm water resistance. The wind resistance seems to reduce the total resistance over a large number of simulated days as the wind hits the vessel from the quarter or astern.

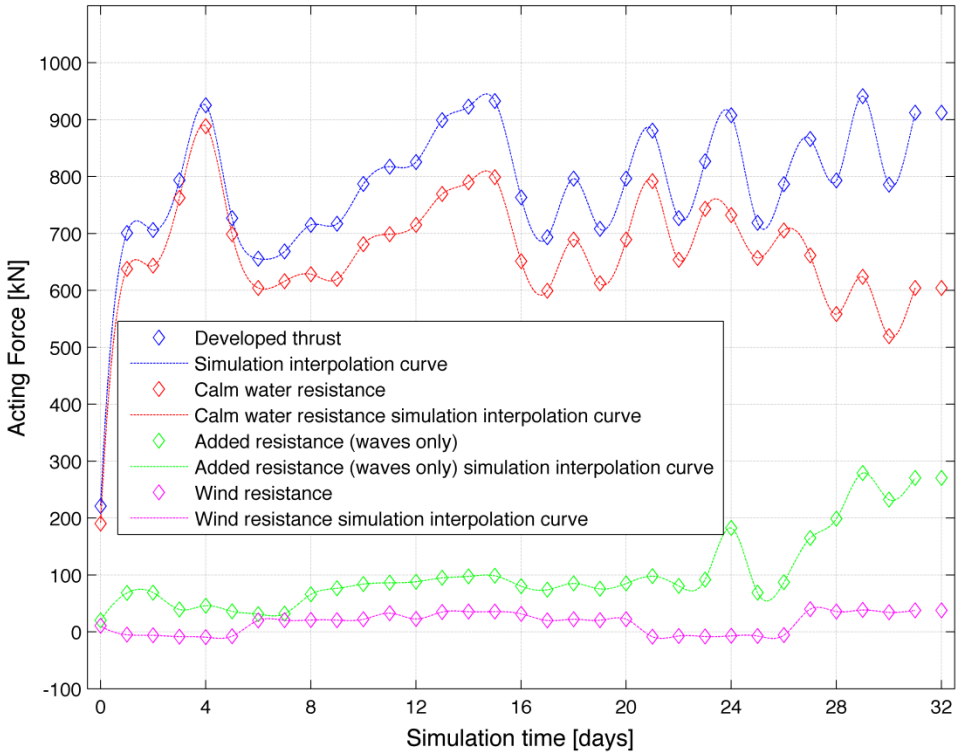


**Figure 6.2: Resistance breakdown for a 32 laden voyage of the examined Post-Panamax vessel**

The daily fuel consumption is calculated by applying corrections due to the air temperature, sea temperature and lower fuel calorific value, as described in Chapter 4. Figure 6.3 illustrates the simulated fuel consumption versus the 'as measured' one. However, in order to explain the differences, Figure 6.4 and Figure 6.5 are introduced. Based on the propeller performance graph, there is a significant power increase when the propeller efficiency drops. The propeller efficiency drop is relevant to the thrust increase in order to keep the vessel speed at the desired level. As a result, it is obvious that the engine power depends on the required thrust, thus torque and the propeller efficiency. Hence, the consumption is approximated given these parameters. In Figure 6.3, the reported fuel oil consumption per day remains almost the same. It can be seen, however, by the simulation results that there are significant engine load variations that overestimate or underestimate the corrected consumption. The uncertainty on the speed and consumption measurements in the reports and during on-board energy audits was discussed in the propulsion committee of the ITTC in 2002.

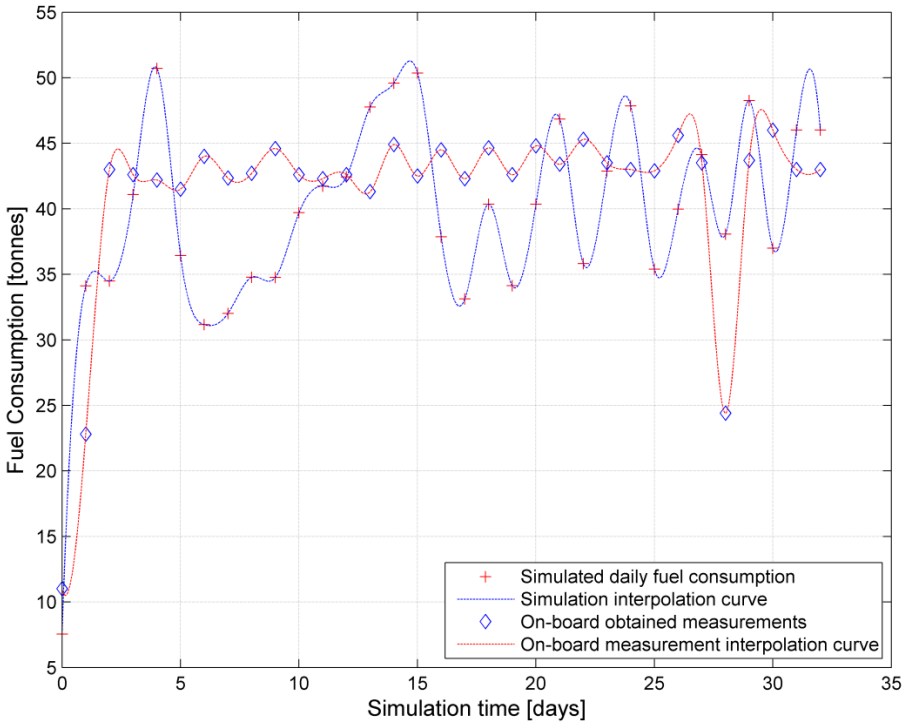


**Figure 6.3: Simulated versus 'as measured' fuel consumption for a 32 laden voyage of the examined Post Panamax vessel**

Based on this sample, it can be concluded that, although the total simulated consumption is underestimated by 56.35 tonnes or 4.14% of the total fuel bill, the daily differences have significant dissimilarities. In order to identify further differences between the simulator estimations and the 'as measured' fuel consumption, five more voyages have been included in the calculation. The results corresponding to the already presented voyage are summarised in Table 6.2. The negative sign denotes that there is an underestimation of the fuel consumption.

**Table 6.2: Simulated versus the 'as measured' fuel consumption for all vessels and voyages**

| | Laden Voyage | | | Ballast Voyage | | |
|---|---|---|---|---|---|---|
| | Vessel 1 | Vessel 2 | Vessel 3 | Vessel 1 | Vessel 2 | Vessel 3 |
| Simulated Fuel consumption | 616.11 | 614.07 | 1302.70t | 978.45t | 276.75t | 390.22t<br>498.66t |
| Measured fuel consumption | 653.40 | 642.20 | 1359.10t | 1206.80t | 354.60t | 438.20t<br>594.40t |
| Fuel difference | -37.29 | -28.13 | -56.35t | -228.35 | -77.85t | -47.98t<br>-95.74t |
| Percentage difference | -5.71% | -4.38% | -4.14% | -18.92% | -21.95% | -10.95%<br>-16.11% |

It is observed that extreme differences in the prediction of fuel consumption exist while the examined vessels operate in ballast condition. The main reason for this difference is the ballast draft calm water resistance, the sailing draft differs to that of the model test data. For this reason, the Hollenbach and the Holtrop-Mennen methods are applied, using the direct approximation of the ballast draft and hull coefficients from the vessel loading conditions as presented on the vessel loading manual. With the calculation of the resistance curve for the heavy ballast condition, the simulated fuel consumption can be recalculated.

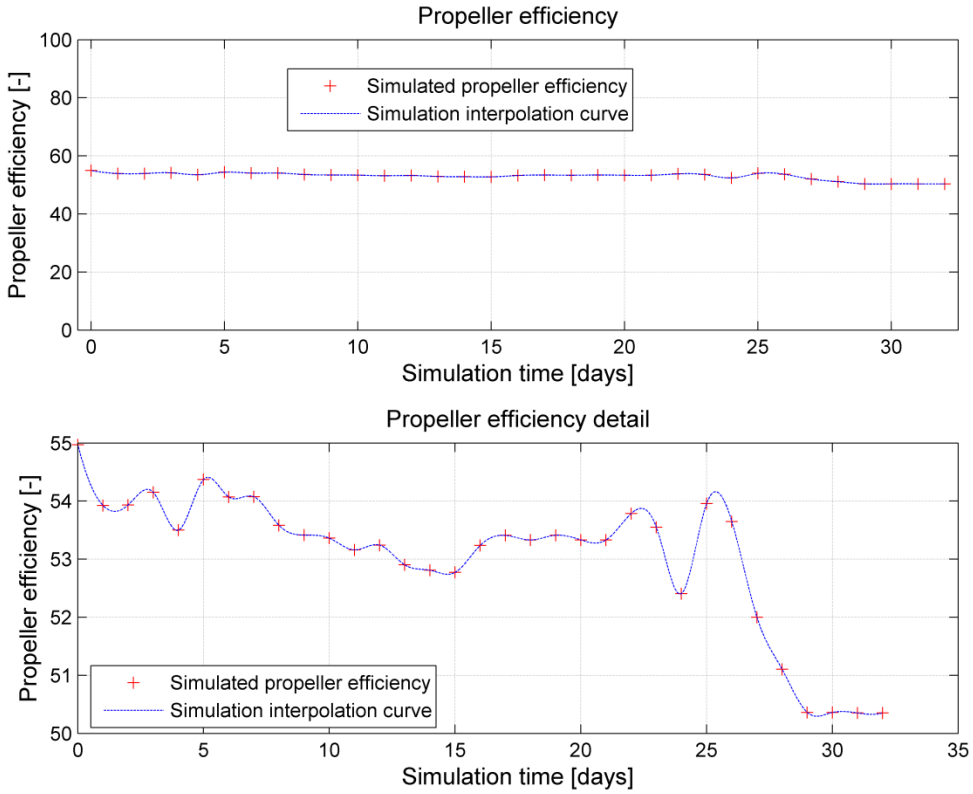


**Figure 6.4: Simulated propeller efficiency for a 32 day voyage of the examined vessel**

Firstly, the resistance method of Hollenbach was applied to the simulation. Nevertheless, it was observed that this method significantly overestimates the total resistance in ballast draft. The method resulted in lower heavy ballast resistance than the normal ballast condition, which has a smaller draft and smaller wetted surface area. In order to avoid this problem, the Holtrop-Mennen method was employed, and the comparison of resistance between the model test resistance in design draft and of the model test resistance in normal ballast is found in Figure 6.6. The power requirements before filtering the overload points are presented in Figure 6.7.

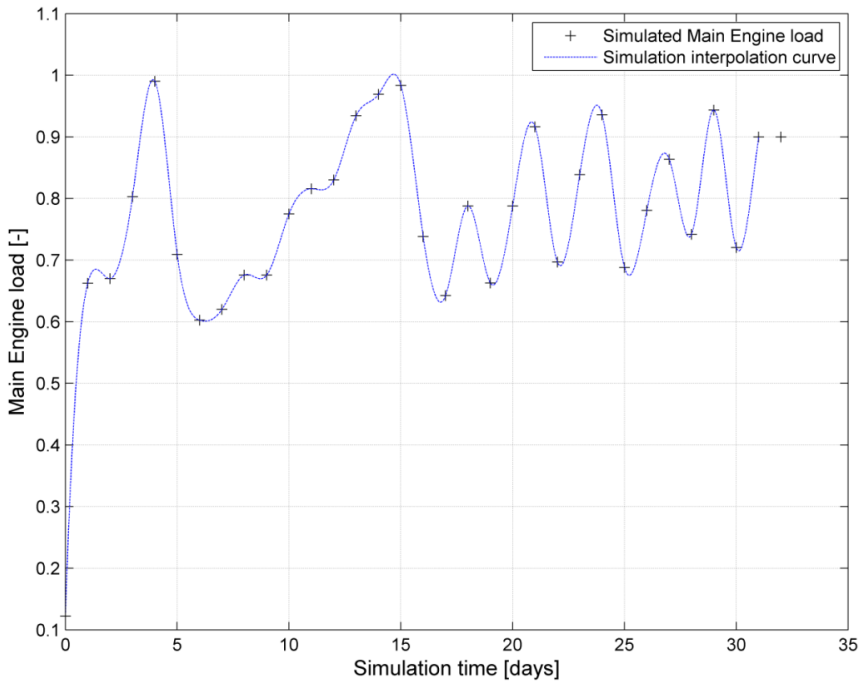


**Figure 6.5: Simulated main engine loading for a 32 day voyage of the examined vessel**

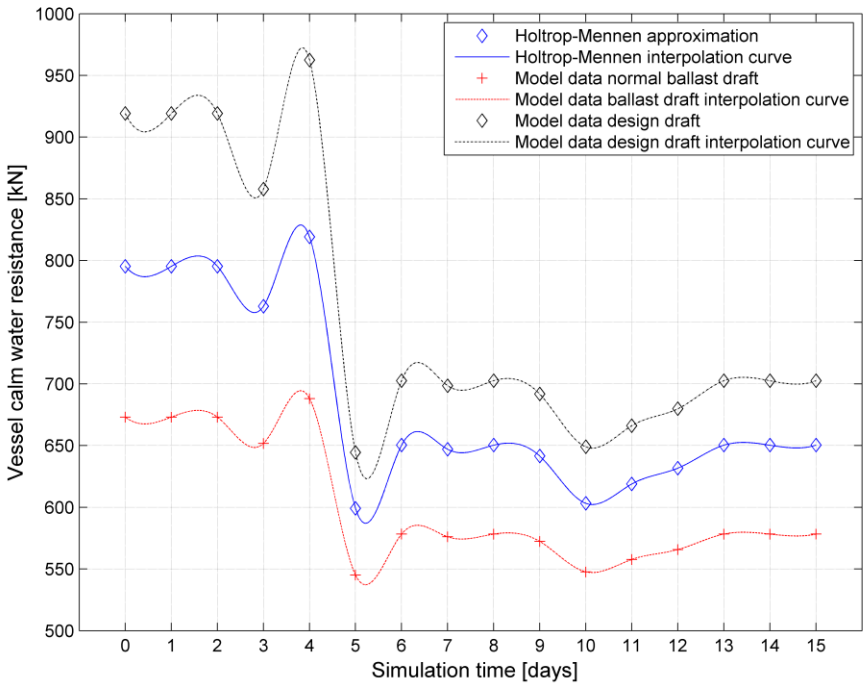


**Figure 6.6: Comparison of resistance curves for design laden condition, approximated by Holtrop-Mennen heavy ballast condition, and normal ballast condition for a 16 day voyage**

It can be surmised from this figure that the Holtrop-Mennen curve is as expected between the resistance curve for design laden draft and the normal ballast draft. The

results can be justified by the fact that the vessel sails with average draft of 8.64m ($T_F$=7.29m and $T_A$=9.99m), which is higher than the 6.140m ($T_F$=4.820 m and $T_A$=7.460 m) and lower that the 12.2m of design draft (even keel). Due to the inexistence of daily draft and trim data, no correction for the arrival condition was performed to the calculations, something that implies a small error in the final values. Thus, by applying the Holtrop-Mennen resistance approximation for the ballast voyages, Table 6.2 is updated by Table 6.3.

It can be concluded from the results presented in Table 6.3 that the error in the approximation of the fuel oil consumption is significantly reduced. In order to assess the ship simulator feasibility in global emission estimation, a comparison of the simulated fuel consumption versus the estimation by IMO, given the reported and corrected for underwater currents vessel speed, is performed. The results of the IMO formula presented in Chapter 2, which calculates the global shipping emissions, will be weighed against the calculation of emissions by the constructed ship simulator results. The outcome of this comparison will measure the implied error of the two bottom-up approaches, thus the method with the lowest deviation from the real consumption data will determine the global shipping air pollution more accurately.

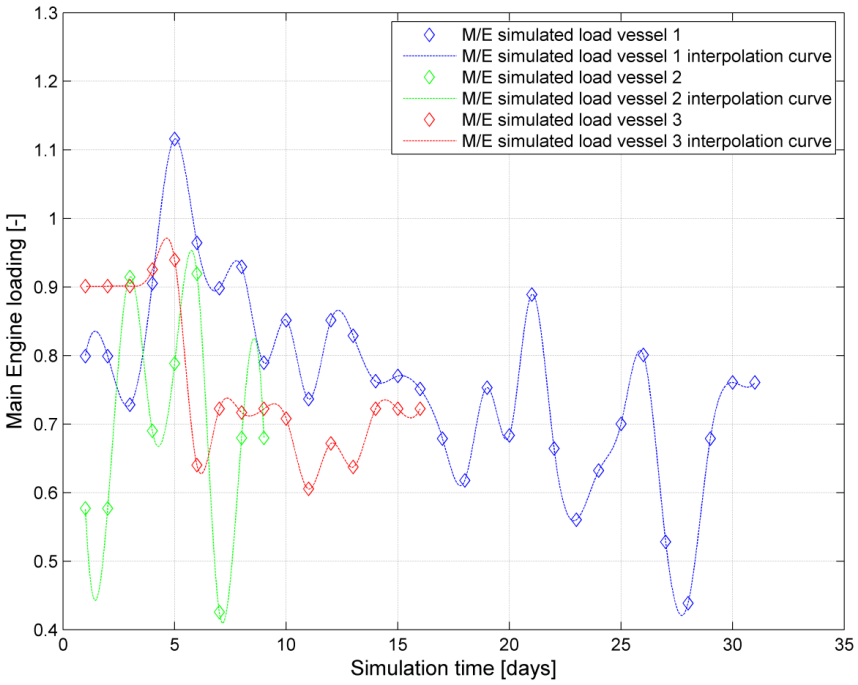


**Figure 6.7: Simulated M/E loads in re-analysed ballast voyages**

Corbett and Koehler (2003) propose in their work to utilise the SFOC curve of the engine instead of the average specific fuel oil consumption value at the NCR. Since this method is more accurate than the original of the IMO, the comparison of the consumptions will be

based on the simulated engine loading and the approximated engine loading. To estimate the fuel consumption, each loading will be multiplied by the corrected SFOC and by the engine MCR times the operational time. Given that an average fuel emission factor is used, there will be no presentation of $CO_2$ emissions, as the latter can be approximated easily, as described in chapter 2. Thus, for the ballast voyage of vessel 1, the simulation reanalysis showed that the simulator underestimated the total fuel oil consumption by 3.93%.

**Table 6.3: Re-analysis of the ballast voyage fuel consumptions**

| | Ballast voyage | | | Re-analysis of ballast voyage | | |
|---|---|---|---|---|---|---|
| | Vessel 1 | Vessel 2 | Vessel 3 | Vessel 1 | Vessel 2 | Vessel 3 |
| Simulated Fuel consumption | 978.45t | 276.75t | 390.22t<br>498.66t | 1159.28t | 307.43t | 461.50t<br>600.44t |
| Measured fuel consumption | 1206.80t | 354.60t | 438.20t<br>594.40t | 1206.80t | 354.60t | 438.20t<br>594.40t |
| Fuel difference | -228.35 | -77.85t | -47.98t<br>-95.74t | -47.52 | -47.17 | 23.30t<br>6.04t |
| Percentage difference | -18.92% | -21.95% | -10.95%<br>-16.11% | -3.93% | -13.30% | 5.32%<br>1.02% |

By applying the approximation of engine loading given the only the corrected vessel speed, the IMO formula resulted in overestimation of the fuel consumption by 8.59%. For the first ballast voyage of vessel 3, the implied error by the IMO formula is 8.63% (overestimation), while the implied error by the ship simulator is 5.32% (overestimation). It can be extracted by the comparison that both approaches introduce uncertainty to the calculation but the total error is lower than the top down approach. Moreover, the ship simulator proved to determine with more accuracy the actual consumed fuel by applying a day-to-day energy approach.

### 6.1.2 Voyage simulation using 2h time step

In this section, the results of the demonstration test case which was presented in sections 4.4 and 5.3 are given. The selected voyage is a 31 day ballast voyage. Because only the daily mean environmental parameters were known, the weather generation model is applied. For the purposes of the simulation, there is no voluntarily speed loss due to bad weather and the speed remains constant as per the performance report. In cases where the engine loading exceeds 100%, the result is filtered and neglected, as there is no physical meaning to this value, since the master always reduces speed to avoid engine overloading and excessive ship motions. The simulated engine loading is presented in Figure 6.8 and the speed setting versus the significant wave height is presented in Figure 6.9.

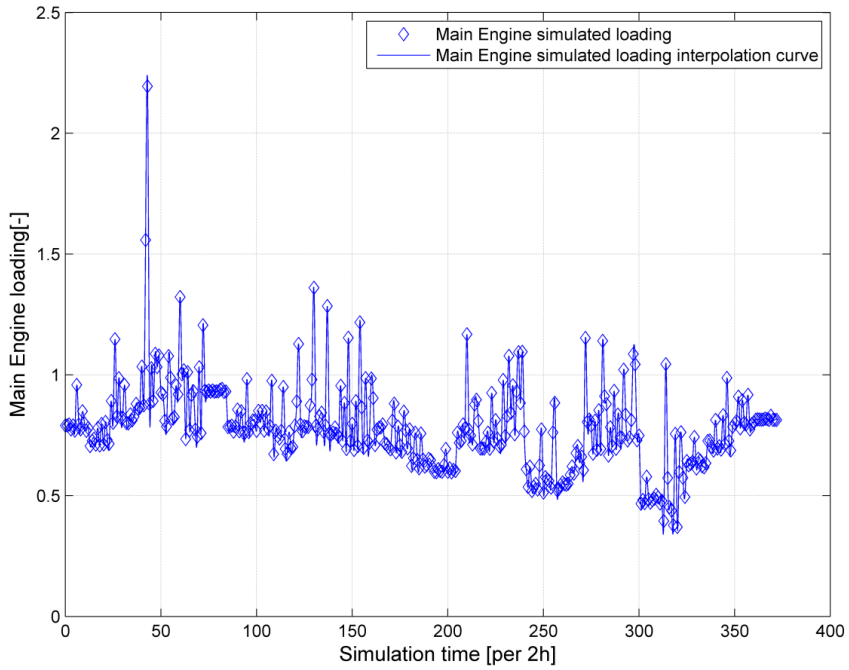


Figure 6.8: Simulated Main Engine loading using 2h weather generation model

Based on the graph depicted in Figure 6.8, it can be said that the engine is overloaded in 25 samples over the generated 373, a fact that supports the initial assumption that the vessel does not alter its speed when sea state increases during each voyage day.

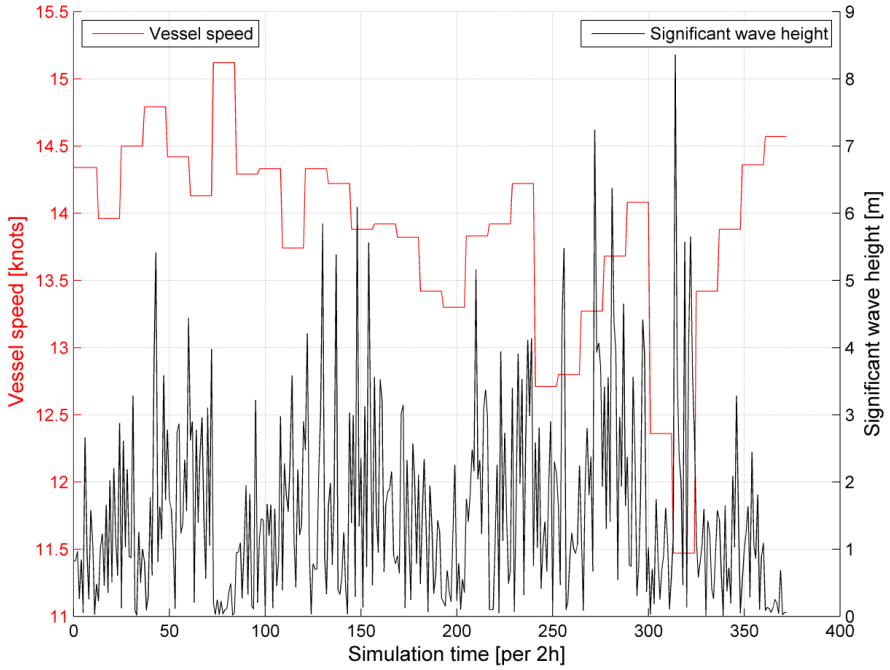


Figure 6.9: Vessel speed and significant wave height correlation applying 2h weather generation model

Concerning the first peak of engine loading around the 45th two-hour segment, the vessel speed is not reduced when the vessel faces waves with a significant wave height value around 5.2 m. Nevertheless, in the extreme weather around the 320th sample, the master reduces the speed and the outcome on the engine loading is obvious in Figure 6.8. In order to finalise the picture on the effect of environmental parameters, the direction of waves is presented in Figure 6.10. This figure demonstrates why the effect of waves is greater in the peak engine loads. This is explained by the fact that head waves dramatically increase the propulsive power for constant speed, while the abeam or astern waves aid the surge forward movement, reducing the total propulsive power. Taking into account the aforementioned information, the simulator is expected to overestimate the total fuel consumption due to the discussed engine overloading. Consequently, the simulated fuel oil consumption equals to 1240.1 tonnes meaning, 33 tonnes more consumed fuel or 2.75% implied error with this working procedure.

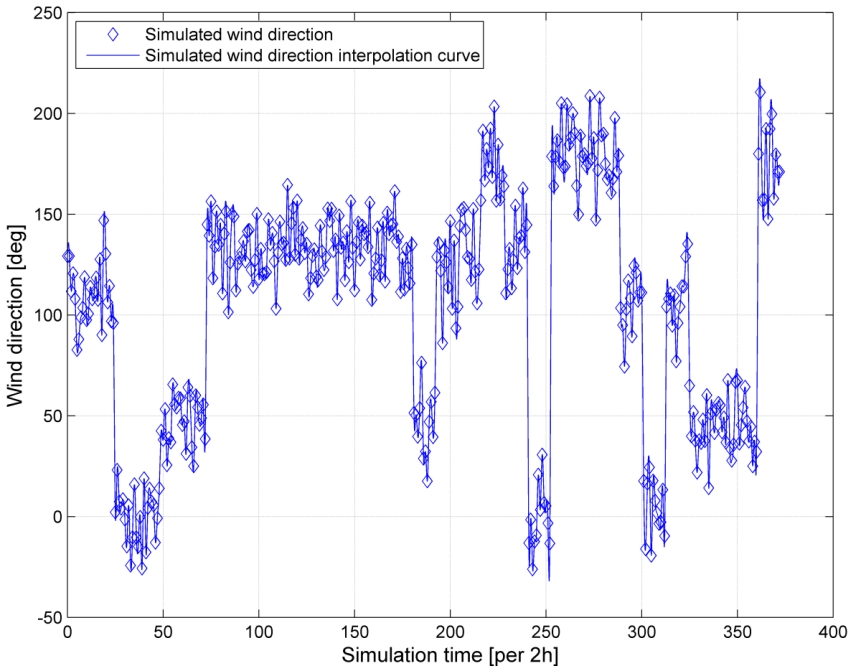


Figure 6.10: Simulated Wind direction using 2h weather generation model

This error will potentially decrease with better tuning of the simulator, by supplying a model to alter the speed based on the simulated significant wave height. Nonetheless, the approximation of fuel consumption yields to a very small deviation from the actual fuel consumption and the results are closer than the IMO study method.

## 6.2 Optimisation of propulsive and auxiliary machinery

This section includes the optimisation scenario results for the investigated Diesel Hybrid topologies, which were presented in Chapter 3 and mathematically represented in Chapter 4. This section includes runs for down-scaled and up-scaled prime movers, so as to assess the aid or not of the Hybrid system to the indirect fuel savings that differently optimised prime movers can contribute.

### 6.2.1 Prime movers operating at normal running conditions

So that to assess the effect of Hybrid power layouts in propulsion and or auxiliary loads, representative power demand vectors should be inserted into the optimisation algorithm. For the propulsion demand and based on the simulation of every sampled voyage, Figure 6.11 is introduced. It can be observed from this figure that the majority of the simulated average power requirement drops between 7000 – 9000kW and less in the range of 9000 – 11000kW. Thus, it can be assumed, that if two representative vectors in these two ranges are fed to the optimisation algorithm, a general conclusion can be extracted. Consequently, a daily power demand with two hour segments will be acquired from the Ship voyage simulator. The selected voyage is the 31 day ballast voyage which was presented in Section 6.1. The minimum simulated power is 7471kW and the maximum 9459kW; hence the power vector is a good representation of the power scatter.

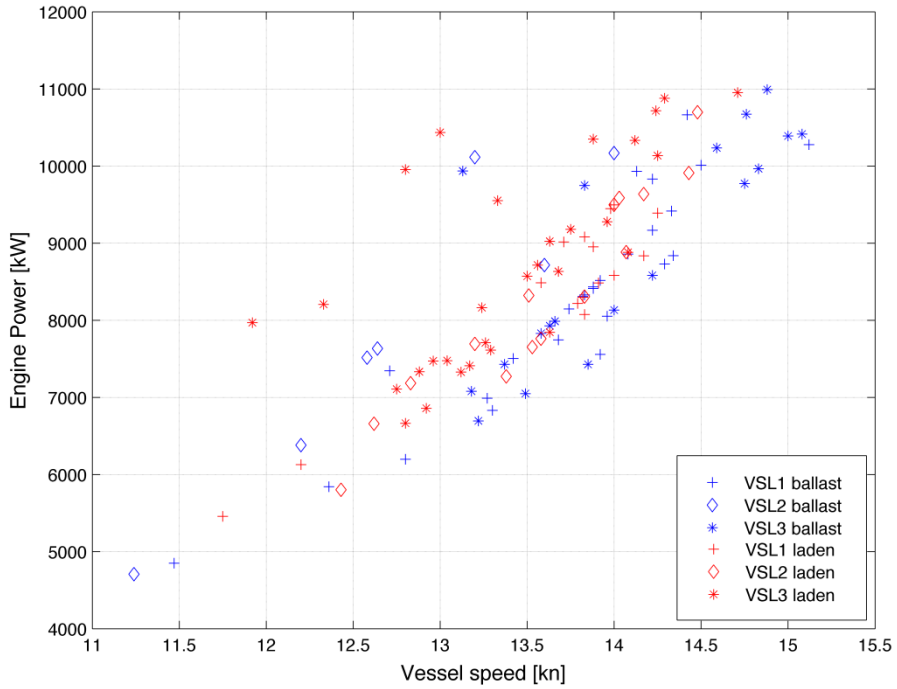


Figure 6.11: Propulsive power versus speed for laden and ballast voyages

Regarding the auxiliary power demand, the actual loading profile was acquired by on-board measurements during sea passage of a sister ship in the same condition as the demonstration vessel. The sampling rate of the data loggers was set to 40 seconds and the loggers were connected to a portable computer. Two representative days of this auxiliary demand are depicted in Figure 6.12.

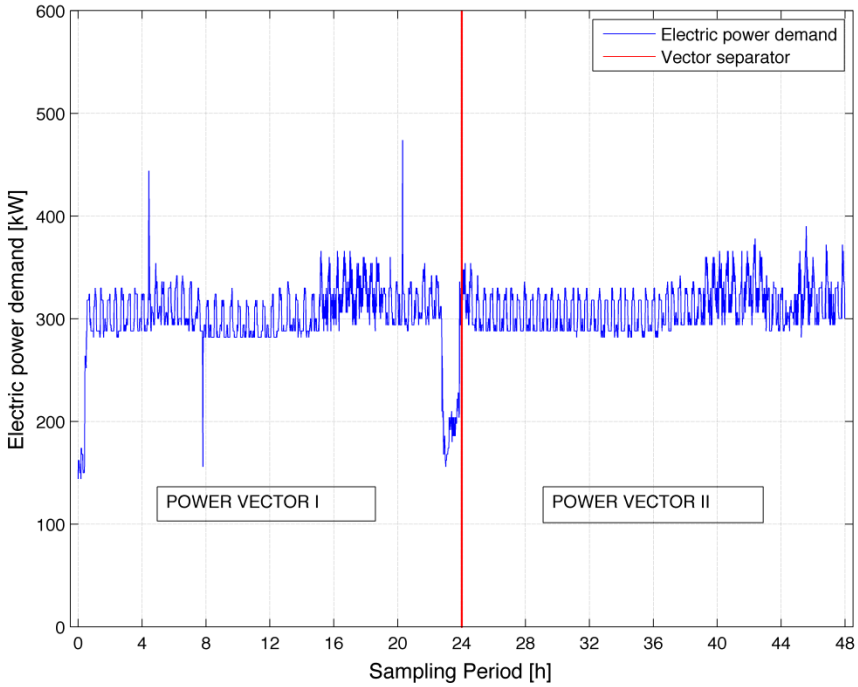


Figure 6.12: Auxiliary Power demand for 48 hours

#### *6.2.1.1 Layout D-A1*

The vessels are equipped with three Diesel generators which provide 600kW electrical output each. At sea operation, only one generator is running, however, for energy demanding situations, a second one is on stand-by so the power is split manually approximately at half of the load. This operation is done mainly for safety reasons and not because of lack of power output. The Hybrid system is initially set up for a case where the battery system can provide energy without charging for at least 24 hours. The installed capacity is set up initially at 14.4MWh, which is the maximum energy that can be supplied by an auxiliary generator on the examined ship during each day. Thus, by applying the optimisation at the power vector I of the loading profile of Figure 6.12, the following Figure 6.13 presenting the power split is introduced.

Based on the results, it was found that the daily consumption difference was in favour of the Hybrid system and the consumption was 1.62 tonnes of HFO in ISO conditions or 5.81% less fuel than the conventional system (Conventional system: 1.72 tonnes of fuel/day in ISO).

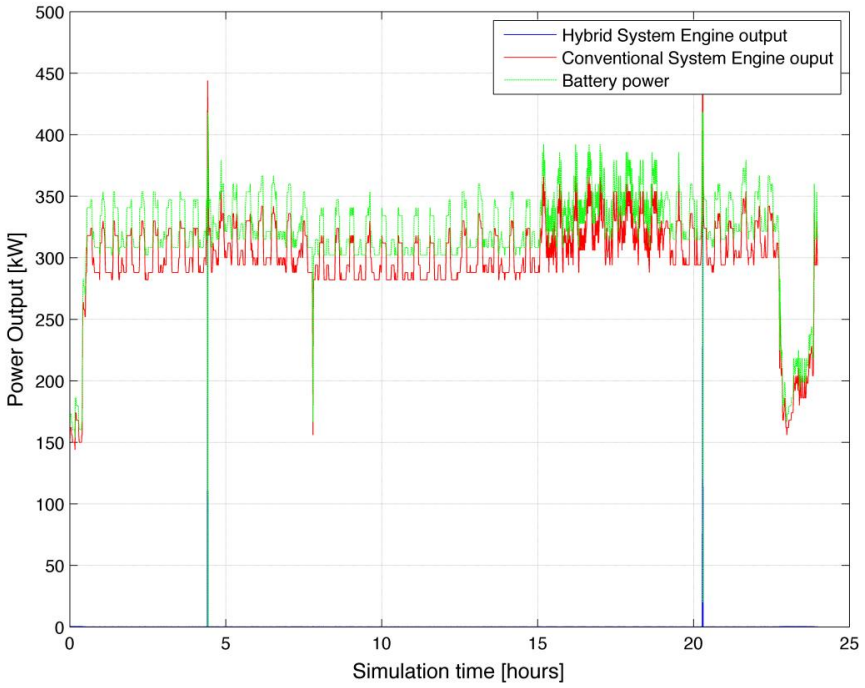


**Figure 6.13: Power split between Auxiliary Engines and batteries of energy capacity of 14.4MWh and comparison with the conventional system**

However, as it is observed from the power demand figure, the maximum instantaneous peak load was 450kW, hence the daily demand is around 10MWh. In addition due to the extreme amount of installed energy in batteries and restrictions in carrying capacity of the vessel, a scenario with the same demand profile was performed, but with reduced energy capacity in the battery. A 10 – 15% of the capacity of the generator can be considered sufficient for load levelling purposes. Thus, the second run involves capacity equal to 2MWh. The power split for this scenario is depicted in Figure 6.14

It was found that the consumption of the hybrid system was lower than the conventional, but the savings are almost negligible (0.0083 tonnes less fuel or 0.48% savings). Figure 6.14 depicts the power split between the battery and the auxiliary engine. It can be surmised from Figure 6.14 that, for specific loads, the usage of the hybrid system is not cost effective. Because of this finding, the engines are switching on and off and the power split is performed either by the battery only or by the auxiliary engine only. In addition, the observed non-stable power split is explained by the pairing of the Auxiliary engine, the reduced size of the battery bank and the implementation of the logic optimisation criteria. Consequently, the regular switch from idle to ~50% load of each generator engine is a product of the fast depletion of the battery bank and the existence of non-favourable charging conditions which do not meet the rule based optimisation criteria (the cycling over batteries after 16$^{th}$ hour reaches 0%). Because the rule set for charging

cannot escape from the loop of no charging solution, the logic has been altered. Furthermore, more battery capacities have been investigated. The results indicate that the saving percentage is improved and the battery is charged by the 16th hour and onwards with increased rate as the $t_{sim}$ approaches the $t_{ref}$, due to the existence of lambda coefficient.

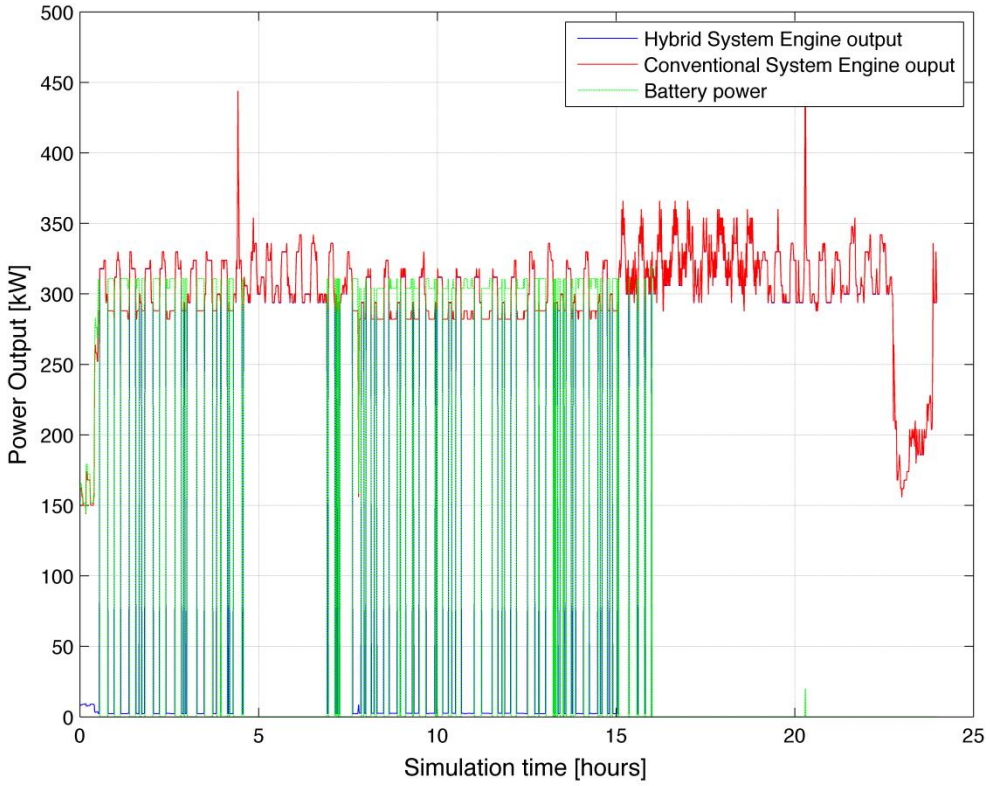


**Figure 6.14: Power split between Auxiliary Engines and batteries of energy capacity 2MWh and comparison with the conventional system**

Three more battery capacities are investigated which are presented in Table 6.4 along with the fuel saving percentage. The capacity of the 7MWh corresponds approximately to a power equivalent of ~300kW for 24 hours, the 10MWh for ~450kW and the 4MWh is a 30% storage capacity of the maximum required energy per day.

**Table 6.4: Effect of logic and installed capacity on the amount of fuel savings**

| Battery installed capacity [MWh] | Auxiliary fuel savings with logic improvements [-] |
|---|---|
| 2 | 0.84% from 0.48% |
| 4 | 2.64% |
| 7 | 4.38% |
| 10 | 5.57% |
| 14.4 | 6.19% from 5.81% |

The saving percentage follows a quadratic curve (shown in Table 6.1) which curves downwards and remains almost flat when the battery capacity reaches 14.4 MWh. The reason for the convex form is that when the installed energy exceeds the daily requirement, the effect of the larger battery bank only reduces the discharging/ charging current per battery string which is already ultra-low, thus the effect is negligible over a 24h examined period.

It can be observed from Table 6.4 that the rule based optimisation is affected by the set applied logic criteria for charging. In addition, it is stated in Dedes et al. (2012a) that the time step is of crucial importance on the feasibility of the Hybrid power system. Given these parameters and taking into account that in layout D-C, the propulsion vector has 2h sample rate, the auxiliary load power demand is transformed to a 2h mean vector. The process involves the sampling of 180000 40sec values and exports a smaller set of data which correspond to 2 hour mean power demands. Hence, the charging parameters are altered. The reference time is reduced from 72h to 48h and 24h respectively. The reference time affects the lambda coefficient, thus the charging percentage and the charging logic. For all the cases, the logic improvements which were explained before apply. The following Table 6.5 presents these effects on a 24h power vector.

**Table 6.5: Effect of $t_{ref}$ and sampling time in savings percentage for 24h sample**

| Case Capacity | 24h vector, 2h sample rate, $t_{ref}$ = 72h | 24h vector, 2h sample rate, $t_{ref}$ = 48h | 24h vector, 2h sample rate, $t_{ref}$ = 24h |
|---|---|---|---|
| 2MWh | 0.53% | 0.52% | 0.45% |
| 4MWh | 2.62% | 2.94% | -0.60% |
| 7MWh | 4.88% | 4.91% | 1.90% |
| 10MWh | 5.52% | 5.52% | 5.52% |
| 14.4MWh | 5.70% | 5.70% | 5.70% |

It can be observed from Table 6.5 that the 2h mean power vector underestimates the savings in cases where the charging effect is of vital importance. The main reason is that given the power demand, the battery SoC may not be sufficient to cover the power for this specific time, but be available for a shorter time, thus the simulation constraints which have to be satisfied during the time step, reject the optimum solution which is to absorb power from the battery bank. In cases were the simulation step is smaller, the decisions of the optimisation algorithm have a lower influence on the drain/ charge rate of the battery system, yielding to a more global optimised solution, as non-favourable conditions are present for a shorter time than before and vice versa. Yet, the time division should be made in accordance with the principle assumption that the system is operating in quasi-steady conditions.

The reference time and the initial state of charge also alter significantly the savings percentage as the lambda coefficient (described in equation 4.10.1) is increased

and the logic criteria imply more charging energy at the same optimisation step when comparing the 24h with the 72h reference time columns. Nonetheless, there is no effect of reference time in cases where there is no battery depletion e.g. 10MWh or 14.4MWh. Thus, it can be concluded that the criteria satisfaction of rule based optimisation may not lead always to the global optimum solution.

Finally, in order to investigate the effect of the Hybrid system in auxiliary fuel savings, a 48h sample was also investigated for 48 and 72h reference time cases. The 48 hour auxiliary demand vector is now consisted of power vectors I and II of Figure 6.12.

**Table 6.6: Effect of $t_{ref}$ and sampling time in savings percentage for 48h sample**

| Case Capacity | 48h vector, 2h sample rate, $t_{ref}$ = 48h | 48h vector, 2h sample rate, $t_{ref}$ = 72h |
|---|---|---|
| 2MWh | 0.74% | 0.72% |
| 4MWh | -0.26% | 2.01% |
| 7MWh | -0.15% | 3.31% |
| 10MWh | 2.32% | 2.62% |
| 14.4MWh | 5.08% | 5.45% |

It can be observed from Table 6.6 that the effect of logic in charging condition again affects significantly the fuel savings especially in cases where the charging power is high and yields to higher fuel consumption than the conventional system. In cases where the fuel savings are in favour of the Hybrid system and notable lower than the conventional system, their percentage is decreased by the logic imposed charging (e.g. in 10MWh 2.62% becomes 2.32%).

#### *6.2.1.2 Layout D-B*

The optimisation runs were made for the three SFOC curves (normal optimised, full load optimised and part load optimised engines described in Figure 3.9). The battery bank energy capacity is set to 8MWh, which is a product of statistical analysis of the hybrid power demand on the subject vessel type. Given the conversion losses presented in Table 3.2, the hybrid system is not feasible in comparison with the operation of the conventional machinery. As a result, sensitivity analysis on the effect of component efficiencies to the degree of hybridisation is performed and is presented in Section 6.2.2.

#### *6.2.1.3 Layout D-C*

For the assessment of layout D-C, and in order to compare the potential findings with layout D-B, the following optimisation scenario was implemented. The propulsion demand is already presented in the beginning of the section. For crosschecking purposes only, the auxiliary loads are decoupled from the calculation and it is assumed that they are covered

by one of the three auxiliary generators. The efficiencies of Hybrid components are described in Table 3.2. The battery energy capacity is set to 8MWh and the MCR of the PTO/PTI system equals 600kW. The Main Engine is optimised for part load operation.

Table 6.7 presents the power split of the propulsion and auxiliary components for layout D-C. The results indicate that, due to conversion losses, the battery system remains idle. Nonetheless, the existence of the PTO/PTI system contributes to fuel savings, which, for the given propulsion demand vector, amount to 7.23% of the fuel bill. The equivalent fuel savings do not take into account the potential savings due to the part load optimisation when compared to the normal optimisation.

**Table 6.7: Power Split for layout D-C system for propulsive load demand**

| Simulation time [h] | Battery Output [kW] | M/E load [-] | A/E 1 load [-] | A/E 2 load [-] | A/E 3 load [-] |
|---|---|---|---|---|---|
| 1 | 0 | 82.30% | 100% | 0 | 0 |
| 2 | 0 | 66.49% | 100% | 0 | 0 |
| 3 | 0 | 69.87% | 100% | 0 | 0 |
| 4 | 0 | 81.64% | 100% | 0 | 0 |
| 5 | 0 | 69.02% | 100% | 0 | 0 |
| 6 | 0 | 65.44% | 100% | 0 | 0 |
| 7 | 0 | 81.48% | 100% | 0 | 0 |
| 8 | 0 | 69.16% | 100% | 0 | 0 |
| 9 | 0 | 66.11% | 100% | 0 | 0 |
| 10 | 0 | 66.84% | 100% | 0 | 0 |
| 11 | 0 | 69.60% | 100% | 0 | 0 |
| 12 | 0 | 69.02% | 100% | 0 | 0 |

The operating principle of Hybrid layout D-C is depicted in Figure 6.15. The total fuel bill is the multiplication of SFOC and the total kW. For this scenario, equations (6.2.1) and (6.2.2) explain the optimisation algorithm solution.

$$SFOC_{M/E} \cdot P_{M/E} + SFOC_{A/E} \cdot P_{A/E} \leq SFOC'_{M/E} \cdot P'_{M/E} \tag{6.2.1}$$

The following constraint applies for the power split:

$$P'_{M/E} = P_{M/E} + P_{A/E} \tag{6.2.2}$$

The SFOC is load dependent, thus, if the engine operates at a less efficient point, the total amount of kW is produced inefficiently. Using the PTO system, the extra kW are produced in a far more inefficient way, although the remaining kW are produced in a more efficient way, leading to fuel consumption savings and not to power savings. The difference of SFOC is clear if Figure 3.8 and Figure 3.9 are compared for given loads. For the examined case, the conventional system fuel consumption is 67.26 tonnes in ISO conditions, while for the proposed layout D-C Hybrid system; fuel consumption for propulsion is 62.40 tonnes in ISO (total difference of 4.86 tonnes HFO). Figure 6.15 explains that in cases where the ship

is required to maintain a predefined speed constant, the RPM of the propeller need to increase in order to match the total resistance with the produced thrust (accounting the wake friction and thrust deduction factors).

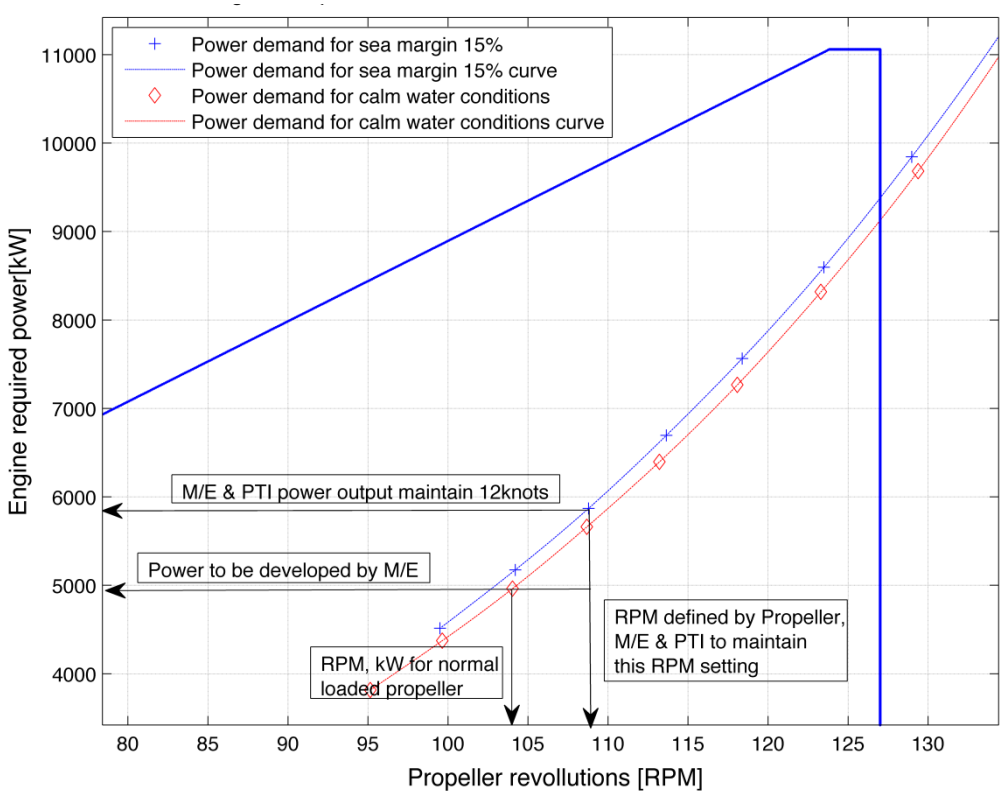


Figure 6.15: Operating principle of D-C Hybrid power layout

However, instead the engine to increase load, M/E will operate in constant power mode and the difference is covered by the PTO/PTI system. Nonetheless, in an ideal solution, the best fuel consumption would be achieved if the M/E working point would be at the fuel optimisation point set up by the engine manufacturer.

In continuation of the layout D-C assessment, auxiliary loads of Figure 6.12 transformed in 2hour mean segments are inserted to the optimisation algorithm. The system leads to fuel savings of 7.23% for the propulsive loads and 5.38% for the auxiliary loads. During this operation, the system is absorbing an amount of energy from the batteries for the cover of auxiliary demand. Nevertheless, because the principle of optimisation does not take into account the overall simulation picture, it identifies the best solution of a specific time step (Guzzella and Sciarretta, 2005), ignoring a different voyage minimum that could be found using Dynamic Programming. The power split and the battery DoD for this scenario are given in Table 6.8. It should be noted that the DoD of the battery at the initial time step is of great importance to the amount of fuel savings. The charging criteria may lead the optimisation algorithm to non-optimum solutions when

compared to the baseline system, but to lead to best fit to purpose solutions in terms of criteria satisfaction.

**Table 6.8: Power Split for layout D-C system for propulsive load and auxiliary demand**

| Simulation time [h] | Battery Output [kW] | M/E load [-] | A/E 1 load [-] | A/E 2 load [-] | A/E 3 load [-] | Battery DoD [%] |
|---|---|---|---|---|---|---|
| 1 | 306.73 | 82.30% | 100% | 0 | 0 | 7.67% |
| 2 | 330.05 | 66.49% | 100% | 0 | 0 | 15.92% |
| 3 | 314.61 | 69.87% | 100% | 0 | 0 | 23.78% |
| 4 | 324.95 | 81.64% | 100% | 0 | 0 | 31.91% |
| 5 | 345.30 | 69.02% | 100% | 0 | 0 | 40.54% |
| 6 | 299.37 | 65.44% | 100% | 0 | 0 | 48.03% |
| 7 | 329.15 | 81.48% | 100% | 0 | 0 | 56.25% |
| 8 | 324.19 | 69.16% | 100% | 0 | 0 | 64.36% |
| 9 | 322.77 | 66.11% | 100% | 0 | 0 | 72.43% |
| 10 | 334.12 | 66.84% | 100% | 0 | 0 | 80.78% |
| 11 | 344.99 | 69.60% | 100% | 0 | 0 | 89.41% |
| 12 | 338.70 | 69.02% | 100% | 0 | 0 | 97.87% |

### 6.2.2 Sensitivity analysis for D-A1 and D-B layouts

This section investigates the effect of the Hybrid components efficiencies at the feasibility or not of the Hybrid solution. In addition, in cases where the Hybrid layout is feasible when using the efficiencies presented in Table 3.2, a battery deterioration model will be inserted in the calculation, so as to identify the edge of operational success. Finally, for the cases where the highest saving percentages have been observed, deterioration with sensitivity analysis is performed.

#### *6.2.2.1 Layout D-A1*

Based on the results of section 6.2.1, the D-A1 Hybrid power layout demonstrates the best potential in terms of fuel savings. Nevertheless, it is probable that during the life time of a ship, the batteries may exceed the maximum number of cycles and start to deteriorate. For this scenario, a linear battery system degradation model is applied to the scenarios presented in 6.2.1. Table 6.9 and Table 6.10 show the effect of battery degradation for examined battery capacities and for a particular charging logic. It is observed that the charging logic again affects the feasibility of the system. Nonetheless, it can be extracted that a 1% difference in battery efficiency decreases by approximately 10-40% the amount of fuel savings. Hence the system is very sensitive to the battery behaviour.

Table 6.9: Fuel savings with battery degradation model for 48h sample with $T_{ref}$ = 48h

| Battery Degradation | Battery capacity | | | | |
|---|---|---|---|---|---|
| | 2MWh | 4MWh | 7MWh | 10MWh | 14.4MWh |
| Baseline | 0.74% | - | - | 2.32% | 5.45% |
| 1% | 0.42% | - | - | - | 3.70% |
| 2% | 0.29% | - | - | - | 0.41% |
| 3% | 0.22% | 0.30% | 0.34% | 0.38% | 0.45% |
| 4% | 0.14% | 0.19% | 0.21% | 0.21% | 0.22% |
| 5% | - | 0.12% | 0.14% | 0.14% | 0.15% |
| 10% | - | - | - | - | - |

A more clear view of the effect in battery deterioration is given in Table 6.10 where the effect of charging logic is reduced. The dash symbol represents no gain in efficiency.

Table 6.10: Fuel savings with battery degradation model for 24h sample with $T_{ref}$ = 72h

| Battery Degradation | Battery capacity | | | | |
|---|---|---|---|---|---|
| | 2MWh | 4MWh | 7MWh | 10MWh | 14.4MWh |
| Baseline | 0.52% | 2.63% | 4.88% | 5.52% | 5.70% |
| 1% | 0.19% | 1.66% | 2.98% | 3.59% | 3.79% |
| 2% | - | 0.77% | 1.34% | 1.61% | 1.81% |
| 3% | - | 0.23% | 0.28% | 0.25% | 0.30% |
| 4% | - | - | - | - | - |
| 5% | - | - | - | - | - |
| 10% | - | - | - | - | - |

It can be concluded that the system in case of degradation of batteries will work at the edge of feasibility. Consequently, a detailed investigation on the number of possible charging/ discharging cycles has to be performed. In case that the results indicate that the battery system exceeds the maximum cycles, the financial feasibility assessment should be re-run and a battery replacement cost needs to be inserted in the calculations. Consequently, the financial feasibility model should be reassessed.

Finally, with the intention of identifying the feasibility of the system in cases where the efficiency of specific components at the early concept design phase is overestimated, the following Table 6.11 is introduced.

When operating in all electric mode, as the layout D-A1, the battery converter and transformer are the key efficiency components. The effect of alternator efficiency (generator electric side) is not investigated in the sensitivity analysis, as the auxiliary engines operate at constant RPM and at that small range the electric machine is optimised. Nonetheless, the variation of power load affects the efficiency but due to unavailable data, this area in this thesis is not covered. Thus, only the combined effect of battery converter/ transformer efficiency is investigated.

**Table 6.11: Battery degradation model with marginal subcomponent efficiency**

| Battery Degradation percentage | Final Degradation coefficient | Battery capacity | | |
|---|---|---|---|---|
| | | 2MWh | 10MWh | 14.4MWh |
| 1% | 0.97 | - | 0.26% | 0.32% |
| 2% | 0.96 | - | - | - |
| 3% | 0.95 | - | - | - |
| 4% | 0.94 | - | - | - |

In this table, only the cases that demonstrate non-negligible savings under the scenarios of battery degradation are presented. Nonetheless, the case of 2MWh capacity is also presented, as this is the lowest capacity which offers reduced installation cost and can easily be stored inside the E/R of the vessels. It can be observed from this table, that the degradation coefficient that reduces by 2% the battery converter and transformer efficiency and applies the linear battery degradation model renders infeasible the 2MWh capacity with only 1% assumed battery deterioration. For the rest of the cases, it is remarkable that the fuel savings potential is dropped significantly, making the system financially not viable.

### *6.2.2.2 Layout D-B*

For the layout D-B and given the conversion losses presented in Table 3.15, the hybrid system is not feasible in comparison with the operation of the conventional propulsion machinery. As a result, a sensitivity analysis on the effect of subcomponent efficiencies is presented in Table 6.12 along with scenarios of component improvements in the future. The least efficient components are the propulsion converter, the propulsion transformer and the gearbox/clutch. It is observed from Table 6.12 that the Hybrid layout D-B for every engine configuration (presented in Figure 3.9) is not feasible. In order to investigate potential feasibility in the future, the subcomponent efficiencies have been increased.

**Table 6.12: Sensitivity analysis for D-B Hybrid power layout**

| $\eta_c$ | $\eta_{T/F}$ | | | | $\eta_c$ x $\eta_{T/F}$ | Layout savings | Feasibility check |
|---|---|---|---|---|---|---|---|
| 0.940 | 0.960 | 0.970 | 0.980 | 0.990 | 0.902<br>0.912<br>0.921<br>0.931 | 0 | Non feasible |
| 0.950 | | | | 0.990 | 0.941 | 0 | Non feasible |
| 0.960 | | | | 0.990 | 0.950 | 0 | Non feasible |
| 0.970 | | | | 0.990 | 0.960 | 0 | Non feasible |
| 0.980 | | | | 0.990 | 0.970 | 0 | Non feasible |
| 0.985 | | | | 0.990 | 0.975 | 0 | Non feasible |
| 0.990 | | | | 0.990 | 0.980 | ~ 0 | Feasible, negligible savings |

It can be observed that only when the combined efficiency of converter and motor transformer reaches 98%, feasibility for the D-B layout is observed, given the examined propulsion load vector. For the feasible scenario, for an installed capacity of 8MWh, the daily consumption difference is only 0.1%, while the battery depletion reached 36% per day, validating the discussion on the sizing of the energy storage system, which was set to an autonomy time of 96 hours. Besides the sensitivity analysis of the efficiencies and the feasibility affecting parameters discussed in 6.2.1, it was observed that Electric Machine MCR is an important parameter of the feasibility of the propulsion system. Because of the motor/generator efficiency curve, if the system is absorbing a small amount of energy from the battery system, the electric machine will operate in a very low loading state, resulting in a significant efficiency drop, leading the optimisation suite to drop a potential hybrid solution. In addition, improper sizing of the battery storage system may result in high discharge currents affecting the battery behaviour, which, based on the runs, is regularly around 97%, something that relies on the number of battery parallel units and parallel battery bank connections.

### 6.2.3 Prime movers operating at special running conditions

This section investigates the applicability of the Hybrid power layouts D-A1 and D-B in cases where the prime mover output cannot meet the energy demand, either due to improper design of the power system (cases of large deviation), or due to designer decision to reduce the total installed power output, or due to emergency/ safety reasons, extra power is required. In addition, the Hybrid power system will be assessed for cases where over-sized engines are installed on the ship. This system is investigated under the same conditions as those applied to the properly matched prime mover in section 6.2.1.1. In order to investigate these special running conditions, the following statistical vector which drops into the range of Figure 6.11 will form the input to the optimisation algorithm for the propulsion layout (D-B-M).

$$P_{shaft} = \begin{bmatrix} 11052 & 11052 & 11031 & 9299 & 7998 \\ 8876 & 10090 & 10184 & 7785 & 10335 \end{bmatrix} \quad (6.3.1)$$

Regarding the auxiliary layout (D-A1-M), the power profile of Figure 6.12 will form the input to the optimisation algorithm again.

#### *6.2.3.1 Layout D-A1-M*

The first scenario to investigate is the possibility of an improper engine match with the electric power requirements. As this has a low probability of occurence in modern ship building, this scenario can represent cases that the electric loads are reduced during the sea passage, in normal environmental conditions without ballast operations.

The Yanmar 6N21L engine is replaced by the MAN 6L23/30, which has an electrical output of 730kW (characteristics were presented in Table 3.3). This engine has significantly higher fuel efficiency, as depicted in Figure 3.8. The battery capacity is set to 2MWh which has the lowest effect in fuel savings as seen in Table 6.4 and Table 6.5. Thus it is considered as the baseline configuration. Figure 6.16 illustrates the power split between the up-scaled auxiliary engine and the power output of the batteries. It can be extracted that the battery system is utilised in low generator loads only, and the system remains idle for the 92% of the simulation time.

Consequently, the battery SoC at the final simulation step is maintained at 87.8%. The higher fuel efficiency over a large operational range of the MAN 6L23/30 engine, results in lower hybridisation degree of the system, when compared to the D-A1 scenario. The effect of D-A1 in combination with this prime mover is restricted due to the steepness of the SFOC curve of the up-scaled engine. The SFOC is flatter over a large operational range.

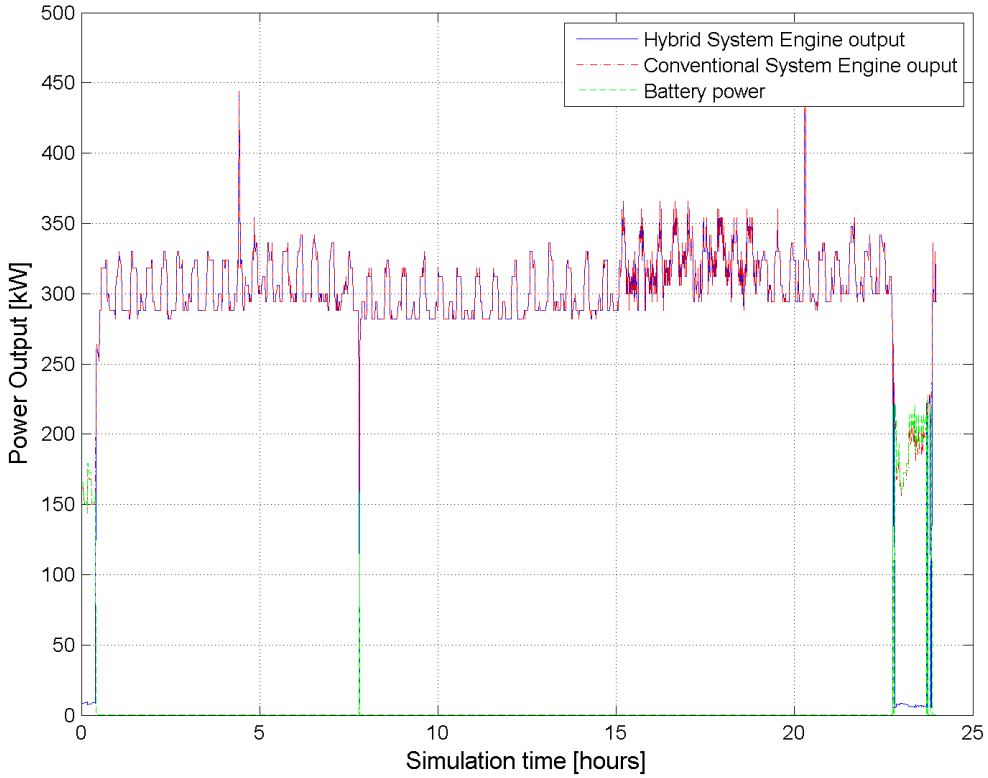


**Figure 6.16: Power split between Auxiliary Engines and batteries of energy capacity 2MWh for A1 layout with up-scaled generator output**

For this scenario, the auxiliary engine consumption is 1.5520 tonnes of HFO, while the savings due to the hybrid configuration reach 0.15% of the auxiliary fuel, which is far less than the equivalent 0.48% of the scenario where the installed energy of the battery system was set to 2MWh.

To simulate the scenario where the designer has reduced the installed power output of the prime movers, the Yanmar 6N21L engine is replaced by the Yanmar 6N18L, which has an electrical output of 475kW (as seen in Table 3.3). The battery capacity is set to 2MWh. The power split between the battery system and the auxiliary engine is presented in Figure 6.17.

The analysis of Figure 6.17 shows that the downscaled auxiliary engine restricts the battery usage, which is now limited to very low currents. This difference is clear when comparing Figure 6.16 and Figure 6.17 at the 23$^{rd}$ and 24$^{th}$ simulation hours. The downscaled layout limits the battery operation there and operates the auxiliary engine instead. The battery peak though, around the 4$^{th}$ hour should be neglected. Nevertheless, it is found that, for the given auxiliary demand profile, although the downscaled auxiliary engine is better suited to the operational purpose, there is a slight increase of the total fuel consumption. The consumption is now 1.58 instead of 1.55 tonnes of HFO. Nonetheless,

this difference is acceptable and is explained by the higher SFOC curve that the Yanmar engine has in comparison with the auxiliary generator set of MAN Diesel. If assuming a downscaled engine with the same 'parent' SFOC curve, then the fuel consumption would certainly be lower with the downscaled generator set. Despite this difference, the battery system affects the fuel consumption and the reduction reaches 0.38% of the auxiliary fuel bill.

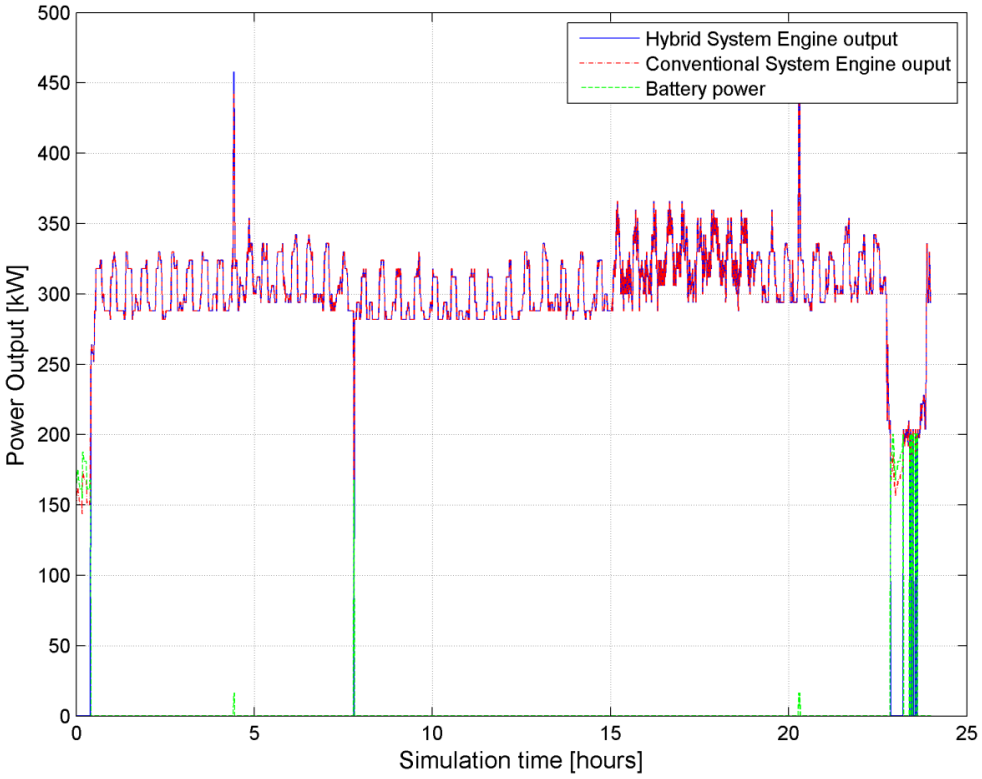


**Figure 6.17: Power split between Auxiliary Engines and batteries of energy capacity 2MWh for A1 layout with downscaled generator output**

### *6.2.3.2 Layout D-B-M*

Based on the findings of layout D-B, the hybrid system is not feasible for normal load optimisation or high load optimisation. For this reason, the 'parent' engine SFOC curve for part-load optimised engines is used. For these simulation runs, the M/E MCR is altered according to Table 3.4. The battery energy capacity is set to 8MWh and to 10MWh. For this optimisation scenario, the MCR of the PTO/PTI system is increased from 600kW to 1200kW and to 1800kW because the investigation involves excessive high load of the M/E as the vessel sailed in Beaufort numbers 5 and 6 in high speed.

For this scenario, the installed MAN 7S50MC-C type engine with MCR at 11060kW is downscaled to 10500 (MCRM1) and then is replaced by the MAN 6S50MC-C type, with a power output equal to 9800kW (MCRM2). No sensitivity analysis is performed

for the downscale scenario. The results of the power split between the propulsion engine and the battery system are given by Table 6.13.

**Table 6.13: Power split and battery DoD for layout D-B and for downscaled M/E**

| Simulation segment [-] | Simulation Time [h] | M/E load [-] | | Battery Power [kW] | | Battery DoD [%] | |
|---|---|---|---|---|---|---|---|
| | | MCRM 1 | MCRM 2 | MCRM 1 | MCRM 2 | MCRM 1 | MCRM 2 |
| 1 | 2.4 | 100% | 99.96% | 948 | 1768 | 28% | 42% |
| 2 | 4.8 | 100% | 99.96% | 948 | 1768 | 57% | 85% |
| 3 | 7.2 | 100% | 100% | 1200 | 631 | 93% | 100% |
| 4 | 9.6 | 100% | 100% | 1200 | 1800 | 57% | 57% |
| 5 | 12 | 77.73% | 83.28% | 0 | 0 | 57% | 57% |
| 6 | 14.4 | 86.26% | 100% | 0 | 1800 | 57% | 14% |
| 7 | 16.8 | 100% | 99.34% | 1200 | 750 | 21% | 32% |
| 8 | 19.2 | 100% | 97.64% | 695 | 1050 | ~0% | 57% |
| 9 | 21.6 | 74.14% | 81.07% | 0 | 0 | ~0% | 57% |
| 10 | 24 | 100% | 97.82% | 79 | 1200 | 0% | 86% |

The power split indicates that there is usage of the battery system in cases (time segments 6 and 7) where the total amount of kW reserved for propulsion does not exceed the M/E MCR, and the Hybrid controller forces the battery system to charge. This can be explained by the shape of the part load curve, which affects the optimisation decisions, the implied logic criteria and the equivalent future fuel saving. The implied battery charging results in equality in fuel efficiency between the initial configuration of 11060kW and when the one with the MCR set at 10500kW.

When the MCR is set at 9800kW there is a slight decrease in fuel efficiency by 0.10% which is negligible. Hence, it can be said that the Hybrid system is maintaining the fuel efficiency of a properly matched engine to a configuration with downscaled prime mover without affecting the operational capability of the vessel and without increasing the total fuel consumption. Thus, the indirect savings occur in slow vessel speeds where the downscaled M/E has high fuel efficiency when compared to the baseline configuration.

The Main Engine is now up-scaled and the PTO/PTI MCR is reduced to 600kW as the M/E power is significantly increased and no large margin for the PTO/PTI system is required. The MAN 6S70MC-C type with a power output equal to 14460kW is selected as the propulsion engine. The batteries are fully charged prior to the application of the shaft power profile. The high power output requirements imply the selection of high load M/E optimisation profile. Consequently, two runs were performed, incorporating part load optimisation for comparison with the downscale scenarios and full load optimisation for Hybrid system assessment.

The hybrid configuration over the reported period is found to be less energy efficient and the total consumption is increased by 0.37% and for the part load configuration the fuel consumption is increased by 0.57%. This is explained by the implied charging current, which marginally increased the power consumption, as the total amount of equivalent fuel savings is reduced by the existence of conversion losses, but mainly due to the charging/discharging battery efficiency.

## 6.3 Chapter summary

This chapter demonstrated the accuracy of the ship simulator. The latter tool in terms of fuel oil consumption estimation has a lower error in calculations which is around 4% compared to the IMO formulae which result in an error of around 10%. Nonetheless, when the ship simulator regenerates the daily parameters and the simulator has a 2 hour step instead of a daily 24 hour step, the implied simulator error drops to 2.75%. This Chapter also validated the fuel savings of Hybrid power system concept for Diesel Hybrid power systems. The D-A1, D-B and D-C scenarios were investigated. For safety reasons and for cases of improper matching of prime movers, optimisation scenarios using downscaled or up-scaled prime movers were also performed.

Regarding the auxiliary demands, the prime mover electrical output and the installed battery energy capacity are the controlling parameters of the hybrid power train feasibility. Depending on the installed capacity, a hybrid system has small but non negligible effects that can lead up to 6.19% savings of the daily auxiliary fuel consumption.

It was also demonstrated the crucial effect of the logic in charging mode which greatly affects the fuel saving percentage. In addition, the reference time which controls when the system is forced to have the energy storage medium charge, also contributes to the savings percentage and hence the feasibility of the system. In addition, it was also underlined the effect of the time step to the optimisation results and also validated the statements of Dedes et al. (2010).

About the layout D-B, it was found that the system is infeasible. The optimisation resulted in zero hybridization degree because of the electromechanical losses that exist from battery towards the PTO/PTI system.

Regarding layout D-C and for part load optimised engine, although the battery operation is restricted due to conversion losses for propulsion loads, the advanced power management yielded to power split between the M/E and the A/E offering fuel savings that reach 7.23% for propulsive loads. In specific loads, it was shown that this is more energy efficient to supply power to M/E with PTI feature than use the electric machine as a shaft generator.

A sensitivity analysis was performed for the D-A1 and D-B scenarios. It emerged that the hybrid system as expected is sensitive to the variation of component efficiencies. For the layout D-B it was found that the system might run at the edge of efficiency only when the efficiencies of the conversion and control components are close to one. Thus it can be concluded that given the SFOC curves and the electrical and electromechnical conversion efficiencies, the layout D-B is not feasible.

For the case of D-A1 scenario, a linear degradation battery model was applied. It was found that the system can withstand in most of the cases a degradation of up to 2% with potential to reach up to 4% depending on the installed battery capacity.

In the test of downscaling and up-scaling the A/E, it emerged for the up-scaled engine that the fuel consumption is reduced primarily due to improved engine fuel efficiency and secondly due to the application of the Hybrid solution. Regarding the downscaled option, the system is less energy efficient due to the less efficient A/E in terms of SFOC but still, the hybrid system offers fuel savings. Nevertheless, for the examined power profile, the battery system operating time was reduced, as the optimisation showed that the battery system reduces the fuel consumption in very low loads.

The same scenario was also applied to layout D-B. It was demonstrated that, for the given power demand, a downscaled M/E along with a high output PTO/PTI system supplied by batteries has almost negligible fuel increase due to conversion losses. The system regularly performed a power split between the battery and the M/E, leading to the conclusion that the system is feasible without any future component improvements. Thus, the downscaled option leads to indirect fuel savings due to smaller engine (lower initial cost) and due to part or low load optimisation which leads to fuel savings. Nonetheless, the run with the up-scaled M/E showed that the system might work at the edge of its overall efficiency and it occasionally results in temporary fuel deficiencies.

(Page left intentionally blank)

# 7 Conclusions

This thesis investigated the potential of Hybrid Power layouts for ocean going vessels, having as prime movers Diesel engines. The thesis applied a systematic approach to the target areas of emission calculation, performance monitoring and energy efficiency. The hybrid potential was based on statistical analysis of thirty-six voyages of all the modern categories of bulkers. The analysis of the Hybrid Power system also included a concept feasibility, constructional feasibility and financial feasibility, using statistical data sampled by the author and structural and geometrical data of the examined ships. In order to estimate global shipping emissions, which are quasi-static phenomena, and also to measure the benefit of Hybrid Power systems, a time domain quasi-steady ship simulator was constructed in a modular, scalable and extendable way.

The combination of energy storage devices for the minimisation of engine transient loads for emissions reduction achieves fuel savings and lowers exhaust emissions compared to conventional machinery installations. The application of this technology involves different propulsion layouts for conventional fuel consumption. To assess over a broad range the Hybrid Power layouts, multiple optimisation scenarios were run. A modified version of the equivalent cost minimisation strategy was adopted and implemented. Moreover, a pseudo multi-objective optimisation for PM and $CO_2$ emission reduction was also demonstrated. Savings ranging from 0.3 to 7.23% for Diesel Hybrid and advanced energy management concept were demonstrated. In addition, a Hybrid power system in combination with downscaled prime movers showed great potential in terms of indirect fuel savings due to better efficiency of the prime mover. Nonetheless, the sensitivity analysis performed for the pure Hybrid scenarios showed that the proposed system might work at the edge of operational feasibility when the energy storage system starts to deteriorate. The following detailed conclusions can be made:

***Exhaust emission estimation***

This thesis demonstrated that the adopted fuel emission factors introduce a small percentage of uncertainty when the fuel factor corresponds to the actual burnt fuel. Moreover, the power based factors, when divided by the engine SFOC, converge with the correct fuel based factor. However, when an average power based factor is used, a greater inaccuracy is introduced to the calculations. Regarding the determination of shipping emissions, the formula of the IMO and the assumptions of the second greenhouse emission study were compared to the results of the constructed ship simulator. It was shown that the constructed ship simulator, using daily mean data, underestimates the shipping emissions in the majority of the acquired sample cases; in terms of error percentage,

however, the simulator is far more accurate than the IMO study. Nevertheless, when the simulator regenerates the environmental conditions over the 24-hour period and recalculates the emissions over the complete voyage, the simulation results overestimate the fuel consumption. However, the introduced error is 75% lower than the implied error, due to the adoption of the IMO formula and of its associated assumptions.

In order to compare the cost and to determine how the hybrid system can interact with up to date energy efficiency measures, this thesis outlined and presented all energy saving devices and techniques. It was discussed how the proposed system is suitable for installation alongside the majority of these measures. However, there are certain cases, mostly in terms of energy efficiency measures targeting the propulsion machinery, which reduce the effect of the hybrid system in certain operational profiles. Nonetheless, the proposed system does not affect the function of these technologies, as the system is capable of being idle when not required. Thus, the hybrid system proved to be an additional energy saving technology, which is compatible with the latest technologies and also increases the overall fuel saving percentage when operated.

### *Simulator model assessment*

For the requirements of the ship simulator, various methods for hull-fluid interaction were implemented. Regarding the calm water resistance, the Hollenbach method proved to converge with the model test data at the design draft, while the Holtrop-Mennen method best fits the ballast draft calm water resistance. However, both methods converge in all drafts for Handysize and Handymax designs. Concerning the added resistance data, three methods were implemented. The Aertssen model proved to give modest results regarding the added resistance due to wind and waves, and better suited the majority of the reported data. However, there are cases where the Kwon method proved to converge with the actual reported data.

For the wind induced loads, the Blendermann method converged with the results of the wind resistance proposed by Isherwood. Since the Blendermann method is more up to date, it is recommended to use this method for simulation purposes.

### *Statistical Hybrid Power system analysis*

The proposed hypothesis was that a combination of energy storage devices for minimisation of engine transient loads for emissions and fuel reduction is a promising alternative to conventional installations of ship machinery. This assumption was initially validated by the statistical analysis of twenty-six voyages of thirteen types of bulkers. The amount of demonstrated potential savings was multiplied by the appropriate emission factors. The likely amount of savings was projected to the world fleet, by multiplying the

results of the sample with the category percentage of the world fleet, in order to assess the global emission benefit by adopting the proposed machinery alternative.

The voyage statistical analysis showed that a Hybrid Power system is a flexible and efficient propulsion system for any type of vessel having a standard mission profile, and not only with an extensive high and low load operation. The minimisation of engine transient loading and the use of load levelling are shown to result in fuel savings and hence emissions reductions. The latter may be reduced further through the optimisation of propulsion and engine components. The overall AES concept proved not to be feasible for laden operation, as the engine fluctuation fuel savings do not compensate for the electromechanical losses. Moreover, the hybrid AES system is more suitable in manoeuvring operation or while sailing within ECA zones. Based on the results of the statistical analysis, the combination of slow speed Diesel and of a hybrid PTO/PTI (scenario D-B) system with fully integrated auxiliary power generation proved to be a feasible alternative.

The statistical analysis concluded that the operation of the fleet greatly affects the fuel consumption and hence the emissions. Differences were observed in similar designs (Handysize and Handymax), which were expected to have a similar engine profile and similar consumption: it emerged that savings were negligible for Handymax vessels, whereas significant savings were found for Handysize. This is primarily due to chartering commands resulting in variations in voyage speeds. A secondary reason is that the relatively small dimensions of the ship make it suitable for a wide range of loads that greatly affect the engine operation. To extract a more universal conclusion, a larger sample has to be investigated, using detailed operational profiles for the voyages.

The installed power requirement is shown to be highest for the Panamax category. On the other hand, larger ships (e.g. Capesize bulkers) operate their engines closer to the optimum points and there is less speed variation. The installation of a large energy storage medium is thus not necessary. Analysis of the Panamax type, being between the HandyMax and Small Capes (also known as Post-Panamax), shows a further increase in the energy storage demand.

From an economic point of view, and not accounting for the benefit of environmental protection, the storage medium with Sodium Nickel-Chloride proved to be the most feasible method, with a potentially high return on initial investment. Post-Panamax type fuel savings demonstrated that the rate of return on the investments for both storage media cases examined is less than three years. Other ship types indicate the system is economically feasible over a 25-year period – with the exception of the Handymax type– with high rates of return in most cases for the Sodium Nickel Chloride

batteries. Meanwhile, whilst other storage media are still very costly when the products reach the market, their cost is likely to drop.

The voyage analysis showed that installing hybrid power technology on-board dry bulk ships can lead to fuel savings of up to 1.27 million USD (at the price of 520$/tonne) per vessel and per year, assuming that 60% of the voyage time ship sails in laden and 40% in ballast condition. This value also depends on the ship's dimensions, the storage medium adopted and the demand for energy availability. The emission reduction is achieved primarily through reducing the consumption of fuel, and further reductions could be achieved by the optimisation of the combustion process or the operation of other engine components. The combination of a hybrid energy storage medium and the flexibility that it offers in the coupling with the propulsor, along with other possible improvements in hydrodynamic ship energy efficiency should allow a notable step improvement in the overall efficiency of the ship's propulsion systems (estimated between 2%-10%), although this requires further systematic design studies (Molland, et al., 2009). The re-allocation of machinery weight and battery system is deemed feasible.

### *Constructional feasibility assessment*

The feasibility of constructing such a hybrid system was investigated for dry bulk ships, by considering realistic loading conditions and the trim of the vessels, together with a description of factors to be considered in any change in weight distribution. Of the considered battery technologies, at the early stage the potential of installing Sodium Nickel Chloride and Redox flow cell batteries was examined. It was observed that installing Sodium Nickel Chloride batteries closely balances the weight saving due to the reduction in carried fuel. For other batteries, a decrease of payload is required to keep the same total displacement. The operational characteristics of the energy storage system were presented alongside a discussion of the appropriate compartments for their housing. It appears as though the operating temperature in Sodium Nickel Chloride batteries is a crucial criterion in the selection of compartments, however they are an attractive choice, since the specific energy per $m^3$ and the energy density per kg is high. For the second selected battery type, namely Vanadium Redox Flow Batteries, large tanks are required to store the electrolytes (reactants) and their energy density per kilogram and per cubic meter is significantly lower.

It was demonstrated that the equivalent propulsion system can be installed in current ships. Two scenarios were investigated; the first includes new-builds using the current concept design, and the second involves an innovative ship design suitable only for new-builds. Thus, concerning the first category, the proposed areas suitable for the installation of energy storage devices proved to be part of the engine room and the steering

gear room. In the cargo length, the lower stool compartments were considered. The Sodium Nickel Chloride batteries will withstand impacts, penetration and spraying with water. Moreover, a fire test has been performed by laboratories, which proved the robustness and the durability of this battery type. Hence, the already successful implementation in the marine environment, through application in modern submarines, is validated. On the other hand, Redox flow cells do not have constraints in terms of the operational temperature. However, the storage of reactants in different tanks raises issues for the coating of the tanks and the pumping requires power. Moreover, the storage of reactants creates potential issues of stability due to the presence of uncontrolled free surfaces and issues of constructional strength due to sloshing effects inside these tanks.

Concerning the second application, the new concept design involves more radical changes. The overall design is strictly dependent on the number of prime movers and the installed energy capacity of the storage medium. The overall feasibility is dependent on the operating profile of the vessel, the cargo loss, the ship's constructional design, the age of the vessel and, finally, the overall price of retrofitting, as any payback period of the system is directly related to the fuel savings that may be achieved due to the installation of the Hybrid Power system.

It was demonstrated that the percentage of cargo loss is lower than 1% for Panamax and Post-Panamax bulk carriers, dependent on the payload weight and the presence of ballast in the examined loading cases.

### *Ship Voyage simulator results*

The ship simulator, which is a quasi-steady time domain simulator, offered significant aid in identifying the power demand from the propeller, which is subject to dynamic changes due to ship added resistance and speed alternations. Primarily, the conventional Hybrid system, which consists of Sodium Nickel Chloride batteries and conventional Diesel Engines or generator sets, was investigated. Three potential layouts were demonstrated. However, because conversion losses, from electrical to mechanical and vice versa, are significant, the latter cannot be levelled by the fuel savings since the fluctuation of engine loading has to exceed the percentage of the loading range covered by the 'flat' section of the fuel consumption curve of a conventional Diesel engine. Hence, concerning the Main Propulsion, for the examined propulsive demand, the part load optimised engine in combination with improved efficiencies give small but non-negligible improvements in efficiency. Regarding the cycling over batteries, the optimisation runs validated the preliminary sizing. The total installed energy capacity proved to be sufficient for the examined application. Furthermore, the cycles per day do not exceed the 0.2 value, which means that for a typical operational profile, consisting of laden and ballast voyages of

maximum 340 days per year, over the expected 25-year service margin of the vessel, the energy storage medium will not exceed the up to date maximum reported cycles of the Sodium Nickel Chloride tests. This reduces the risk of battery replacement under normal conditions and thus the total cost of the system remains as presented in the financial feasibility of the Hybrid Power system.

### *Optimisation algorithm results*

The adopted ECMS strategy is described as rule based optimisation. Logic criteria are imposed by the designer and the algorithm has to satisfy the constraints, the rules and find also the optimum (for implied rules) solution. The following parameters have been noted as of big influence on the optimisation algorithm solutions.

The reference time which controls when the system is forced to have the energy storage medium charging, also contributes to the savings percentage and also affect the feasibility of the system. It was also found that the effect of lambda coefficient in combination with the rule based (logic criteria) optimisation can lead the system to infeasible solutions. In addition, it was also underlined the effect of the time step to the optimisation results and also validated the statements of Dedes et al. (2010).

Regarding the auxiliary demands, the prime mover electrical output and the installed battery energy capacity are the controlling parameters of the hybrid power train feasibility. Depending on the installed capacity, hybrid has small but non negligible effects and can reach up to 6.19% of daily auxiliary fuel consumption.

Regarding layout D-C and for part load optimised engine, it was demonstrated that, although the battery operation is restricted due to conversion losses, the power split for propulsive loads is feasible. The propulsion demand is covered by the main Diesel engine and a small percentage is supplied though the PTO/PTI system which is powered by the auxiliary engine. In specific loads, it demonstrated savings up to 7.23% and can be concluded that PTI system is more fuel efficient than the PTO (shaft generator) mode.

Sensitivity analysis was performed for the D-A1 where savings were observed and to the D-B layout due to the lack of feasibility with the current technological improvements. It emerged that the Hybrid system is too sensitive on the variation of component efficiencies, however, it can withstand a small overall efficiency drop of 2%. For the layout D-B it was found that the system might run at the edge of efficiency only when the efficiencies of the conversion and control components are close to one. Thus it can be concluded that given the SFOC curves and the electrical and electromechnical conversion efficiencies, the layout D-B is not feasible.

For the case of D-A1 scenario, a linear degradation battery model was applied. It was found that the system can withstand in most of the cases a degradation of up to 2% with potential to reach up to 4% depending on the installed capacity.

Concerning the test of downscaling and up-scaling the A/E, it emerged for the up-scaled engine that the fuel consumption is increased.. Regarding the downscaled option, the Hybrid power system despite the introduction of conversion losses, the total consumption in high loads (which exceed engines MCR) are almost the same than using a normal set engine. The fuel savings occurs by optimising the engine in part and low load configuration. Thus, hybrid couples the benefits of other fuel saving measures to operational envelopes that before it was not possible to be applied.

The same scenario was also applied to layout D-B. The ship simulator constructed a 24-hour voyage profile. Regarding the downscaled option, the Hybrid power system although introduces conversion losses, the total consumption in high loads (which exceed engines MCR) are almost the same as using a normal set engine. The fuel savings occurs by optimising the engine in part and low load configuration. Thus, hybrid couples the benefits of other fuel saving measures to operational envelopes that before it was not possible to be applied. The system is feasible without any future component improvements. Nonetheless, the run with the up-scaled M/E showed that the system might work at the edge of its overall efficiency and it occasionally results in temporary fuel deficiencies.

Consequently, it can be concluded that the Diesel Hybrid power train is a feasible solution for marine application in ocean going ships with no extreme variations in engine loading, although the results are not as remarkable as in automotive applications, where the ICE efficiency curves are not as flat as in marine Diesel engines. Furthermore, there are parameters that cannot be described in terms of total fuel savings, which further improve the benefits of the Hybrid Power concept. These parameters are the operating temperatures and pressures (e.g. $NO_x$ and PM formulation, material life cycle) and the loading of the engine, which directly affects the external abatement technologies for emission reduction.

The optimisation scenarios used M/E SFOC curves without having any degradation model applied to the performance of the main engine are something that reduces the benefit of the hybrid system. It was observed during energy audits that the deterioration of the engine performance does not follow the curve trend of the SFOC as it was manufactured and tuned by the engine builder. Thus, an experimental SFOC curve should be inserted to the optimisation algorithm so as to compare directly the statistical analysis with the results of the optimisation Thus, the differences between the statistical analysis and the actual optimisation results rely on two major parameters. The first is the

static efficiency of the components which add uncertainty to the calculation and the second the actual SFOC curve of each ship. Nonetheless, the statistical analysis gives a good indication on the potential of the system in full scale application, while the optimisation results give modest benefits as the developed algorithms compare both systems in ideal conditions.

***Novelty***

This research project was the first which investigated the concept of Hybrid propulsion and Hybrid auxiliary power train for ocean going ships consisting of battery storage system Diesel prime movers and advanced energy management. The project modified the Hybrid topologies proposed by the automotive industry and adapted the non-linear optimisation procedure of the ECMS strategy for marine applications for the first time. In addition a simple pseudo multi-objective optimisation algorithm was presented aiming at lowering PM and $NO_x$ emissions except $CO_2$ which remained the primary goal. The assessment of the marine Hybrid topologies was completed by taking into account the numerous restrictions in the application of such systems in shipping. Moreover, in the investigation the financial and constructional feasibility has been demonstrated, something than has not been done up to this date. Furthermore, the author had access to a number of sensitive technical and operational information, which allowed this project to be in line with the actual shipping business and in accordance with existing machinery and hull designs. Nevertheless, in order to be able to increase the usage of the findings and to demonstrate further the applicability of the proposed systems, a time domain quasi- steady simulation tool was built. The constructed model library can assist future studies involving simulation in this domain. Finally, the application of the simulator tool can assist shipping companies which are aiming at higher fuel efficiency for their fleet. Currently, only few marine consultancy companies offer Excel® based tools for performance assessment and emission estimation with the exception of Marorka Company which develops a combination of performance monitoring, engine control and prediction software for large maritime companies. Therefore, the ship simulator which utilises a logical amount of computer power can be an accurate and cheap alternative.

## 7.1 Discussion

'What will be the future in marine power systems', 'which principles will define the modern ship design', 'will the current market define the ship design for the next 25 years'? These are some questions that arise and introduce scepticism among the ship designers. Based on the findings of this research project, it is believed that the Hybrid power train will dominate the ship industry in the future. Probably the first attempt will be the installation

of multiple prime movers coupled to clutches rotating a single propeller slow speed vessel, accepting the trade-off of increased complexity. Another potential solution is to design slow speed twin skeg vessels which will allow a more flexible approach in engine propeller matching. However, the flexibility, the reliability and the excessive operational profile of the proposed Hybrid system make it applicable to future ship designs. The main advantage of this system is that can be combined with the majority of up to date energy efficiency measures. Moreover it can also improve the prime mover efficiency by decoupling them from the power demand, allowing operation in more efficient points. This means that the powering system is suitable for many purposes, something that is not dictating the maximum or the minimum speed (a common problem of future ships which are designed nowadays for slow steaming). A more traditional designer may say that the ships are designed for the current market because ship-owners do not give much weight to the future requirements as they want to maximise their current profits. This statement is clear by taking into consideration the number of ordered and cancelled vessels and the vessel dimensions that dominated the shipping sector. Nonetheless, this statement will not be valid for long. Ship-owners, influenced by the global economic recession have already identified the risks of their past choices and nowadays they pay close attention to the requirements of flag states IMO, EU and of course the charterers including the Oil Majors. Especially IMO takes many decisions which are not always validated by actual shipping data, something that drives the industry in strange paths. Consequently, systems that can serve many purposes without major retrofits and comply with future IMO regulations should be the first choice of ship-owners willing to adapt without problems to them. In terms of installed power, always stored energy and propulsion redundancy can decrease the risks of collision, grounding and even total loss of the ship. To conclude, the traditional machinery layout is likely to reach its end. Major changes of propulsion machinery in combination with future ship designs are considered certain. Regarding the future of Hybrid propulsion, Det Norske Veritas (DNV) had announced the installation of a Hybrid power module on board the supply vessel 'Viking Lady' for assessment. This module is consisted of an unknown type battery and a controller which will perform the energy management. The excessive low and high needs of electrical power does not render this case suitable for assessment of the D-B layout, however, the results will validate or not the proposed topologies D-A1 and D-A2. Hence, the Hybrid system for Diesel powered vessels will be judged by the shipping community in shorter time from the publication of this thesis than initially believed, and if the statistical and simulation results are validated, then the proposed options may become reality.

## 7.2 Implications for future application

There are currently no projects underway which attempt to merge specified databases of meteorological data, ship characteristics and AIS data in order to create the appropriate file for data loading to the simulator. As a result, by using the time domain quasi-steady ship simulator proposed in this thesis, the fuel consumption and thus emissions can be estimated by the application of an accurate real time bottom up approach. This tool will be accurate enough to assess potential fuel saving device that are installed on-board, especially if this will save historical data in a global fleet database. However, none of the current projects for emission inventories based on AIS data can actually estimate real time fuel consumption, as the data of ship hull and weather are available in different databases.

Regarding the ship simulator, further investigation of the models that can describe more accurately every ship type of the examined sample is proposed. However, this requires an extensive database of confidential data, which can only be provided by shipping companies or by the shipyards. In addition, a detailed RAO of added resistance versus significant wave height and wave direction would be an interesting contribution to the ship simulator library. In addition, a dynamic approach should also be considered, but not for emission calculation as these phenomena are quasi-static.

Concerning the optimisation suite, it is proposed to refine and improve the logic criteria and re-run simulation cases. It would be of great interest if future comparisons between the results of the ECMS strategy and the results of a DP were made.

Finally, the dynamic coupling in a laboratory environment of the PTO/PTI system in fluctuating power profile with a Diesel engine requires further testing. In addition, a dynamic controller for this purpose has to be designed and implemented. It is recommended to perform laboratory tests, adding to the previous laboratory layout a Sodium Nickel Chloride battery pack, so as to validate the simulated battery efficiency curves. The latter efficiencies were obtained from experimental data, but not for marine application and not in such a large energy capacity.

# References

G. H. Abd-Alla. Using exhaust gas recirculation in internal combustion engines: a review. *Energy Conversion and Management*, 43(8):1027–1042, 2002. ISSN 0196-8904.

T. Abram. *Reactor thermal Hydraulics* - lecture notes SESG6026, University of Southampton MSc. The University of Manchester, Dalton Institute, 2011.

A. K. Adnanes and Norges teknisk-naturvitenskapelige universitet Institutt for marin teknikk. *Maritime electrical installations and diesel electric propulsion*. Citeseer, 2003.

G. Aertssen. Service Performance and Seakeeping Trials on MV Lukuga. *Trans. RINA*, page 293, 1963.

G. Aertssen. Service Performance and Seakeeping Trials on MV Jordaens. *Trans., RINA*, 108(4), 1966.

G. Aertssen. Service-Performance and Sea Keeping Trials on a Stern Trawler. *Transactions of the North-east coast institution of engineers and shipbuilders*, page 13, 1967.

G. Aertssen. Service Performance and Trials at Sea. In *12th International Towing Tank Conference*,1969.

G. Aertssen and M. F. Sluys. Service Performance and Seakeeping trials on a large Containership. *Trans. RINA*, 114, 1972.

R. Alvarez, P. Schlienger and M. Weilenmann. Effect of hybrid system battery performance on deter- mining CO2 emissions of hybrid electric vehicles in real-world conditions. *Energy Policy*, 2010. ISSN 0301-4215.

M.D. Amiridis, T. Zhang, and R.J. Farrauto. Selective catalytic reduction of nitric oxide by hydrocar- bons. *Applied Catalysis B: Environmental*, 10(1-3):203–227, 1996. ISSN 0926-3373.

H. E. Anderson. *Predicting wind-driven land wild fire size and shape,* United States Ministry of Agriculture, Research Paper INT-305, 1983.

K. Andersson and H. Winnes. Environmental trade-offs in nitrogen oxide removal from ship engine exhausts. *Proceedings of the Institution of Mechanical Engineers, Part M: Journal of Engineering for the Maritime Environment*, 225(1):1, 2011. ISSN 1475-0902.

P. Andreadis, C. Chryssakis, and L. Kaiktsis. Optimization of injection characteristics in a large marine diesel engine using evolutionary algorithms. *Optimization*, 1:1448, 2009.

S. Ansolabehere, J. Deutch, M. Driscoll, P.E. Gray, J.P. Holdren, P.L. Joskow, R.K. Lester and E.J. Moniz. The future of nuclear power: an interdisciplinary MIT study, 2008.

M. E. Aughey. *Ship Hull Characteristics Program*. Joint Meeting of the Chesapeake & Hampton Roads Section of the Society of Naval Architects and Marine Engineers, September 1968.

A.P. Ault, M. J. Moore, H. Furutani and K.A. Prather. Impact of emissions from the los angeles port region on san diego air quality during regional transport events. *Environmental science & technology*, 43(10):3500–3506, 2009.

A. Azaron and F. Kianfar. Dynamic shortest path in stochastic dynamic networks: Ship routing problem. *European Journal of Operational Research*, 144(1):138–156, 2003.

J. Baker. New technology and possible advances in energy storage. *Energy Policy*, 36(12):4368–4373, 2008. ISSN 0301-4215.

T. van Beek. *Technology Guidelines for Efficient Design and Operation of Ship Propulsor*. Marine news, Wartsilla, 2004.

G. Barabino, M. Carpaneto, L. Comacchio, M. Marchesoni, and GP Novella. A new energy storage and conversion system for boat propulsion in protected marine areas. In *Clean Electrical Power, 2009 International Conference on*, pages 363–369. IEEE.

F. Barnaby and J. Kemp. Too hot to handle? the future of civil nuclear power. *Executive summary*, pages 7–14, 2007.

F. Barnaby, J. Kemp and Oxford Research Group. *Secure Energy?: Civil Nuclear Power, Security and Global Warming*. Oxford Research Group, 2007.

W. B. van Berlekom, P. Tragardh and A. Dellhag. Large tankers-wind coefficients and speed loss due to wind and sea. *Naval Architect*, (1), 1975. ISSN 0306-0209.

W. B. van Berlekom. Wind forces on modern ship forms–effects on performance. *Trans. Of the North East Institute of Engineers and ship Builders*, 97(4):123–132, 1981.

S. J. Bijlsma. *On minimal-time ship routing*. Staats drukkerij, 1975.

W. Blendermann. Parameter identification of wind loads on ships. *Journal of Wind Engineering and Industrial Aerodynamics*, 51(3):339–351, 1994. ISSN 0167-6105.

H. Bohm and G. Gutmann. *Proceedings of the 13th international Electric vehicle symposium*, Vol. II p.701, 1996.

H. Bohm and J. L. Sudworth. *Extended abstracts of the Electrochemical Society*, Abstract No 138, "ZEBRA-Battery: A Viable Candidate for EV", Vol. 94-2. The electrochem. Society, Pennington, NJ, 1994.

N. Bose, *Marine Powering Prediction and Propulsors,* The society of Naval Architects and Marine Engineers, 2008.

P. Van den Bossche, J. Matheys, and J. Van Mierlo. Battery environmental analysis. *Electric and Hybrid Vehicles: Power Sources, Models, Sustainability, Infrastructure and the Market*, page 347, 2010.

V. Brslica. Plug-in hybrids and new energy storages. *In Vehicle Power and Propulsion Conference, 2009. VPPC'09. IEEE*, pages 516–523. IEEE.

B. Burger, D. Kranzer. Extreme high efficiency PV-power converters, *Power Electronics and Applications, 2009. EPE '09. 13th European Conference on* , vol., no., pp.1-13, 8-10 Sept. 2009

P. Cariou. Is slow steaming a sustainable means of reducing $CO_2$ emissions from container shipping? *Transportation Research Part D: Transport and Environment*, 2011.

J. S. Carlton, Marine Propellers and Propulsion, 2nd Edition, Butterworth & Heinemann, Oxford, 2007.

S. L. Ceccio. *Friction drag reduction of external flows with bubble and gas injection,* Annual review of Fluid Mechanics 42, pp. 183-203, 2010.

F. Celik. *A numerical study for the effectiveness of a wake equilising duct,* Ocean Engineering 34, pp. 2138-2145, 2007.

S.G. Chalk and J.F. Miller. Key challenges and recent progress in batteries, fuel cells, and hydrogen storage for clean energy systems. *Journal of Power Sources*, 159(1):73–80, 2006. ISSN 0378-7753.

Chatzilau, K., Prousalidis, I.M., Gyparis, I.K. and Vallianatos, P., *Evolution of Electric Propulsion and overview of design in an All Electric Ship*. Athens : Hellenic Chamber of Mechanics, 2006.

C. Chryssakis, A. Frangopoulos, and L. Kaitsis. Computational Study of In-Cylinder NOx Reduction in a Large Marine Diesel Engine Using Water Injection Strategies. In *26th CIMAC World Congress. Bergen, Norway, June 2010*. CIMAC, 2010.

J. F. Cole. Battery energy-storage systems–an emerging market for lead/acid batteries. *Journal of power sources*, 53(2):239–243, 1995.

J. J. Corbett, P. S. Fischbeck and S.N. Pandis. Global nitrogen and sulfur inventories for ocean-going ships. *Journal of Geophysical Research*, 104(D3):3457–3470, 1999.

J. J. Corbett and H.W. Koehler. Updated emissions from ocean shipping. *J. Geophys. Res*, 108(D20): 4650–64, 2003.

J. J. Corbett, J.J. Winebrake, E.H. Green, P. Kasibhatla, V. Eyring, and A. Lauer. Mortality from ship emissions: a global assessment. *Environmental science & technology*, 41(24):8512–8518, 2007.

J. J. Corbett, H. Wang, and J.J. Winebrake. The effectiveness and costs of speed reductions on emissions from international shipping. *Transportation Research Part D: Transport and Environment*, 14(8): 593–598, 2009.

J. J. Corbett, D. A. Lack, J. J. Winebrake, S. Harder, J. A. Silberman and M. Gold. Arctic shipping emissions inventories and future scenarios, Atmos. Chem. Phys., 10 9689, 2010.

Cotzias Shipping Group. S&P Monthly Report. Piraeus, June 2010.

C. Daniel and J. O. Besenhard. Handbook of Battery materials *Wiley VCH, Weinheim* 1999

S. B. Dalsøren, M. S. Eide, Ø. Endresen, A. Mjelde, G. Gravir, and I. S. A. Isaksen. Update on emissions and environmental impacts from the international fleet of ships: the contribution from major ship types and ports. *Atmospheric Chemistry & Physics*, 9:2171–2194, 2009.

P. de Vos and E. Versluijs. Application of Dynamic Models during Design of a Hybrid Diesel-Fuelled PEMFC System with Fuel Reformer. In *Practical design of ships and other floating structure symposium, 2009. PRADS'09*, pages 681–689. COPPE UFRJ, 2010.

E. K. Dedes. Modular thermodynamic implementation and simulation of the closed cycle period for a cylinder of a large marine Diesel engine. Master's thesis, School Naval Architecture and Marine Engineering, National Technical University of Athens, July 2009.

E. K. Dedes, D. A. Hudson, and S. R. Turnock. Design of hybrid diesel-electric energy storage systems to maximize overall ship propulsive efficiency. In *Practical design of ships*

*and other floating structure symposium, 2010. PRADS'10*, pages 703–713. COPPE UFRJ, 2010.

E. K. Dedes, D. A. Hudson, and S. R. Turnock. Assessing the potential of hybrid energy technology to reduce exhaust emissions from global shipping. *Under Review Energy Policy*, 2012a.

E. K. Dedes, D. A. Hudson, and S. R. Turnock. Technical feasibility of Hybrid Powering systems to reduce exhaust emissions of bulk carriers. *IJME transactions of RINA*, 2013a.

E. K. Dedes, S. R. Turnock, D. A Hudson, and S. Hirdaris. Possible power train concepts for nuclear powered merchant ships. In *Low Carbon shipping conference, Strathclyde University, Glascow*, 2011c.

M. St Denisand W.J. Pierson. On the motion of ships in confused seas. *SNAME Transactions* 61, 280–332, 1953.

J. Deutch, E. Moniz, S. Ansolabehere, M. Driscoll, P. Gray, J. Holdren, P. Joskow, R. Lester and N. Todreas. The future of nuclear power. *an MIT Interdisciplinary Study, http://web.mit.edu/nuclearpower*, 2003.

K. C. Divya and J. Østergaard. Battery energy storage technology for power systems–An overview. *Electric Power Systems Research*, 79(4):511–520, 2009. ISSN 0378-7796.

DNV. Nuclear powered ships. Technical Report 2010-0685, Det Norske Veritas DNV, 2010.

C.H. Dustmann. Advances in ZEBRA batteries. *Journal of Power Sources*, 127(1-2):85–92. ISSN 0378-7753, 2004.

C. Elliott and P. Dearsley. Creating systems that work: Principles of engineering systems for the 21st century. *The Royal Academy of Engineering*, 14:27, 2007.

EMEP/CORINAIR. Atmospheric emission inventory guidebook. Technical report, UN ECE, 2002.

Ø. Endresen, E. Sørgaard, J.K. Sundet, S.B. Dalsøren, I.S.A. Isaksen, T.F. Berglen, and G. Gravir. Emission from international sea transportation and environmental impact. *Journal of Geophysical Research*, 108(D17):4560, 2003.

Ø. Endresen, E. Sørgard, H.L. Behrens, P.O. Brett and I.S.A. Isaksen. A historical reconstruction of ships' fuel consumption and emissions. *Journal of geophysical research,* 112(D12):D12301, 2007.

ENTEC UK Limited. Quantification of emissions from ships associated with ship movements between ports in the european union. Technical report, European Commission, 2002. DG ENV.C1.

ENTEC UK Limited. Defra UK Ship Emissions Inventory. Technical report, Department for Food and Rural Affairs, 2010. 21897-01.

V. Eyring, H. W. Kohler, J. Van Aardenne, and A. Lauer. Emissions from international shipping: 1. the last 50 years. *Journal of Geophysical Research*, 110(D17):D17305, 2005.

V. Eyring, I.S.A. Isaksen, T. Berntsen, W.J. Collins, J.J. Corbett, O. Endresen, R.G. Grainger, J. Moldanova, H. Schlager, and D.S. Stevenson. Transport impacts on atmosphere and climate: Shipping. *Atmospheric Environment*, 44(37):4735–4771, 2010.

O.M. Faltinsen, K. J. Minsaas, N. Liapis, and S.O. Skjordal. Prediction of resistance and propulsion of a ship in a seaway. In *Proc. 13th Symposium on Naval Hydrodynamics,* 1980.

Fathom Consulting. *Energy Efficiency. The Guide,* Fathom Tech, London, 2011.

A. V. Fiacco and G. P. McCormick. Nonlinear programming: sequential unconstrained minimization techniques, Society for industrial Mathematics 4, 1990.

A.E. Fitzgerald, C. Kingsley, and S.D. Umans. *Electric machinery*. Tata McGraw-Hill, 2002. ISBN 0070530394.

E. J. Foeth, *Decreasing frictional resistance by air lubrication,* 20th International Hiswa Symposium in Yacht Design and Yacht Construction, Amsterdam, 2008.

G. Fontaras, P. Pistikopoulos, and Z. Samaras. Experimental evaluation of hybrid vehicle fuel economy and pollutant emissions over real-world simulation driving cycles. *Atmospheric Environment*, 42(18): 4023–4035, 2008. ISSN 1352-2310.

C.A. Fragkopoulos. *Shipboard Energy Systems*. Athens: National Technical University of Athens, 2007.

E.G. Frankel, H. Chen, and National Maritime Research Center. *Optimization of ship routing*. National Maritime Research Center, 1980.

A. Fratta, P. Guglielmi, G. M. Pellegrino, F. Villata. DC-AC conversion strategy optimized for battery or fuel-cell-supplied AC motor drives. *Proceedings of the 2000 IEEE International Symposium on Industrial Electronics,* vol.1, no., pp.230,235, 2000 doi: 10.1109/ISIE.2000.930518

H. Fujii and T. Takahashi. Experimental study on the resistance increase of a large full ship in regular oblique waves. *J. Soc. Nav. Archit. Japan*, 137, 1975.

L. Gaines, M. Singh, Argonne National Laboratory, and United States. Dept. of Energy. *Impacts of EV Battery Production on Recycling*. GPO, 1996.

R. Galloway and C. Dustmann. ZEBRA® Battery-Material Cost Availability and Recycling. In *proceeding of international electric vehicle symposium (EVS-20), Ling Beach, Canada*, pages 1-9, 2003.

W. S. Gearhart and M. W. Mc Bride. Performance assessment of propeller boss cap fin type device*, 22nd ATTC, St Johns*, 1989.

J. Gerritsma and W. Beukelman. Analysis of the resistance increase in waves of a fast cargo ship. *International Shipbuilding Progress*, 19(217):285–293, 1972.

S. Grammatico, A. Balluchi, E. Cosoli. *A series-parallel hybrid electric powertrain for industrial vehicles*. Vehicle Power and Propulsion Conference (VPPC)'10 IEEE, pp. 1-6, 2010.

J. Gravina, J. I. R. Blake, R. A. Shenoi, S. R. Turnock, S. R. Hirdaris. Concepts for a Modular Nuclear Powered Containership. *17th International Conference on Ships and Shipping Research*. Naples, 2012.

A. Greig and R. Bucknall. Challenges for Electric Ship Design in a Low Carbon Economy. *Marine Live Workshops*, Athens 2012.

G. Grigoropoulos, T. Loukakis and A. Perakis. Seakeeping standard series for oblique seas (A synopsis), *Journal of Ocean Engineering*, Vol. 27, pp. 111-126, 2001.

H. Grimmelius, P. de Vos, M. Krijgsman and E. van Deursen. Control of Hybrid Ship Drive Systems, 2011. University of Delft.

D. Griffiths. *Marine Low Speed Diesel Engines*. Institute of Marine Engineers, 2006. ISBN 1902536339.

J. Gurche (ed). Encyclopedia of Electrochemical power sources. Elsevier 4, 2009.

H. E. Guldhammer and S. A. Harvald. *Ship Resistance, Effect of Form and Principal Dimensions*. Akademisk Forlag Copenhagen, 1974.

C.T. Gupta and L.C.A. Batra. Marine Engine Emissions and their Control: Present and the Future. 2010.

L. Guzzella and A. Sciarretta, *Vehicle propulsion systems*. 2005, Springer.

W.J. Hall. Assessment of CO2 and priority pollutant reduction by installation of shoreside power. *Resources, Conservation and Recycling*, 54(7):462–467, 2010. ISSN 0921-3449.

G. J. Haltiner, H. D. Hamilton, and G. 'Arnason. Minimal-time ship routing. *Journal of Applied Meteorology*, 1:1–7, 1962.

G.L. Hanssen and R.W. James. Optimum ship routing. *Journal of Navigation*, 13(03):253–272, 1960.

N. Hatziargyriou, T. Karakatsanis, M. Papadopoulos, Probabilistic load flow in distribution systems containing dispersed wind power generation, *EN: IEEE Trans. Energy Conversion. – Vol. 8*, N°1, pp. 159 – 165, 1993.

J. Heywood. Internal combustion engine fundamentals (ISE). *Mcgraw-Hill*, 1988.

W. Henschke. *Schiffbautechnisches Handbuch*. 2nd edn, Verlag Technik, Berlin, 1965.

K. Hirota, K. Matsumoto, H. Orihara and H. Yoshida. Verification of Ax-Bow Effect based on Full Scale Measurement*, Journal of the Kansai Society of Naval Architects 241*, pp. 33-40, 2004.

J. Hinnenthal. Robust pareto-optimal routing of ships utilizing ensemble weather forecasts. In *Maritime Transportation and Exploitation of Ocean and Coastal Resources: Proceedings of the 11th International Congress of the International Maritime Association of the Mediterranean, Lisbon, Portugal, 26-30 September 2005*, volume 1, page 1045. Taylor & Francis, 2006.

HMS-Sultan. *Sustainable energy Nuclear Power - lecture notes SESG6026, University of Southampton MSc, HMS Sultan*. Nuclear Department Defence Academy, 2008.

W. Hock and K. Schittkowski. A Comparative Performance Evaluation of 27 Nonlinear Programming Codes, *Computing Vol. 30*, p. 335, 1983.

W. A. Hockberger. Ship design margins-issues and impacts. *Naval Engineers Journal*, 88(2):157–170, 1976.

J. Holtrop, G. G. J. Mennen. An approximate power prediction method, *International Shipbuilding Progress*, Vol. 29, pp. 166-170, 1981.

J. Holtrop. A statistical re-analysis of resistance and propulsion data. *International Shipbuilding Progress*, 31(363):272–276, 1984. ISSN 0020-868X.

U. Hollenbach, O. Reinholz. Hydrodynamic Trends in Optimising Propulsion*, SPM '11 International Symposium on Marine Propulsors, Hamburg*, 2011.

U. Hollenbach and J. Friesch . *Efficient hull forms – What can be gained*. 1st Intennational Conference on Ship Efficiency, Hamburg. 2007.

H. Hori. Feasibility of a nuclear ship at crude oil price 100 *per barrel, 2008*.

D. T. Hountalas, G. C. Mavropoulos, and K. B. Binder. Effect of exhaust gas recirculation (EGR) temperature for various EGR rates on heavy duty DI diesel engine performance and emissions. *Energy*, 33(2):272–283, 2008. ISSN 0360-5442.

*IAEA: news centre*. Retrieved May 2011, from International Atomic Energy Agency: www.iaea.org, May, 2011.

IMO. Study of Greenhouse gas emission from ships. Technical report, Norwegian Marine Technology Research Institute - MARINTEK, 2000. MT00 A23-038.

IMO. Second greenhouse gas emission study. Technical report, International Maritime Organisation, 2009.

R. M. Isherwood. Wind resistance of merchant ships. *RINA Supplementary Papers*, 115, 1974.

ITTC. The specialist committee on unconventional propulsors, *22nd International Towing Tank Conference, Seoul*, 1999.

ITTC. Testing and Extrapolation Methods Propulsion, Performance Propulsion Test, Propulsion Committee of 23rd ITTC. *International Towing Tank Conference, Bali,* 2002.

R.W. James. Application of wave forecasts to marine navigation. 1957.

A. M. Jaruchi. *Analysis and modelling of energy source combinations for electric vehicles*. PhD Thesis, University of Manchester, 2010.

V. Jenkins, J. S. Carlton, and R. Smart. The nuclear propulsion of merchant ships. *The Royal Academy of Engineering*, 2010.

J.M.J. Journée. Prediction of Speed and Behaviour of a Ship in a Seaway*, ISP, Volume 23, No. 265*, 1976.

J.M.J. Journée and J.H.C. Meijers. Ship Routeing for Optimal Performance, *Transactions IME, February,* 1980.

A. Junglewitz, *Der Nabeneinfluib beim Schraubenpropeller,* PhD thesis, University of Rostock, 1996.

C. G. Justus. *Winds and wind system engineering,* Franklin Institute Press, Philadelphia, PA, 1978.

M. Kashiwagi. Impact of hull design on added resistance in waves—application of the enhanced unified theory. *Proceedings of the 10th International Marine Design Conference, Trondheim, Norway*, 2009.

Y. Khersonsky, M. Islam, and K. Peterson. Challenges of connecting shipboard marine systems to medium voltage shoreside electrical power. *Industry Applications, IEEE Transactions on*, 43(3):838–844, 2007.

E. Koutroulis, D. Kolokotsa, and G. Stavrakakis. Optimal design and economic evaluation of a battery energy storage system for the maximization of the energy generated by wind farms in isolated electric grids. *Wind Engineering*, 33(1):55–81, 2009.

Y. J. Kwon. Speed loss due to added resistance in wind and waves. *The Naval Architect*, March: 14–16, 2008.

N. P. Kyrtatos. *Marine Diesel Engines, Design and Operation*. Symmetria, 1993. ISBN 9602660023.

N. P. Kyrtatos. Marine Diesel Engines and technologies for emission reduction. In *EnergyReS Scientific Forum*. EnergyReS, 2009.

D. A. Lack, et al.. Particulate emissions from commercial shipping: Chemical, physical, and optical properties, *J. Geophys. Res.*, *114*, D00F04, doi:10.1029/2008JD011300, [printed 115(D7), 2010.

J.R. Lamarsh and A.J. Baratta. *Introduction to nuclear engineering*. Prentice Hall, 2001.

Young-Joo Lee, A. Khaligh, A. Emadi. Advanced Integrated Bidirectional AC/DC and DC/DC Converter for Plug-In Hybrid Electric Vehicles. *Transactions on Vehicular Technology, IEEE,* vol.58, no.8, pp.3970,3980, 2009. doi: 10.1109/TVT.2009.2028070

C. Lewis. The advanced induction motor. In *Power Engineering Society Summer Meeting, 2002 IEEE*, volume 1, pages 250–253. IEEE, 2007. ISBN 0780375181.

D. Lehman. *Improved Propulsion with Tuned Rudder Systems*, 1st International Conference on Ship Efficiency, Hamburg, 2007.

H. Liljenberg. *Utilising pre-swirl Flow – Reducing Fuel Costs*. SSPA Highlights 2, 2006.

C. Lin, J. Kang, J.W. Grizzle and H. Peng. Energy Management Strategy for a Parallel Hybrid Electric Truck. In *Proceedings of the Armerican Control Conference,* 2001.

D. Linden and T. B. Reddy. *Handbook of batteries 3rd Edition*. McGraw-Hill Handbooks, 2002.

S. Liu, A. Papanikolaou, and G. Zaraphonitis. Prediction of added resistance of ships in waves. *Ocean Engineering*, 2011.

Lloyds Maritime Information Services. *Lloyd's Fairplay Ship Database,* 2007.

H.K. Lo and M.R. McCord. Adaptive ship routing through stochastic ocean currents: General formulations and empirical results. *Transportation Research Part A: Policy and Practice*, 32(7):547–561, 1998.

M. S. Longuet-Higgins, *On the Statistical Distribution of the Heights of Sea Waves*, Journal of Marine Research, 11(3), PP. 245-266, 1952.

P. Lorange. *Shipping Company Strategies: Global Management under Turbulent Conditions*, Emerald Group Publishing Limited, 2005.

MAN Diesel. MAN BW S50MC-C7 project guide. Technical report, MAN Diesel Copenhagen, 2007.

MAN Diesel. *SFOC optimisation methods*. Technical report, MAN Diesel Copenhagen, 2009a.

MAN Diesel. *Emission control MAN B&W Two-stroke diesel engines*. Technical report, MAN Diesel Copenhagen, 2009b.

J.F. Manwell and J.G. McGowan. Lead acid battery storage model for hybrid energy systems. *Solar Energy*, 50(5):399–405, 1993.

JF Manwell, JG McGowan, EI Baring-Gould, W. Stein, and A. Leotta. Evaluation of battery models for wind/hybrid power system simulation. In *Proceedings of EWEC*, 1994.

J.F. Manwell, J.G. McGowan, U. Abdulwahid, and K. Wu. Improvements to the hybrid2 battery model. In *American Wind Energy Association, Windpower 2005 Conference, Massachusetts*, 2005.

R. Manzoni, M. Metzger, and G. Crugnola. Zebra electric energy storage system: From RnD to market. *Presented at HTE hi. tech. expo–Milan*, 25:28, 2008.

H.S. Marcus, J.L. Beaver. *An early conceptual design and feasibility analysis of a nuclear-powered cargo vessel*. PhD thesis, Massachusetts Institute of Technology, 2009.

MARPOL. *MARPOL 73/78 revised ANNEX VI*, MEPC59. Technical report, Internation Maritime Organisation, 2005.

MARPOL. *MARPOL ANNEX I - oil pollution*. Technical report, Internation Maritime Organisation, 2006.

Mathworks. *Building an S - Function*. Mathworks Inc., 2002.

V. Matthias, I. Bewersdorff, A. Aulinger and M. Quante. The Contribution of Ship Emissions to Air Pollution in the North Sea Regions, Env. Poll., 158 (2010) 2241, 2010.

H. Maruo. The excess resistance of a ship in rough seas. *International Shipbuilding Progress*, 4(35), 1957. H. Maruo. The drift of a body floating on waves. *Journal of Ship Research*, 4(3):1–10, 1960.

H. Maruo. Resistance in waves. *Researches on seakeeping qualities in Japan, SNAJ, 60th Aniversary Series*, 8:67–102, 1963.

J.A. McDowall. Status and outlook of the energy storage market. In *Power Engineering Society General Meeting, 2007. IEEE*, pages 1–3. IEEE, 2007.

De Meyer, P., Maes, F., Volckaert, A. 2008. Emissions from international shipping in the Belgian part of the North Sea and the Belgian seaports, *Atmospheric Environment 42*, p. 196, 2008.

MER. Early nuclear tankers. *Marine Engineers Review*, pages 27–29, March 2011.

M.R. Mohamed, S.M. Sharkh, and F.C. Walsh. Redox flow batteries for hybrid electric vehicles: progress and challenges. In *Vehicle Power and Propulsion Conference, VPPC'09. IEEE,* pages 551–557. IEEE, 2009.

A. F. Molland and S. R. Turnock. *Marine Rudders and Control Surfaces: Principle, Data, Design and Applications,* Butterworth & Heinemann, Oxford, 2007.

A.F. Molland, S.R. Turnock, and D.A. Hudson. Design metrics for evaluating the propulsive efficiency of future ships. *Proceedings of the 10th International Marine Design Conference, Trondheim (IMDC'09)*, Norway, 2009.

A.F. Molland, S.R. Turnock, and D.A. Hudson. *Ship resistance and propulsion: practical estimation of ship propulsive power*. Cambridge University Press, 2012.

A.F. Molland. *The Maritime Engineering Reference Book*. Butterworth-Heinemann, 2008. ISBN 9780750689878.

R. Moody. *Preliminary power predictions during the early design stages of a ship*. Masters Dissertation, Cape Technikon, South Africa, 1996.

R.F. Mulligan. A simple model for estimating newbuilding costs. Maritime Economics andLogistics 10, 310–321, 2008.

C. Mussardo, G. Rizzoni and Y. Guezennec. A-ECMS: An adaptive algorithm for hybrid electric vehicle energy management. *European Journal of Control*, 2005. Vol. 11, p.p. 509-524.

S. Naito. *Propulsive performance of ships in actual seas*. Proceedings of Seventh Osaka Colloquium on Seakeeping and Stability, Osaka, Japan, 2008.

R. Nilsen and I. Sorfonn. Hybrid power generation systems. In *Power Electronics and Applications, 2009. EPE'09. 13th European Conference on,* pages 1–9. IEEE, 2009

NKK. *A New Energy-saving Bow Shape at Sea*. Technical Report 86, Japan, 2002.

Nocedal, J. and S. J. Wright. *Numerical Optimization*, Second Edition. Springer Series in Operations Research, Springer Verlag, 2006.

N. Norbin. Statens Skeppsprovnings anstalt, *Transactions of RINA*, *Vol.114*, 1972.

M. K. Ochi, *Ocean Waves: The Stochastic Approach,* Cambridge University Press, 2005.

M. Ohkusu. Added resistance in waves of hull forms with blunt bow. In *Proceedings of 15th Symp. On Naval Hydrodynamics*, pages 135–148, 1984.

M.W.C. Oosterveld and P. Van Oossanen. *Further computer-analyzed data of the Wageningen B-screw series*. Netherlands Ship Model Basin, 1975.

K. Ouchi. *Research and Development of PBCF (propeller boss cap fins) to enhance propeller efficiency,* The Motor Ship 10th International Marine Propulsion Conference, London, 1988.

K. Ouchi, M. Tamashima, T. Kawasaki, H. Koizuka. *A research and development of PBCF (propeller boss cap fins) – 2nd report: Study on propeller slipstream and actual ship performance,* Journal of Society of Naval Architects 195, Japan, 1989.

K. Ouchi, M. Tamashima, T. Kawasaki, H. Koizuka. *Research and development of PBCF (propeller boss cap fins) – Novel energy saving device to enhance propeller efficiency,* Naval Architecture and Ocean Engineering 28, Ship and Ocean Foundation, 1992.

M.J. Osborne. A resolution to the NPV-IRR debate? *The Quarterly Review of Economics and Finance*, 50(2):234–239, 2010. ISSN 1062-9769.

C.P. Padhy, D. Sen, and P.K. Bhaskaran. Application of wave model for weather routing of ships in the north indian ocean. *Natural Hazards*, 44(3):373–385, 2008.

N.A. Papadakis and A.N. Perakis. Deterministic minimal time vessel routing. *Operations Research*, 38(3):426–438, 1990.

G. Papalambrou and NP Kyrtatos. Control Development for Smoke Reduction Through Inlet Manifold Air Injection During Transient Loading of Marine Diesel Engines. *ASME*, 2009.

G. Papalambrou, N. Alexandrakis, N. P. Kyrtatos, E. Codan, I. Vlaskos, V. Pawils, and R. Boom. Smokeless Transient Loading of Medium/High-Speed Engines Using a Controlled Turbocharging System. In *25th CIMAC World Congress. Vienna, Austria, May 2007*. CIMAC, 2007.

A. Papanikolaou. *Ship Design, Preliminary design*. Symeon, 1991. ISBN 9607346378.

C.D. Parker. Lead-acid battery energy-storage systems for electricity supply networks. *Journal of Power Sources*, 100(1-2):18–28, 2001.

A. Paxian, V. Eyring, W. Beer, R. Sausen and C. Wright. *Present-Day and Future Global Bottom-Up Ship Emission Inventories Including Polar Routes*, Environmental Science Technology, 44 1333, 2010.

Petromedia LTD. *bunkerworld*. Retrieved March 12, 2010, from http://www.bunkerworld.com , 2010.

R.F. Pocock. Nuclear ship propulsion. 1970.

G. Politis. Ship Resistance and Propulsion. National technical University of Athens, lecture notes, 1991.

C. Ponce de Leon, A. Fr´ıas-Ferrer, J. Gonz´alez-Garc´ıa, DA Sz´anto, and FC Walsh. Redox flow cells for energy conversion. *Journal of Power Sources*, 160(1):716–732, 2006. ISSN 0378-7753.

J. Prousalidis, S.A. Gertsos and C.A. Frangopoulos. Electric Propulsion: from infancy to adolesence. In proceedings of *IMDC 2003: 8th International Marine Design Conference, Athens, 2003*.

J. Prousalidis, IK Hatzilau, P. Michalopoulos, I. Pavlou, and D. Muthumuni. Studying ship electric energy systems with shaft generator. In *Electric Ship Technologies Symposium, 2005 IEEE*, pages 156–162. IEEE, 2005. ISBN 0780392590.

J. Prousalidis, E. Styvaktakis, E. Sofras, IK Hatzilau, and D. Muthumuni. Voltage dips in ship systems. In *Electric Ship Technologies Symposium, 2007. ESTS'07. IEEE*, pages 309–314. IEEE, 2007. ISBN 1424409470.

H. N. Psaraftis and C. A. Kontovas. Balancing the economic and environmental performance of maritime transportation. *Transportation Research Part D 15:* 458–462, 2010.

H.N. Psaraftis and C.A. Kontovas. CO2 emissions statistics for the world commercial fleet. *WMU Journal of Maritime Affairs*, 8(1):1–25, 2009.

H. N. Psaraftis and C. A. Kontovas. *Ship Emissions Study*. Athens: NTUA, LMT, 2008.

D. Radan. Power electronic converters for ship propulsion electric motors. *Department of Marine Technology NTNU*, 2004.

R. K. Rajput. *Engineering thermodynamics: A computer approach (si units version)*. Jones and Barlett, 2009.

G. Rousseau, D. Sinoquet, A. Sciarretta and Y. Milhau. Design Optimisation and Optimal Control for Hybrid Vehicles. *International Conference on Engineering, 2008. EngOpt 08*.

G.D. Rodriguez. Operating experience with the chino 10 mw/40 mwh battery energy storage facility. In *Energy Conversion Engineering Conference, 1989. IECEC-89., Proceedings of the 24th Intersociety*, pages 1641–1645. IEEE, 1989.

C. J. Rydh. Environmental assessment of vanadium redox and lead-acid batteries for stationary energy storage. *Journal of Power Sources,* Vol. 80, pp 21-29, 1999.

N. Salvesen. Second-order steady state forces and moments on surface ships in oblique regular waves. In *Int. Symp. On Dynamics of Marine Vehicles and Structures in Waves, Univ. College, London*, 1974.

P. Schenzle. *Windschiffe im 21sten Jahrhunbert?,* Jahrbuch der Schiffbautechnischen Gesellschaft, Springer, 2010.

N. J. Schouten, M. A. Salman and N. A. Kheir. Fuzzy Logic Control for Parallel Hybrid Vehicles. *IEEE Transactions on control systems technology*. Vol. 10, 2002.

R. Schulze. *SVA - Nabenkappenflossen fur Schiffspropeller,* Report 2218, SVA Potsdam, 1995.

H. Schneekluth. Wake equalising duct*, The Naval Architect 103*, April, pp. 147-150, 1986.

H. Schneekluth and V. Bertram, *Design for Efficiency and Economy,* Butterworth & Heinemann, Oxford, 1998.

D. F. Shanno. On broyden-fletcher-goldfarb-shanno method, *Journal of Optimization Theory and Applications 46*, pp. 87-94, 1985.

K. D. A. Shearer and W.M. Lynn. Wind Tunnel Tests on Models of Merchant Ships. *Trans. NECI*, 76(Part 5): 229–260, 1960.

W. Shi, H. T. Grimmelius, D. Stapersma. Analysis of ship propulsion system behaviour and the impact on fuel consumption, *International Shipbuilding Progress, Vol. 57*, 2010.

C.S.N. Shiau, C. Samaras, R. Hauffe, and J.J. Michalek. Impact of battery weight and charging patterns on the economic and environmental benefits of plug-in hybrid vehicles. *Energy Policy*, 37(7):2653–2663, 2009.

A. Shintani and R. Inoue , Influence of hull form characteristics on propulsive performance in waves. *SMWP*, December, 1984.

SNAME. *Marine Diesel Power Plant Practices*. The Society of Naval Architects and Marine Engineers, 1990. ISBN 960254533X.

B.K. Sovacool. Valuing the greenhouse gas emissions from nuclear power: A critical survey. *Energy Policy*, 36(8):2950–2963, 2008.

LLC Starcrest consulting Group. The port of San Diego 2006 emissions inventory. Technical report, 2008.

R. L. Steigerwald. Power electronic converter technology. *Proceedings of the IEEE* , vol.89, no.6, pp.890,897, 2001 doi: 10.1109/5.931484

J. L. Sudworth. The sodium/nickel chloride (ZEBRA) battery. *Journal of Power sources*, 100(1-2):149–163, 2001. ISSN 0378-7753.

T. M. O'Sullivan, C. M. Bingham and R. E. Clark. Zebra Battery Technologies for the All Electric Smart Car. *International Symposium on Power Electronics. Electrical Drives, Automation and Motion, 2006 SPEEDAM 06*.

D. Sutanto and W. R. Lachs. Battery energy storage systems for sustainable energy development in Asia. *Electric power systems research*, 44(1):61–67, 1998.

J. Szlapczynska and R. Smierzchalski. Adopted isochrone method improving ship safety in weather routing with evolutionary approach. *International Journal Of Reliability Quality and Safety Engineering*, 14(6): 635, 2007.

T. Tarasiuk. A few remarks about assessment methods of electric power quality on ships-Present state and further development. *Measurement*, 42(8):1153–1163, 2009. ISSN 0263-2241.

R. V. Thomson and P. S. Katsoulakos. The Application of Emulsified Fuels in Diesel Engine Designs: Experimental Results and Theoretical Predictions. *Transactions of Institute of Marine Engineers*, 97, 1985.

F. R. Todd, *Series 60 - Methodical Experiments with Models of Single-Screw Merchant Ships*. The David W. Taylor Model Basin, Report 1712. Washington D.C., 1963.

R. L. Townsin and YJ Kwon. Approximate formulae for the speed loss due to added resistance in wind and waves. *Tran. RINA*, 125:199–207, 1983.

R. L. Townsin, B. Moss, J. B. Wynne, and IM Whyte. Monitoring the Speed Performance of Ships. *University of Newcastle, England*, pages 159–177, 1975.

E. Tzannatos. Ship emissions and their externalities for the port of Piraeus-greece. *Atmospheric Environment*, 44(3):400–407, 2010.

UNCTAD. Review of Maritime Transport. In *United Nations Conference on Trade and Development*. United Nations, 2008.

US Army, *Shore protection manual*. Corps of Engineers ; Coastal Engineering Research Center (U.S.) Volume 1, 1984.

J T. B. A. Van Kessels, Energy management for automotive power nets. Eindhoven : Technische Universiteit Eindhoven, 2007 - Proefschrift.

A. Versluis, Computer Aided Design of Ship form by Affine Transformation. *International Shipbuilding Progress*, 24 (274), 147-160, 1977.

DS Vlachos. Optimal ship routing based on wind and wave forecasts. *Applied Numerical Analysis & Computational Mathematics*, 1(2):547–551, 2004.

VLCC Workgroup- F.R. Adolfen, V. Bertram, S. Collins, D. Connoly et al.. *Fuel Saving Options for VLCCs*. 2009.

E. I. Vrettos and S. A. Papathanassiou. Operating policy and optimal sizing of a high penetration RES-BESS system for small isolated grids. *Energy Conversion, IEEE Transactions on*, PP(99):1 –13, 2011. ISSN 0885-8969. doi: 10.1109/TEC.2011.2129571.

R. Wagner. Large lead/acid batteries for frequency regulation, load levelling and solar power applications. *Journal of power sources*, 67(1-2):163–172, 1997.

L. Wang, D.J. Lee, W.J. Lee, and Z. Chen. Analysis of a novel autonomous marine hybrid power gener- ation/energy storage system with a high-voltage direct current link. *Journal of Power Sources*, 185(2): 1284–1292, 2008.

C. Whall, D. Cooper, K. Archer, L. Twigger, N. Thurston, D. Ockwell, A. McIntyre, and A. Ritchie. Quantification of emissions from ships associated with ship movements between ports in the European Community. *Final Report for the European Commision, Entec UK Limited*, 2002.

PA Wilson. A review of the methods of calculation of added resistance for ships in a seaway. *Journal of wind engineering and industrial aerodynamics*, 20(1-3):187–199, 1985.

D. Woodyard. *Pounder's marine diesel engines and gas turbines*. Butterworth-Heinemann, 2009. ISBN 0750689846.

H. Klen Woud, D. Stapersma, Science Institute of Marine Engineering, and Technology. *Design of propulsion and electric power generation systems*. IMarEST, 2003. ISBN 1902536479.

A. A. Wright. *Exhaust emissions from combustion machinery*. Institute of Marine Engineers, 2000. ISBN 1902536177.

GJ Van Wylen and RE Sonntag. *Fundamentals of classical thermodynamics, SI version, 744 pp*. John Wiley and Sons, New York, 1978.

Liangfei Xu, Guijun Cao, Jianqiu Li, Fuyuan Yang, Languang Lu and Minggao Ouyang and Francisco Macia Perez (Ed.). Equivalent Consumption Minimization Strategies of Series Hybrid City Buses, *Energy Management*, ISBN: 978-953-307-065-0, InTech, 2010.

M. Zheng, G.T. Reader, and J.G. Hawley. Diesel engine exhaust gas recirculation–a review on advanced and novel concepts. *Energy Conversion and Management*, 45(6):883–900, 2004. ISSN 0196-8904.

R. Zoppoli. *Minimum-Time Routing as an N-Stage Decision Process*. Institute of Electronics, University of Genoa, Genoa, Italy, 1972.

(Page left intentionally blank)

# Appendix I

In this appendix, the calculation process for specific mathematical models is presented. In addition, mathematical models which were implemented but were not used further in this project are also described.

### Holtrop and Mennen calm water resistance calculations

The total calm water resistance using the Holtrop-Mennen method was given in Chapter 4 by equation (4.1.6). Thus, the components of resistance are given below:

The appendage resistance can be determined from equation (I.1.1)

$$R_{APP} = 0.5 \cdot \rho \cdot V^2 S_{APP} \cdot \left(1 + k_2\right)_{eq} \cdot C_F \tag{I.1.1}$$

where,

$S_{APP}$ : Wetted surface area of appendices [m²]

$C_F$ : Coefficient of frictional resistance of the ship according to ITTC-1957 [-]

The wave resistance $R_W$ is determined according to the Froude number (Fn). Hence, for $F_n$>0.55

$$R_{W-B} = c_{17} \cdot c_2 \cdot c_5 \cdot \nabla \cdot \rho_w \cdot e^{\left(m_3 \cdot F_n^d + m_4 \cdot \cos\left(\lambda \cdot F_n^{-2}\right)\right)} \tag{I.1.2}$$

For $F_n$ <0.4 the following equation is introduced:

$$R_{W-A} = c_1 \cdot c_2 \cdot c_5 \cdot \nabla \cdot \rho_w \cdot e^{\left(m_1 \cdot F_n^d + m_4 \cdot \cos\left(\lambda \cdot F_n^{-2}\right)\right)} \tag{I.1.3}$$

$C_i$ , $m_i$, $\lambda$ are coefficients determined in Holtrop and Mennen (1972) and Holtrop (1984)

For 0.4< $F_n$ <0.55 an interpolation formula is suggested:

$$R_W = R_{W-A0.4} + \frac{\left(10 \cdot F_n - 4\right) \cdot \left(R_{W-B0.55} - R_{W-A0.4}\right)}{1.5} \tag{I.1.4}$$

The additional resistance due to the presence of a bulbous bow near the surface is determined by:

$$R_B = \frac{0.11 \cdot e^{\left(-3 \cdot P_B^{-2}\right)} \cdot F_{ni}^3 \cdot A_{BT}^{1.5} \cdot \rho \cdot g}{\left(1 + F_{ni}^2\right)} \tag{I.1.5}$$

The additional pressure resistance due to the immersed transom is determined by:

$$R_{TR} = 0.5 \cdot \rho_w \cdot V^2 \cdot A_{TR} \cdot c_6 \tag{I.1.6}$$

The model-ship correlation resistance $R_A$ is given by:

$$R_A = 0.5 \cdot \rho_w \cdot V^2 \cdot S \cdot C_A \tag{I.1.7}$$

**Hydrodynamic induced loads calculations**

If the propeller is assumed as an actuator disk of known diameter and area, which is advancing over an undisturbed fluid at speed $V_o$, the speed at the rudder, whose leading edge is at distance X downstream of the propeller disk, can be determined by:

$$T = \rho \cdot A_1 \cdot V_1 \cdot \left(V_2 - V_0\right) \tag{I.2.0}$$

$V_O$ : Undisturbed fluid speed at propeller [m/s]
$V_1$ : accelerated speed at the propeller disk [m/s]
$V_2$ : accelerated speed downstream of propeller disk [m/s]

By applying the Bernoulli equation and by arranging appropriately (I.2.0), it can be said that:

$$\frac{2 \cdot T}{\rho \cdot A_1} = \frac{8 \cdot K_T}{\pi J} \cdot V_0^2 \tag{I.2.0}$$

The Velocity $V_2$ can be calculated using:

$$V_2 = \sqrt{\frac{8 \cdot K_T}{\pi} \cdot n^2 \cdot D^2} \tag{I.2.0}$$

While $V_1$ equals to:

$$V_1 = \frac{V_0 + V_2}{2} \tag{I.2.0}$$

Molland and Turnock (2007) propose a Guetsche type correction to $V_1$ to account for the flow acceleration between the propeller and the rudder. The rudder velocity is noted as $V_{RR}$. Thus, the correction for the rudder velocity, which takes into account the distance from the propeller, is determined by:

$$K_R = 0.5 + \frac{0.5}{\left(1 + \left(\frac{0.15}{X / D_p}\right)\right)} \tag{I.2.0}$$

X : Distance between rudder and propeller

Finally, the rudder velocity is found using (I.2.0)

$$V_{RR} = V_0 \cdot \left(1 + K_R \cdot \left(\sqrt{\left(1 + \frac{8 \cdot K_T}{\pi \cdot J^2}\right)} - 1\right)\right) \tag{I.2.0}$$

**Miscellaneous calculations for double screw vessels**

The wake, thrust deduction and relative rotation propulsion coefficients for double screw vessels are presented here. The thrust deduction factor is approximated using the following the expressions of Holtrop and Mennen (1981) and SSPA laboratory, which have better accuracy versus the actual coefficients of other approximations found in the literature. Consequently,

$$t = 0.325 \cdot C_B - 0.01885 \cdot \frac{D}{\sqrt{B \cdot T}} \tag{I.3.1}$$

$$t = w \cdot \left(1.67 - 2.3 \cdot \frac{C_B}{C_{WP}} + 1.5 \cdot C_B\right) \tag{I.3.2}$$

The wake coefficient is approximated by Holtrop and Mennen (1981) and Kruger (1976), respectively. Thus,

$$w = 0.3095 \cdot C_B + 10 \cdot C_V \cdot C_B - 0.23 \cdot \frac{D}{\sqrt{B \cdot T}} \tag{I.3.3}$$

$$w = 0.81 \cdot C_B - 0.34 \tag{I.3.4}$$

The relative rotation efficiency is calculated by the formula proposed by Holtrop and Mennen (1981).Therefore,

$$\eta_R = 0.99737 + 0.111 \cdot (C_P - 0.0225 \cdot lcb) - 0.06325 \cdot \frac{P}{D} \tag{I.3.5}$$

**Wind Generation parameters**

The wind model is a four-component model and is given by (4.8.10).The following equations describe each subcomponent of (4.8.10).

The base wind component ($V_{WB}$) is a constant number. This component is assumed to be always present when the Beaufort number exceeds 3.

The gust wind velocity component is described by the equation:

$$V_{WG} = \begin{cases} 0 & t < T_{1G} \\ V_{\cos} & T_{1G} < t < T_{1G} + T_G \\ 0 & t > T_{1G} + T_G \end{cases} \tag{I.4.1}$$

where,

$$V_{\cos} = \frac{MX_G}{2} \cdot \left( 1 - \cos\left( 2 \cdot \pi \left( \frac{t}{T_G} - \frac{T_{1G}}{T_G} \right) \right) \right) \tag{I.4.2}$$

The wind bust model is considered an essential component of wind velocity for dynamic studies (Anderson et al. 1983), especially when investigating transient loads.

The ramp wind velocity component is described by the equation:

$$V_{WG} = \begin{cases} 0 & t < T_{1R} \\ V_{ramp} & T_{1R} < t < T_{2R} \\ 0 & t > T_{2R} \end{cases} \tag{I.4.3}$$

where,

$$V_{ramp} = MX_R \cdot \left(1 - \frac{\left(t - T_{2R}\right)}{\left(T_{1R} - T_{2R}\right)}\right) \tag{I.4.4}$$

It should be noted that $T_{2R}>T_{1R}$.

The final wind velocity component is a random noise component, which is defined by:

$$V_{WN} = 2 \cdot \sum_{i=1}^{N} \left(\sqrt{\left(s_V \cdot \omega_i \cdot \Delta\omega\right)} \cdot \cos\left(\omega_i \cdot t + \varphi_i\right)\right) \tag{I.4.5}$$

where,

$$\omega_i = \left(i - \frac{1}{2}\right) \cdot \Delta\omega \tag{I.4.6}$$

Thus,

$$s_v\left(\omega_i\right) = \frac{2 \cdot K_N \cdot F_T{}^2 \left|\omega_i\right|}{\pi^2 \cdot \left(1 + \left(\frac{F_T \cdot \omega_i}{\bar{u}_w \cdot \pi}\right)^2\right)^{(4/3)}} \tag{I.4.7}$$

The surface drag coefficient ($K_N$) equals 0.004, the Turbulence scale factor ($F_T$) equals 2000. The following parameters have been attained from empirical data but, according to Anderson et al. (1983), they provide results of excellent accuracy when used. Thus, the sampling rate should be equal to at least 50 and the Δω ranging from 0.5 – 2.0 rad/s.
The wind noise component equation can be replaced using a Gaussian white noise generator. White noise has been used in sea wave modelling, offering pseudo-realistic conditions and not smooth and/or perfect representations of the actual sea environment.

# Appendix II

This appendix contains tabular data which area applicable to conventional Diesel installation. Detailed tables of equipment located into a conventional engine room are presented in Appendix Table 3. This information is of vital importance to assess the constructional feasibility of the Hybrid system which is presented in Chapter 3.

**Appendix Table 1: Electric Components in E/R of a modern cruise ship**

| No | Component | Installed No | Volume | Weight |
|---|---|---|---|---|
| 1 | Propulsion Transformers type I | 4 | 159.94 | 47200 |
| 2 | Component | 1 | 6.48 | - |
| 3 | Propulsion Converter type II | | | |
| 4 | Component 1 | 2 | 18.30 | 23600 |
| 5 | Component 2 | 2 | 41.47 | - |
| 6 | Component 3 | 2 | 49.28 | 23600 |
| 7 | Component 4 | 2 | 33.28 | - |
| 8 | Propulsion Converter type I | | | |
| 9 | Component 1 | 1 | 27.66 | - |
| 10 | Component 2 | 2 | 65.28 | 23600 |
| 11 | Component 3 | 1 | 26.93 | - |
| 12 | Component 4 | 1 | 16.64 | - |
| 13 | Engine Transformers type II | 2 | 28.56 | 11600 |
| 14 | Component 1 | 1 | 3.60 | 557 |
| 15 | Engine Transformers type I | 3 | 69.12 | 24000 |
| 16 | Component 1 | 1 | 3.60 | 557 |
| 17 | Main Switchboards | 1 | 104.40 | 3300 |
| 18 | Secondary Switchboard 1 | 1 | 35.28 | 684 |
| 19 | Secondary Switchboard 2 | 1 | 56.88 | 275 |
| 20 | Motor Load Control | 2 | 12.672 | - |
| 21 | Electric Motors | 2 | 274.56 | 300000 |
| | SUM: | | 1033.94 | 458.98 |

**Appendix Table 2: Comparison of propulsion technologies**

| Arrangement Components | Conventional 2-stroke Diesel | Hybrid Diesel-Electric System - All Electric Ship |
|---|---|---|
| Prime Mover | 2-stroke Marine Diesel Engine | 4-stroke Marine Diesel Generator sets |
| Auxiliary Power | 3 4-stroke generator sets, 1 emergency | Covered by the main propulsion unit (Fully electrified vessel) |
| Components | Shaft generator (if Applicable), Shafts and bearings | Marine type electric cables, Transformers, Converters/ inverters (motor speed control), Rectifiers (Storage system existence), Electric motors |
| Propulsor and manoeuvrability | Large diameter Fixed Pitch propeller, steering gear | FP propeller(s), CP propeller(s) with steering gear or Podded Propulsor (no steering gear) |

**Appendix Table 3: Weight, volumes of machinery equipment, tanks and rooms in engine room for 2-stroke Diesel propulsion system**

| No | Component | Installed No | Volume [$m^3$] | Weight [Kg] |
|---|---|---|---|---|
| 1 | Main Engine | 1 | 436.48 | 255000 |
| 2 | Auxiliary Engine | 3 | 94.88 | 6030 |
| 3 | A/C refrigeration Unit Acom. | 1 | 3.31 | N/A |
| 4 | Auxiliary air Reservoir | 1 | 0.45 | 218 |
| 5 | Bilge & Fire | 1 | 5.20 | N/A |
| 6 | Cabinet solenoid Valve | 1 | 0.20 | N/A |
| 7 | Central Cooler | 1 | 13.13 | 1858 |
| 8 | Compressors & Pumps General | 20 | 27.30 | 3097 |
| 9 | Control air Compressor | 1 | 3.02 | 700 |
| 10 | Deck Service air Compressor | 2 | 6.05 | 700 |
| 11 | Deck Service air Reservoir | 1 | 1.34 | 446 |
| 12 | DO Trans. P/P | 1 | 0.11 | N/A |
| 13 | Drain Cooler with Tank | 1 | 7.20 | N/A |

| | | | | |
|---|---|---|---|---|
| 14 | Drink Hydrophore Unit | 1 | 2.04 | N/A |
| 15 | Emergency air Compressor | 1 | 1.34 | 300 |
| 16 | Fresh Water Generator | 1 | 4.38 | 595 |
| 17 | Fresh Water Hydrophore Unit | 1 | 3.00 | N/A |
| 18 | FWD Seal | 1 | 0.44 | N/A |
| 19 | HFO Trans. P/P | 1 | 0.46 | N/A |
| 20 | Hot water Calorifier | 1 | 3.51 | 300 |
| 21 | Hyd Power Pack | 1 | 1.53 | 60 |
| 22 | Jacket Water cooler D/G | 3 | 0.79 | N/A |
| 23 | LO Purifier | 1 | 9.58 | 242 |
| 24 | LO Purifier Feed Pump | 2 | 0.19 | N/A |
| 25 | LO Trans Pump | 1 | 0.08 | 38 |
| 26 | Local fire P/P | 1 | 0.45 | N/A |
| 27 | M/E & G/E FO Supply Unit | 2 | 31.00 | 220 |
| 28 | M/E J.W. Pre-heater | 1 | 0.31 | 200 |
| 29 | M/E Jacket F.W. Cooler | 1 | 0.19 | 319 |
| 30 | M/E Jacket Water Pump | 1 | 0.94 | 115 |
| 31 | M/E LO Cooler | 1 | 4.70 | 3820 |
| 32 | Main air Compressor | 1 | 0.96 | 480 |
| 33 | Main Air Reservoir | 2 | 15.87 | 4530 |
| 34 | Main Central CFW P/P | 3 | 0.94 | 1764 |
| 35 | Main CSW P/P | 1 | 6.00 | 320 |
| 36 | Oily Water Separator | 1 | 8.75 | 650 |
| 37 | Oily Water Separator P/P | 1 | 0.06 | 65 |
| 38 | Purifier | 1 | 49.03 | 1410 |
| 39 | Ref. Prov. Plant | 1 | 1.57 | N/A |
| 40 | Sewage System | 1 | 10.00 | N/A |
| 41 | Shaft & Bearings | 1 | 21.68 | 29945 |
| 42 | Composite Boiler | | 3.00 | 20000 |
| COMPARTMENTS INSIDE E.R. | | | | |
| 42 | Control Room | 1 | 469.46 | N/A |
| 43 | Engine Room Store | 1 | 606.16 | N/A |
| 44 | Engine Room Workshop | 1 | 417.30 | N/A |
| TANKS INSIDE E.R.* | | | | |
| 45 | DO SERVICE | 1 | 33.00 | 35.6 |
| 46 | DO SETTLING | 1 | 39.50 | 29.7 |

| | | | | |
|---|---|---|---|---|
| 47 | HFO SERVICE | 1 | 42.30 | 38.7 |
| 48 | HFO SETTLING | 1 | 42.30 | 40.8 |
| 49 | HFO STORAGE 4 P | 1 | 254.80 | 245.9 |
| 50 | HFO STORAGE 4 S | 1 | 419.30 | 404.8 |
| 51 | SLUDGE | 1 | 12.30 | Depended |
| 52 | L/S FO SERVICE | 1 | 40.10 | 38.7 |
| 53 | L/S FO SETTLING | 1 | 40.10 | 38.7 |
| 54 | CYLINDER OIL STORAGE | 1 | 70.30 | 62 |
| 55 | G/E LO STORAGE | 1 | 29.60 | 26.1 |
| 56 | M/E LO STORAGE | 1 | 36.80 | 32.4 |
| 57 | M/E LO SETTLING | 1 | 29.60 | 26.1 |
| 58 | GRAY WATER TANK | 1 | 26.40 | Depended |
| SUMMATION (items marked with * not accounted) | | | 6301 | 334 |
| Engine Room Free Volume: | | | 2910m$^3$ | |

# Appendix III

This appendix elaborates on the statistical approximation of the energy storage requirements using the same procedure as presented in Chapter 3.

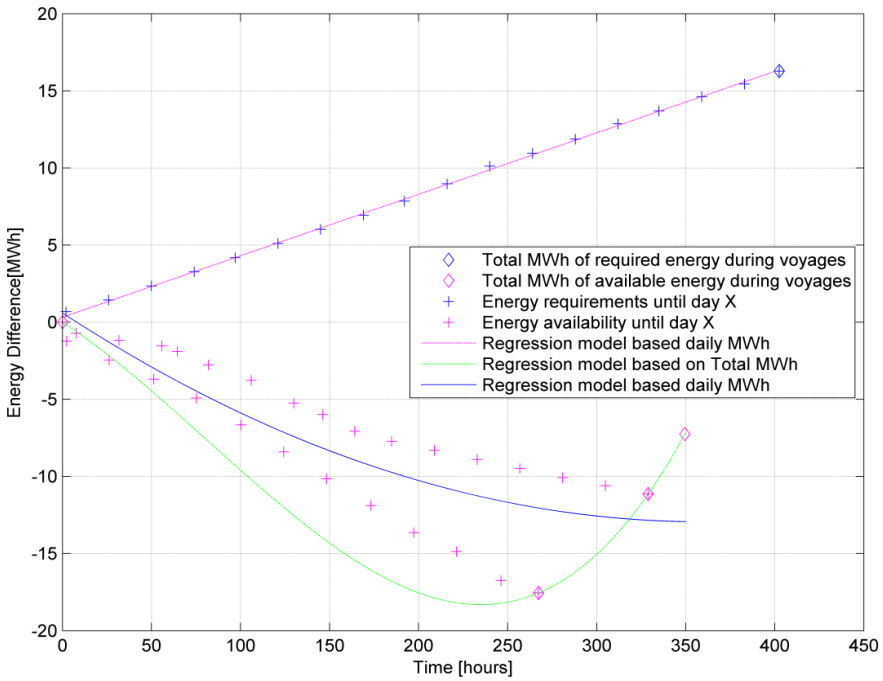


**Appendix Figure 1: Energy profile regression analysis for Handysize type**

As a result, Appendix Figure 1 presents the regression analysis for the Handysize bulk carriers, Appendix Figure 2 for the handymax type, Appendix Figure 3 for the Panamax type and Appendix Figure 4 for the capsize bulkers. For the Post-Panamax category, the result is presented with detailed explanation in Chapter 3.

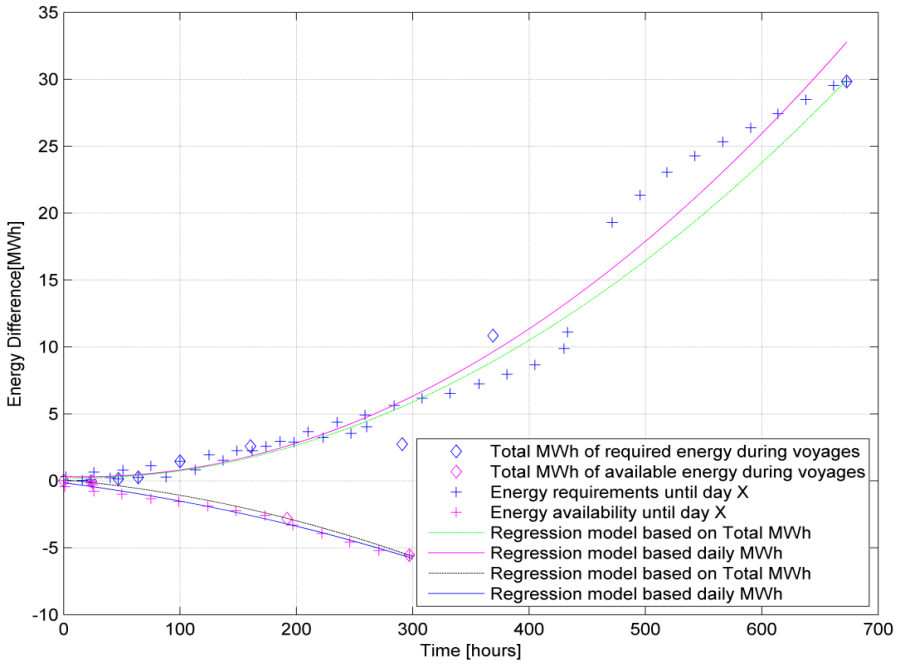


**Appendix Figure 2: Energy profile regression analysis for HandyMax type**

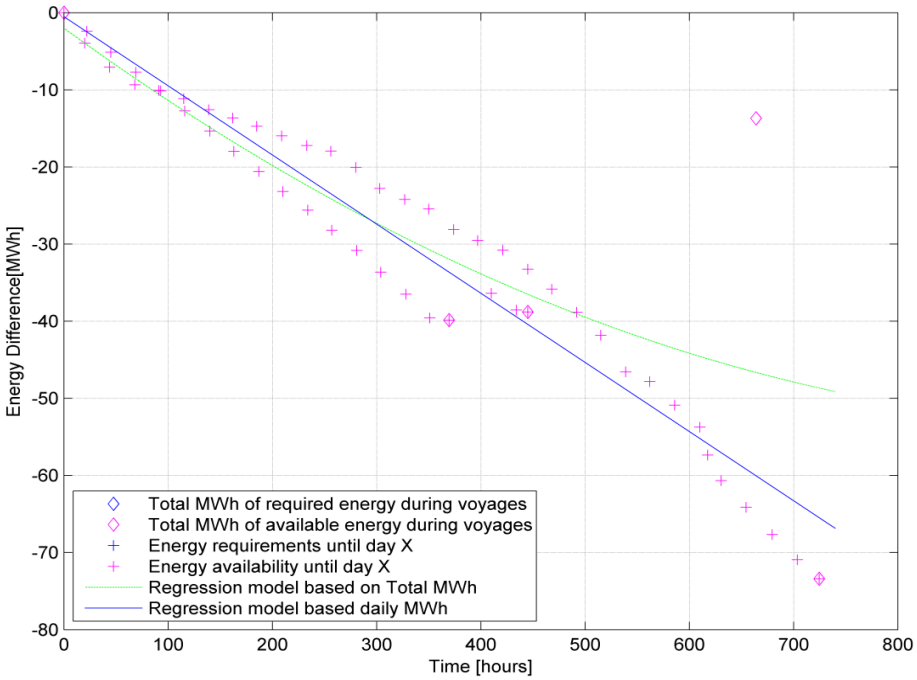


**Appendix Figure 3: Energy profile regression analysis for Panamax type**

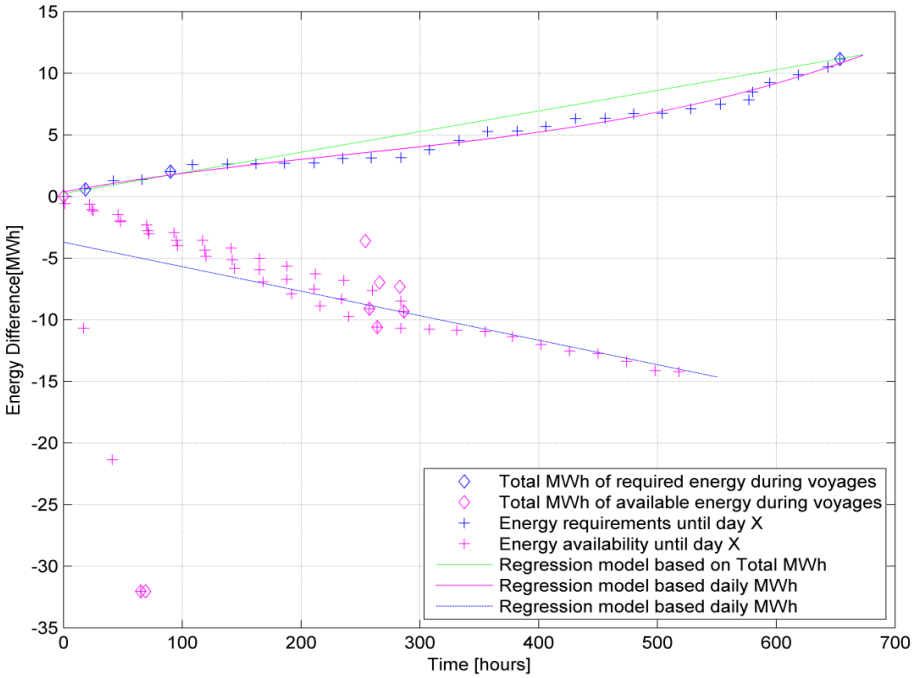


**Appendix Figure 4: Energy profile regression analysis for Capesize type**

# Appendix IV

Currently there are 600 nuclear reactors in service globally, of which one third are marine applications, all but a few military based. Nuclear propulsion has many potential advantages in terms of reduced emissions, as nuclear fission itself has zero $CO_2$, $NO_x$, $SO_x$ and PM emissions, although the overall nuclear fuel cycle has a certain amount of emissions associated with it. The energy in nuclear propulsion originates from the released energy of the fission of $^{235}U$ which arises from the kinetic energy of the charged fission fragments, the gamma rays due to fission, the subsequent beta and gamma decay and the energy of neutrinos (Lamarsh and Baratta, 2001). No chemical reactions as in hydrocarbons occur and the energy is considered clean and carbon free in terms of operation. Nevertheless, emissions occur through plant construction, Uranium mining and milling and plant decommissioning. Although no large fleet of nuclear powered vessels exists as yet, an assessment is required to compare fossil fuel direct emissions with nuclear lifecycle indirect emissions.

The possible environmental impact of nuclear powered vessels (submarines or merchant and naval surface ships) requires assessment; it is noted, however, that a number of submarine accidents have occurred and no nuclear major contamination has been reported (Pocock, 1970). In May 2011, a Russian icebreaker reported excess of radioactivity. IAEA categorised the event at scale 0 (IAEA: news centre, 2011). In stationary nuclear power plants though, severe accidents have occurred the last decades. The most severe of all was the Chernobyl disaster in 1986, which led to deaths due to radiation and environmental contamination. The most recent accident happened in 2011 in Fukushima, Japan. The latter has not led to deaths related to radioactive release until the present day. Based on the official reports so far, in terms of radioactive release, the Fukushima situation can be compared to the Three Mile Island accident in the United States in 1979. Nevertheless, there is a significant difference between naval nuclear and civil nuclear applications. This difference is the output power and the size of the plant, which, in marine applications, the nuclear reactor is considered a propulsion unit of maximum thermal power of 100MW and not an electric generation plant of several hundreds of GW with multiple nuclear reactors.

In terms of radioactivity, in PWR designs (where small modular reactors (SMR) are part of that category), the safety system must protect the three barriers to release of radioactivity: the fuel cladding, the primary cooling circuit and the containment. It is an obvious risk that ship is a small system, the danger being that there might be an exposure to radioactive material by radiation or by inhalation of particles. Based on extensive design experience derived from more than 800 years of PWR operation, this risk in modern

reactors that operate under normal conditions is considered low (DNV, 2010). In the case of a ship, the containment compartment is shielded and protected with double bulkheads, double bottom and double skin in case of collision and grounding. The probability of collision to the amidships is increased compared to the stern. Unfortunately, there is a trade-off between the risk of exposing the reactor to high accelerations and the risk of collision and potential breach of the containment compartment.

The safe operation of ships requires the availability of propulsion power, steering capability, navigation, and auxiliary power generation. Currently, this is mainly secured by ensuring that each component complies with the general standards, having enhanced reliability and performance. In nuclear powered ships, due to the high initial cost of the reactor, it is believed that only one nuclear reactor providing enough output for the propulsion and auxiliary loads will be installed. In case of a reactor failure, a back-up propulsion system should be fitted, to ensure that the ship can return safely to a convenient port and all the emergency functions can run. A combination of diesel generator and batteries is the suitable solution. Although Diesel generators can provide enough power to propel and provide enough electricity for cooling the decay heat of the reactor, as in land based power plants, a second back-up system is required. Integrating the solution of Hybrid Nuclear, batteries seem to offer both load levelling in terms of demand, and can offer at the same time a back-up system in case of total failure. Furthermore, for a nuclear powered ship, the energy storage coupling is also investigated for optimisation of the secondary steam generation plant, which affects the overall efficiency of the turbo-generators or of the propulsion turbines. The mechanical efficiency of the turbo-generators and the turbine isentropic efficiency depends on the pressure ratio and hence the power loading of the component (Rasjput, 2009). As a result, the objective of load levelling practice is transformed from GHG reduction to nuclear fuel burn-up reduction in order to increase the refuelling interval.

Regarding the safety of the nuclear reactors, the basic principles to design the secondary safety systems are diversity (different principles of operation), redundancy (multiple components and systems to guard against the individual failure of components), and independence (systems have to be physically separated); they must be failsafe and testable (tested without disrupting operation, or with redundancy). Modern reactor designs are always under-moderated and they operate with a negative reactivity coefficient. In case of rapid or extreme load change, turbine failure or loss of primary coolant, the reactor will self-shut down to avoid damage. In terms of the ship accelerations imposed on the reactor, the designer has to calculate the operational margins and match the design with the operational profile of the ship.

In the last few decades, terrorist attacks and nuclear major accidents in Chernobyl and Fukushima have ensured a general public awareness of the potential hazards associated with the use of nuclear power. In shipping, another aspect arises as harbours are usually located close to areas of large population density. Although the risk of terrorist threat may be limited in secured ports, and the low enriched Uranium (LEU which contains <20% of $^{235}U$) fuel is not suitable for nuclear weapons, still the political implications and the general public opinion is believed to be against nuclear powered ships entering the harbours. Hence, at least initially, the ship types which seem attractive are bulk carriers and tankers. They are capable of loading /unloading away from the shore and, as shown in , share a significant proportion of $CO_2$ emissions. Furthermore, due to the high initial cost which is 2.5 times the cost of conventional vessels, the HFO consumption of these ships should be high to justify a radical change in ship design (DNV, 2010).

Implications arise concerning the operation of nuclear vessels. Firstly, not all ports can accept these vessels. Secondly, transatlantic or transpacific voyages, during which usually large vessels operate as liners, decrease the flexibility for chartering. Thus nuclear powered vessels with port restrictions obstruct free economy.

Furthermore, the construction and repairs of such ships is limited to licenced shipyards, which, again, bound the economy and potentially the construction and repair cost would remain high due to the lack of competition.

The manning and operational costs of such vessels are still an issue. Nuclear ships will require fully qualified and thus expensive personnel on board. The rest of the crew can be as it is currently. However, specialised crew increases the operational cost of the vessel.

From the shipping company view, the daily performance monitoring of the fleet and the maintenance surveying that superintendent engineers perform in dry-dockings should change. Superintendent engineers have to attend continuing professional development (CPD) courses in nuclear engineering so they can understand the principles of operation and, of course, be aware of and able to identify any failures in materials caused by radioactive exposure. Nevertheless, small modular reactors can be considered as black boxes and might be property of the developing company, so no company engineers have to attend such an inspection but rather, as in the early days of radio, the nuclear company would provide the operators.

**Appendix Table 4: Global fleet (until 2007) and power trends per vessel category**

| Dry Bulk Carriers | Number of Vessels | Specified MCR up to [kW] |
|---|---|---|
| Small and Coastal | 753 | 2,860 |
| Handysize | 1,774 | 7,780 |
| Handymax | 1,732 | 10,600 |
| Panamax | 1,383 | 12,200 |
| Post – Panamax | 98 | 15,200 |
| Capesize >120.000 | 722 | 18,660 and 21160 for VLBC |
| Total: | 6,462 | |
| | | |
| **Container Vessels** | **Number of Vessels** | **Specified MCR up to [kW]** |
| Feeder – Feedermax | 1,120 | 8,500 |
| Handysize | 1,143 | 21,500 |
| Sub-Panamax | 689 | 30,000 |
| Panamax | 568 | 47,000 |
| Post-Panamax | 712 | 78,000 |
| New Panamax | - | 91,000 |
| ULCV | - | 106,000 |
| Total: | 4,232 | |
| | | |
| **Oil Tanker Vessels** | **Number of Vessels** | **Specified MCR up to [kW]** |
| Small | 115 | 3,840 |
| Handysize-Handymax | 240 | 8,800 HS and 10,600 HM |
| Panamax | 177 | 12,100 |
| Aframax | 648 | 16,000 |
| Suezmax | 332 | 18,700 |
| VLCC/ ULCC >200,000dwt | 516 | 30,000 and 44,000 |
| Total: | 2,028 | |

The limitations that currently seem to exist in nuclear merchant shipping dictate that a potential ship-owner has to be willing to be the first mover, to have a strong financial position and decide that this potential is going to be a long term investment. Due to the fact that the acceptance of a ship might be limited and hence trade restrictions might occur, the ship-owner must be willing to accept the high risks of an unknown territory. However, in case of success, the benefits of the prime mover can be significant.

Traditional P&I clubs cover third-party liability in case of accidents. When having a nuclear fleet, a new trust would probably be required to cover any radiological pollution that might occur after a serious accident. It can be said that the situation will be volatile and a lot of steps are required before the actual operation of nuclear powered merchant vessels can occur.

Finally, the spent fuel of global nuclear powered shipping should be considered. PWR designs create hazardous depleted fuel. In terms of fuel economy, the worst thing to perform is to bury the depleted fuel. The study of Deutch et al. (2003) showed that the discovered Uranium resources are sufficient for the next 70 years, without accounting for

the potential of nuclear shipping demand. Therefore, fuel recycling has to begin before any nuclear renaissance. Technological improvements in fast reactor technology (Lamarsh and Baratta, 2010) should allow the depleted fuel to be re-used, and thus the nuclear fuel cycle can close and the actual burnt fuel can breed more, providing practically unlimited fuel for 1500 years. However, with the technology currently available, it would take almost 40-50 years to breed more fuel.

The nuclear propulsion renaissance involves a new type of nuclear reactor. The Small Modular Reactor (SMR) and all the secondary circuits are contained into a closed to crew box of known and small dimensions, which potentially equal the dimensions of a Fifty feet (FEU) container. This reactor type has higher enrichment than the Pressurised Water Reactor that is still used in naval applications. Its output is initially set to 25 MWe, which, according to Appendix Table 5 can fit almost all categories if more than two reactors are installed.

Because an SMR is still under design for marine applications, it can be assumed that due to the assembly materials and their decreased volume, the associated emissions are the lowest reported for Nuclear installations (Sovacool, 2008), a fact that makes the nuclear potential attractive right from the beginning.

To summarise all the above, the research project aims to reduce air emissions from global shipping using a Hybrid Power concept, which consists of high efficiency batteries, electric generators and a slow speed Diesel engine. Although the all-electric ship concept was investigated, efficiency issues made the solution for slow speed vessels unattractive. The nuclear potential of a pusher barge system is also investigated in terms of machinery sizing and efficiency. This thesis is accompanied by a ship simulator, which incorporates multiple optimisation algorithms for calculation of savings, if any, in fuel consumption, which are dependent on given operational scenarios.

The simulation offers an assessment tool for ship energy efficiency, of optimal routing and of decision support for the operations department of the maritime companies. Moreover, it is a tool for the shipping company's technical department to control the deterioration of the performance of their fleet. Finally, the structural and financial feasibility of the hybrid system is demonstrated and thus the alternative system proposal is validated in terms of most design aspects.

In the short history of nuclear power, many types of reactors have been proposed for civil and naval applications. Power reactor systems consist primarily of five types of reactors. The first and most commonly used category is that of light water reactors. Pressurised water (PWR) and boiling water reactors are well-established light water designs. The second category includes gas-cooled reactors, the third fast reactors and the fourth evolutionary pressurised water or boiling water reactors. Recently, a fifth category

of small modular reactors (SMR) was introduced. Modular reactors are designed by Mitsubishi, Toshiba and Hyperion Energy. Especially for the Hyperion Energy design, the principal characteristics are found in Appendix Table 5.

**Appendix Table 5: Small Modural Reactor principal characteristics**

| |
|---|
| Reactor Power: 70$MW_{thermal}$ |
| Electrical output : 25$MW_{electrical}$ |
| Lifetime: 8 - 10 years |
| Size: 1.5m w by 2.5m h |
| Weight: Less than 50tons including pressure vessel, fuel and primary coolant LBE |
| Structural material : Staineless steel |
| Coolant: PbBi |
| Fuel: Stainless clad, uranium nitride ($U_2N_3$) |
| Enrichment: %U-235 less than 20% |
| Refuel on site: No |
| Sealed core: Yes |
| License : Design certification |
| Passive shutdown : yes |
| Active Shutdown: Yes |
| Transportable : Yes; intact core |
| Factory fuelled : Yes |
| Safety and Control Elements: 2 redundant shutdown systems & reactivity control rods |

Not every design is feasible for marine applications, however, except PWR design which is dominant category in naval vessels (aircraft carriers and submarines); fast reactors are present in the navy of Russia. Currently, concept designs for vessels equipped with SMR are underway as well. So as to have a clear picture of reactor designs, a comparison of characteristics is made. It will be based on the several operation parameters and on efficiency. The first and most important is the burn-up. This term describes the energy produced per unit of mass fuel [GWdays/tonne]. A typical value of a PWR design is 45000 GWdays/tonne compared to a gas fired boiler which is 0.4 GWdays/tonne. The second parameter is the thermal to electrical efficiency. This efficiency comprises the steam generator efficiency and the electric generator efficiency, which varies according to the load. Other important parameters for the consumption of fuel are the operating temperatures and pressures. Appendix Table 6 contains a comparison of civil reactor

designs in general. In marine applications, as previously mentioned, PWR and fast Reactors have already been installed on naval vessels. Gas reactors, despite their high efficiency and operating temperatures, are not viable due to their low power density. Advanced boiling water reactor (BWR) designs should however be investigated in the future.

**Appendix Table 6: Characteristics of civil reactor commercial designs (Pocock, 1970; HMS-Sultan, 2008)**

| Reactor Type | PWR | BWR | MAGNOX | AGR |
|---|---|---|---|---|
| Fuel | 3% LEU | 2.2% LEU | Natural Uranium | 2% LE $UO_2$ |
| Cladding | Zircalloy | Zircalloy | Magnesium alloy | St. Steel |
| Moderator | Light Water | Light Water | Graphite | Graphite |
| Coolant | Light Water | Light Water | Carbon dioxide | Carbon Dioxide |
| Outlet Temp. | 318 | 318 | 360 | 620 |
| Steam Temp. | 285 | 286 | 345HP 330LP | 540 |
| Steam Pressure | 69 | 75 | 150 | 40HP 11LP |
| Efficiency | 32% | 32% | 33% | 42% |
| Power Density | High | High | Low | Low |
| Burn-up | High | High | Low | Low |

Light water reactors consist of a pressure vessel, where the nuclear fuel, the control rods and the moderator are present. The moderator is responsible for slowing the fission neutrons, which increases the probability of the latter hitting another fuel atom core and sustaining the fission. A good moderator should be cheap, should have a small absorption cross sectional area so not to scatter the nuclei, and be chemically compatible with the core materials. In light water reactors, the moderator also acts as a coolant. Therefore, it should have good heat transfer capability and, over the range of operational and fault temperatures, should have well-defined thermal properties. The main difference between a boiling water reactor and a pressurised water reactor is the existence of a secondary steam cycle. In PWR such a circuit exists. The steam is produced by steam generators and the heat transfer occurs into a heat exchanger inside the reactor compartment. The temperature at the primary circuit is on average at 325$^{o}$C and the pressure is kept at 155 bar to prevent the water from boiling, thus changing phase. Single-phase coolant reassures the undisturbed heat exchange of the primary circuit. On the other hand, boiling water reactors do not have a secondary steam cycle. The coolant boils and

then passes through an expander (turbine), which produces torque. No containment structure is present as in PWR designs. Furthermore, the dangerous instabilities of the two-phase condition of the coolant are avoided at high pressures. This means that the design is robust. There are obvious advantages to BWR reactors. As is known, for a given amount of water, more heat can be absorbed as latent heat (heat necessary to vaporise a liquid) than as sensible heat, which only changes the coolant temperature. However, the water is contaminated and the turbine should be shielded. Furthermore, the power density of a BWR is lower than a PWR, necessitating the existence of thicker and larger pressure vessel. Similar to the BWR concept, the RMBK type (Soviet design) utilised graphite as a moderator and did not have a pressure vessel (Lamarsh and Baratta, 2001).

Fast reactors or Breeder Reactors differ on the principle of operation and fuel type. Thermal reactors utilise enriched fuel and consume $^{238}U$ while in operation. However, Ansolabehere et al. (2008) state that Uranium reserves are depleting, thus technology for recycling depleted fuel and breeder technology is investigated. A fast reactor is found in four types: the liquid metal cooled breeder reactor (LMFBR), the gas-cooled breeder reactor (GCFR), the molten salt breeder reactor (MSBR) and the light-water breeder reactor (LWBR). The principle behind the operation is to fuel the reactor with isotopes of plutonium as core, and the blanket to be natural or depleted Uranium and breed 'fresh' fuel. The number of fission neutrons emitted per neutron absorbed by Plutonium increases monotonically with increasing neutron energies above 100 keV. Thus, no moderator is present and the effort is to sustain the velocity of neutrons. The breeder ratio and breeding gain increase with the average energy of the neutron, including fission in the system (Lamarsh and Baratta, 2001).

Gas cooled reactors, fed by natural Uranium and graphite moderated, were constructed in US, UK and France for conversion of $^{238}U$ to $^{239}Pu$ for military purposes. They formed the base of nuclear civil applications in nations without access to enrichment facilities. The coolant is mainly $CO_2$, which as a gas can operate at high temperatures, increasing the thermal efficiency, which can reach 40%. The steam is superheated compared to the previous mentioned designs, and their characteristics are an average temperature of $540^{O}C$ and pressure of approximately 160 bar. However, the gas has poor heat transfer properties and requires higher surface to exchange the same amount of heat, thus the energy density is low compared to PWR or BWR designs. Furthermore, $CO_2$ is susceptible to leakage, is compressible, hence it requires more pumping power and has negligible moderating properties due to the tremendously low density (Abram, 2011).

The Small Modular Reactor (SMR) is more like a nuclear battery than a reactor propulsion layout. It has a 36% thermal to electrical efficiency, competitive to the European Pressurised Reactor (EPR) design of the French Areva company. These reactors

are modular, can fit into a twenty-foot container (TEU) and weigh approximately two tonnes per installed MWe. The fuel is LEU.

The marine environment is dynamic with continual variation in load applied to the vessel structure with resultant motions. Unlike commercial nuclear power plants, marine nuclear reactors must be rugged and resilient enough to withstand several decades of rigorous operations at sea, subject to a ship's pitching and rolling and rapidly changing demands for power, keeping the vessel speed close to that required by the operator. These conditions, combined with the harsh environment within a reactor plant, which subjects components and materials to the long-term effects of irradiation, corrosion, high temperatures and pressures, necessitate an active, thorough and far-sighted technology effort to verify reactor operation and enhance the reliability of operating plants. A nuclear reactor is a device that should not operate under non-stable structural conditions. The nuclear reactor should be placed near the amidships where the longitudinal centre of buoyancy is found at design or scantling draft. The reactor compartment has to be shielded and protected from groundings, collisions and impacts. The attractive characteristics of the SMR reactor are that the coolant circuit operates with atmospheric pressure, thus there is no sloshing effect caused by the vessel motions. And the reactor operation remains undisrupted.

Unlike other shore-based electric generator plants, the marine reactor has to operate at continuous fluctuating load. Depending on the sea state, a rise of total resistance may lead to a power change of ~10%. Moreover, if the fluctuation of required loading exceeds 5%, the nuclear reactor is not capable of serving the energy demand for safety issues. If this is the case, the vessel inevitably has to reduce speed. For the peak auxiliary loads, there is no direct problem with the nuclear operation, as they share a very small percentage of the total installed power, hence the peak effects are negligible. Although the rapid load change, which does not exceed 5% at a small time step, is the least important aspect in modern nuclear reactors in respect of accident probability, because designs are under-moderated and have always negative temperature coefficient, the operation of turbo-machinery in non-optimum conditions increases the fuel consumption whether the fuel is a HFO or nuclear. Despite the fact the Uranium price has been constant in the last decades, with the exception of recent problems in mines of Canada which actually increased the price of $^{238}U$ up to four times, it is important to have fully optimised and the least energy intensive systems from the early design stage. Minimising fuel usage will either reduce or even completely remove the need for through life refuelling with potentially large cost savings. Reactor technology, however, still limits the possibility for drastic improvements in steam generation efficiency. The following graphs explain the

steam cycles occurring in conventional and nuclear steam power plants. Appendix Figure 5 depicts a steam cycle with superheating.

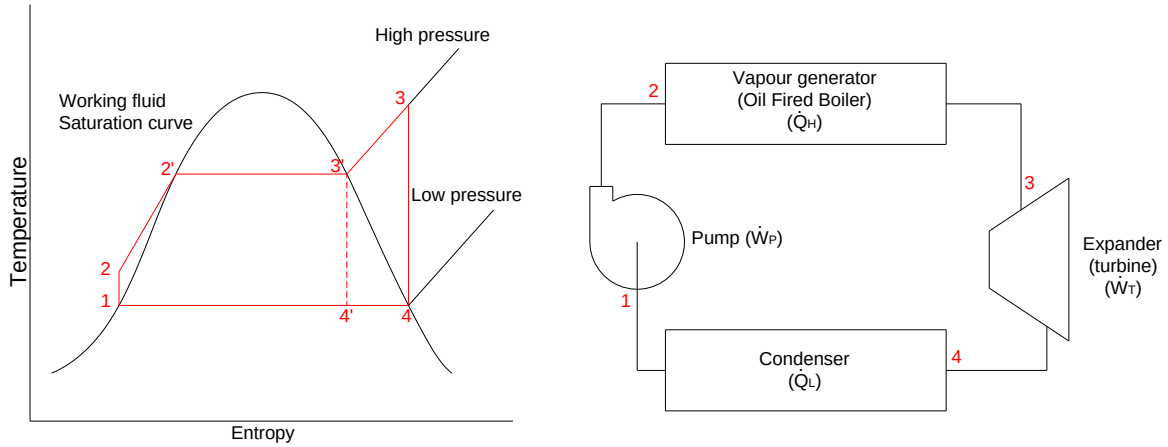


**Appendix Figure 5: Steam Cycle with superheating 3'-3 and one expander (turbine)**

Superheating is a better way of increasing Rankine efficiency by the extra area of (3' 3 4 4') (Van Wylen and Sonntag, 1978). Superheated steam ensures longer turbine life because of the absence of erosion from high-velocity water particles that are suspended in wet vapour (Rajput, 2009). Moreover, the Rankine cycle efficiency can be improved by increasing the average temperature (2' - 3') at which heat is supplied (2- 3'), or by decreasing the temperature at which heat is rejected (points refer to Appendix Figure 5). Appendix Figure 6 represents the actual nuclear cycle where no superheating is possible, as the cycle has to operate at lower temperatures due to reactor constraints (Nuclear cycle typical values are: $T_{3'}$= 285°C, $X_{3'}$ ~=0.9975, $P_{3'}$= 69bar, while typical steam, $T_3$=600°C, $X_3$>1, $P_3$= 80bar).

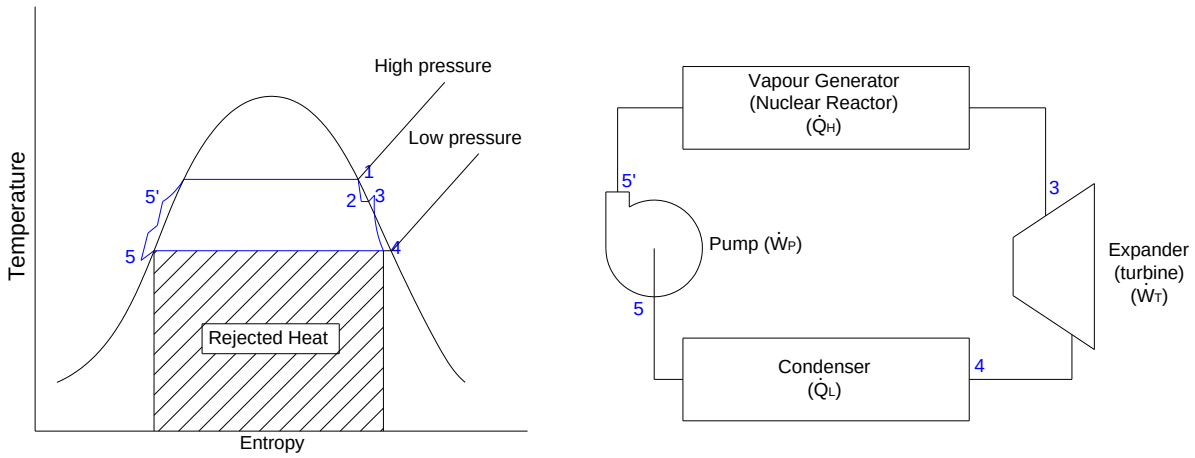


**Appendix Figure 6: Nuclear steam cycle using two expanders, with reheating (2-3) between high pressure (HP) (1-2) turbine and low pressure (LP) turbine (3-4) and preheating/ compression (5-5')**

To increase efficiency and to protect the low pressure turbine from operating with steam of dryness <0.9 (X<0.9), reheating occurs after the high pressure turbine (HP) and

the steam efficiency increases. Thus, in order to increase the propulsive efficiency and reduce the fuel burn up, the secondary circuit efficiency should be targeted.

If the coolant and moderator is light water ($H_2O$), in order to keep it in a single phase, the reactor maximum temperature should always be under 550$^oC$. Although operation with a two-phase coolant is possible (in BWR designs), it is very difficult to control, therefore BWR designs have lower safety limits. Thus, operational risk increases and other methods for Rankine efficiency increase have to be examined. It has been observed that by increasing the secondary steam cycle boiler pressure, the cycle efficiency tends to rise and reaches maximum value at about 166bar. Thermal efficiency of the cycle increases if the $T_{max}$ (without superheating) is higher and by keeping the $T_{min}$ lower or equal to the initial cycle. This means too that high temperature reactors have increased efficiency.

The net efficiency of the Rankine cycle is given by equation (IV.1.1):

$$n_{Rankine} = \frac{W_T - W_P}{Q_1} = \frac{\left(h_1 - h_2\right)\cdot\left(h_{f4} - h_{f3}\right)}{\left(h_1 - h_{f4}\right)} \quad \text{(IV.1.1)}$$

Turbo-generator work can be defined by the following equation (IV.1.2):

$$\dot{W} = \dot{m}\cdot\left(h_0 - h_p\right)\cdot\eta_{overall} \quad \text{(IV.1.2)}$$

The mass flow, pressure drop and efficiency of the turbine are described by manufacturer system maps. Usually these systems are optimised for a broad range of operation and at high loads, but in every other load their efficiency drops. Typical turbo-generator efficiency values for example for an LNG operated LNG carrier vessel vary from 0.93 to 0.96.and remain almost constant at high loads (Rajsput, 2009).

Taking into account the prime mover efficiencies, the Hybrid Power concept involves a two-stroke Diesel Engine with auxiliary four stroke Diesel Generator Sets. Due to the fact that 4-stroke Diesel Engines have reduced efficiency in low output powers, as the basis of the optimisation scenario, a regular Diesel Generator is used. Furthermore, a lower output generator will be used to measure the impact of low efficiency in combination with the Hybrid system. Moreover, an oversized generator is used, which has higher efficiency than in the initially examined cases. The same approach is followed for the main propulsion Engines. However, it should be noted that the selection of a downscaled or up-scaled Main Diesel engine is not a product of the optimisation algorithm.

**Nuclear Hybrid Series-Parallel Propulsion**

Hybrid nuclear propulsion combines the advantages of direct steam propulsion, the flexibility of electrical systems in manoeuvring and while ship is at berth, and safety features. The safe operation of the ship requires the availability of propulsion power, steering capability, navigation, and auxiliary power generation. Currently, this is mainly secured by ensuring that each component complies with the general standards, having enhanced reliability and performance. In nuclear powered ships, due to the high initial cost of the reactor, it is believed that only one nuclear reactor providing enough output for the propulsion and auxiliary loads will be installed. In the event of a reactor failure, a back-up propulsion system should be fitted, to ensure that the ship can return safely to a convenient port and all the emergency functions can run. A combination of diesel generator and batteries is a suitable solution. Although Diesel generators can provide enough power to propel and provide enough electricity for cooling the decay heat of the reactor, as in land based power plants, a second back-up system is required. The basic principles for designing the secondary safety systems are diversity (different principles of operation), redundancy (multiple components and systems to guard against the individual failure of components), independence (systems have to be physically separated); they also need to be failsafe and testable (tested without disrupting operation, or with redundancy).

Integrating the solution of Hybrid Nuclear, batteries seem to offer both load levelling in terms of demand, can actually downscale the reactor installed thermal power and can offer, at the same time, a back-up system in case of total failure. In normal conditions the majority of the power generation comes from a nuclear reactor, which produces steam through the steam generators attached to the secondary circuit. The main characteristics of the steam are low quality, due to the absence of superheating, and the existence of reheating between the HP and LP turbines at all stages of operation.

The ship will be considered to operate in four normal and one emergency modes of operation, which define the Hybrid Nuclear scenarios. Appendix Figure 7 illustrates the proposed Nuclear Hybrid configuration. The green line represents an alternative steam and electric circuit, which is controlled by the optimisation algorithm described in Chapter 4. When the system operates using the alternative circuit, HP turbines are by-passed and the excess of power demand that cannot be covered by the LP turbo-generators is boosted by the energy storage module.

**Scenario Nuclear – A (N-A):**

The first scenario is identified as normal, where the main propulsion turbine provides the power to the propulsor and a secondary turbo-generator, which utilises a part of the steam flow, provides at sea basic loads only. No battery operation takes place.

**Scenario Nuclear – B (N-B):**

The second mode is called 'slow steaming', in which no propulsion occurs from the main turbine. The ship uses the electric motor to cover the propulsion demand. However, while the electric loads are significantly higher than the auxiliary, a second turbine, which will be optimised for this operation, has to be installed. In this scenario, steam oriented for the main turbine will pass thought the main propulsion generator and the rest through the turbo-generator for auxiliary 'at sea' loads as in scenario one. In this operation, load levelling is investigated. For the needs of load levelling or to power the vessel at specific voyage periods, the battery system covers the demand. The latter system consists of multiple Sodium Nickel Chloride battery banks. The purpose of the system is to identify the optimum power split between the high and low pressure turbines in terms of isentropic efficiency and of generator efficiency. For that reason, the operation of the battery system is inevitable during normal sea going operation. However, in order to simulate these scenarios, the following assumptions have to be made.
Firstly, the cost of reactor refuelling is not known and cannot be compared with the cost of replacing the battery banks, if the latter exceed the maximum cycles. Secondly, the reactor thermal efficiency is taken equal to the nominal (36%), as reported by the manufacturer. Thirdly, for simulation purposes, the basic system for comparisons is the one with isentropic efficiency around 96% and with generator efficiency around 96% for the high and low pressure turbine, dependent on power load. As a result, the mathematical implementation of the system will be formed not by the component sub-efficiencies but from the efficiency drop for each component when the system operates in non- optimised conditions.

**Scenario Nuclear – C (N-C):**

The third scenario is while the ship is manoeuvring. This scenario is identical to the second; however, due to significantly lower propulsion loads than at slow steaming but with higher electric loads, the main propulsion generator should operate only. In case of reactor limit operation, the ship should be able to withstand operation using energy storage devices only. Because the propulsion is performed by the electric motor, steam re-heating in the turbo-generator can be performed again having increased efficiency. In cases of modular ship designs where the reactor is not present, the energy comes directly from the battery system.

**Scenario Nuclear – D (N-D):**

The fourth scenario is when the vessel is berthed. According to the port restrictions, either the nuclear reactor can operate at low loads driving only one turbine (preferably the electric propulsion turbine, as electric loads are higher than at sea, but lower than manoeuvring) maintaining low burn up, thus increasing the refuelling interval.

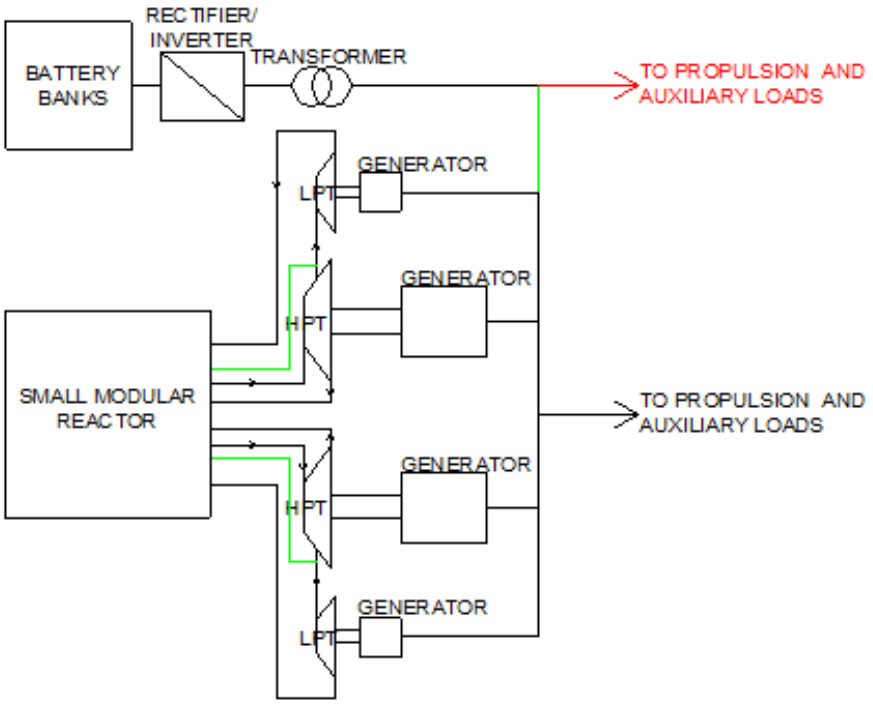


**Appendix Figure 7: Nuclear Hybrid AES propulsion system for conventional and pusher barge vessels**

## Nuclear Hybrid optimisation

It is already stated that reactor efficiency remains practically the same in every operational load. However, the efficiency of the secondary system is related directly to the operational load of the turbine generator. As a result, in order to decrease the rate of fuel burn up and thus increase the refuelling interval, the total absorbed power from the nuclear reactor has to be minimised. Thus, in order to reduce the consumption, the objective functions for charging and discharging should be defined. Because the fuel efficiency of the SMR is constant, the efficiency term is omitted from the equations, so the problem yields to reduction of total produced power. The concept of the reduction of power instead of the direct fuel consumption from Diesel engines has been modelled by Grimmelius et al. (2011), in order to reduce the $CO_2$ emissions from a Hybrid tug. The authors, in order to constrain excessive battery cycling limited the battery power split per time step, using logic criteria. This was achieved by introducing the lambda coefficient, which was described

previously in Chapter 4. Consequently, the objective functions are determined by equations (IV.1.3) and (IV.1.4).

When the storage medium is discharging:

$$\min P_{nf} = NF_{cons.} \cdot \left( x_2 + x_3 + \frac{x_1}{\eta_{T/F,inv} \cdot w\left( \frac{x_1}{N_{BB} \cdot V_{Bat}} \right)} \right) \tag{IV.1.3}$$

When the storage medium is charging:

$$\min P_{nf} = NF_{cons.} \cdot \left( x_2 + x_3 - \eta_{T/F,inv} \cdot w\left( \frac{x_1}{N_{BB} \cdot V_{Bat}} \right) \cdot x_1 \right) \tag{IV.1.4}$$

where,

$x_1$ : Battery power [kW]

$x_2$ : Nuclear reactor output for HP turbine [kW]

$x_3$ : Nuclear reactor output for LP turbine [kW]

The overall minimum is the solution out of (IV.1.3) and (IV.1.4) that yields to the minimum power/nuclear fuel bill.

The lower and upper bound vector of the power split is given by:

$$\begin{bmatrix} lb \\ ub \end{bmatrix} = \begin{bmatrix} 0 & 0 & 0 \\ \lambda \cdot \mathrm{Bat}_{\mathrm{cap.}} & MCR_{t_{HP}} & MCR_{t_{LP}} \end{bmatrix} \tag{IV.1.5}$$

For safety reasons, and based on manufacturer recommendations, the reactor is constrained to operate between 25% and 90% of the Maximum thermal output (or electrical output if assuming constant generator efficiency).

The linear inequality constraint matrices following the same form of ECMS strategy for Diesel Hybrid systems and are given by:

$$A = \begin{bmatrix} 0 & 1 & 1 \end{bmatrix} \tag{IV.1.6}$$

$$\boldsymbol{b} = \begin{bmatrix} 0.90 \cdot NR_{\max} \end{bmatrix} \tag{IV.1.7}$$

The non-linear constraint when the storage medium is discharging is determined by:

$$\frac{P_{shaft}+P_{aux.}}{\eta_C\cdot\eta_{T/F}\cdot\eta_{loss}} = x_2\cdot\eta_m\left(x_2\right)\cdot\eta_{is}\left(x_2\right)+x_3\cdot\eta_m\left(x_3\right)\cdot\eta_{is}\left(x_3\right)+ \\ +\eta_{T/F,inv}\cdot w\left(\frac{x_1}{N_{BB}\cdot V_{Bat}}\right)\cdot x_1 \tag{IV.1.8}$$

The non-linear constraint when the storage medium is charging is determined by:

$$\frac{P_{shaft}+P_{aux.}}{\eta_C\cdot\eta_{T/F}\cdot\eta_{loss}} = x_2\cdot\eta_m\left(x_2\right)\cdot\eta_{is}\left(x_2\right)+x_3\cdot\eta_m\left(x_3\right)\cdot\eta_{is}\left(x_3\right)- \\ -\eta_{T/F,inv}\cdot w\left(\frac{x_1}{N_{BB}\cdot V_{Bat}}\right)\cdot x_1 \tag{IV.1.9}$$

The lower and upper bound vector of the power split in charging condition is given by:

$$\begin{bmatrix} lb \\ ub \end{bmatrix} = \begin{bmatrix} \lambda\cdot \mathrm{Bat}_{\mathrm{cap.}} & 0 & 0 \\ DoD_{in}\cdot \mathrm{Bat}_{\mathrm{cap.}} & MCR_{t_{HP}} & MCR_{t_{LP}} \end{bmatrix} \tag{IV.1.10}$$

The linear constraints that are applicable to the optimisation vector X for the charging condition are expressed by matrices (IV.1.6) and (IV.1.7). The initial vector $x_{0,}$ which enables the system to converge to the minimum solution more rapidly, is given by:

$$x_0 = \begin{bmatrix} \left(\dfrac{\lambda\cdot\dfrac{\mathrm{Bat}_{\mathrm{cap.}}}{\Delta t_{sim}}}{w\left(\lambda\cdot\dfrac{\mathrm{Bat}_{\mathrm{cap.}}}{\Delta t_{sim}}\right)\cdot\eta_{T/F,inv}}\right) & \left(\dfrac{P_{\mathrm{AES}}}{2}-x_0\left(1\right)\right) & 0 \end{bmatrix} \tag{IV.1.11}$$

## Nuclear configuration voyage simulation

In order to set up the nuclear machinery configuration, the fluctuations in engine loading should be identified. Moreover, a statistical analysis of the average fluctuations in electric load should be taken into consideration. For this reason, Figure 6.5 and Figure 6.7 should be used. According to the analysis of these figures, it can be stated that the daily mean engine fluctuation does not regularly exceed 8%. Based on an interview with nuclear engineers designers of the SMR, it is expected that the reactor will be able to alter the power output by 5% in one second. This is expected to hold true for power changes lower than 15%. Above the 15% level, the rate of change is expected to be lower, i.e. about 0.2% per second. The idle condition for the reactor is expected to be at the operating temperature but at minimal power output in order to maintain this temperature. Consequently, for the speeding case after the ship has sailed from the harbour, it is implied that the reactor should take about 10 minutes to go from idle to full power.

Thus, given a more complete image of engine loading per two-hour period, which is presented in Figure 6.8, the M/E fluctuations in engine loading do not pose problems in serving the energy demand in real time and without the need to instantaneously reduce speed. Nevertheless, despite the fact that the propulsion loads do not impose problems to the reactor operation, as the fluctuation due to the propeller inertia and the governor setting exceed the response of 20 seconds, the study of the electric loads should be performed.

The electric load analysis performed by the yard is shown in Appendix Table 7, while the average measured electric power demand for laden and ballast voyages is presented in Appendix Figure 8.

**Appendix Table 7: Electric load analysis per voyage condition for the examined Post-Panamax vessels**

| Condition: | Total Load [kW] | Continuous Load [kW] | Internment Load [kW] |
|---|---|---|---|
| Normal sea going | 522.5 | 402.7 | 363.1 |
| Manoeuvring with ballasting | 991.2 | 961.1 | 151.7 |
| Manoeuvring without ballasting | 765.4 | 715.3 | 151.7 |
| Cargo Handling | 823.0 | 655.5 | 507.5 |
| At Harbour | 478.2 | 370.4 | 326.4 |

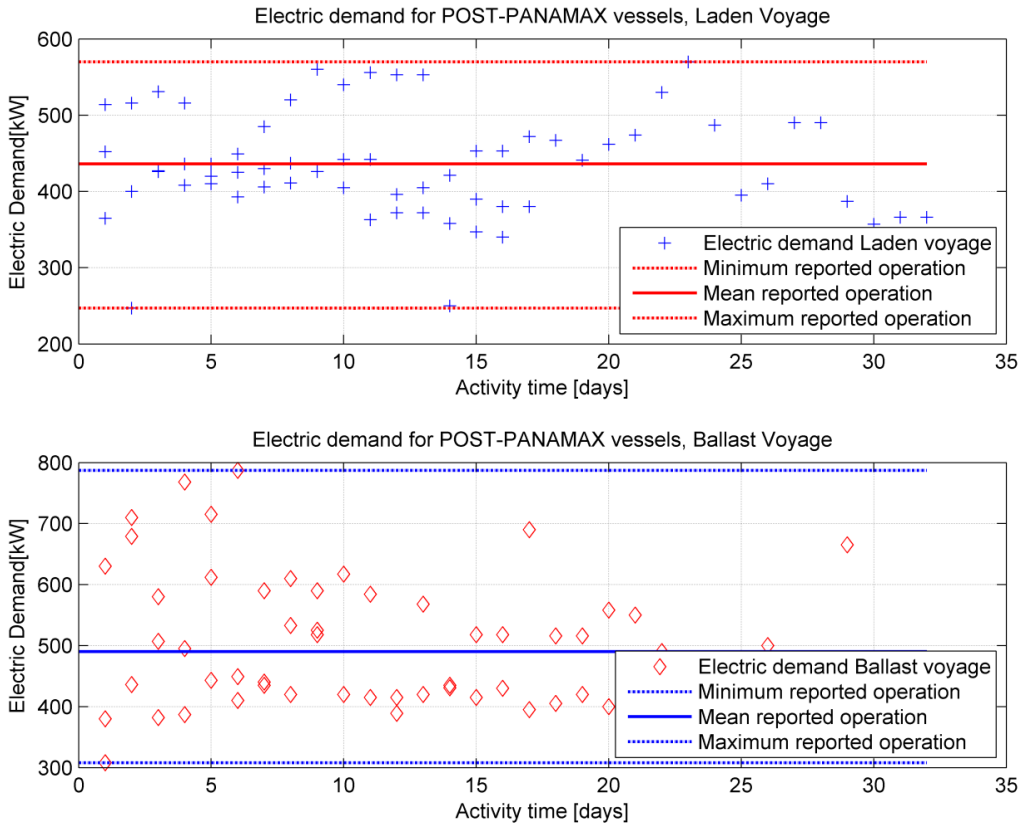


**Appendix Figure 8: Average electric power demand for laden and ballast voyages for 3 Post-Panamax sister ships**

In order to determine the auxiliary power demand more accurately, on board measurements during laden ocean going voyage for the examined ship were performed. The acquired power profile is depicted in Appendix Figure 9. The Diesel engine output before the alternator is 660kW, leading to an average load of 330kW or 320kWe (generator efficiency defined in Table 3.3). The sampling rate was set at 40-second intervals, and the obtained profile matches the reported electric values presented in . Thus, the question raised is, assuming a constant power output obtained from the ship simulator, whether the fluctuating auxiliary power demand will cause a problem in the nuclear operation. The answer is no, because the A/E fluctuation over the 40-second sample is almost 7% of the A/E MCR, resulting in a fluctuation of approximately 46kW. The Nuclear reactor maximum electrical power output is 20000kW. Thus, a continuous fluctuation of 46kW out of the 20MW is 0.23% of the power output, which is a negligible transient. Thus, the electric loads do not cause problems to the normal nuclear reactor operation. Thus, the assumption that the Hybrid Nuclear propulsion is required in order to stabilise the reactor operation, increase the operational safety and improve the primary circuit efficiency, is not valid.

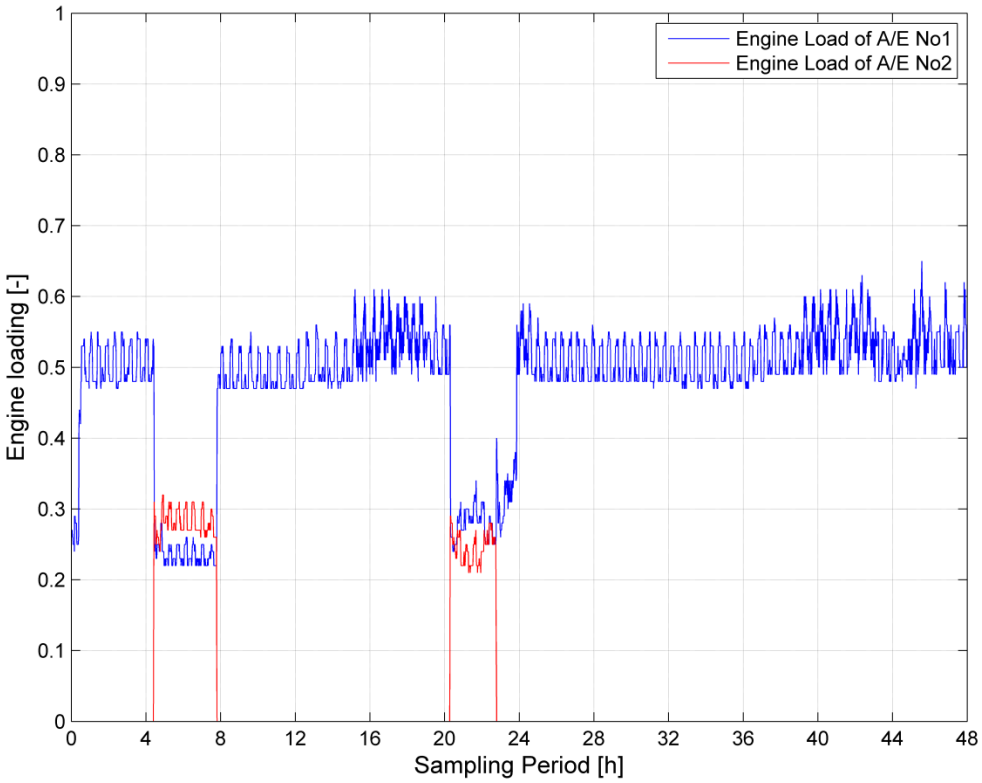


**Appendix Figure 9: Shipboard energy audit measurements of A/E loads**

Thus, the investigation of Hybrid Nuclear propulsion will be focused only on maximising the secondary steam circuit efficiency, which is dependent on the turbine load.

To produce a typical power profile for the main propulsion of the nuclear Hybrid ship equipped with electric propulsion, the ship simulator will be used, but with some modifications on the requested power from the prime mover. Due to the existence of electric motors, power converters, propulsion transformers and transmission losses, the following relationship should be applied:

$$P_{demand} = \frac{P_{shaft}}{\sum_{i=1}^{n} \eta_{component}} \qquad \text{(IV.2.1)}$$

The efficiencies of the electric components are presented in Table 3.2. However, in order to simplify the propulsion problem, the efficiency of the propulsion motors will be taken as constant and equal to 96% instead of the relationship between load and efficiency (shown in Figure 3.7). Hence, the prime mover power, as modified for electric propulsion, is defined by:

$$P_{\text{AES}} = \left( \frac{P_{\text{shaft}}}{\sum_{i=1}^{n} \eta_{components}} \right)_{\text{AES}} = \frac{1}{\sum_{i=1}^{n} \eta_{components}} \cdot \left( \frac{P_{\text{shaft}}}{0.99} \right)_{\text{Conventional}} \quad \text{(IV.2.2)}$$

To finalise the total power demand of the vessel operation, electric load which depends on the operational scenario is added to the calculation. This average load is defined by the electric load analysis and concerns typical ocean going operation. In order to export a global result to the calculation, the power profile of Appendix Figure 9 will not be used in the Nuclear Hybrid scenario.

For the baseline approximation of nuclear fuel consumption, the following assumptions are made:

- Approximately 85% of reactions leads to fission
- One fission releases approximately 200MeV of energy
- 1 mol of $U_2N_3$ weights 518.078g
- Avogadro number equals $6.02 \text{x} 10^{23}$ atoms/mol
- Small Modular Reactor efficiency equals to 36%

As a result, the number of fissions to meet the power demand is given by (IV.2.3):

$$A = \frac{P_{demand}}{\eta_{\text{reactor}} \cdot 3.2 \cdot 10^{-11}} \quad \text{(IV.2.3)}$$

The number of atoms involved in the fission process is approximated by:

$$No_{atoms} = \frac{A}{85\%} \quad \text{(IV.2.4)}$$

Hence, the consumption of $U_2N_3$, which is the fuel of the examined SMR, is calculated by:

$$FC_N = \frac{\frac{No_{atoms}}{6.02 \cdot 10^{23}} \cdot 518.078}{10^6} \quad \text{(IV.2.5)}$$

The result of (IV.2.3) should be minimised using the optimisation algorithm presented in this Appendix.

## Optimisation of Nuclear Hybrid installation

The assessment of the Hybrid Nuclear installation was performed on the basis of the efficiency of the secondary circuit only. The results indicate that it is more energy efficient to have multiple turbine sets (denoted as High Pressure or Low Pressure), instead of two turbo generators. Thus, the following vector represents an average shaft loading. The power demand to one motor is half of IV.3.1, as to propulsion motors cover the shaft demand.

$$P_{AES} = \begin{bmatrix} 9300 & 8900 & 9100 & 7800 & 7200 & 6900 \end{bmatrix} \qquad \text{(IV.3.1)}$$

To this power demand, an additional average power demand for auxiliary services was included in the optimisation scenario. The average electric load equals to 575kW, which is the maximum reported current, as shown in Appendix Table 7 and is higher than the normal sea going operation. For the presented optimisation scenario, the $P_{AES}$, including the auxiliary loads, is divided by the number of electric motors, which is set to two. The motors are connected to a gearbox with an efficiency of 98%. The HP turbo-generator maximum output is set to 4000kW and the LP turbo-generator maximum output to 2000kW. The nuclear electric output is set to 12000kWe, with nominal thermal to electrical efficiency of 36%. The installed battery energy capacity is set to 8000kWh and the batteries are depleted for the optimisation scenario.

The results indicate that the proposed hybrid system with multiple turbines is indeed less energy efficient by 3.27% than the conventional system for the given power profile. For the propulsive and auxiliary demand of (IV.3.1), the Hybrid-Nuclear configuration attempts to maintain the highest loads over the two turbines. This is explained by the fact that the isentropic and motor efficiency of the HP turbine reaches its maximum value when it operates near 100% of the load. Hence, with initially depleted batteries and without the existence of the λ coefficient constraint, there was no need for the system to reduce the load of turbines and utilise stored energy over the simulation period and for the remaining simulation time, so the applied logic criterion was set continuously to the charging condition. Nevertheless, it is stated that the logic criteria are set in order to determine which of the Hybrid conditions (charging or discharging) yields to the optimum global solution.

In order to evaluate the effect of the constrained optimisation, a second run is also performed inserting the λ coefficient constraint, following exactly the same optimisation procedure outlined in Chapter 4. Appendix Figure 10 depicts the progressive charging of the battery during the simulated 24-hour operation. It can be extracted that

the battery is now charging for 83.3% of the simulation time, until it reaches the $SoC_{ref}$ value, which is 35%.

The charging effect is of great importance to the percentage of power savings or power losses. For the unconstrained system, where the battery was fully charged after two hours of operation, power losses reached 3.71%, while, in this scenario, losses amounted to 959.30kW or 3.27% with progressive charging. However, the results showed that the baseline system without batteries attached is more energy efficient, as conversion losses do not exist. In addition, these two scenarios showed that, when the battery system was utilised and the SoC differed from $SoC_{ref}$, having a high propulsive power demand, the system was more energy efficient in charging the batteries the as soon as possible, in order to maximise energy savings. Consequently, in order to evaluate the effect of the battery system in the Nuclear Hybrid solution, the manoeuvring condition is selected, as the turbines work at the edge of the thermal efficiency and the turbo-generators at low loads. The principle is to have a condition that slightly exceeds the maximum output of LP or the HP turbine.

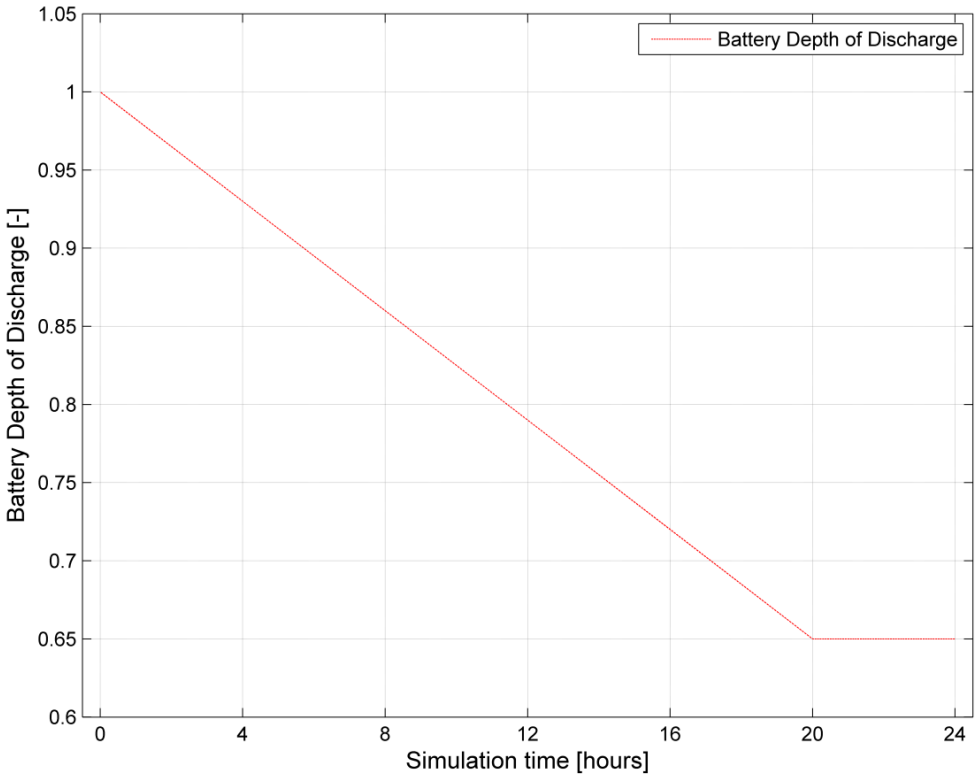


**Appendix Figure 10: Battery Depth of Discharge in Hybrid Nuclear configuration applying λ coefficient constraint**

This scenario will evaluate the need for batteries for load levelling purposes in the Hybrid Nuclear configuration. The power demand vector for each propulsion electric

motor is the equal power split of the propulsion demand vector. Hence, the following vector represents the artificial load to the LP and HP turbines. To this load, the average auxiliary load, which equals 765kW for the ship manoeuvring without ballasting condition, is added to the calculation. This artificial loading represents the manoeuvring of the vessel until it reaches berth using tug assistance. The battery system is fully charged prior to this operation.

$$P_{AES_I} = \begin{bmatrix} 5200 & 4300 & 3900 & 2800 & 2300 & 1900 \end{bmatrix} \quad \text{(IV.3.2)}$$

Appendix Figure 11 illustrates the power split between the HP, LP and battery system. It can be concluded from this graph that the battery system interacts and absorbs or provides energy to the system over the examined simulation. The battery system remains idle only for 16.7% of the simulation time. Moreover, the LP turbine is operating near its maximum power output, increasing the energy efficiency of the system. Because the cycling over batteries is constrained by the λ coefficient, it is impossible to meet the power demand without running the HP turbo-generator. Thus, it is inevitable to perform a power split between the battery and the low-pressure turbo-generator only. Nonetheless, compared to the baseline vessel, the system is more energy demanding.

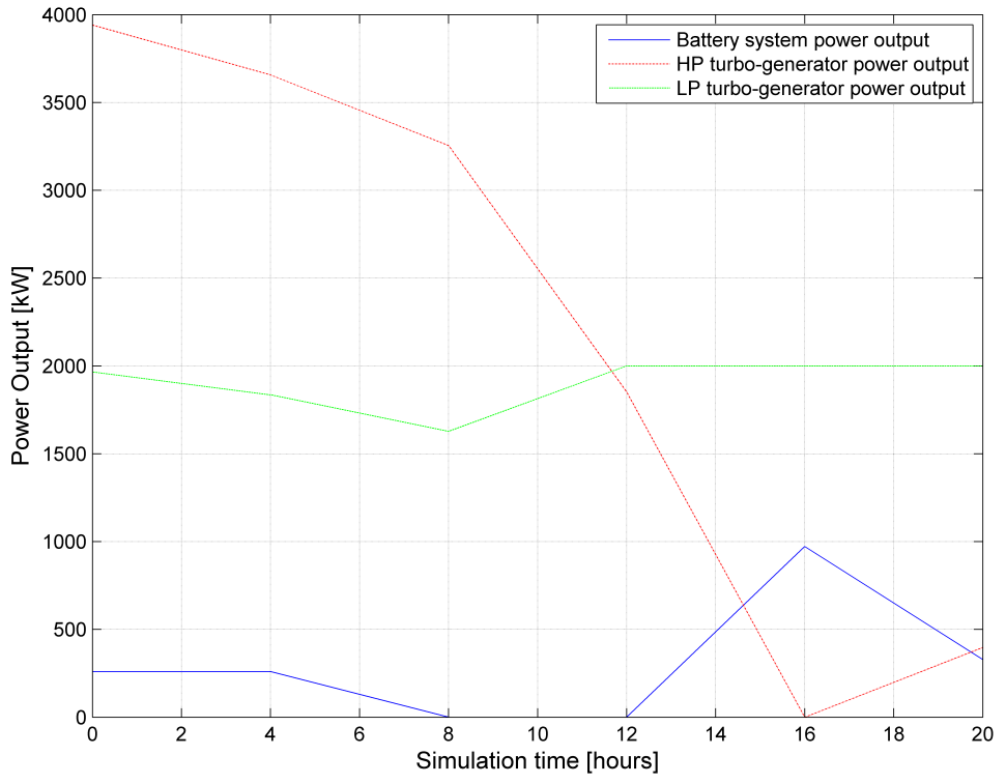


**Appendix Figure 11: Power split between battery system, LP and HP turbo-generators for Nuclear Hybrid configuration**

In order to finalise the feasibility assessment of the system, an artificial load during cargo handling operations will be inserted to the calculations, for the purpose of assessing the usefulness of the battery system. The power vector is given by (IV.3.3). The system is fully charged prior to the application of this power vector, and the energy capacity is set to 8000kWh.

$$P_{aux} = \begin{bmatrix} 655 & 507 & 680 & 540 & 630 & 600 \end{bmatrix} \quad \text{(IV.3.3)}$$

The results of this run are presented in Appendix Table 8. It is found that the battery system operates and aids the LP turbine to cover the auxiliary demands, and there is a 8-hour slot during which the system operates in battery only condition. Moreover, the system is charging during certain periods, and the discharging, charging and idle split is 50.0%, 33.3% and 16.7%, respectively. The savings percentage, as compared to the baseline configuration, is 2.13%.

**Appendix Table 8: Power Split and battery DoD of Nuclear Hybrid system**

| Simulation time [h] | Battery Output [kW] | HP turbo-generator output [kW] | LP turbo-generator output [kW] | Battery DoD [%] |
|---|---|---|---|---|
| 0-4 | 0 | 0 | 897.3 | 0 |
| 4-8 | 325.0 | 0 | 398.8 | 16.25 |
| 8-12 | -325.0 | 0 | 1203.4 | 0 |
| 12-4 | 596.0 | 0 | 0 | 29.80 |
| 4-8 | 696.9 | 0 | 0 | 64.64 |
| 8-0 | -120.0 | 0 | 843.6 | 64.59 |

***Results***

Regarding the nuclear power renaissance, the SMR design seemed a feasible solution which reduces the accident risk. Moreover container ships > 8000 TEUs with the current price of HFO are financially viable. Nevertheless, there are many parameters which still need to overcome such as the large difference of initial cost, the high manning cost, the expensive insurance and the operational restrictions imposed by the regulatory frameworks of each country. Moreover, the increase of nuclear waste due to the potential application in shipping is considered as an important factor. Therefore, the installation of Fast reactors was discussed as a potential solution to the nuclear waste problem which are significantly reducing the environmental impact and increasing the Uranium resources for 1500 years of reactor operation. Nonetheless, it would take almost 40-50 years to breed more fuel with the current technology, thus requires short term future action in terms of shipping policy.

The nuclear configuration showed contradicting results regarding the total power efficiency. There are cases where the existence of both HP and LP turbo-generators affects

the overall energy efficiency, resulting in the conclusion that the system is not feasible, i.e. in high loads. Nonetheless, it was demonstrated that, when the power demand is higher than the maximum power output for each of turbo-generators, but less than their combined output power, the system absorbs power from the energy storage medium, increasing the power efficiency by up to 2.13%. However, this case is only applicable in manoeuvring or cargo handling conditions and not in ocean going.